The University Of Sheffield.

Determining the performance characteristics of flat plate and photovoltaic thermal collector for sustainable cooling systems integration

PhD Thesis

by

Mohammad Saleh Alobaid

Submitted in accordance with the requirements for the degree of PhD

The University of Sheffield

Department of Mechanical Engineering

Jan 2019

I confirm that the research work is my work and the appropriate credit has been given where reference has been made to the work of others

This copy has been supplied on the understanding that it is copyright material and that no quotation from the thesis may be published without proper acknowledgement.

The right of Mohammad Alobaid to be identified as Author of this work has been asserted by him in accordance with the Copyright, Designs and Patents Act 1988.

© 2016 The University of Sheffield and Mohammad Alobaid

Acknowledgements

This thesis has been carried out with the full support and patience of my supervisor, Dr. Ben Richard Hughes. I wish to acknowledge the contributions of Dr. Hughes for his constant support and of all those in the research team of the 2050 Energy Engineering Group, under Dr. Hughes' supervision, who have given direct or indirect support.

Dedicated to the memory of my father, SALEH ALOBAID, who spent every moment of his life strengthening me towards success and improving my knowledge. You passed away while I was studying away from home but your support has made my PhD journey possible.

I would also express my thankfulness to my mum who was very patient during my journey while waiting for the moment of success. I would also never forget to thank a very special person, my wife, for her continuing support and understanding during every single moment of my journey, which made it possible. I appreciate my lovely boys; I could never imagine what the journey would have been like without such a lovely family, while I was away from home, with their love and understanding of the difficulties in this journey.

This research was made possible by Majmaa University through a grant from the Saudi Arabian government fund. The statements made are solely the responsibility of the author.

Abstract

Improvement of the overall performance of solar cooling systems is achievable by optimising inlet conditions for the highest thermal efficiency of solar collectors such as flat plate collectors (FPC) and photovoltaic thermal collectors (PVT). This study has highlighted the recent advances in the field of solar absorption cooling systems from the point of view of the solar collector's types and has conducted an extensive review of the use of FPC and PVT for absorption cooling systems. The aim of this study is to investigate and optimise the thermal efficiency of FPC and PVT for sustainable cooling systems.

The effect of inlet temperature (T_{in}) and flowrate ($\dot{m}$) on thermal efficiency (η_{th}) of FPC was investigated. Computational Fluid Dynamics (CFD) was employed to simulate a FPC and the results validated with experimental data from literature. Increasing inlet water temperature of FPC from 298 K to 370 K reduced thermal efficiency by 30%. There was no significant impact when the total flowrate of FPCs exceeded 36.4 x10^{-3} kg/s/m^2.

CFD was also employed to simulate a PVT and was validated by the literature. The effect of T_{in} and $\dot{m}$ on thermal efficiency(η_{th}) and electrical efficiency (η_{elc}) for the PVT was investigated. Increasing inlet water temperature of PVT from 273 K to 373 K reduced thermal efficiency by 7% while there was a significant reduction in electrical efficiency by 45% due to the increase in photovoltaic layer temperature. There was no significant impact when the total flowrate of the PVT exceeded 35 x10^{-3} kg/s/m^2.

The inlet conditions of FPC and PVT were optimised for the highest efficiency in accordance with the minimum absorption cooling driving temperature currently available in the market. A multi-objective optimisation study was applied to the computational model of the FPC by employing the response surface optimisation method in ANSYS16.1. The optimum flowrate of the FPC was $\dot{m}$ =0.0067 kg/s/m^2 with an inlet temperature of 321 K for thermal efficiency of 84 %. A multi-objective optimisation study was also applied to the computational PVT model. The optimum flowrate of the PVT was $\dot{m}$ =0.0165 kg/s/m^2 with an inlet temperature of 337.36 K for thermal and electrical efficiency of 81.32 % and 11.26 % respectively. The study has managed to optimise inlet conditions for FPC and PVT coupled with a cooling system at specified conditions. Optimising the inlet conditions has a significant impact to increase solar coefficient of performance (SCOP).

Contributions to knowledge

Journal papers:

1- Alobaid, M., Hughes, B., O'Connor, D., Calautit, J., Heyes, A. *A review of solar driven absorption cooling with photovoltaic thermal system*. Renewable & Sustainable Energy Reviews, 2017. https://doi.org/10.1016/j.rser.2017.03.081

2- Alobaid, M., Hughes, B., O'Connor, D., Calautit, J., Heyes, A. *Improving Thermal and Electrical Efficiency in Photovoltaic Thermal (PVT) systems for Sustainable Cooling System Integration*. Sustainable Development of Energy, Water and Environment Systems. https://doi.org/10.13044/j.sdewes.d5.0187

3- Alobaid, M., Hughes, B., Heyes, A., O'Connor, D. *Determining the Effect of Inlet Flow Conditions on the Thermal Efficiency of a Flat Plate Solar Collector*. Fluids, 2018. 3(3): p. 67. https://doi.org/10.3390/fluids3030067

Conference papers:

1- Alobaid, M., Hughes, B., O'Connor, D., Calautit, J., Heyes, A. *Development of sustainable cooling systems in hot countries*. Sustainable Development of Energy, Water and Environment Systems – Conference, 4-9 September 2016, Lisbon, SDEWES 11th.

2- Alobaid, M., O'Connor, D., Hughes, B. *Development of photovoltaic thermal systems in hot countries*. Sustainable Energy Technologies - Conference, 17-20th July 2017, Bologna, SET2017 16th.

Table of Contents

List of Tables

List of Figures

Nomenclature

A_c	Collector area (m^2)
COP	Coefficient of performance
PV	Photovoltaic panel
Q	Heat transfer rate (kW)
Q_u	Useful energy output from the solar collector (kW)
T_{in}	Inlet temperature of the coolant (^oC, K)
T_{out}	Outlet temperature of the coolant (^oC, K)
T_{bs}	Back surface of Tedlar temperature (^oC, K)
T_{cell}	PV cell temperature (^oC, K)
U_L	Overall heat transfer coefficient (W/m^2 K)
U_T	Overall heat transfer coefficient from solar cell to flowing water through Tedlar (W/m^2 K)
U_{tT}	Overall heat transfer coefficient from glass to Tedlar (W/m^2 K)
U_b	Overall back loss coefficient from flowing water to ambient(W/m^2 K)
L_g	Thickness of cover glass (m)
L_{si}	Thickness of photovoltaic layer (m)
T_{pm}	Mean temperature for the absorber plate collector (K)
T_a	Ambient temperature (K)
T_{sc}	Reference cell temperature (K)
T_f	Fluid Temperature (K)
$\dot{m}$	Mass flowrate of the coolant (kg/s)
C_p	Specific heat of the coolant (kJ/kg K)
G	Incidence solar irradiance normal to the surface (W/m^2)
F_R	Heat Removal factor

h	Heat transfer coefficient (W/m^2)
h_T	Heat transfer coefficient back surface of Tedlar to fluid (W/m^2 K)
h_f	Convective heat transfer coefficient inside the water duct (W/m^2)
h_{p1}	Penalty factor due to the glass cover of PV module
h_{p2}	Penalty factor due to the absorber below PV module
η	Efficiency
η_o	Reference efficiency
η_{tot}	PVT overall efficiency
η_{th}	PVT thermal efficiency
η_{elc}	PVT electrical efficiency
β	Photovoltaic temperature coefficient
τ	Transmittance
α	Absorbance
ϵ	Emittance
a	Acceleration vector (m/s^2)
u	Local velocity component in x direction (m/s)
v	Local velocity component in y direction (m/s)
w	Local velocity component in z direction (m/s)
ρ	Density (kg/m^3)
k	Conductivity (W/m k)
S_h	Volumetric heat source

Chapter 1. Introduction

1.1 Introduction

The demand for energy is increasing around the world due to population growth and industrialisation. Fossil fuels such as oil and natural gas are considered primary sources of energy. In 2035, more than 80% of energy consumption will be produced by fossil fuels in some developed countries (Fumo et al. 2013). Producing energy by traditional methods increases gas emissions and accelerates global warming. Alternative renewable sources of energy such as solar energy, wind energy and geothermal energy are required (Eicker et al. 2014).

In response to the need for alternative energy sources, solar cooling technologies have become an important factor especially in hot countries due to the huge amount of solar radiation and the need for cooling. Solar cooling systems are environmentally friendly compared to conventional cooling systems and are an important technology for reducing gas emissions (Prasartkaew 2013). Integrating solar technologies with cooling systems has become a key factor in meeting the energy demand while reducing CO_2, and gas emissions.

The potential for solar energy and the opportunity to utilise it for cooling purposes depend on the geographical location. Theoretically, 0.6 % of the area of Europe would need to be covered by solar photovoltaic panels (PV) to satisfy Europe's total electricity consumption (Šúri et al. 2007). Europe, North America, most of Latin American and western Asia have a 100-200 W/m^2 average annual rate of solar radiation while in the Middle East, the value reaches 250 W/m^2. During the summer time, the average solar radiation in Saudi Arabia is 540 W/m^2 (Pazheri et al. 2012). Accumulated solar radiation for different cities in Saudi Arabia is in the range of 3.28 to 7 $kWh/m^2/day$ (Abd-ur-Rehman and Al-Sulaiman 2016). Pazheri et al. (2012) estimated that a 20 MW solar plant, which would need an area of 1.25 km^2, can generate 200 to 300 GWh/year and could save 500,000 barrels of oil per year. In Europe, the residential sector accounts for 40% of energy consumption, with heating purposes representing about 68% of this sector

(Hepbasli and Alsuhaibani 2011; Pampuri et al. 2016). In contrast, cooling systems consume 72% of residential electricity in residential sectors in hot climatic conditions (Sadiq Munfath Khan and Orfi 2014). In Saudi Arabia, air-conditioning systems in the residential sector consume approximately 65% of the energy demand (Al-Ugla et al. 2016).

1.2 Solar cooling systems

Figure 1-1 shows a schematic diagram of a solar heating and cooling absorption system which consists of solar collector coupled with an absorption chiller, storage tank, cooling space and controllers. Solar energy is absorbed by the solar collectors and transferred to the fluid before it is circulated to the storage tank through a close cycle with a circulating pump. The storage tank is set up at specified temperature in order to supply the heat energy to the absorption chiller at the required driving temperature (T_g). The heat is rejected from the absorption chiller through the cooling tower. Chilled water is supplied from the absorption chiller to the space in a temperature range of 6 ^oC to 26 ^oC (Al-Alili et al. 2014). In case of heating, the hot water is supplied to the space directly from the storage tank.

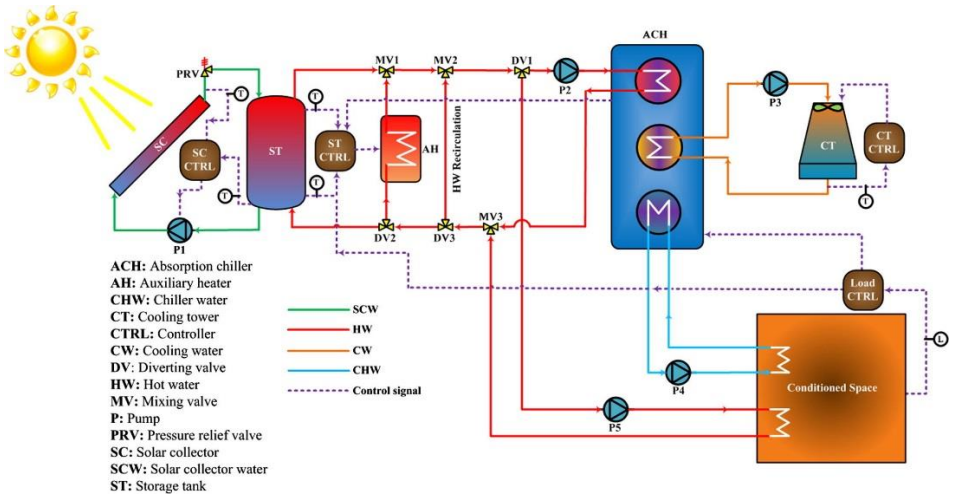

Figure 1-1 Schematic diagram of solar heating and cooling absorption system (Shirazi et al. 2016).

1.2.1 Background of Solar Absorption Cooling System

Absorption cooling system is one of the most popular designs to produce cooling by utilizing thermal energy such as solar energy, geothermal energy and waste energy. Figure 1-2 shows ammonia-water single absorption refrigeration cycle. In this system, ammonia serves as a refrigerant and water as transport medium. Ammonia-water solution, which is rich in NH3, is pumped from the absorber, through the regenerator exchanger for heat recovery, to the generator. The heat, which is utilised by the solar collector, is added to the solution in the generator then by raising its temperature and pressure, the mixture is separated into vapour and liquid solutions. The vapour, which is rich in ammonia, leaves the generator in a high pressure through the rectifier to reach the condenser as pure NH3 while the remains water passes back to the generator. The weak solution is throttled back to the absorber through the regenerator to recover the heat. In the absorber, the solution is cooled and pure NH3 is transferred from the evaporator to make a strong solution once more. The other section of the cycle is a typical basic refrigerant cycle, which consists of condenser, expansion valve and evaporator (Cengel et al. 2011).

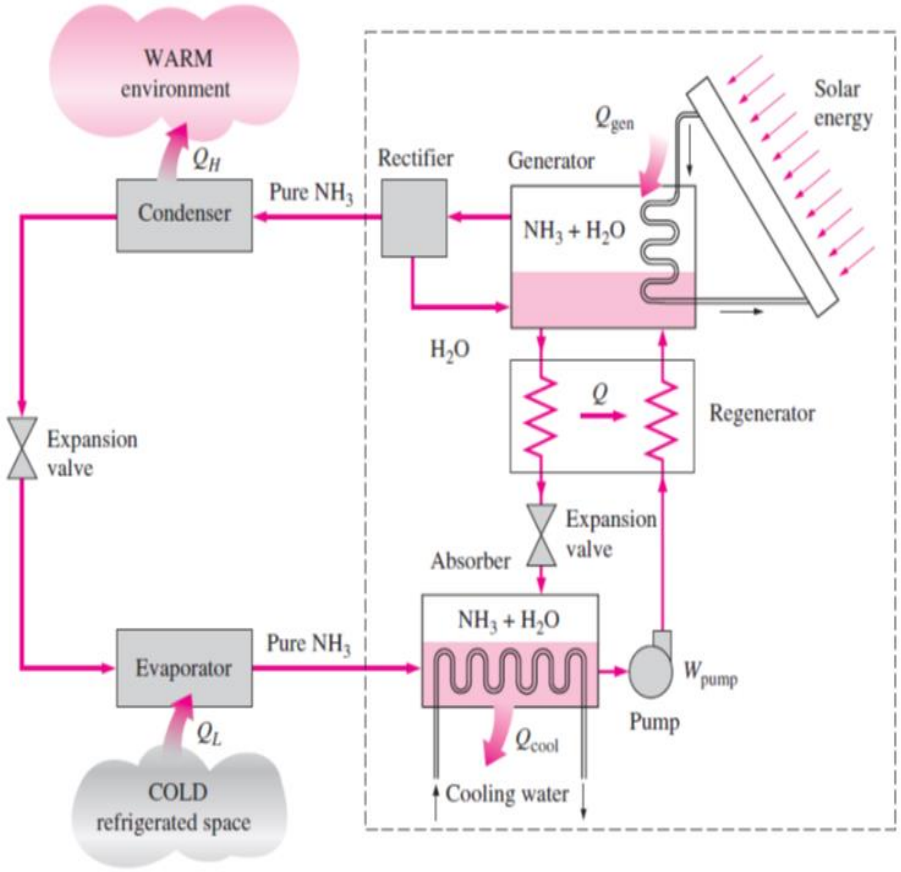

Figure 1-2 Solar absorption refrigeration cycle (Cengel et al. 2011).

Generation temperature of single effect absorption chillers are in the range of 70 ^{o}C to 100 ^{o}C and the COP in the range of 0.5 to 0.8. Double effect absorption chiller required a generation temperature of 140 ^{o}C to 180 ^{o}C and the COP in the range of 1.1 to 1.4 (Allouhi et al. 2015). Double effect absorption refrigeration cycle consists of two stages of generators, two condensers and two heat exchangers. The primary heat is supplied to the high pressure generator in the system while the low pressure generator receive the heat (at 90 ^{o}C) from the high pressure condenser as well as from the high pressure generator (Hassan and Mohamad 2012).

1.2.2 Solar cooling system performance

Performance indicators have been discussed in the literature to evaluate solar cooling systems (Fong et al. 2010; Allouhi et al. 2015). Solar fractions is an efficiency indicator that measure the ratio of the total energy collected by the solar collectors to the energy required for the system and can be written as:

$$SF = \frac{Q_s}{Q_S + Q_{aux}} \quad (1\text{-}1)$$

Where SF is the solar factor of the system, Q_s is the energy that produced by solar collectors and Q_{aux} is the additional energy from the auxiliary devices. Another efficiency indicator is solar coefficient of performance (SCOP) which calculates the ratio of the cooling energy required Q_e (usually representing the energy removed from the zone and absorbed by the evaporator) to the energy produced by the solar collectors Q_s and is written as (Bellos et al. 2016):

$$SCOP = \frac{Q_e}{Q_S} \quad (1\text{-}2)$$

The coefficient of performance of the absorption chiller (COP) is the ratio of the cooling energy required (Q_e) to the input energy in the generator section (Q_g):

$$COP = \frac{Q_e}{Q_g} \quad (1\text{-}3)$$

Single effect solar absorption systems have been estimated to be relatively more efficient and less costly (Raja and Shanmugam 2012). The majority of research has analysed the incorporation of solar collectors, such as the flat plate collector and the evacuated tube collector (FPC and ETC), with absorption chillers, but most has not emphasised their efficiencies. From previous studies, there is still a lack of information on the combination of photovoltaic thermal collectors (PVT) with absorption chillers.

1.2.3 Solar collectors

Solar collectors such as flat plate collectors (FPC) convert solar radiation to useful thermal energy and can be designed to deliver energy to fluid up to a level of 100 ºC above the ambient temperature (Duffie and Beckman 1980). Solar collectors is a key parameter that affects the overall cost of solar cooling system. Solar collectors represents 35% of the overall cost while the percentage cost of chillers was 15 % as illustrated in Figure 1-3. The high impact of the solar collectors cost requires further effort to select the optimum types and operation conditions of the collectors coupled with solar cooling systems.

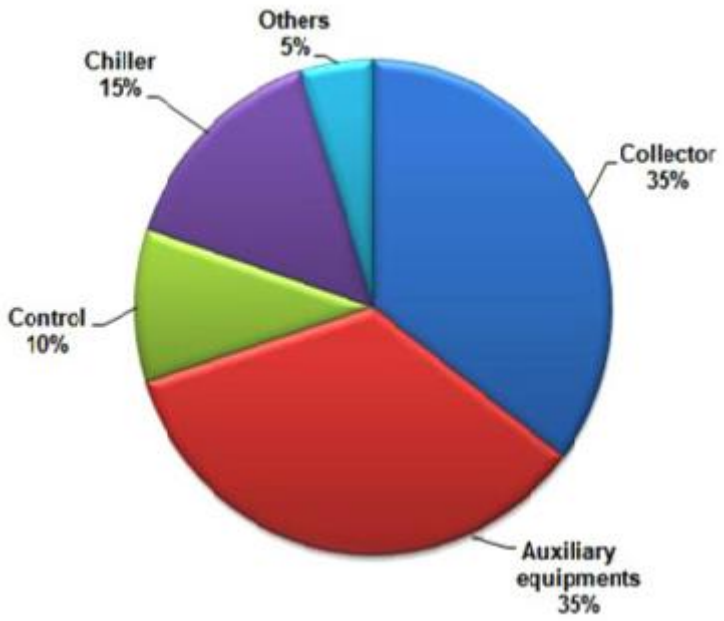

Figure 1-3 Percentage cost of solar cooling system components (Allouhi et al. 2015).

Flat plate collectors are the most common devices that can power a single absorption chiller which needs to be driven by hot water in the range of between 70 ºC and 120 ºC. Single absorption chillers also need to be supplied by electricity; that is, power from an electricity grid or other sources such as photovoltaic (PV) devices. PVTs and CPVTs (a combined photovoltaic thermal collector) can also supply both electricity and hot water to the system. Research into photovoltaic thermal systems (PVT) is important in solar technologies, as PVT systems are designed to produce both electrical and thermal energy;

this can improve performance of the overall system. The PVT performance is based on several factors that include PVT materials, design, ambient temperature, inlet and outlet fluid temperature and photovoltaic (PV) cell temperature.

In the last few years, there has been a growing interest in reducing the initial cost and improving the efficiencies of solar collectors, which reduces overall investment in the solar cooling system. Flat plate collectors and photovoltaic thermal collectors have been used for several solar cooling projects in order to produce both electricity and thermal energy. The average electrical efficiency of a photovoltaic thermal collector that associated with a cooling system was 10.4% and can be improved by 23.8% due to cooling the photovoltaic panel (Fang et al. 2010).

Five types of solar collectors were compared in Figure 1-4 concerning their efficiencies for different inlet and ambient temperatures at high and low solar radiation (1000 W/m^2 and 500 W/m^2).

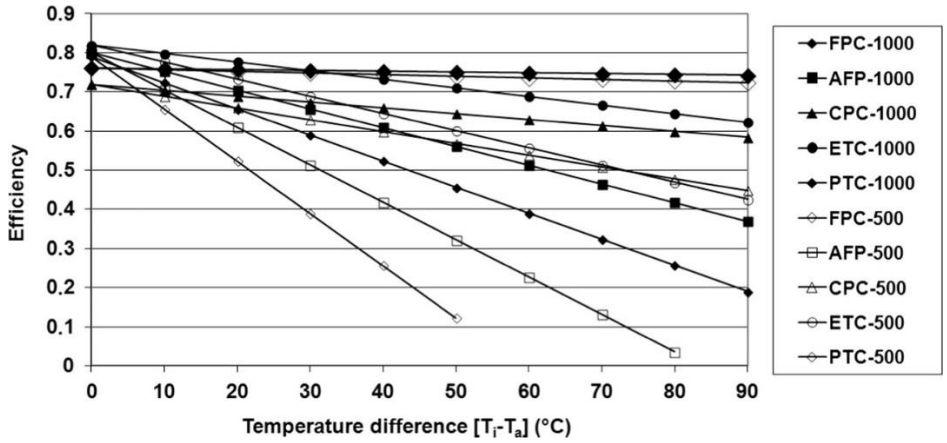

Figure 1-4 Thermal **e**fficiency of various collectors for different inlet and ambient conditions (Allouhi et al. 2015).

Figure 1-5 shows another comparison for several types of solar collectors based on the efficiencies of published works at 1000 W/m^2 solar radiation. It can be observed that the efficiency of flat plate collectors was relatively higher at low T_M (T_M = plate mean temperature – ambient temperature) compared to the other types of collectors which

included evacuated tube collectors and parabolic trough collectors. In contrast, due to a higher heat loss coefficient for flat plate collectors, the efficiency of flat plate collectors was relatively lower at T_M > 100 ^oC (Moss et al. 2018).

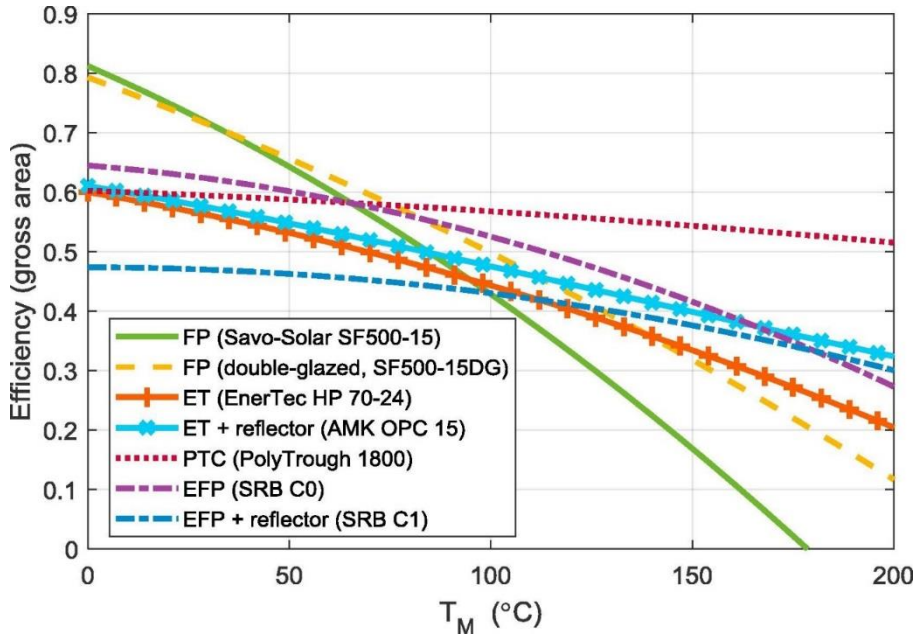

Figure 1-5 Thermal efficiency of various collectors versus T_M (plate mean temperature – ambient temperature) (Moss et al. 2018).

The cost for different types of solar collectors and temperature ranges are reported in Table 1-1. It can be observed that flat plate collectors were approximately 40 % lower cost compared to the other types of solar collectors which is a practical choice to be utilise in solar cooling systems . In addition, Figure 1-4 and Figure 1-5 illustrated that flat plate collectors can achieve a heat at a level of outlet temperature in the range 70 ^oC to 100 ^oC with relatively reasonable efficiency which meet the target temperature of single absorption chillers. In the other hand, the method to manufacture and maintenance flat plate collectors is not complicated compared to the other collectors types (Michael et al. 2015). However, sheet and tube flat plate collector is one of the best options to be coupled with single absorption cooling systems.

Table 1-1 Temperature ranges and cost for different types pf solar collectors.

Collector type	Temperature range ^{o}C (Allouhi et al. 2015)	Cost (Euro/m^2) (Asadi et al. 2018)
FPC	30-200	150
ETC	50-200	250
CPC	60-300	225
PTC	50-400	215

Thermal performance of flat plate collectors is affected by transmitted solar radiation through the top cover, which is based on the cover transmissivity. As illustrated in Figure 1-6, parts of transmitted radiation is reflected from the absorber and some heat is transferred as a heat loss to the ambient, which is in the range of 10-35% as (Hossain et al. 2011). The absorbed heat is based on the absorptivity of the absorber plate. However, the percentage of heat flow and losses is affected by the materials of the collectors, ambient conditions and operation conditions.

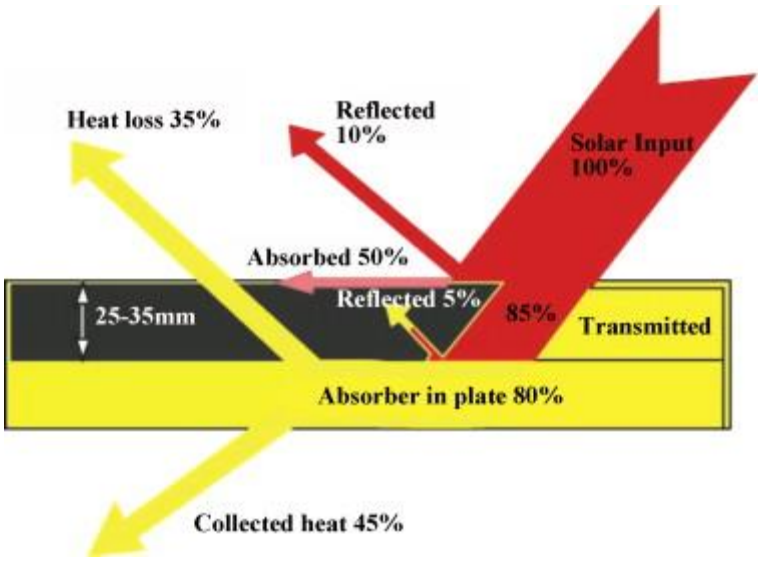

Figure 1-6 Heat flow and losses in a flat plate collector (Hossain et al. 2011).

1.3 Determining overall efficiency in solar cooling system

Research into solar cooling systems has mostly aimed to increase the annual solar fraction of the system by investigating a parameter of the system, such as the collector inclination angle or the size of the storage tank (Agrouaz et al. 2017). Other research into solar cooling systems aimed to maximise the overall efficiency by minimising the area of collecting, improving the storage tanks strategies, and increasing the coefficient of performance (COP) of the chiller of the cooling system (Al-Ugla et al. 2015; Ketfi et al. 2015; Buonomano et al. 2018). Some of the research in the field compared the thermal efficiency (or the collecting area) between several types of collectors such as FPC, evacuated tube, compound parabolic, and parabolic trough in order to achieve the highest overall efficiency of the system (Praene et al. 2011).

For the thermally driven solar cooling system, the overall energy performance can be maximised by minimising the driving temperature (Buonomano et al. 2018). Specifically, minimising the heat source temperature in solar absorption cooling systems enhances the overall efficiency (Aman et al. 2014). On the other hand, the outlet water temperature of collectors is a key factor that affects the overall efficiency in solar cooling absorption systems (Li et al. 2014). The efficiency of solar collectors was improved by minimising the average temperature of the solar temperature (Buonomano et al. 2018). Of previous studies in solar cooling systems, as is highlighted in chapter 2, there is no study that shows the optimum inlet temperature and flow rate of FPC and PVT for a specified required driving temperature.

A mathematical method has been used to predict solar collectors' efficiency in order to use it as an input parameter in transient system software, or an analytical method for a solar cooling system (Ketfi et al. 2015; Bellos et al. 2016). In most research, thermal efficiency was calculated without taking into account the flow rate of the solar collector, which affects the accuracy of the overall evaluation of the solar cooling system. Transient software such as TRNSYS has been used widely in order to maximise the cooling production of solar absorption systems or to select the optimum type of absorption chiller (Fong et al. 2011; Martínez et al. 2012; Fong and Lee 2014; Martínez et al. 2016). TRNSYS was used to study the impact of a parameter on the overall system

economically, environmentally and efficiently, but there is no study that calculated thermal efficiency and predicted the outlet temperature of a FPC and PVT using 3-D CFD models in order to select an optimum flow rate and inlet temperature for a specified temperature.

1.4 Research aim and objectives

There is an opportunity to increase the coefficient of performance of a solar cooling system (SCOP) by enhancing the efficiency of the FPC and PVT collector. The majority of previous research investigated the incorporation of solar collectors such as FPC with absorption chillers, but has not investigated the efficiency of the collector for specified outlet temperature. On the other hand, most research into solar cooling systems used a theoretical method to calculate the thermal efficiency of the collector without taking into account the flow rate or the inlet temperature of these equations. In addition, some research optimised the driving temperature of the absorption chillers based on the conditions of the study, without taking account of the fact that the absorption chillers in the market have been designed for an optimum inlet temperature in order to achieve the highest COP. In this study, the effect of flow rate and inlet temperature on thermal and electrical efficiency were optimised in accordance with the minimum absorption cooling driving temperature available in the market in order to increase the SCOP of a solar cooling absorption system.

The aim of this research is to investigate and optimise the thermal efficiency of the flat plate collector (FPC) and photovoltaic thermal collector (PVT) for a sustainable cooling system. In order to achieve this aim, key objectives are listed below:

1. To conduct a comprehensive critical review of the literature in the area of FPC and PVT solar absorption cooling systems.
2. To investigate the effect of inlet temperature on thermal efficiency (FPC and PVT).
3. To investigate the effect of flowrate on thermal efficiency (FPC and PVT).
4. To investigate the effect of PVT systems on overall performance.

5. To determine the optimum inlet conditions of FPC and PVT (multi-objective optimisation).

1.5 Research Approach and Methodology

A 3-D CFD model for an FPC and PVT were developed in order to predict the outlet temperature and determine thermal efficiency accurately. The output from the CFD model is utilised to establish new efficiency curves and equations with which to calculate thermal efficiency for FPC and PVT at low and high level flow rate, in order to generalise the results of this study for other conditions. Inlet conditions for the collectors were optimised for the highest efficiency in accordance with the minimum absorption cooling driving temperature available in the market so as to increase the solar coefficient of performance (SCOP) of the solar cooling absorption system.

The performance of an array comprising several panels of a PVT is based on several factors, including PVT materials, design, ambient temperature, inlet and outlet fluid temperature and PV cell temperature. A mathematical model was developed for a PVT system to calculate the anticipated system performance and the results were validated with experimental data from the literature.

Multi-objective optimisation is considered in this study, as explained in chapter 3. A set of design experiments points (DOE) was generated in ANSYS in accordance with the design parameters of the FPC and PVT. Space filling type was considered in this study according to (Mwesigye et al. 2015). Automated refinement was applied to create the response surface and the Kriging meta-model is used to enhance the accuracy. A multi-objective algorithm is employed in this study in order to select the optimum inlet temperature and flow rate of the FPC and PVT for highest thermal efficiency.

Figure 1-7 shows a workflow for the method that is considered in this study.

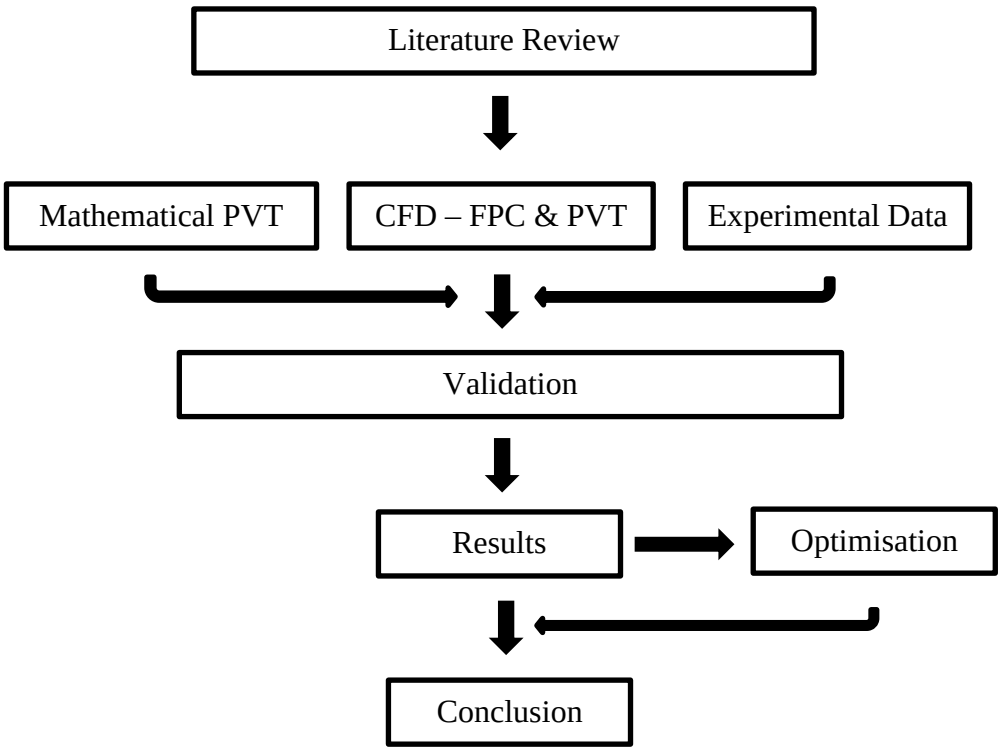

Figure 1-7 Flow chart of the methodology of the study.

1.6 Structure of the thesis

The thesis includes six chapters as follows:

Chapter 1 presented an introduction on the increasing energy demand and the potential to utilise solar energy for cooling systems by employing FPC and PVT. The chapter specified the aim of this research and its objectives and concluded with the thesis outline.

Chapter 2 provides a critical review of research in the field of FPC and PVT. An extensive review of literature on the use of FPC and PVT for cooling systems, in particular absorption cooling systems, was conducted. The gaps in the current research into the use of FPC and PVT for solar cooling systems were highlighted.

Chapter 3 presents the methods of research employed in this study to determine and enhance the performance of FPC and PVT. The research included a computational CFD

model of a FPC, a computational CFD model of a PVT, and a mathematical model of a PVT.

In chapter 4, the effects of inlet temperature on thermal efficiency for the FPC and PVT, which is the second objective of the study, are investigated by employing the computational CFD models for FPC and PVT. In addition, the effects of flow rate on thermal efficiency for FPC and PVT, which is the third objective of the study, were also investigated. A mathematical model of PVT was employed in this chapter in order to study the effect of a PVT system on the overall performance and so to achieve the fourth objective.

In chapter 5, multi-objective optimisation with response surface method is applied to the computational model of the FPC and PVT in order to achieve the highest efficiency for a specified outlet temperature (the fifth objective in the study). The inlet conditions of the flat plate collector (FPC) and photovoltaic thermal collector (PVT) were optimised in accordance with the minimum absorption cooling driving temperature currently available in the market.

Presented in chapter 6 are the specific conclusions in relation to each objective of the thesis, along with indications for future work in the use of FPC and PVT for solar cooling systems.

Chapter 2. Review of the Literature

2.1 Introduction

This chapter presents a critical review of research in the field of FPC and PVT collectors. An extensive literature review in the use of FPC and PVT for cooling systems, especially absorption cooling systems, is conducted. This includes experimental and computational studies with a focus on collectors' efficiencies and the optimisation methods. Section 2.2 collates review papers in the field of solar cooling systems. In section 2.3, previous work relating to thermal collectors for absorption cooling systems which included experimental, theoretical and simulation studies, was reported. Section 2.4 presented flat plate collectors (FPC) and focused on their use in different cooling systems as found in the literature. Section 2.5 surveyed the research into photovoltaic thermal collectors (PVT) and focused on their use in different cooling systems. Section 2.6 established the use of the computational fluid dynamics (CFD) method to investigate the performance of FPC and PVT in the literature. Multi-objective optimisation methods are presented in section 2.7 and a summary of this chapter is given in section 2.8. Section 2.9 then highlights the gaps in the current research into flat plate collectors and photovoltaic thermal collectors.

2.2 Review papers in the field of solar cooling systems

In the last decade, many researchers have focused on solar cooling systems and different types of solar thermal cooling systems have been reviewed (Kim and Infante Ferreira 2008; Al-Alili et al. 2014). The use of solar collectors such as FPC and ETC for thermally driven solar cooling systems, and of photovoltaic panels (PV) to provide electricity for vapour compression air conditioning units, has been discussed (Baldwin and Cruickshank 2012; Ferreira and Kim 2014; Allouhi et al. 2015). The application of thermally driven systems such as absorption, adsorption, desiccant and ejector systems has been highlighted in the review papers (Deng et al. 2011; Sarbu and Sebarchievici 2013; Ghafoor and Munir 2015). Options for thermal and cold storage have also been

discussed (Chidambaram et al. 2011). However, the existing reviews have limitations because they were specific to a particular region or application (Baldwin and Cruickshank 2012).

Al-Alili et al. (2014) reviewed solar thermal air conditioning technologies and reported a number of research outcomes from the point of view of working fluid temperature, collector type, collector area, storage volume and COP values. The authors evaluated research depending on conditions such as the temperature of evaporators, condensers and generators. In this research, evaporator temperature was in the range of -9 °C and 26 °C, condenser temperature was in the range of 24 °C and 45 °C, and generator temperature was in the range of 74.1 °C and 120 °C. The paper analysed six experimental and five simulation studies and reported that the average area of solar collector for a solar absorption cooling system was 4.67 m^2/kW_c (4.67 m^2/KW_c means that 4.67 m^2 of solar collectors would be required to produce 1 kW of cooling). The areas required of evacuated tube collectors ranged between 2.7 and 9.4 m^2/kW_c, while these areas were 1.4 to 3.3 m^2/kW_c for the flat plate collector (Al-Alili et al. 2014).

Review papers that focus on solar cooling absorption technology are scarce; Zhai et al. (2011) provided a literature survey of solar cooling absorption systems but did not mention the use of PVT and only included one project that used CPVT with single absorption chillers (Zhai et al. 2011). PVT increases the efficiency of solar energy conversion (Rosell et al. 2005). The main advantage of PVT systems is to utilise the surface area of the collector to produce both electrical and thermal energy with high performance (Aste et al. 2016). Raja and Shanmugam (2012) also reviewed solar absorption systems, aiming to reduce the initial cost of the systems. The authors discussed auxiliary components that were typically used in the systems such as backup heating and some solar collector types. The paper mentioned that FPC and ETC are reliable economically with absorption systems but did not report any existing PVT collectors and only one CPVT project was mentioned (Raja and Shanmugam 2012). Different types of absorption solar cooling systems which included single effect, double effect and half effect absorption cycles were also reported in the review papers (Hassan and Mohamad 2012, Siddiqui and Said 2015, Aliane et al. 2016). The required heat

source temperature, refrigeration output, capacity range, COPs and fluid pairs are reported for single-effect absorption refrigeration cooling technologies in Table 2-1.

Table 2-1 Single-effect Absorption refrigeration cooling technologies (Kim and Infante Ferreira 2008; Deng et al. 2011).

Capacity kW	**Working fluid pairs**	**Driving temperature °C**	**Chilled water Temperature °C**	**COP**	**Cooling applications**
5–7000	LiBr–H_2O	70–90	5–10	0.5–0.8	Industrial refrigeration
10–6500	H_2O–NH_3	100–200	−60 - 0	0.25–0.6	Large capacity for industrial refrigeration, and small size for light commercial use
10–90	H_2O–NH_3	80–200	5–10	0.5–0.6	Residential and small commercial building cooling

Table 2-2 illustrates small capacity absorption chillers currently in the market which are in the range of 4.5 kW to 17.6 kW. Table 2-2 also shows that COP is in the range of 0.63 to 0.77 and the driving temperature for absorption chillers is in the range of 75 ^oC to 90 ^oC.

Table 2-2 Small capacity absorption chillers available in the market (Ghafoor and Munir 2015).

Manufacturer	Capacity (kW)	Working fluid pairs	Driving temperature (^oC)	Cooling temperature(^oC)	Chilled water Temperature °C	COP
Rotartica (Spain)	4.5	H2O–LiBr	90/85	30/35	13/10	0.67
Climatewell (Sweden)	10	H2O–LiCl	83/--	30/--	--/15	0.68
Pink (Austria)	10	NH3–H2O	85/78	24/29	12/6	0.63
Sonnenklima (Germany)	10	H2O–LiBr	75/65	27/35	18/15	0.77
EAW (Germany)	15	H2O–LiBr	90/80	30/35	17/11	0.71
Yazaki (Japan)	17.6	H2O–LiBr	88/83	31/35	12.5/7	0.7

The incorporation of solar collectors such as ETC and FPC with absorption chillers was highlighted but there is a lack of data in the use of photovoltaic thermal collectors (PVT) with absorption chillers (Bataineh and Taamneh 2016).

Based on the performance and the initial cost of solar cooling systems, single effect absorption systems were estimated to be more efficient with lower costs. The majority of previous research analysed the incorporation of solar collectors such as ETC and FPC with absorption chillers, but most did not report their efficiencies. In previous review papers, there is a lack of data on the combination of photovoltaic thermal collectors (PVT) with absorption chillers (Raja and Shanmugam 2012). In these studies, absorption systems show the opportunity to achieve a relatively high COP (0.5 – 0.8) for generation of temperatures in the range of 70°C to 90°C (Kim and Infante Ferreira 2008; Raja and Shanmugam 2012).

The aim of this review is to establish the current developments in the field of photovoltaic thermal collectors (PVT) for cooling purposes and to identify the opportunity to use PVT and FPC for absorption cooling systems. The review also discusses current developments in the field of solar absorption cooling systems from the point of view of solar collecting options. In addition, the review covers experimental and computational studies and focuses on collectors' types, thermal efficiencies and the methods of evaluation.

2.3 Thermal collectors' absorption cooling systems

The dominant driving power in solar absorption cooling systems is the thermal power from solar collectors. Solar radiation is absorbed by solar collectors then delivered to a storage tank through a hydraulic pump. A backup heater is fixed with the storage tank and the temperatures in the system should be managed to meet the required temperature for the absorption chiller. The most common working fluid in absorption systems are H_2O/LiBr (Water is refrigerant) and NH_3/H_20 (Ammonia is refrigerant) (Allouhi et al.

2015). Figure 2-1 shows a schematic diagram of a thermal solar absorption system, made up of solar collector, storage tank and absorption chiller.

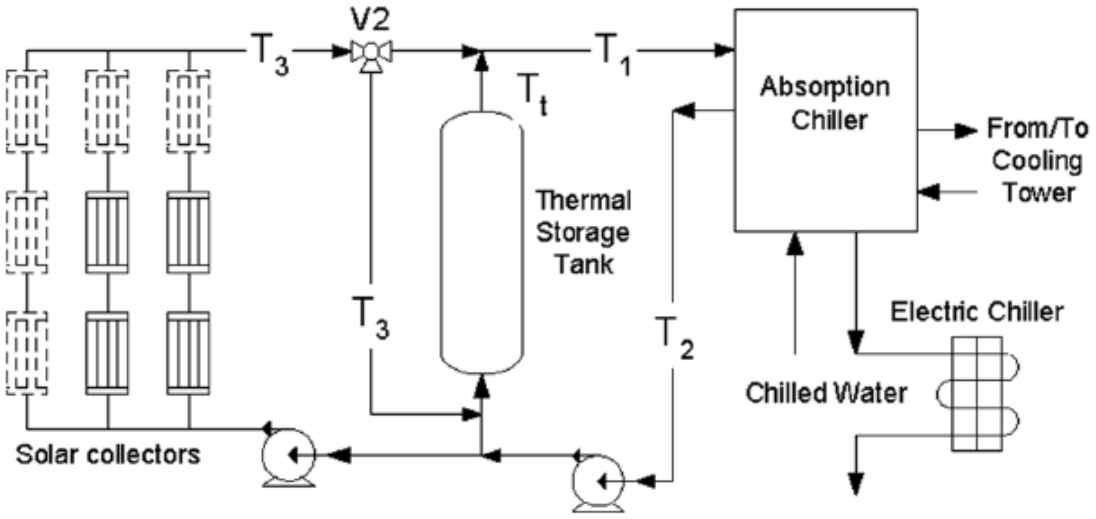

Figure 2-1 Schematic diagram of solar cooling system with multi solar collectors (Fumo et al. 2013).

Fang et al. (2010) carried out a comparison study of different solar cooling systems, which included solar electric compression refrigeration, solar mechanical compression refrigeration, solar absorption refrigeration, solar adsorption refrigeration and solar solid desiccant cooling, based on their performance throughout the year. The study was based on the simulation program TRNSYS to calculate the performance indicators which included solar fraction (SF), coefficient of performance (COP), and primary energy consumption in order to meet a cooling load of 29 kW_c. The driving temperature, which is the water temperature supplied to the generator as shown in Figure 2-2, was in the range of 67-90 °C. The work further found that the solar absorption system achieved a solar factor of 50% throughout the year and the COP was 0.77 (Fang et al. 2010).

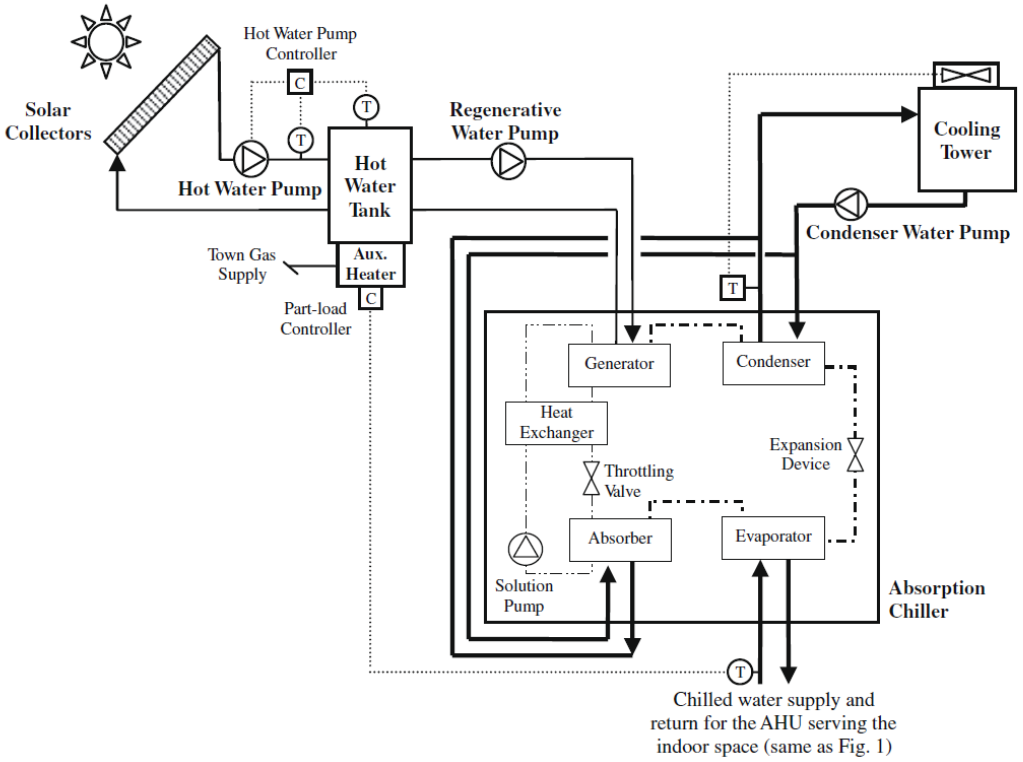

Figure 2-2 Solar absorption refrigeration system with cooling tower and air handling unit (AHU) (Fong et al.).

Hartmann et al. (2011) also carried out a comparison between a solar electric compression refrigeration system and a solar adsorption refrigeration system to evaluate the primary energy savings and the cost involved in meeting the demand for heating and cooling of a typical building in Germany and Spain. The cooling and heating load throughout the year, the performance of a photovoltaic PV system and the performance of a FPC system were simulated in TRNSYS for varying solar collector areas. The study highlighted that the annual cost of a solar cooling system was 128% higher than a conventional compression chiller in Spain and 134% in Germany, whilst the annual cost for solar electric cooling varied between 102–127% in Spain and 102–125% in Germany. They concluded that, for the same energy saving in the PV cooling systems with a defined PV field area, six times this area would need to be covered by FPC solar collectors (Hartmann et al. 2011).

Fumo et al. (2013) carried out a theoretical comparative analysis of solar thermal cooling systems based on the reduction of the required primary energy and its cost. The two setups included evacuated tube collectors, an absorption chiller, and a solar electrical system, which included photovoltaic panels and a vapour compression system. The reference system was an air-cooled vapour compression system that consumed electricity from the grid as displayed in Figure 2-3.

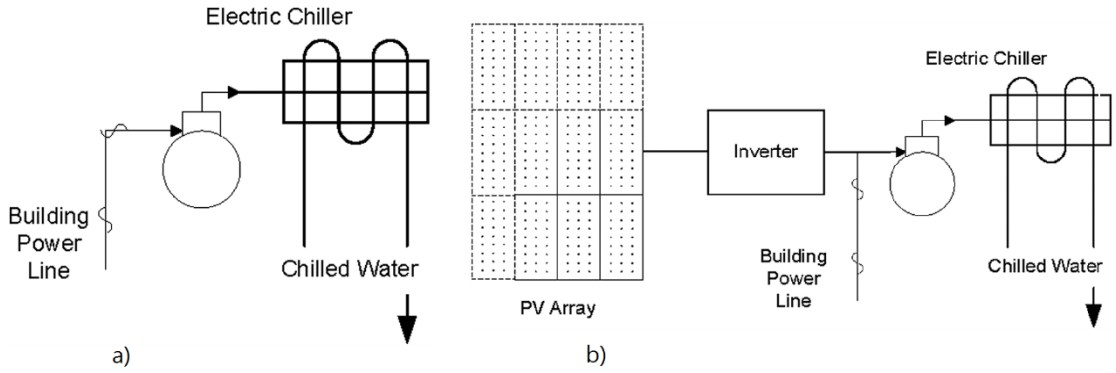

Figure 2-3 Schematic diagram of a) reference system and b) photovoltaic cooling system. Modified from (Fumo et al. 2013).

The authors highlighted that 12 m^2 of evacuated tube solar collector were required to produce 1 ton of refrigeration (3.517 kW_c) for a solar absorption cooling system and 7 m^2 of PV panels were required for a solar electric cooling system. They also established the energy saving curve for both the PV and thermal systems, based on specific parameters and conditions such as electric rate of $0.1/kWh as shown in Figure 2-4.

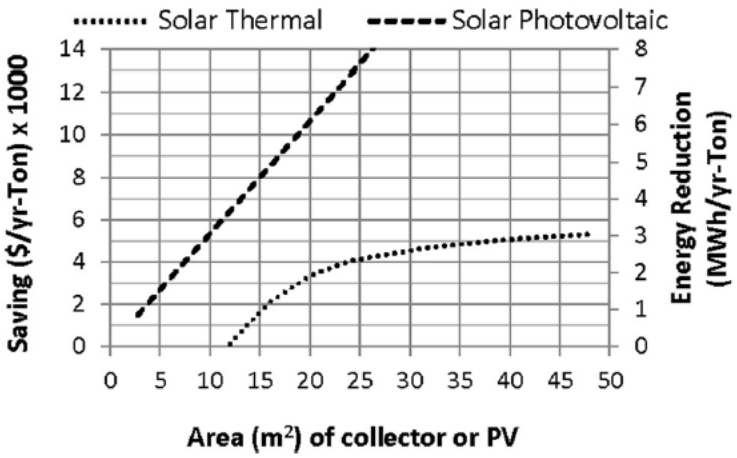

Figure 2-4 Cost and energy savings based on electric rate of $0.1/kWh and specific parameters and conditions in the United States (Fumo et al. 2013).

These findings can be considered an initial assessment for solar cooling systems. However, they are preliminary results and further investigation is needed to validate the results (Fumo et al. 2013).

Eicker et al. (2014) carried out an economic evaluation of photovoltaic (PV) and thermal cooling systems based on primary energy savings in a case study building with 309.9 m^2 floor area. This study included a reference system with a 30-50 kW_c vapour compression chiller derived by grid electricity and 1500 L cold storage tank. The study included a PV cooling system (compression chiller and PV modules), thermal solar cooling system (flat plat collector or compound paraphilic collector), 5000 L hot storage tank, 1000 L cold storage tank and 25 kW_c absorption chiller. The solar cooling system required a specific collector area of 2.5 m^2/kW_c, and a 130-170 m^3/h air volume cooling tower per kW_c. The PV cooling system was simulated in INSEL and FORTRAN whilst the thermal cooling system was simulated using TRANSOL 3.0 and TRNSYS. The findings in the study indicated that the solar collector efficiencies were 31% and 23% for CPC and FPC respectively. The primary energy consumptions for each cooling system are shown in Figure 2-5.

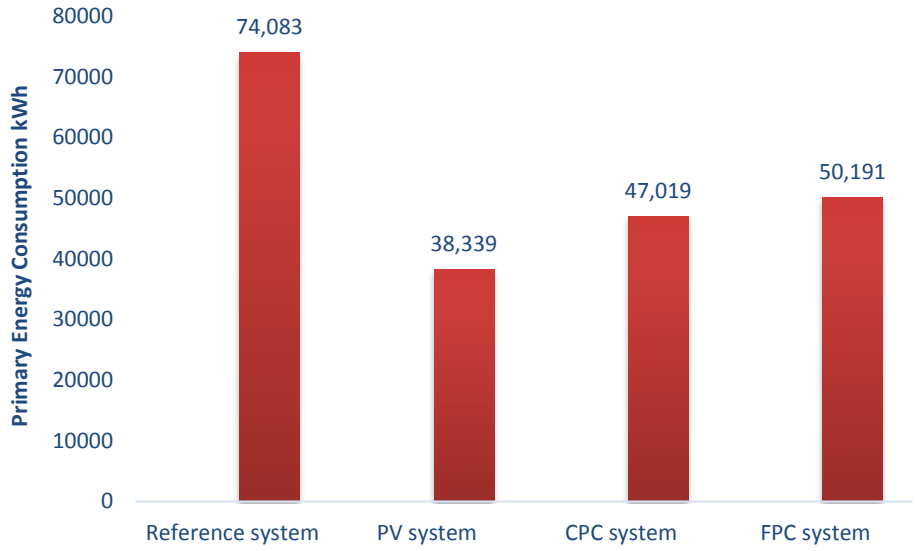

Figure 2-5 Primary energy consumptions for reference, PV, CPC and FPC cooling systems.

The coefficient of performance (COP) of the absorption chiller is the ratio of the cooling energy required (Q_e) to the input energy in the generator section (Q_g) while it is the ratio to the input to the compressor in the compression cycle (Kim and Infante Ferreira 2008; Bellos et al. 2016). The annual COP values were calculated as 3.19, 0.79 and 0.77 for the compression chiller, CPC-absorption chiller and FPC-absorption chiller respectively. The study concluded that reduction of the initial cost of the solar cooling system is a key factor in enabling the system to compete in the market, and reported valuable specific cost parameters for the initial assessment of the solar cooling system. They also suggested parametric studies of the system to reduce the energy demand (Eicker et al. 2014).

2.3.1 Experimental studies

Outdoor testing methods were mainly used in the literature in order to implement the performance of solar cooling systems. The coefficient of performance for the overall solar cooling system in this review was in the range of 0.17–1.25 whilst solar collector efficiency was in the range of 0.24–0.64. Flat plate collectors (FPC) were employed in some of these studies and the normalised area to produce cooling was in the range of 3–9.4m^2/kW_c. Evacuated tube collectors (ETC) were used for other research and the normalised area was in the range of 2–7.2 m^2/kW_c. For FPC, ETC, compound parabolic concentrator (CPC) and parabolic trough solar collectors (PTC), the average area to produce cooling in the experimental studies for single and double effect absorption chillers was in the range of 2-12 m^2/kW_c and 2-5 m^2/kW_c respectively. The deviation in the normalize area to produce cooling was due to the fact that each project was implemented in different operation condition, different designs and different capacities. These key findings for solar absorption systems and other details for each experimental project are summarised in Table 2-3.

Table 2-3 Summary of the solar absorption cooling system, experimental studies.

Collector type	A_c (m^2)	Solar collector Efficiency	Chiller Type	Cooling Capacity (kW)	COP	Experimental Type	References
FPC	42.2	0.31	$LiBrH_2O$ Single effect	4.5	0.53	Outdoor	(Lizarte et al. 2012)
	90	0.24-0.40	$LiBrH_2O$ Single effect	30	0.8	Outdoor	(Praene et al. 2011)
	90	0.51	$LiBrH_2O$ Single effect	30	0.3-0.41	Outdoor	(Marc et al. 2010)
	500	0.51-55	$LiBrH_2O$ Double effect	100	0.37-0.46	Outdoor	(Sumathy et al. 2002)
ETC	72	0.55	Single effect $LiBrH_2O$	35	0.17-0.50	Laboratory	(Ketjoy and Mansiri 2013)
	220	0.61	Single effect LiBrH2O	55	0.69	Outdoor	(Darkwa et al. 2012)
	12	0.64	Single effect $LiBrH_2O$	4.5	0.58	Outdoor	(Agyenim et al. 2010)
	72	--	Single effect $LiBrH_2O$	10	0.7	Outdoor	(Pongtornkulpanich et al. 2008)
	42	---	Double effect NH_3-H_2O	10.1	0.69	Outdoor	(Said et al. 2016)
CPC	27	0.37-0.46	Double effect $LiBrH_2O$	10	-----	---	(Li et al. 2014)
	61.4	0.47-0.59	Single effect $LiBrH_2O$	10	0.19	Outdoor	(Lu et al. 2013)
	96	0.43-0.45	Single effect $LiBrH_2O$	8	0.25-0.38	Outdoor	(Yin et al. 2013)
	42	0.32	Double effect NH_3-H_2O	10	0.8	Outdoor	(Khan et al. 2016)
PTC	39	NA	Double effect $LiBrH_2O$	16	0.8 - 0.91	Outdoor	(Balghouthi et al. 2012)
	56	0.35- 0.45	Single effect $LiBrH_2O$	23	0.11 - 0.27	Outdoor	(Li et al. 2016)
LCC	352	0.35	Double-effect $LiBrH_2O$	174	1.1–1.25	Outdoor	(Bermejo et al. 2010)

A_C: Collector area (m^2)
ETC: Evacuated solar collector tubes
PTC: Parabolic trough solar collectors
CPC: Compound parabolic concentrator
LCC: Linear concentrating collector

FPC is reliable economically with absorption systems (Raja and Shanmugam 2012) and Table 2-3 showed that the maximum thermal efficiency in experimental projects of FPC with absorption chiller systems was 55%. However, further investigations are needed to optimise operation conditions in order to increase thermal efficiency of FPC with single absorption chiller.

2.3.2 Theoretical analysis and simulation studies

Theoretical and simulation studies that evaluated solar cooling absorption systems in the literature are reported in this section. TRNSYS, MATLAB and theoretical methods were used widely in previous research. Based on the simulation and theoretical studies which is summarised in Table 2-4, the coefficient of performance (COP) for solar absorption cooling systems was in the range of 0.25–0.80 whereas the solar collector efficiencies were in the range of 6% 63%. The normalised area of FPCs to produced cooling was in the range of 2.18–3 m^2/kW_c whereas it was in the range of 1.27–6 m^2/kW_c for ETCs. For FPC, ETC, CPC and PTC, the average area to produce cooling in the simulation and theoretical studies for both single and double effect absorption chillers was in the range of 1.27 to 12 m^2/kW_c. These key findings for solar absorption cooling systems and details about collector types, their areas and efficiency, cooling capacity and COPs for each theoretical and simulation project are summarised Table 2-4.

Table 2-4 showed that the maximum thermal efficiency in theoretical and simulation studies of FPC with absorption chiller systems was 50%. However, operation conditions for the collectors were not optimised therefor this will be consider in this study in order to increase thermal efficiency of FPC with single absorption chiller.

Table 2-4 Summary of the solar absorption cooling system, theoretical and simulation studies.

Collector type	A_c (m^2)	Solar collector Efficiency	Chiller Type	Cooling Capacity (kW)	COP	Method	Reference
FPC	---	0.06-0.50	Single effect $LiBr/H_2O$	10-105	0.35	TRANSYS	(Mateus and Oliveira 2009)
	90	0.39	Single effect $LiBr/H_2O$	30	0.8	TRANSYS	(Praene et al. 2011)
	38.4	0.29	Single effect $LiBr/H_2O$	17.6	0.69	TRANSYS	(Martínez et al. 2012)
	----	-----	Single effect NH_3/H_2O	10	0.6	Analytical method	(Aman et al. 2014)
	---	---	--	10	0.33	Transol	(Agrouaz et al. 2017)
	38.4	0.28-0.47	Single effect $LiBr/H_2O$	17.6	----	TRNSYS	(Martínez et al. 2016)
ETC	31,54, 25	0.37, 0.45, 0.26	$LiBr/H_2O$ Single effect	15	0.67, 0.67, 0.64	TRNSYS	(Eicker and Pietruschka 2009)
	45	0.63	Single effect $LiBr/H_2O$	35.17	0.7	Theoretical	(Falahatkar and Khalaji Assad 2011)
	60	----	Single effect NH_3/H_2O	10	0.54	TRNSYS	(Al-Alili et al. 2012)
PTC	52	0.63	Double effect $LiBr/H_2O$	16	NA	TRNSYS	(Qu et al. 2010)
CPC	96	0.45-0.43	Single effect $LiBr/H_2O$	8	0.25 -0.38	MATLAB	(Yin et al. 2013)

A_C: Collector area (m^2)

ETC: Evacuated solar collector tubes

PTC: Parabolic trough solar collectors

CPC: Compound parabolic concentrator

2.4 Flat plate solar collectors

Solar collectors such as flat plate collectors (FPC) convert solar radiation to useful thermal energy and can be designed to deliver energy to fluid up to a level of 100 ^{o}C above the ambient temperature (Duffie and Beckman 1980). Main features of absorber materials plate, which is the main part in FPC, are reported in Table 2-5.

Table 2-5 Main features of absorber materials (Aste et al. 2014)**.**

Absorber material	Thickness (mm)	Density (kg/m^3)	Thermal conductivity (W/m K)	Heat capacity (J/kg K)
Copper	~0.3	8920	380	350
Aluminum	~1	2700	160	900
Steel	~2	7860	50	450
Polymer	~2–3	900–1500	0.2–0.8	1200–1800

The absorber plate transfers the absorbed energy to a fluid, which moves through pipes or ducts system. FPCs' configurations include front cover and back insulation to reduce heat losses from the collector (Duffie and Beckman 1980; Hajabdollahi and Hajabdollahi 2017). Figure 2-6 illustrates a schematic diagram of FPC.

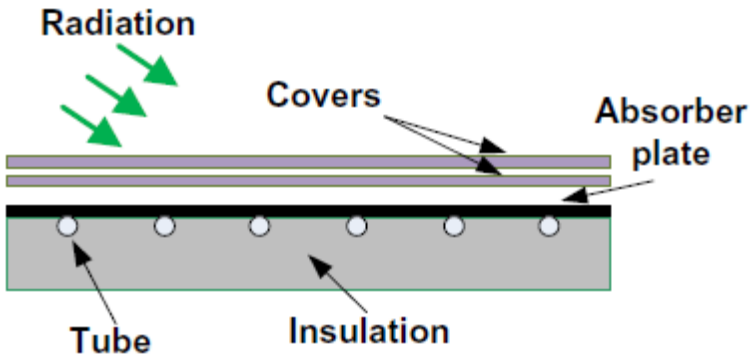

Figure 2-6 Schematic diagram of Flat plate collector (Hajabdollahi and Hajabdollahi 2017).

The operating conditions and configuration of flat plate collectors depend on the application of the solar collector system. Previous research into FPCs focused on heating applications in the winter season but has not made substantial progress on other application such as cooling (Alobaid et al. 2017). In these applications, inlet temperatures were in the range of ambient temperature in most of the research in this field (Liang et al. 2015). The opportunity to utilise the outlet water temperature of the FPC for cooling systems such as absorption cooling systems, adsorption-cooling systems and desiccant cooling systems has not been investigated for different range of inlet temperature and flowrate. Such applications need a different range of inlet temperatures and flowrate to operate as intended.

Ayompe et al. (2011) carried out work on a forced circulation solar water heating system with FPC. The model was simulated in TRNSYS and outlet fluid temperature was validated with an experimental set-up with maximum mean error of 16.9% (Ayompe et al. 2011). Zhang et al. (2016) employed a mathematical method to calculate thermal performance of FPC collectors with maximum error of 6.1%. The geometry of the collector was 2 m in length, 1 m in width and 0.065 m in thickness. Inlet temperature was in the range of 21.1 ^{o}C to 45.1 ^{o}C, while the outlet temperature was in the range of 37 ^{o}C to 55.4 ^{o}C and the average thermal efficiency was 51.4%. The authors concluded that thermal efficiency, outlet water temperature and heat transfer effectiveness were affected significantly by the flow rate. With regard to thermal efficiency, the recommended water flow rate was 0.06-0.08 kg/s (Zhang et al. 2016).

Shojaeizadeh et al. (2015) studied the effect of solar radiation, ambient temperature and inlet fluid temperature on FPC performance. Theoretical analysis was employed to calculate the useful rate of thermal energy that was delivered by the FPC, which is expressed by calculating energy absorbed by the absorber and lost from the top and bottom surfaces. In this study, inlet water temperature (T_{in}) was in the range of 296 K to 420 K, inlet flowrate ($\dot{m}$) was in the range of 0 to 0.2 kg/s, ambient temperature (T_a) was in the range of 294K to 324 K and global solar radiation (G) was in the range of 185 to 1100 W/m^2. MATLAB toolbox was used to optimise the efficiency of the system. The

optimum values were T_{in} = 401.67 K, $\dot{m}$ = 0.067 kg/s, T_a =294 K and G =1100 (Shojaeizadeh et al. 2015).

2.4.1 Efficiency of FPC with sustainable cooling systems

The overall thermal efficiency of solar absorption cooling systems is significantly low. Experimentally, the thermal efficiency of FPC coupled with an absorption chiller was 0.27, which restricted the coefficient of performance of the solar cooling system (SCOP) significantly to 0.06 (Lizarte et al. 2012). Bellos et al. (2016) reported that the thermal efficiency of the collector was 0.42; SCOP was 0.31 and the specific area of the collector to produce cooling was 3.317 m^2/kW. The authors reported that the optimum driven temperature for FPC and single absorption chiller was 378 k (105 ^oC). The driving temperature is the most important parameter that affected the COP of absorption chillers and the thermal efficiency of collectors. High value of driving temperature leads to high value of absorption chiller COP but decreases the thermal efficiency of the solar collector. Enhancing the SCOP for single absorption chillers coupled with solar collector was the aim of many researchers, pursued by studying the impact of the important parameters in the system such as the driving temperature (Praene et al. 2011, Bellos et al. 2016).

The thermal collectors' efficiency was in the range of 0.06–0.64 and sufficient efficiency could be achieved in the range of 60–80 °C outlet temperature. FPCs have been investigated experimentally to supply thermal energy for cooling application systems with thermal efficiency in the range of 0.24 to 0.55. Using theoretical and simulation methods for the same application, thermal efficiency was in the range of 0.24 to 0.5. The performance of the solar collector regarding thermal efficiency and the increase in the inlet temperature was highly affected by ambient temperature, inlet temperature, solar radiation and the configuration of the collectors. More details on the use of FPC in absorption systems were reported in Table 2-3 and Table 2-4.

2.5 Photovoltaic thermal collectors

2.5.1 Photovoltaic

The use of solar energy to produce electricity has been a subject of research for several decades. The effect of photovoltaic was discovered in 1839 by the French scientist Becquerel (Jesch 1981). Then, research in the photovoltaic field was developed and the first project to produce electricity by the use of the photovoltaic technique was conducted in 1954 in the United Kingdom by Heywood (Heywood,1954; Cited in (Jesch 1981)).

The photovoltaic effect property occurred when photovoltaic cells absorbed photons of light and released electrons which could be utilised as electric current (Knier 2002). A photovoltaic module consists of a number of solar cells made of semiconductor materials such as silicon. These cells are electrically linked to each other and attached in a frame. The module is the combination of many cells in one frame, while the array is a combination of a group of modules, as in Figure 2-7.

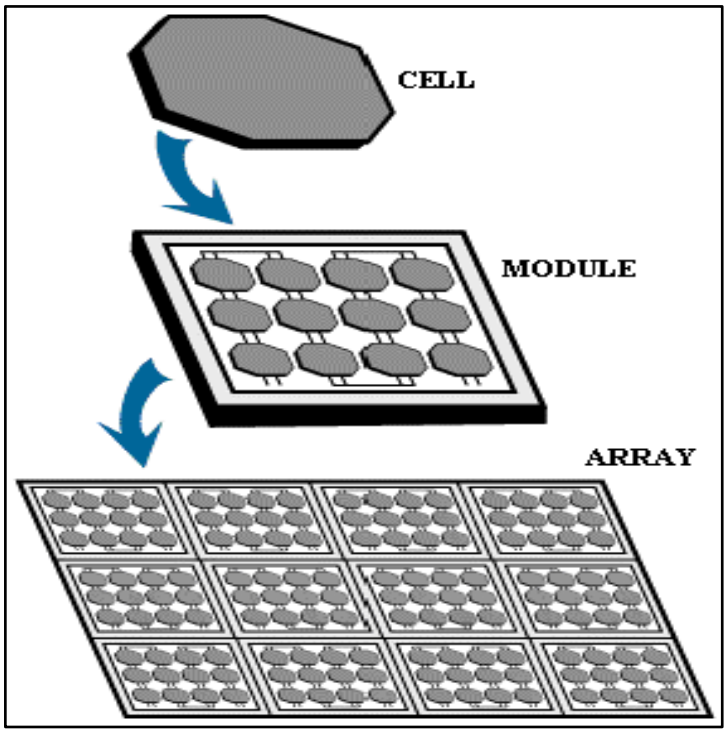

Figure 2-7 Photovoltaic array assembly (Knier 2002).

The main factors that affected electric efficiency were the materials, the design of the module and the temperature of PV cells (Dubey and Tay 2014). According to Chow

(Chow 2010), photovoltaic efficiencies were in the range of 4% to 17%, which means that a large amount of incident energy is converted to heat. The absorbed heat increased PV cells' temperature to 50 ^{o}C above the ambient temperature and then dropped the cells' efficiency by about 0.4% per degree raised for c-Si cells. Since the cells' temperature was a key factor in enhancing photovoltaic efficiency, the effect of cooling PV modules by active water was examined in previous research. It was also reported that PV efficiency was improved from 8.6% to 12.5% due to a drop in PV temperature from 68^{o}C to 38 ^{o}C for a PV module (Hoffmann 2006). Electrical efficiency was raised from 9% to 14% by employing active cooling (Parida et al. 2011). Bahaidarah et al. (2013) examined an active cooling PV system in Saudi Arabia. The experimental test setup for the PV included an insulated water tank, a pump, a flow meter and a cooling panel. In this experiment, electrical efficiency was increased by 9% due to a 20% decrease in the cells' temperature (Bahaidarah et al. 2013).

Dubey and Tay (2014) investigated variations of cell temperature and PV efficiency throughout the day. There were gradual decreases in PV efficiency from morning to midday from 13.5% to 11.5% because of the rise in solar cell temperature from 35 ^{o}C to about 60 ^{o}C. Then, there was an increase in PV efficiency from midday to sunset to 12.5% due to the decrease in cell temperature to below 50 ^{o}C. Figure 2-8 shows the hourly variation of PV efficiency with cell temperature during the day (Dubey and Tay 2014).

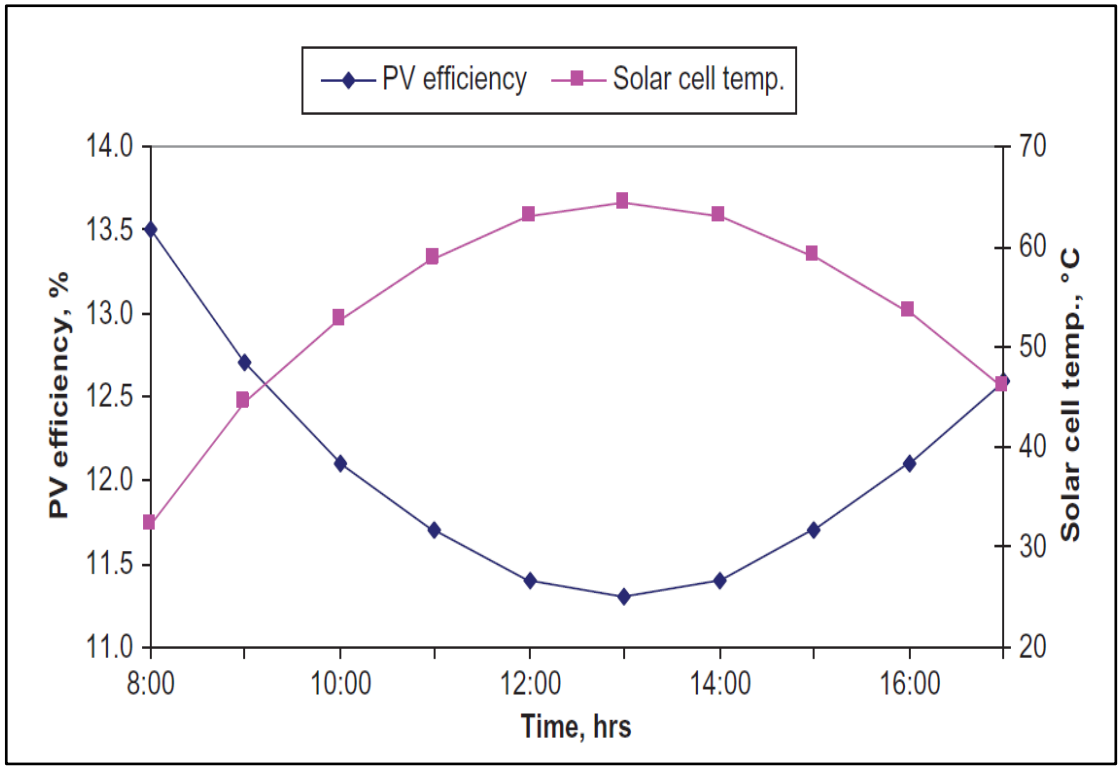

Figure 2-8 Hourly variations of cell temperature and cell efficiency (Dubey and Tay 2014).

Aste et al. (2014) reported that PV technologies have different features such as efficiency, which was in the range of 13% to 22% for crystalline and 7% to 13% for amorphous silicon. Another feature is the temperature coefficient which represents the effect of cells' operating temperature on the efficiency of the PV module. For crystalline silicon, the temperature coefficient was in the range of 0.3 to 0.5 (%/k), while it was 0.2 to 0.3 (%/K) for amorphous silicon. The study also highlighted that cell thickness was in the range of 0.2 mm to 0.5 mm for crystalline silicon whereas it was in the range of between 0.0002 m and 0.0006 m for amorphous silicon. Crystalline silicon cost about 0.55 to 0.85 (Euro/W_p) whereas the cost was between 0.35 and 0.45 (Euro/W_p) for amorphous silicon. Crystalline silicon (c-Si) delivers higher electrical efficiency than the thin film technology and the most used groups are monocrystalline silicon cells (mono-sc-Si) and polycrystalline silicone cells (pc-Si), which have slightly lower efficiency (Aste et al. 2014). Thin film PV is relatively lower cost and lower temperature coefficient, which means lower sensitivity to the operation temperature. Therefore, it is

recommended for employment in the design of PVT systems for cooling applications (Calise et al. 2012).

2.5.2 PVT configuration and applications

Photovoltaic thermal collectors utilise solar radiation to produce electricity and thermal energy. The main components of a PVT system are the PV cells to produce electricity, channels for the fluid, absorber plate and thermal insulation to minimise the heat losses to the ambient. Sheet and tube PVT is the most common configuration where PV cells are installed with flat plate collector as shown in Figure 2-9. Water is the most common fluid used to remove the heat from the panel but there are many options such as air or nano-fluid.

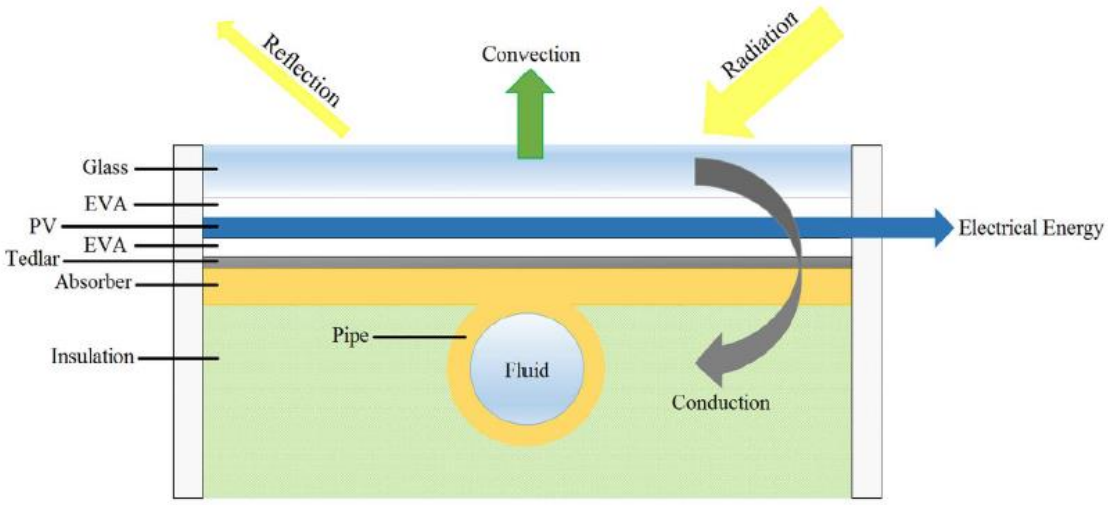

Figure 2-9 Schematic diagram of photovoltaic thermal collector (Hosseinzadeh et al. 2018).

Solar radiation is transmitted through the glass cover and absorbed by the PV cells. Electricity is produced by the photovoltaic which also transfers the heat to the absorber by conduction. The heat then transfer to the copper pipe that attached to the absorber which transfers the heat to the fluid inside the pipe by convection (Aste et al. 2016). Part

of absorbed solar radiation in PVT systems converts to electricity by the PV, which reduces thermal efficiency. In addition, compared to the thermal absorber, the PV has lower absorption and increases thermal resistance in the module (Michael et al. 2015). However, Attaching PV cell directly on the absorber in a PVT system could increase thermal efficiency by 50% due to the decrease in thermal resistance (Michael et al. 2015). Thermal efficiency of the module was calculated by measuring the inlet and outlet temperature (Duffie and Beckman 1980; Chow 2010; Dubey and Tay 2014) ($\eta_{th} = C_p \dot{m} \frac{T_o - T_i}{G\ A_c}$). With generating electricity, electrical power was consider by some researcher by subtracting the electrical power from the absorbed energy in the absorber which reduces the calculated thermal efficiency (Khanjari et al. 2016; Hosseinzadeh et al. 2018).

Increasing the PVT temperature reduces electrical efficiency. The operation temperature of photovoltaic module recommended to be maintain below 85 ^{o}C (Michael et al. 2015). Increasing the temperature of PV from 65^{o}C to 90 ^{o}C decreased the electrical efficiency by about 10% (Shyam et al. 2015). Lari and Sahin (2018) investigated PVT with phase change technology in order to supply hot water and electricity for a residential building. Theoretical analysis was used with Engineering Equation Solver (EES). The results showed an increase of 11.7% in electrical efficiency compared to uncooled photovoltaic system (PV) (Lari and Sahin 2018). The effect of the surface temperature of photovoltaic on efficiency was also investigated using experimental work. The efficiency was increased by 35% due to cooling the panel by water and the output water was used for residential applications (Peng et al. 2017).

Liang et al. (2015) studied the dynamic performance of a PVT heating system which consisted of a PVT, hot water storage tank, heat exchanger to transfer the heat to a piping system, and electric backup heater to maintain the temperature of the under floor system within the design points. TRNSYS was used to calculate the performance of a 32m^2 PVT system which included inlet and outlet temperature and electrical power. They annually achieved 131 kWh/m^2 electric energy and the solar factor was 31.7%. However, further investigations are needed to validate the results and provide thermal and electrical efficiency for the PVT throughout the year (Liang et al. 2015).

Cristofari et al. (2009) developed a finite different model for PVT in order to study thermal and electrical efficiency. This model used water as working fluid to supply hot water and pc-Si PV to supply electricity for residential purposes. They reported that yearly average thermal efficiency was approximately 55%, with electrical efficiency of 12.7%. They also reported the advantages of using copolymer in the PVT, which can reduce the cost and weight of the module (Cristofari et al. 2009).

Dubey and Tay (2014) developed a model of 52 PVT modules that produced 10 kW_p as a nominal electrical capacity. Several assumptions had been made to solve energy equations and calculate the performance of the system. The assumptions included that heat capacity for the materials in the system was neglected compared to the heat capacity of the water, one-dimensional heat transfer and steady state method were applied in the study, and there was no temperature stratification in the storage tank. In the experimental condition, the authors established the optimum flowrate for the PVT system as approximately 0.039 kg/(s m^2). The average thermal and electric efficiencies were 34% and 12% respectively (Dubey and Tay 2014). Further investigations are needed to validate the mathematical model in this study.

Fudholi et al. (2014) examined different designs of PVT collector in the lab under different solar radiation levels by using a solar simulator. Figure 2-10 shows a web flow, direct flow and spiral flow as pipe system designs for the PVT module.

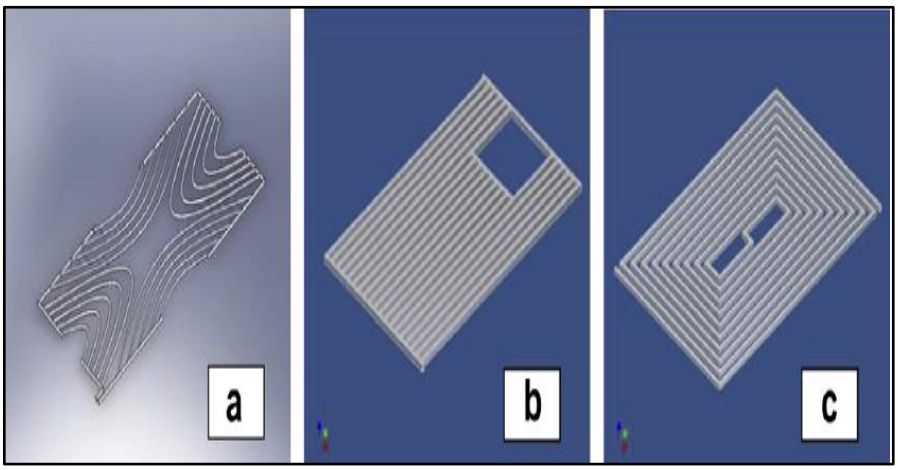

Figure 2-10 a) Web flow absorber, (b) Direct flow absorber and (c) Spiral flow absorber (Fudholi et al. 2014).

The spiral flow showed the highest performance among the PVT pipe system designs. Electrical and thermal efficacy was 13.8% and 54.6% respectively (Fudholi et al. 2014). Further research that considers ambient temperature will lead to more accurate results since the ambient temperature is an important parameter for calculating energy losses, PV's cell temperature and the overall performance of the PVT.

2.5.3 Efficiency of PVT with sustainable cooling systems

Fortuin et al. (2014) reported the important parameters that affected overall efficiency of PVT which included transmittance (τ) and absorbance (α). They also analysed the solar energy received by the surface of the PVT module which converts to electricity, and thermal energy losses to the environment, as illustrated in Figure 2-11.

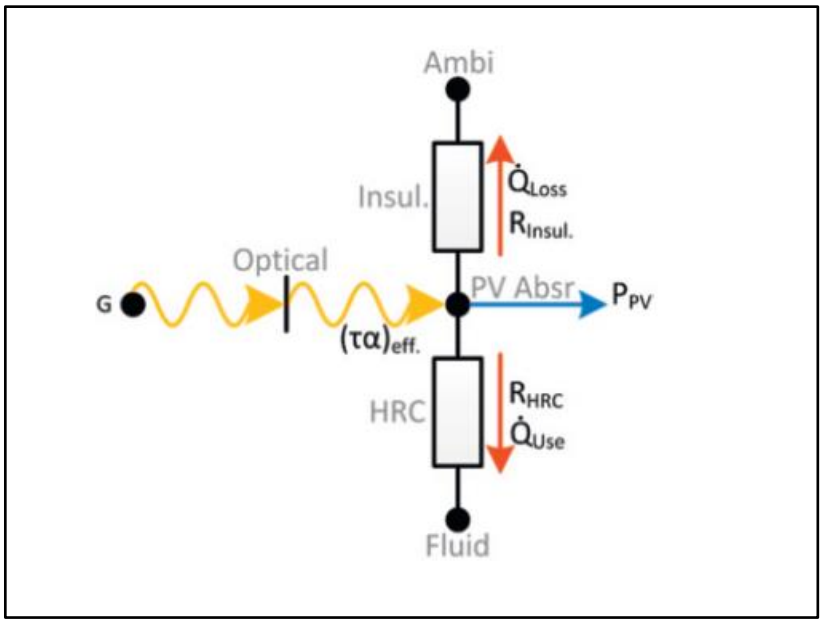

Figure 2-11 Illustration of thermal analysis model of a PVT collector (Fortuin et al. 2014).

The authors figured out the relation between the incoming irradiance and the temperature of the PVT surface for two different wind speed. The surface temperature increased with an increase in irradiance and decreased with an increase in wind speed (Fortuin et al. 2014).

Vokas et al. (2006) investigated the use of PVT instead of FPC with absorption chiller, in order to meet the cooling and heating domestic load throughout the year. The study highlighted that the performance was highly affected by the geographical region, and

electrical efficiency of the PVT was improved due to the reduction of its operating temperature. The study also revealed that FPC produced 54% of the heating load and 31.87% of the cooling load, which in the case of PVT were 11.9% and 21.4% respectively. Electrical performance for PVT and parameters for FPC were not reported and the results were not validated; further justification is needed to explain the decrease in thermal efficiency of PVT (Vokas et al. 2006).

Mittelman et al. (2007) studied the performance and economic viability of using concentrating photovoltaic thermal collectors (CPVT) for cooling and power generation. The plant consisted of 2660 m^2 of CPVT, a water lithium bromide (LiBr-H20) chiller with cooling capacity of 1MW, and natural gas backup heater. A thermal model of the system was analysed theoretically, considering mass and energy balance at each component. The generation temperature was in the range of 65–120°C, electrical efficiency was in the range of 0.19-0.21 and thermal efficiency was 58%. The authors reported that PV cell temperature was 10–30°C higher than the outlet coolant temperature. In this system, it was considered that the thermal energy was used directly to the absorption chiller without use of a storage tank, which is expected to increase the overall efficiency of the system. Figure 2-12 describes the photovoltaic thermal (PVT) module (Mittelman et al. 2007).

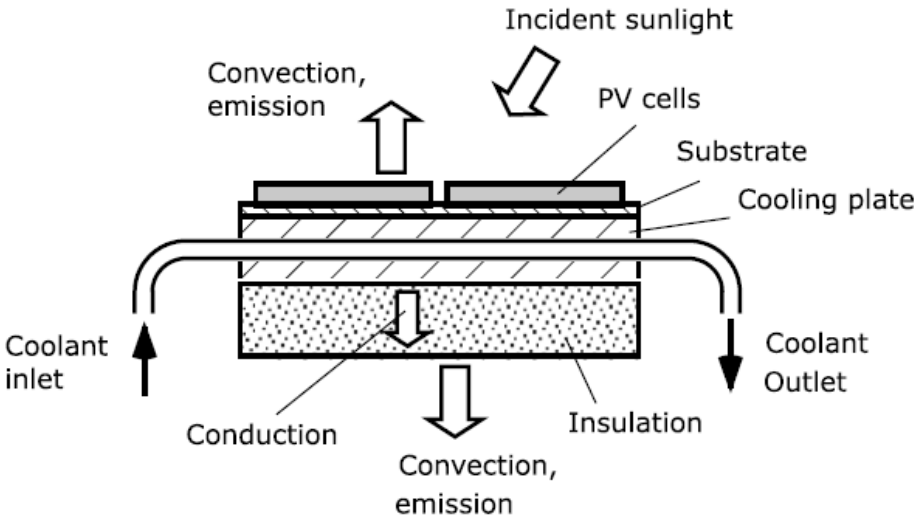

Figure 2-12 PVT Module with heat transfer to the coolant and heat losses(Mittelman et al. 2007).

Calise et al. (2012) investigated the performance of a solar cooling and heating system based on energy saving and economic analysis by considering a specific case study of a university building in Italy. PVT collectors of 1000 m^2 were simulated in TRNSYS to produce both electrical and heat energy to supply a 325 kW_c single lithium bromide absorption chiller that operates at 80°C. The annual produced electricity was $6.04x10^8$ kJ while the thermal energy was $1.84x10^9$ kJ. The system which included a storage tank, an auxiliary heater and a cooling tower, is shown in Figure 2-13.

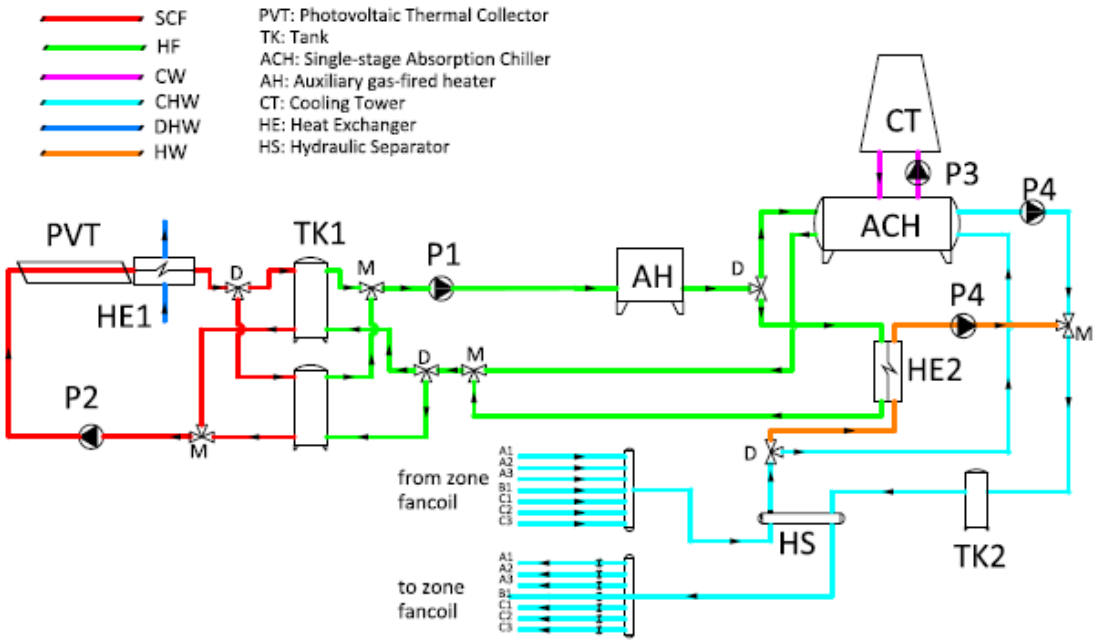

Figure 2-13 Schematic diagram of solar absorption cooling system with photovoltaic thermal collector, cooling tower (Calise et al. 2012).

The findings of this study indicated that PVT performance was significantly affected by ambient and operating temperature. They also found that the PVT system can produce an average of 10% electrical efficiency at an outlet fluid temperature in the range of 50–80°C. The authors reported that the type of cover of PVT systems is an important factor that affects the PVT performance. They highlighted that the tube and sheet c-Si PVT systems show a good ratio of energy production for cooling and heating. In the study, it was shown that surplus electricity was produced and sold to the grid or supplied to the building to meet domestic demand (Calise et al. 2012).

Calise et al. (2013) investigated a dynamic simulation system for cooling, heating and building demand for electricity in order to find the optimal capacity of a solar collector. The study considered a case study in Italy that included a 325 kW double stage absorption chiller (LiBr-H2O) and CPVT collector area of 996m^2 as shown in Figure 2-14. TRNSYS was used to simulate the project throughout the year.

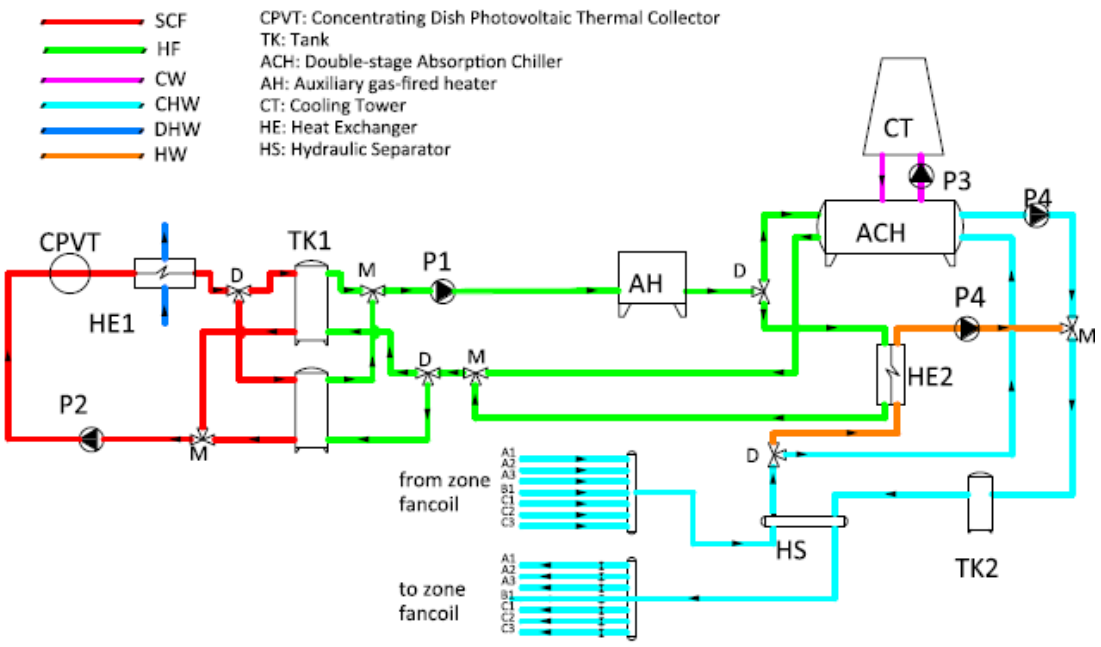

Figure 2-14 Schematic diagram of solar absorption cooling system with concentrating photovoltaic thermal collector, cooling tower (Calise et al. 2013).

The findings of this work highlighted that research in concentration photovoltaics to drive double effect absorption chillers is very attractive due to the utilisation of the same area to produce both electrical and thermal energy and the reduction in the area of PV cells from the concentration of the solar radiation. Average thermal and electrical efficiency throughout the year were 32% and 13.3% respectively. Primary energy saving and simple payback period were 84.4% and 15.2 years respectively. Furthermore, the study highlighted the need for a public fund for the CPVT cooling systems to enable them to compete with conventional systems. The authors reported that no prototype for this system was examined. Further research is needed to define the optimal value of the capacity and area for solar collectors (Calise et al. 2013).

Bunomano et al. (2013) presented a dynamic simulation code in MATLAB to study the performance of solar cooling systems based on energy saving. The roof of this building was covered by 130 m^2 of evacuated tube collectors or concentrating photovoltaic thermal collectors to power a single absorption chiller as in Figure 2-15. The work was validated with literature data showing a good correlation with a maximum error of 10%. The findings of the study indicated that in the case of evacuated tube collectors (ET),

solar energy contributed up to 74% of the energy demand while could reach 100% in the case of concentrated thermal collector (CPVT). Further research is needed in different countries, taking into account gas emission factors and energy prices in these countries (Buonomano et al. 2013).

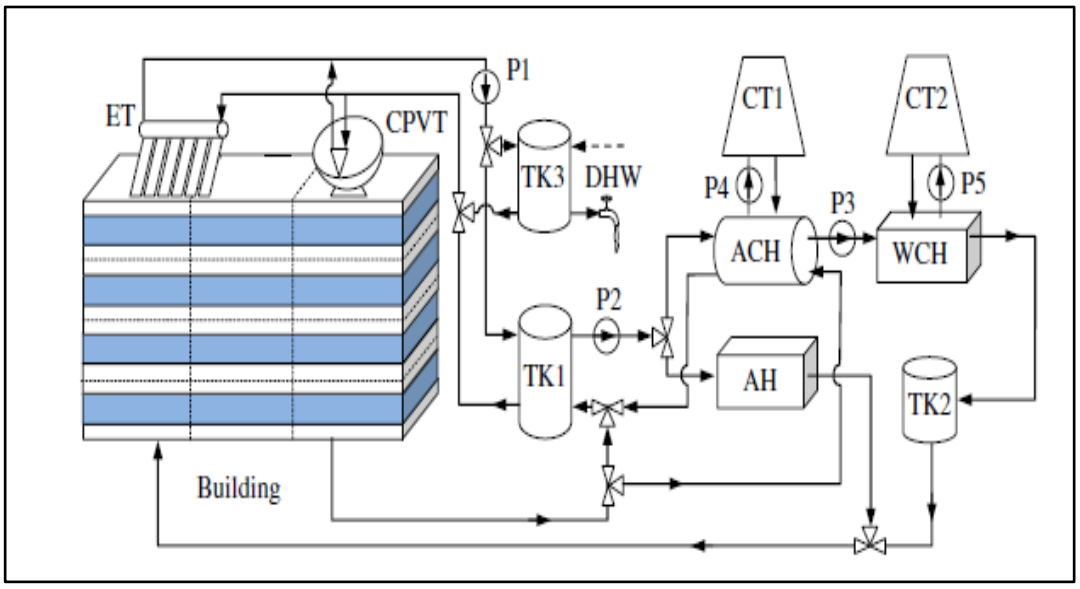

Figure 2-15 Solar absorption cooling heating system with concentrating photovoltaic thermal and evacuated tube collectors (Buonomano et al. 2013).

Sanaye and Sarrafi (2015) adopted a multi-objective optimisation approach for a combined solar cooling, heating and power generation system (CCHP) based on energy and economic evaluation. The main components in this system included PV panels, CPVT collectors, evacuated tube collectors and single effect absorption chiller as in Figure 2-16.

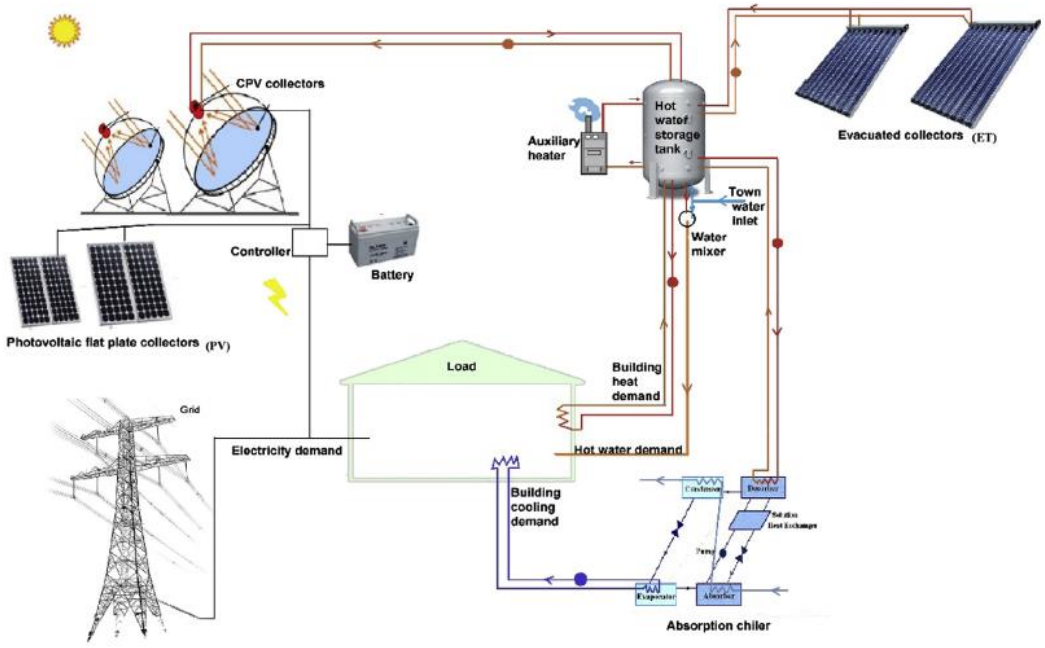

Figure 2-16 Combined solar cooling, heating and power generation system (Sanaye and Sarrafi 2015).

TRNSYS was employed to calculate cooling and heating load for a 150 m^2 case study building in Tehran. LINMABP technique was used to select the optimum value for each component of solar collectors, and size for the storage tank and the battery. The work found a good correlation with which to predict photovoltaic efficiency with 11% mean percentage error (Sanaye and Sarrafi 2015).

In the literature, there are limited experimental and simulated projects that used PVT collectors with absorption chillers because the PVT system is more expensive than the conventional collectors and may produce more electricity than is required for the absorption cooling system. Most of the reviewed projects exported electricity to the grid or utilised it for other purposes such as domestic load. In the following studies, PVT was used for other cooling systems.

Guo et al. (2017) reviewed the utilisation of PVT for desiccant cooling and dehumidification which required a temperature in the range of 50 ^oC to 60 ^oC. The study concluded that the design parameters that affected performance and outlet temperature of the PVT included mass flow rate, glazed cover and hydraulic channel geometry. The increase in flowrate improved thermal and electrical efficiency while decreased outlet

temperature. Adding a glass cover to the PVT improved thermal efficiency and increased outlet temperature but decreased electrical efficiency due to the increase in the photovoltaic cell temperature. It was reported that minimising the hydraulic diameter in PVT design could increase the outlet temperature (Guo et al. 2017).

Fang et al. (2010) investigated electrical and thermal performance of a PVT heat pump air-conditioning system. The PVT modules consisted of photovoltaic cells, aluminum plate, copper tube and insulation material. The study reported that the average photovoltaic efficiency was improved by 23.8% over the conventional PV due to the reduction of its temperature (Fang et al. 2010).

Al-Alili et al. (2012) investigated a hybrid PVT system to supply thermal energy for solid desiccant and electricity for vapour compression systems. The cooling section included a condition zone, desiccant wheel cycle, 17.5 kW vapour compression unit and heat recovery wheel as in Figure 2-17.

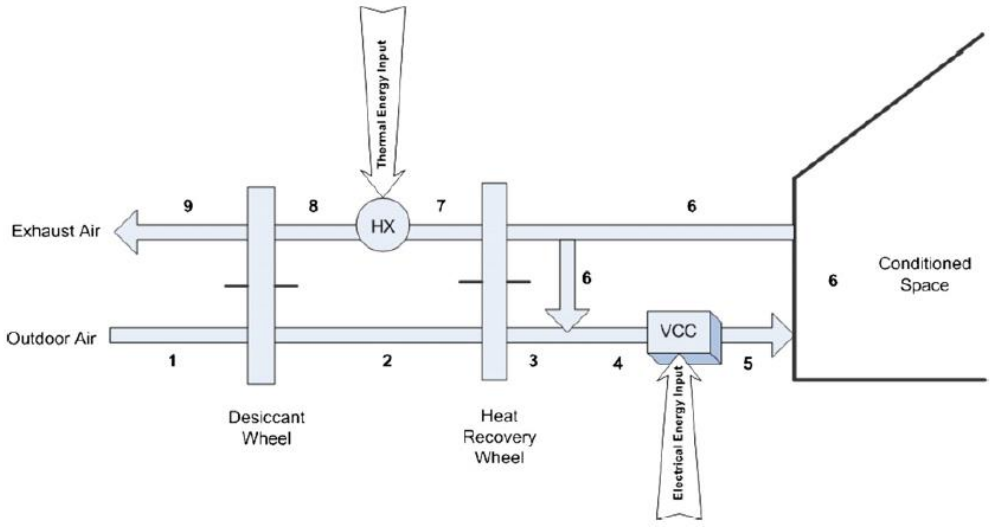

Figure 2-17 Solar solid desiccant and vapour compression cycle (VCC) (Al-Alili et al. 2012).

The main components of the solar section were solar collectors, a thermal storage tank, batteries and a backup heater to maintain the supplied air temperature to the desiccant wheel within the acceptable range. The COP was defined by the ratio of the total cooling capacity for both compression and desiccant cycles to the total energy input to the

system. Thermal performance of the system was analysed throughout the year using TRNSYS and parametric studies were made by varying the CPVT collector area from 5 m^2 to 80 m^2, storage tank volume from 0.5 m^3 to 4 m^3 and the numbers of batteries from 9 to 16 batteries. The findings of this study indicated that the overall performance was significantly affected by CPVT area. In addition the authors highlighted that in a hot and humid climate, the solid desiccant with vapour compression system is more effective than a standalone vapour compression system (Al-Alili et al. 2012).

Lin et al. (2014) investigated the use of PVT collectors with phase change materials (PCMs) in order to provide heating and cooling. The PVT performance was evaluated using TRNSYS and MATLAB and the system mainly consisted of a 68 m^2 building model and 40 m^2 of PVT module. They reported that, in the winter case, the average thermal and electrical efficiencies were 12.5% and 8.31%, while maximum PV cell temperature and electrical power were 44.2°C and 1.35 kW respectively. In the summer case, the average thermal and electrical efficiencies were 13.6 % and 8.26 %, while the maximum PV temperature and electrical power were 71.7 °C and 1.98 kW respectively. Figure 2-18 illustrates the PVT collectors and PCM integrated with ceiling ventilation system (Lin et al. 2014).

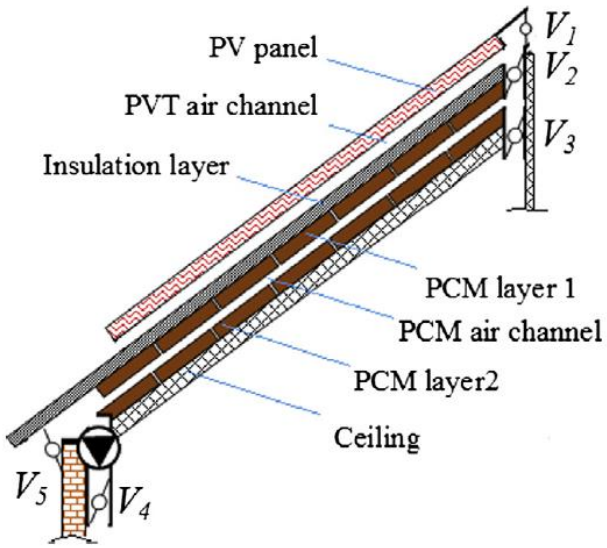

Figure 2-18 Schematic diagram of PVT collectors and PCM integrated with ceiling ventilation system (Lin et al. 2014).

Beccali et al. (2009) investigated the use of single glazed PVT solar collectors for different desiccant cooling systems without heat storage in a hot and humid climate in order to study primary energy saving. TRNSYS was employed to evaluate the options that provide cooling for a 107m^2 floor area building. The packing factor, which is defined as the ratio of the PV cells to the glazed area of PVT, was also investigated (100% means that PV covers all the glazed area), as in Figure 2-19.

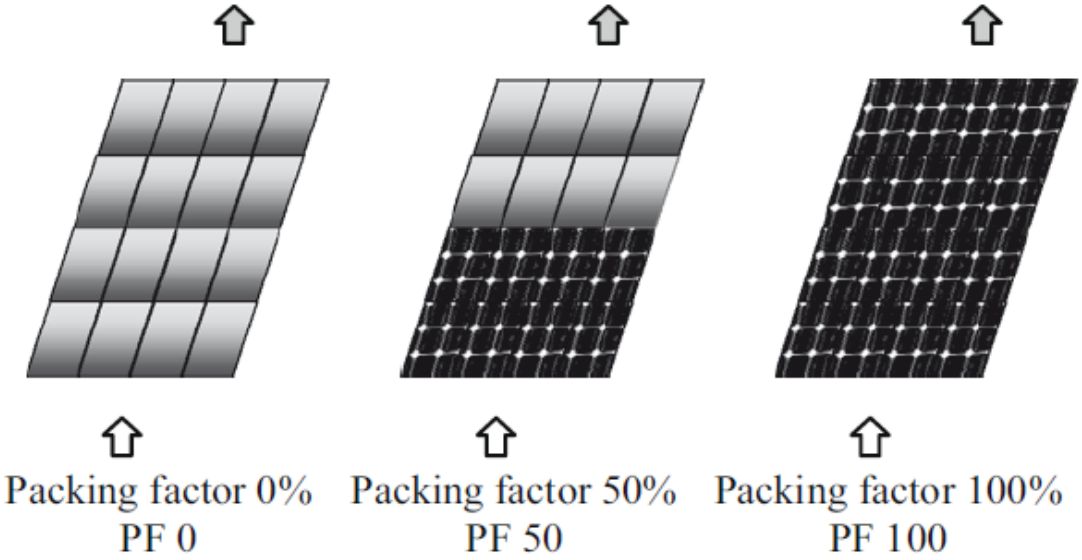

Figure 2-19 Photovoltaic thermal solar collector with different packing factors(Beccali et al. 2009).

By varying the PVT area from 30 m^2 to 50 m^2 for all cases with the desiccant standard system, the simple payback period was in the range of 9.6 to 13.7 years. They reported that maximum temperature for the outlet PVT was in the range of 62 °C to 70 °C and integrated PVT with cooling technologies was more efficient compared to PV with vapor compression systems (Beccali et al. 2009) .

2.5.4 Summary of combined photovoltaic and thermal collector

From previous studies in combined photovoltaic and thermal collectors, the main factors that affected the efficiency were the materials and the operation temperatures of PV cells and PVT module. Photovoltaic efficiencies were in the range of 13% to 22% for crystalline and 7% to 13% for amorphous silicon. PV cells' temperature could be 50 ^{o}C above the ambient temperature. PV cell temperature was also 10–30°C higher than the outlet coolant temperature. The increase in electrical efficiency of PVT due to the active cooling was in the range of 11.7% to 35% compared to uncooled photovoltaic systems (PV). Combined photovoltaic and thermal technologies have been employed in several cooling applications. The operation temperature was in the range of 65–120°C. The annual average electrical efficiency of 10% was produced at an outlet fluid temperature in the range of 50–80°C. The operation temperature of photovoltaic module recommended to be maintain below 85 ^{o}C. Thermal efficiencies for the concentrated photovoltaic thermal collectors (CPVT) in solar cooling systems was in the range of 0.22 to 0.63 while it was in the range of 0.30 to 0.39 for PVT. With respects to multi junction solar cells technology and CPVT, electrical efficiency could reach 40% (Xu and Kleinstreuer 2014; Calise et al. 2014). Electrical efficiency was in the range of 0.08-0.35 for CPVT and approximately of 0.10 of the PVT projects in Table 2-6 .

For CPVT and PVT, the areas to produce cooling in for solar cooling systems were in the range of 1.8-3 m^2/kW_c and 2.86-4.37 m^2/kW_c respectively as in Table 2-6. These key findings on photovoltaic thermal cooling systems, and more details about collectors' types, their areas and efficiency, cooling capacity, and COPs for each photovoltaic thermal project, are summarised in Table 2-6.

Table 2-6 Summary of the use combination of PVT with solar cooling system, simulation and experimental studies.

Collector type	Area (m^2)	Thermal Efficiency	PV Efficiency	Cooling System	Cooling Capacity (kW)	COP	Method	References
CPVT	2660	0.58	0.19-0.21	LiBr/H2O Single effect	1000	0.6-0.75	Theoretical analysis.	(Mittelman et al. 2007)
	130	---	0.35	Single effect $LiBr/H_2O$	61-72	0.7	TRNSYS & Matlap	(Buonomano et al. 2013)
	12 + (Geothermal)	0.22-0.58	0.10-0.2	Single effect $LiBr/H_2O$	700	0.8	TRNSYS	(Calise et al. 2014)
	---	0.59	0.10-0.13	----	---	---	CFD	(Xu and Kleinstreuer 2014)
	996	0.32	0.13	Double effect. $LiBr/H_2O$	325	---	TRNSYS	(Calise et al. 2013)
	---	0.63	0.25	Adsorption system.	----	0.5	Polysun	(Garcia-Heller et al. 2014)
PVT	1000	0.3	0.10	Single effect. $LiBr/H_2O$	325	0.816	TRNSYS	(Calise and Vanoli 2012)
	---	---	0.104	Heat pump	2.0-2.7	2.88	Experimental	(Fang et al. 2010)
	70	---	---	Adsorption chiller.	16.7	0.13-0.47	Mathmatical method	(Papoutsis et al. 2017)
	70	---	-----	Adsorption chiller	16	0.51	Mathmatical method	(Koronaki et al. 2016)
	20	0.36-0.39	0.10	Adsorption chiller	7	0.55	TRNSYS	(Calise et al. 2016)
FPC& PV	40-180	---	0.15	Adsorption chiller.	50	0.68	Simulation SACE.	(Hartmann et al. 2011)
	112.5 (124 PV)	0.27	---	Single effect LiBr/H2O	30	0.7	TRANSOL EDU3.0 INSEL 7.0 for PV.	(Eicker et al. 2014)
ETC & PV	40-50	0.54	0.18	LiBr/H2O Single effect	---	0.7	---	(Fumo et al. 2013)

A_c: Collector area (m^2)
ETC: Evacuated solar collector tubes
PTC: Parabolic trough solar collectors
CPC: Compound parabolic concentrator

2.6 CFD method for solar collectors

In this section, research into FPC and PVT that employed the CFD method is presented, focusing on boundary condition and percentage error of validation.

2.6.1 CFD method for FPC

Rangababu et al. (2015) investigated FPC to improve thermal efficiency. The authors presented a CFD model with a heat flux boundary condition on the top and assumed that other sides of the collector were fully insulated. Mixed radiation model was applied on the glazed cover. Outlet water temperature was validated to analytical and experimental data with errors of 30% and 20% respectively (Rangababu et al. 2015).

A FPC of 1.96 m x 1 m with 20 pieces of heat pipes has been studied by Wang et al. (2015) using CFD with FLUENT and DO radiation model. A convection boundary condition was applied on the top of the glass with regard to the wind velocity (v) and heat transfer coefficient (h) of h= 5.7+3.8 v and h= 2.8+3.8 v on the other surfaces that contact the ambient. The authors highlighted the importance of the instantaneous efficiency curve ($\eta_{th} = F_R\ (\tau\alpha) - \frac{F_R\ U_L\ (T_i - T_a)}{G}$) for the thermal performance of FPC and compared the results for the efficiency with an experiment from the literature with good agreement. Thermal efficiency increased with the increase in the mass flowrate and the maximum was 85.1 % (Wang et al. 2015).

Gunjo et al. (2017) investigated the effect of inlet water temperature, solar radiation, ambient temperature and mass flowrate for a FPC. FLUENT was employed to determine absorber and outlet water temperature. The model was validated to an experiment with maximum relative error of 5.2%. The authors highlighted that thermal efficiency increases with the increase in ambient temperature and solar radiation. Typical meteorological data during the test day has been applied to the study with ambient temperature of 23 ^{o}C to 34 ^{o}C, inlet water temperature of 27 ^{o}C to 30 ^{o}C, and solar radiation of 400 W/m^2 to 920 W/m^2. Maximum outlet temperature of 50.8 ^{o}C was achieved for an inlet water temperature of 47.1 ^{o}C, while the maximum thermal efficiency during the experiment time was 59% (Gunjo et al. 2017).

Hung et al. (2017) employed CFD to investigate the performance of FPC. The authors highlighted that layers thicknesses, mass flowrate and the length of the collector were the main factors affecting the performance of the collector. A fiberglass wool was employed as insulation to reduce losses from the bottom. Increasing the length of FPC raised the outlet temperature but decreased the efficiency. Efficiency and outlet temperature increased with the increase in glass transmittance (Hung et al. 2017).

2.6.2 CFD method for PVT

Hosseinzadeh et al. (2018) employed CFD (FLUENT) to investigate PVT performance. Heat generation rate was applied on the top surface of the model to represent the absorbed solar radiation. The model was validated with an average error of 3.25 % to predict outlet water temperature. Several parameters were optimised such as absorbed solar radiation, wind speed, inlet temperature and mass flowrate based on the Tagguchi optimisation method using Minitab software. The authors highlighted that inlet temperature, absorbed energy and flowrate were key parameters affecting the efficiency of the PVT (Hosseinzadeh et al. 2018).

The performance of PVT was investigated using COMSOL software for a high radiation level. The investigation included flowrate, outlet temperature, cell temperature, and thermal and electrical efficiency. The authors reported that the overall efficiency was affected significantly by the flowrate, being increased by the increase in flowrate. The optimum results of the study were 180 L/h for the flowrate, and 10.6 % and 81.6% for electrical and thermal efficiency respectively at 5000 W/m^2 radiation (Nasrin et al. 2018).

2.7 Multi-objective optimisation

Lee and Kim (2015) applied the multi-objective optimisation technique using MATLAB to enhance heat transfer and reduce pressure drop in heat exchanger technology. Latin hypercube sampling was used based on two geometrical objectives (Lee and Kim 2015). Multi objective optimisation was also presented using MATLAP toolbox in order to reduce experimental and computational cost (Kulkarni et al. 2015). Three geometrical

parameters were selected for the optimisation in order to maximise heat transfer and minimise pressure drop for solar heater collector. The optimisation showed accurate results by selecting design points based on the Latin hypercube method and Kriging type for the response surface.

Six variables were taken as parameters in order to enhance the efficiency of the flat plate collector, which was in the range of 12 % to 74 %. The authors highlighted that the flowrate and solar intensity were the most important parameters for optimising the system. Despite the fact that solar intensity is uncontrollable because it is an environmental condition, solar intensity was taken as a parameter in the study. Further investigation is required, focusing on inlet temperature and flowrate (Hajabdollahi and Hajabdollahi 2017).

A multi-objective algorithm was employed to optimise seven geometrical parameters for a linear Fresnel collector in order to increase the efficiency. A 2-D CFD model was presented using ANSYS design modeller, and central composite design was applied to select 79 design points. Auto refinement Kriging regression was used in the response surface (Moghimi et al. 2015). ANSYS design modeller was also used by Mwesigye et al. (2015) to study the performance of the parabolic trough collector by applying multi-objective optimisation. A space filling type of design of experiment was used with automated refinement Kriging Meta model. Nusselt number and pressure drop were optimised to enhance the heat transfer of the collector by Mwesigye et al. (2015).

Response surface optimisation was combined with CFD to improve building ventilation. Central composite design was used in the design of the experiment to provide design points, and a screening method was used to propose optimal solutions (Sofotasiou et al. 2016). The authors reported that the optimisation technique coupled with CFD in the ANSYS design modeller is a helpful tool for evaluating multi-parameters problems. CFD was used as a model to investigate different parameters that affecting the performance of FPC. The CFD model in ANSYS can be linked with a multi objective optimisation algorithm in order to enhance the performance of FPC and PVT by optimising their parameters (as in this study). The inlet parameters (such as inlet temperature and flowrate) can be defined in the CFD model as well as the outlet parameters (such as outlet temperature and cell temperature). Thermal efficiency can also be defined as an output

parameter in order to be controlled and optimised by using response surface optimisation method, which is available in ANSYS.

2.8 Summary

Based on the research into solar absorption systems, there is an opportunity to increase the solar coefficient of performance (SCOP) of the system by increasing the thermal efficiency of the collector. Some previous research has investigated the incorporation of solar collectors such as FPC and PVT with absorption chillers, but has not investigated the efficiency of the collector for specified outlet temperature. The majority of research that used simulation or an analytical method to investigate solar cooling systems determined the efficiency of solar collectors based on equations from the literature (Ketfi et al. 2015; Bellos et al. 2016) without taking into account the effect of flowrate or the inlet temperature on these equations. In addition, some research optimised the driving temperature of the absorption chillers based on the condition of the study without taking into account that the absorption chillers in the market have been designed for an optimum inlet temperature in order to achieve the highest COP.

The outlet temperature from the collector in solar cooling systems is a key factor that affect the overall performance (Li et al. 2014). Minimising the operation temperature leads to maximisation of the collector's thermal efficiency and overall performance of the system (Buonomano et al. 2018). In solar absorption cooling systems, reducing heat source temperature leads to enhancement of overall efficiency (Aman et al. 2014). Of previous research into solar cooling systems, there is no study that shows the optimum inlet temperature and flowrate of FPC or PVT for a specified required outlet temperature.

The investigation in previous studies on FPC and PVT were carried out mostly in low temperature climates (Cristofari et al. 2009; Calise et al. 2013; Liang et al. 2015). The majority of the research into FPC and PVT focused on geometry; and type of materials of the collector and absorber, in order to enhance performance in specified environments. The application in the majority of these studies consisted of using the collector for heating, where inlet temperature is mainly chosen as the ambient temperature; (Cristofari et al. 2009; Fang et al. 2010; Dubey and Tay 2014; Tsai 2015; Liang et al. 2015). Some

previous research investigated the incorporation of solar collectors such as FPC and PVT with absorption chillers, but there is a lack of research that investigated FPC or PVT using a 3-D CFD model for a specified required temperature.

2.9 Gaps in the current research on FPC and PVT for solar cooling systems.

This chapter presented a comprehensive review of the development of solar cooling system which included experimental and computational research. The study also included an alternative method of utilising solar energy for cooling purposes. The review highlighted different solar collectors which can be integrated with cooling technologies in order to improve the overall performance of the system. However, the following issues are not resolved in the literature:

- There is no research that reviewed a solar driven absorption system with a photovoltaic thermal system.
- There is no research that investigated the effect of inlet temperature on efficiency of FPC and PVT for a specified outlet temperature.
- There is no research that investigated the effect of flowrate on efficiency for FPC and PVT for a specified outlet temperature.
- The effect of PVT systems on performance is rarely investigated; that is the effect of the number of the panel that connected in series.
- There is no study that used multi-objective optimisation method for a specified outlet temperature of a PVT based on a 3-D CFD.
- There is no study that optimised the flowrate and inlet temperature for the heist efficiency of PVT and FPC for a specified outlet temperature.

This work will use analytical and computational fluid dynamics (FLUENT), which was identified in the study as a means of filling the research gap. The aim of the study is to investigate and optimise the thermal efficiency of FPC and PVT for sustainable cooling systems.

Chapter 3. Research Method

3.1 Introduction

This chapter presented the methods of research employed in this study to determine and enhance the performance of a flat plate collector and photovoltaic thermal collector. The research included a computational model of a flat plate collector (FPC), a computational model of a PVT, and a mathematical model of a photovoltaic thermal collector (PVT). Section 3.2 discussed the computational fluid dynamics (CFD) method that was employed to determine the performance of the computational FPC and PVT models. A computational model of FPC which is employed to determine thermal performance is presented in section 3.3. Section 3.4 presents a computational model of PVT which is intended to determine thermal and electrical performance. In order to study the effect of PVT systems on performance, a mathematical model of PVT is presented in section 3.5. Section 3.6 presented the multi-objective optimisation method that is applied to the FPC and PVT model in order to optimise the inlet conditions.

3.2 Computational Fluid Dynamic (CFD)

Fluid problems can be solved analytically, experimentally or numerically. Governing equations of fluid problems are solved in discrete form with accurate results using numerical simulation. CFD has been developed to act essentially as an efficient tool for addressing thermal and fluid problems, which helps to save the time and reduce the cost required to solve such problems. In order to solve a certain problem of a CFD model successfully, the modelling goal needs to be defined, model geometry and mesh need to be created, the solver and physical model need to be set up, and the solution needs to be monitored and examined. In order for the solution to be computed and monitored, the convergence should have occurred (in other words, variations in the solution from one iteration to the next should be negligible). The accuracy of the solution depends on the physical model, mesh study and the setup of the problem (Ansys 2015).

3.2.1 Governing equations for fluid flow

The main governing equations that represent the conservation law of physics for fluid flow are:

- Conservation of mass (continuity equations).
- The sum of forces on a fluid particle is equal to the rate of change of momentum (Newton's second law).
- The rate of heat addition to the fluid particle and the rate of work done on a fluid particle are equal to the rate of change of energy (first law of thermodynamics).

Differential equations of the fluid flow are difficult to solve mathematically (White 2011). Some useful solutions were found by adding assumptions such as steady flow and incompressible flow.

In order to write Newton's second law for fluid, the acceleration vector (**a)** of the flow is considered as in equation 3-1:

$$a = \frac{dV}{dt} = i\frac{du}{dt} + j\frac{dv}{dt} + k\ \frac{dw}{dt} \qquad (3\text{-}1)$$

u represents local velocity component in x direction, *v* represents local velocity component in y direction and *w* represents local velocity component in z direction. Each of the three components of velocities is a function of time and position in the computational zone (*x, y, z, t*). Therefore, the chain rule is applicable for each scalar component of velocities, taking into account that (*u, v, w*) can be represented by the derivation of position component to the time (*u= dx/dt, v = dy/dt , and w= dz/dt.* Then the acceleration of fluid particle in x-direction can be written as in equation 3-2:

$$\boldsymbol{a_x = \frac{du}{dt} = u\frac{\partial u}{\partial x} + v\frac{\partial u}{\partial y} + w\frac{\partial u}{\partial z}} \qquad (3\text{-}2)$$

Similarly, the acceleration of fluid particle in y-direction can is written as in equation 3-3:

$$a_y = \frac{dv}{dt} = u\frac{\partial v}{\partial x} + v\frac{\partial v}{\partial y} + w\frac{\partial v}{\partial z} \qquad (3\text{-}3)$$

The acceleration of fluid particle in z-direction is written as in equation 3-4:

$$a_z = \frac{dw}{dt} = u\frac{\partial w}{\partial x} + v\frac{\partial w}{\partial y} + w\frac{\partial w}{\partial z} \qquad (3\text{-}4)$$

3.2.2 Conservation of mass

The conservation of mass is also known as the continuity equation. Figure 3-1 shows the control volume of a fluid with inlet mass flow in x direction $\rho u\ dA$. The flow through each side of the control volume according to (White 2011) is approximately one-dimensional flow. Therefore, the outlet mass flow on x direction is equal to the inlet flow plus the change in flow through x direction $\left(\rho u + \frac{\partial}{\partial x}\ \rho u\ dx\right) dy\ dz$. Applying conservation of mass to the three directions of the control volume with the same approach provides the following relations, known as the continuity equation:

$$\frac{\partial \rho}{\partial t} + \frac{\partial}{\partial x}(\rho u) + \frac{\partial}{\partial y}(\rho v) + \frac{\partial}{\partial z}(\rho w) = 0 \qquad (3\text{-}5)$$

Or

$$\frac{\partial \rho}{\partial t} + \nabla.(\rho V) = 0 \qquad (3\text{-}6)$$

Where ∇ is a vector operator, which is defined as:

$$\nabla = \vec{\imath}\frac{\partial}{\partial x} + \vec{\jmath}\frac{\partial}{\partial y} + \vec{k}\frac{\partial}{\partial z} \qquad (3\text{-}7)$$

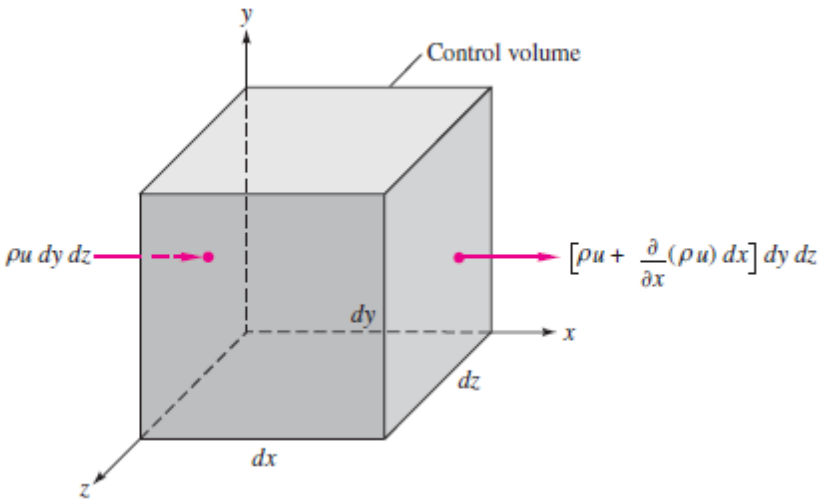

Figure 3-1 Elemental Cartesian fixed control volume showing the inlet and outlet mass flows on the x direction (White 2011).

3.2.3 Momentum and Navier-Stokes equations

By considering the Newtonian second law, net forces acting on a fluid element are equal to the mass of the fluid multiplied by its acceleration, as in equation 3-8:

$$\vec{F} = m\,\vec{a} \qquad (3\text{-}8)$$

As stated by Newton‘s second law for a fluid particle, the rate of change of momentum equals the summation of forces acting on the particle (Calautit et al. 2013). The rates of change of x, y and z-momentum per unit volume can be written as:

$$\rho\frac{Du}{Dt}\,,\ \rho\frac{Dv}{Dt},\ \rho\frac{Dw}{Dt} \qquad (3\text{-}9)$$

Body forces and surface forces are the two types of forces that act on fluid particles. Figure 3-2 represents the stresses on an element fluid particle in the x-direction.

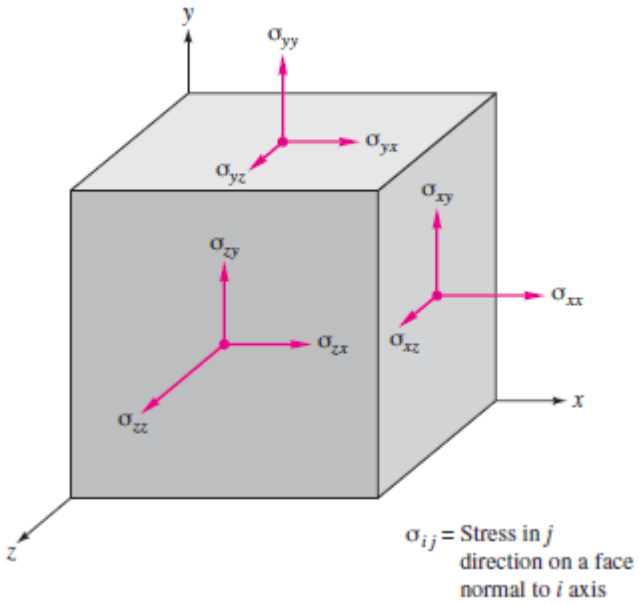

Figure 3-2 Stresses on an element fluid particle (White 2011).

The momentum is represented by considering that; the rate of change of momentum is equal to the summation of forces in the same direction (White 2011). Figure 3-3 shows forces in the x direction on the control volume of a fluid.

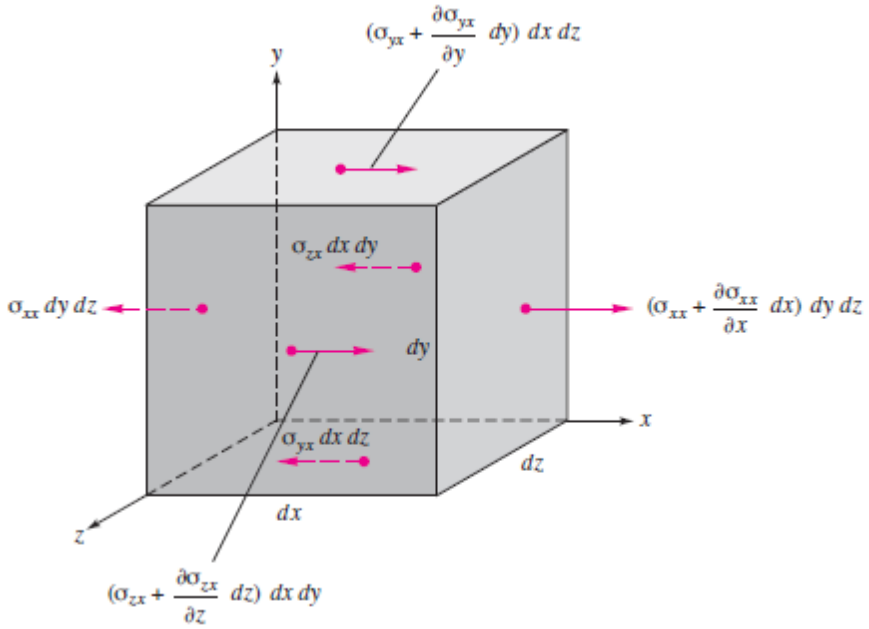

Figure 3-3 Forces in the x direction on the control volume of a fluid (White 2011).

3.2.4 The differential equation of energy

The first law of thermodynamics represents the energy change in an element by the net flux in plus the rate of work done on the element. The energy equation can be represented in the following form (Ansys 2015):

$$\frac{\partial}{\partial t}(\rho E) + \nabla \cdot (\vec{v}(\rho E + p) = \nabla.[k_{eff} \nabla T - \sum h_j \vec{J}_j + (\bar{\tau}_{eff} . \vec{v})] + S_h \qquad (3\text{-}10)$$

Where k_{eff} is the effective conductivity, $\vec{J}_j$ is the diffusion flux j, $k_{eff} \nabla T$ energy transfer by conduction, $h_j \vec{J}_j$ species diffusion, $\bar{\tau}_{eff} . \vec{v}$ viscous dissipation and S_h heat sources.

The energy equation in static solid zones is represented as in equation 3-11 (Ansys 2015):

$$\frac{\partial}{\partial t}(\rho h) = \nabla.[k \nabla T] + S_h \qquad (3\text{-}11)$$

Where ρ is the density, h is sensible enthalpy, k= conductivity and S_h is volumetric heat source.

3.3 Computational model of FPC

Flat plate collectors (FPC) convert solar radiation to useful thermal energy and can be designed to transfer energy to fluid up to a level of 100 ^{o}C above the ambient temperature. The absorber plate is the main components of the FPC. It transfers the absorbed energy to a fluid, which moves through riser pipes. The configuration of the FPC in this study included front glass cover and back insulation to reduce heat losses from the collector. (Duffie and Beckman 1980; Hajabdollahi and Hajabdollahi 2017)

3.3.1 Thermal efficiency using CFD

CFD was employed to solve fluid flow and heat transfer equations for FPC. CFD applies conservation law and integrates the governing equations (continuity, momentum and energy equations) over all the control volumes at solid and fluid zones for the FPC. A three-dimensional CFD model was developed in order to determine the performance of the FPC. Total energy absorbed by the absorber (Q_s) was determined based on the global solar radiation (G), glass transmissivity (τ) and the absorptivity of the plate (α) (Duffie and Beckman 1980). Constant heat flux was applied on the top of the absorber plate whereas fully insulated boundary condition was applied to the other surfaces that are in contact with the surroundings (Khanjari et al. 2016).

The radiative heat loss for a solar collector (PV) represent about 25% of the total losses which included reflective, transmissive and thermal losses respectively (Lu and Yao 2007; Michael et al. 2015). In this study the transmissive and reflective losses was considered based on the equation 3-12 (Duffie and Beckman 1980) . Convective losses was consider based on equation 3-13. The radiative losses was neglected as in (Khanjari et al. 2016; Gunjo et al. 2017; Ebrahim Ghasemi and Akbar Ranjbar 2017). The benefit from that is to minimise the computational cost especially in the multi-objective optimisation stage in the study. Radiation coefficient (h_r) can be estimated using the following (Rejeb et al. 2016): $h_r = \varepsilon_p \sigma (T_p^2 + T_{sky}^2)(T_p + T_{sky})$. where, ε is emissivity (for the absorber copper ε=0.07 as in Shojaeizadeh et al. (2015) and Hawwash et al. (2018), σ is Stefan Boltzmann constant, T_{sky} is sky temperature, T_p is panel temperature and $T_{sky} = 0.0522 * T_{pamb}^{1.5}$. Based on an ambient temperature of 318 K, wind velocity of 1/s

and delta T of 20 K, the radiative coefficient would represent 8.7% of the convective coefficient. In the case of ε=0.10 as in Gunjo et al.(2017), the radiative coefficient would represent 12.5 % of the convective coefficient. Adding transparent cover (as it is consider in this study) would significantly reduce radiation losses from the collector (Fudholi et al. 2014; Gunjo et al. 2017).

Total energy absorbed by the FPC was calculated as in the following equation (Duffie and Beckman 1980):

$$Q_s = \alpha\ \tau\ G \qquad (3\text{-}12)$$

Where Q_s represents the net energy absorbed by the absorber, G represents global solar radiation, τ represents glass transmissivity and α represents absorptivity of the absorber.

Part of the energy absorbed by the FPC is transferred to the surroundings and was represented by convective boundary condition which was applied on the bottom layers as in (Cerón et al. 2015). The convective heat transfer coefficient was determined based on equation 3-13 (Gunjo et al. 2017):

$$h_b = 2.8 + 3V_w \qquad (3\text{-}13)$$

Thermal efficiency is the ratio of the collected energy (useful energy that is transferred to the fluid) to the energy that reaches the flat plate collector. Thermal efficiency is calculated by the following expression (Duffie and Beckman 1980; Chow 2010; Dubey and Tay 2014):

$$\eta_{th} = C_p\ \dot{m}\ \frac{T_o - T_i}{G\ A_c} \qquad (3\text{-}14)$$

Where C_p represents specific heat of the coolant (kJ/kg K), $\dot{m}$ is the mass flowrate of the coolant (kg/s), A_c is the collector area (m^2), T_i is the inlet temperature of the coolant (K), T_o is the outlet temperature of the coolant (K), and G is global solar radiation normal to the cover glass (W/m^2).

Outlet temperature (T_o) for the computational FPC model is determined as an output from the CFD model. Mass weighted average method was used to predict fluid temperature with respect to the variation of the velocity across the pipe.

3.3.2 Thermal efficiency using analytical theory

Overall heat transfer coefficient is an important characteristic for the solar collector to calculate the lost heat from the collector to the ambient. In theory, by knowing the temperature of the absorber plate and the overall heat transfer coefficient of the FPC, useful energy of the FPC can be determined by equation 3-15 (Duffie and Beckman 1980; Al-Ajlan et al. 2003; Bahaidarah et al. 2013; Dubey and Tay 2014):

$$Q_u = A_c \left[\alpha\tau\, G - U_L \left(T_{pm} - T_a \right) \right] \qquad (3\text{-}15)$$

Where:

- Q_u: Useful energy output from the solar collector.
- A_c: Collector area, m^2.
- τ: Transmittance
- α: Absorbance
- G: Solar radiation reaching the surface of solar collector, W/m^2.
- U_L: Overall heat transfer coefficient (including the effects of conduction, convection and radiation), W/m^2 k.
- T_{pm}: Mean temperature for the absorber plate collector, K.
- T_a: Ambient temperature, K.

Collector heat removal factor (FR) is another important characteristic of the solar collector which represents the ratio of actual useful energy gain of the collector to the useful gain if the collector surface is assumed to be at the inlet fluid temperature (Duffie and Beckman 1980). Mathematically, FR is given by equation 3-16:

$$F_R = \frac{m \cdot C_p \,(T_o - T_i)}{A_c[\alpha\tau\, G - U_L(T_i - T_a)]} \qquad (3\text{-}16)$$

Heat removal factor (F_R) and inlet fluid temperature (T_i) were added to equation 3-17 (Duffie and Beckman 1980; Shojaeizadeh et al. 2015); to be written as:

$$Q_u = F_R A_c [\alpha\tau G - U_L (T_i - T_a)] \quad (3\text{-}17)$$

Equation 3-17 was derived by Duffie and Beckman (Duffie and Beckman 1980) and reported as one of the most important equations in the field of solar thermal energy. In the literature, it is a widespread formula for experimental and theoretical research because there is no need to measure the plate temperature in order to calculate the useful energy for FPC.

By calculating useful energy, one can calculate FPC outlet fluid Temperature (T_o) can be calculated as in equation 3-18:

$$T_o = T_i + \frac{Q_u}{m \cdot Cp} \quad (3\text{-}18)$$

Thermal efficiency of FPC can then be written as in equation 3-19 by knowing the heat removal factor (F_R) and collector overall heat loss coefficient (U_L):

$$\eta_{th} = F_R (\tau\alpha) - \frac{F_R U_L (T_i - T_a)}{G} \quad (3\text{-}19)$$

The plots of thermal efficiency versus energy loss parameter (($T_i - T_a$)/G) (if U_L, F_R, and ($\tau\alpha$) were all constant) would be straight lines with intercept F_R ($\tau\alpha$) and slope $-F_R U_L$.

Stagnation water temperature T_{max} (or maximum equilibrium temperature) which represents any part of the collector is a function of Q_s, U_L and ambient temperature. The theoretical maximum temperature can be used as preliminary indicator to design solar collector. T_{max} can be evaluated as in equation 3-20 by estimated zero water flowrate (or useful energy equal zero) at equation 3-17 (Duffie and Beckman 1980):

$$T_{max} = T_a + \frac{Q_s}{U_L} \qquad (3\text{-}20)$$

3.3.3 Experimental setup to validate the computational FPC model

The 3D CFD model of the flat plate collector was validated to the experiment from the literature and achieved results more accurate than those in the literature. This model was used to investigate the impact of flowrate and inlet temperature on the FPC's performance. The experimental layout and structure of the FPC in this study consists of a glass cover, an absorber made of copper, header and riser water pipes, and insulation.

3.3.3.1 Geometry description and meshing

A benchmark model was selected based on experimental geometry from the literature (Gunjo et al. 2017). The FPC was characterised by absorber plate with 1.65 m length, 1 m width and 5 x 10^{-3} m thickness, riser copper pipes along the absorber plate with 0.0125 m diameter, and glass wool insulation with 0.04 m. The distance between riser pipes is 0.1125 m and the pipes were attached to the absorber plate. The tube risers are connected to two main headers at the inlet and the outlet as in Figure 3-4.

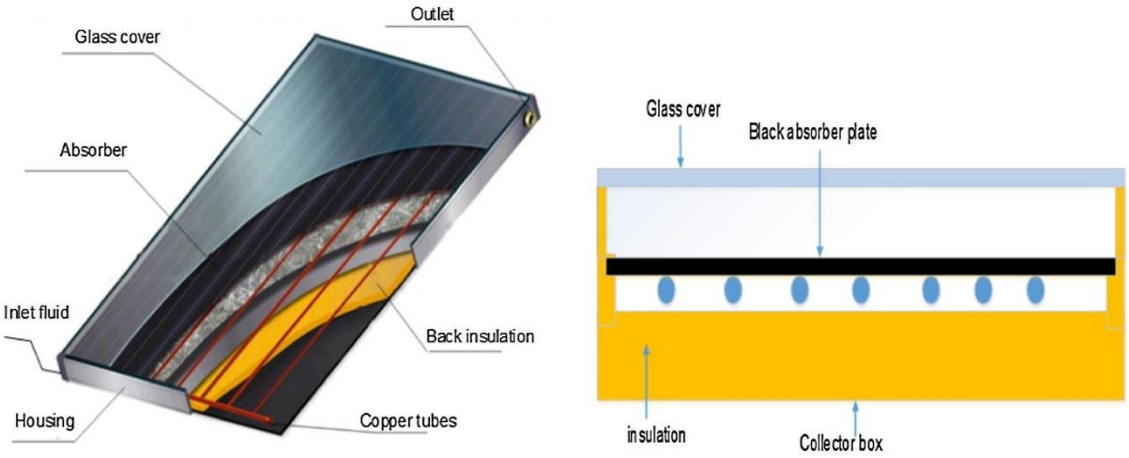

Figure 3-4 Flat plate collector (cross section) (Hawwash et al. 2018).

In order to maximise the absorbed energy and then maximise thermal energy of the collector, a selective coating are consider as in the experiment (10% emittance). Specification of the FPC and materials properties are given in Table 3-1.

Table 3-1: Specification and materials properties of the flat plate collector (Rejeb et al. 2016; Gunjo et al. 2017; Hung et al. 2017).

Material	**Density (kg/m^3)**	**Thermal conductivity (W/m K)**	**Heat capacity (J/kg K)**	
Glass	2500	1.4	750	τ =0.93
Absorber	8954	386	385	α =0.95
Insulation	200	0.044	840	
Description		**Dimension**	**Units**	
Absorber plate length		1.65	m	
Absorber plate width		1	m	
Plate thickness		0.0005	m	
Number of riser pipe		10	--	
Diameter of riser pipe		0.0125	m	
Pipe thickness		0.0007	m	
Distance between riser to riser (centre to centre)		0.1125	m	
Thickness of the insulation (Glass wool)		0.04	m	

In order to reduce the time cost of the simulation, the model in the CFD is simplified to a single riser tube attached on the bottom of the absorber. The flowrate in the riser tube is the ratio of the total flowrate of the collector to the number of risers. Figure 3-5 shows the geometry of the computational domain for the FPC generated in ANSYS Design modeller.

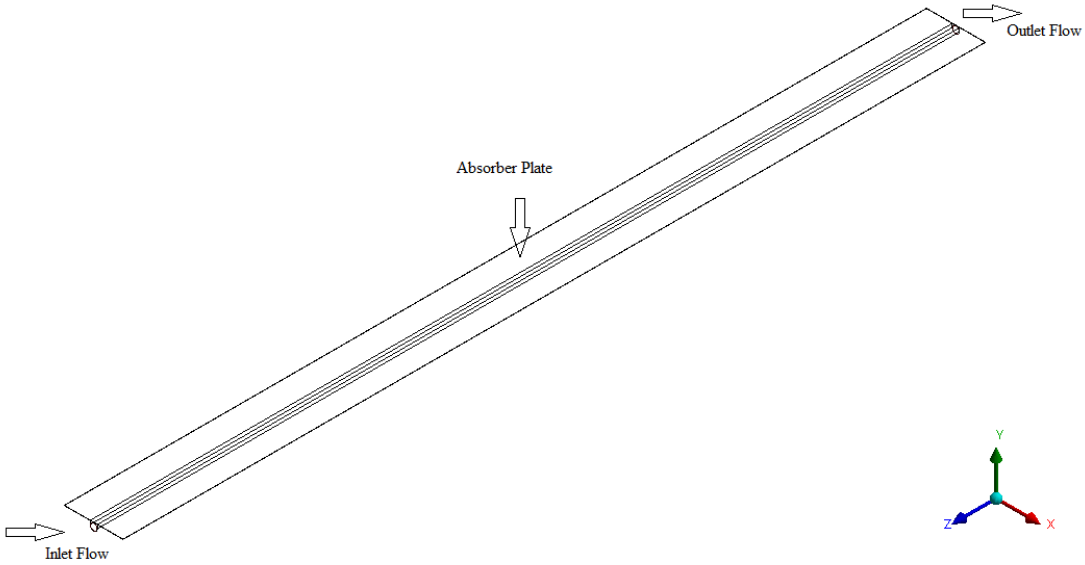

Figure 3-5 Computational domain for the FPC.

3.3.3.2 Grid independence

Grid independence study is necessary to enable CFD simulations to give accurate computational results that are not affected by the number of grids or the size of cells in the computational domain. A sequence of coarse, medium and fine meshes was generated. The mesh was generated in ANSYS mesh tool with automatic method. A grid independence study was applied to the computational domain, which consists of absorber plate, riser pipe and water inside the pipe as in Figure 3-6.

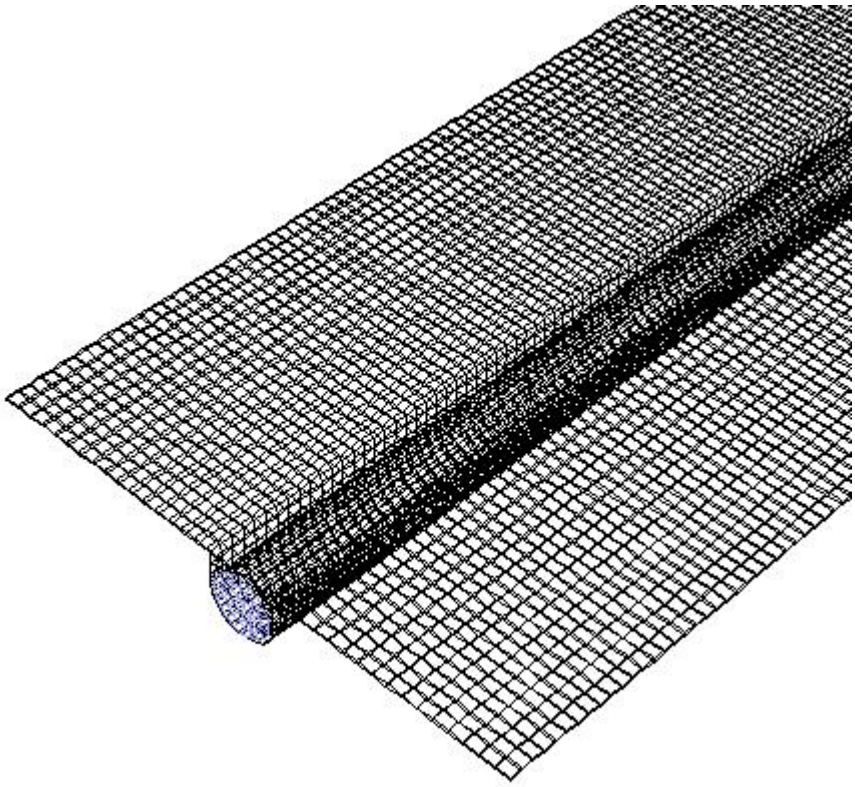

Figure 3-6 Example of a mesh for the computational domain of the FPC

A grid independence study was carried out on the computational domain, which consisted of an absorber plate, riser pipe and water inside the pipe. Numerical sensitivity tests were applied on the outlet fluid temperature and average temperature of the absorber plate. As in Figure 3-7, the difference between simulation results was decreased by increasing the number of elements in the mesh domain. For both outlet water temperature and temperature of the plate, the results for 126,768 and 204,881 elements were approximately the same. Therefore, a mesh size of 126,768 was chosen for the simulation in order to reduce the computational time.

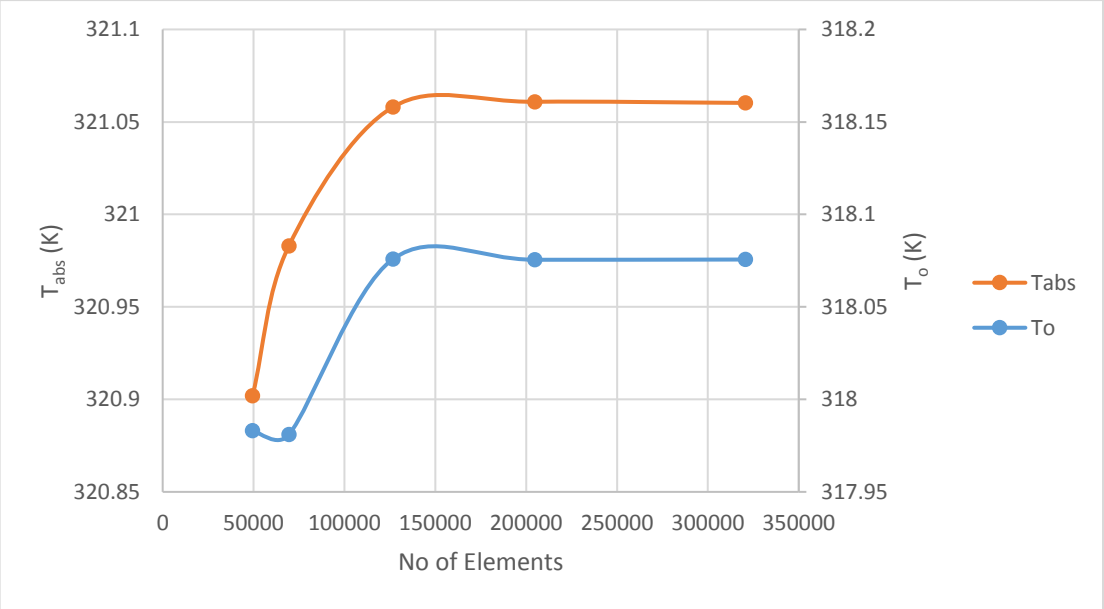

Figure 3-7 Grid independent study for the FPC computational domain.

3.3.3.3 Boundary conditions

The investigation in this study was carried out based on the following assumptions:

- Uniform flow normal to the inlet of the riser and steady state system are considered (Cerón et al. 2015).
- Physical properties for materials are constant (Zhou et al. 2017).
- The flow in each riser is 1/10 of the total mass flowrate.
- Solar radiation is vertical to the absorber plate (Khanjari et al. 2016).
- Due to a selective coating on the absorber which reduces emittance, radiation heat loss is neglected (Khanjari et al. 2016; Gunjo et al. 2017; Ebrahim Ghasemi and Akbar Ranjbar 2017).
- Sides of the collector are fully insulated.
- There is perfect contact between riser pipe and the absorber plate.
- Heat loss from the bottom occurs by convection (Gunjo et al. 2017).

Heat flux was applied on the top of the absorber and the value of the flux was calculated based on the transmittance of the glass and the absorbance of the absorber plate as in equation 3-12. Momentum boundary condition at the inlet was represented by constant

mass flowrate ($\dot{m}$) normal to the boundary while the thermal inlet boundary was represented by constant inlet temperature (T_{in}). Convective boundary condition was applied on the bottom layers and convective heat transfer coefficient determined based on equation 3-13. Zero heat flux has been applied to the other surfaces that are in contact with the surroundings.

Steady state in CFD describes the behaviour of the system in low computational cost with respect of governing equations, which included the conservation of mass, momentum and energy. The steady state model is commonly applied with solar collectors to investigate thermal performance (Fudholi et al. 2014; Xu and Kleinstreuer 2014; Yazdanifard et al. 2016; Gunjo et al. 2017) and the extinction of the last work in Gunjo et al. (2017). However, the steady state model is more efficient when the average weather conditions (hourly, daily, weekly or monthly) is used as an input parameters in the model (Tagliafico et al. 2014).

3.3.3.4 Model validation

In order to validate the CFD model, operation parameters, which included intensity of solar radiation, ambient temperature and fliuid inlet temperature for the FPC, were set based on Gunjo et al. (2017). Wind speed was considered to be 1 m/s in this study. Figure 3-8 shows real weather data (ambient temperature and solar radiation) and inlet water temperature during the experiment day, which were applied as input conditions for the validation in this study.

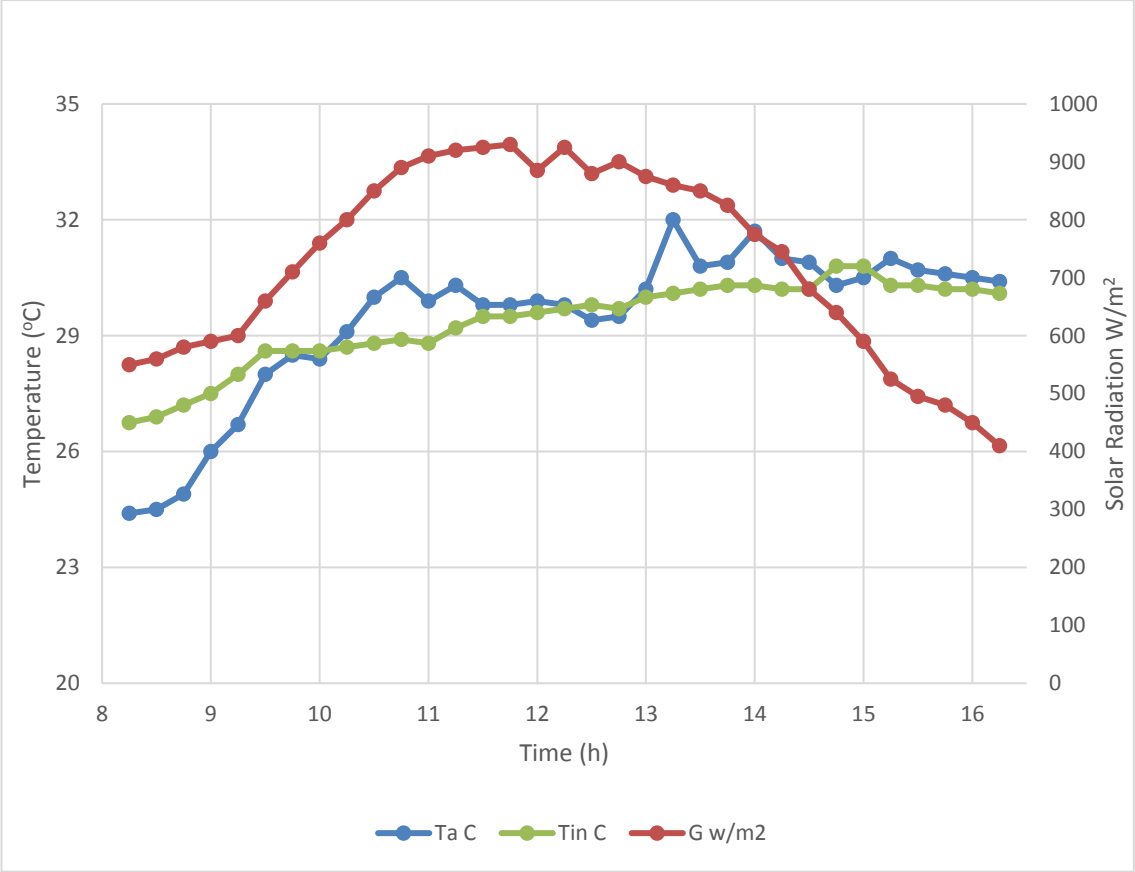

Figure 3-8 Ambient temperature, inlet water temperature and solar radiation during the experiment day.

To validate the CFD model of the flat plate collector in this study, one-hour interval has been considered as an input parameter for each hours based on the conditions on Figure 3-8 . The simulation output for each hour individually (outlet temperature) of the FPC in this study was determined and compared to the experiment in Gunjo et al. (2017). Figure 3-9 shows that outlet water temperature in this study followed the trend of the experiment with a relative error of 0.47% to 1.5%. This validation shows the accuracy of this model for predicting outlet temperature as compared to the literature; for example, Rangababu et al. (2015) and Gunjo et al. (2017), who achieved 20-30% and 5.2% for the maximum relative error respectively.

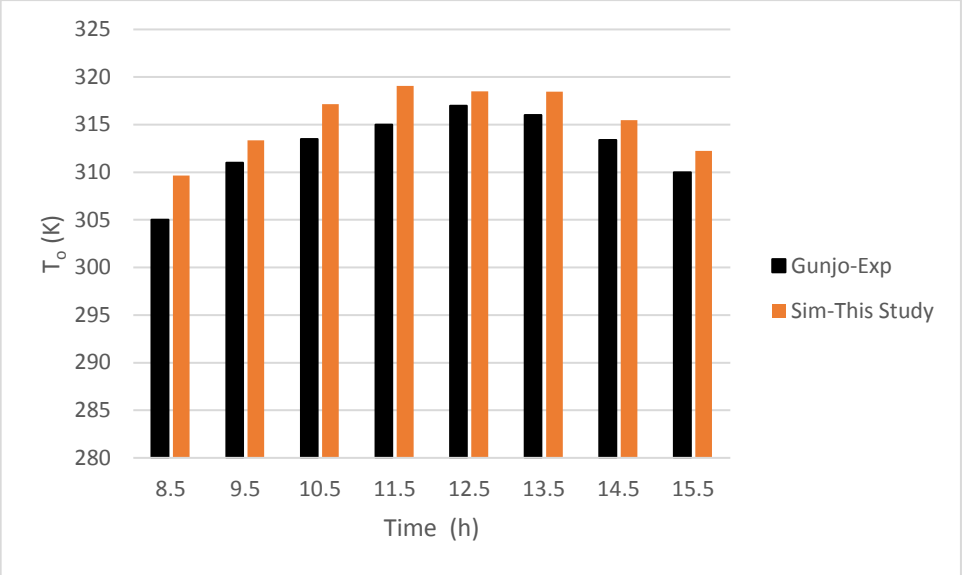

Figure 3-9 Outlet fluid temperature in this study and the experiment in the literature.

3.4 Computational model of PVT

In this study, a 3-D CFD model was developed in ANSYS workbench in order to investigate the performance of a photovoltaic thermal collector (PVT). ANSYS-FLUENT applies conservation law and integrates the governing equations (continuity, momentum and energy equations) over all the control volumes at solid and fluid zones for the PVT. Three-dimensional CFD model was presented in order to determine the performance of the PVT. Pressure based type has been selected in FLUENT solver which take the momentum as primary variable. The materials properties then was added for the photovoltaic layer, absorber plate and insulation based on materials properties in Table 3-2. Then the materials were defined (in cell zone condition section) for each part of the model. Thermal boundary conditions was applied on the top of the PV layer as a constant heat flux. Momentum boundary condition was defined at the pipe inlet as mass flow rate normal to the boundary. Due to the stratification of the fluid inside the pipe, mass-weighted average was considered to calculate the outlet temperature while the average temperature of the PV surface was considered. In order to link the CFD model with the response surface optimisation in the ANSYS workbench, a parameter set were defined for both input and output parameters.

The CFD model of the PVT was employed to predict outlet fluid temperature and determine thermal and electrical efficiency. Energy absorbed (Q_s) by the photovoltaic layer (PV) was determined based on the global solar radiation (G), glass transmissivity (τ) and absorptivity (α) of the photovoltaic layer (PV). As discussed in the FPC section, constant heat flux was applied on the top of the PV sheet and convective heat transfer was applied on the bottom layers. Convective heat transfer coefficient was also determined based on equation 3-13 as explained in section 3.3.

Thermal efficiency of PVT is determined as in equation 3-14, which was discussed in section 3.3. Useful energy and thermal efficiency of PVT can also be represented as in equation 3-17 and 3-19 in order to calculate the overall heat loss coefficient (U_L) and heat removal factor (F_R) of the computational PVT model.

PV's cell temperature in this study is the average temperature of the photovoltaic sheet, which is an output result from the CFD model. The solar cell type was Solarex MSX60, Poly-crystalline silicon which has a reference efficiency of 15 %. This was chosen from Yazdanifard et al. (2016) to validate the model with the data in the same work. Outlet temperature (T_o) is also determined for the computational PVT model as an output from the CFD.

Electrical efficiency of the photovoltaic is expressed by the empirical relationship in the field presented by (Evans 1981). This method for predicting the electrical efficiency of PVT has been widely used in the field of PVT, as in equation 3-21 (Hosseinzadeh et al. 2018):

$$\eta_{ele} = \eta_o[1 - \beta\,(T_{sc} - 298\ K)] \qquad (3\text{-}21)$$

3.4.1 Computational method validation of PVT

The CFD model was validated to the literature and achieved results more accurate than those in the literature. This model was used to investigate the performance of PVT and optimise its inlet temperature and flowrate in order to achieve high efficiency for a specific outlet temperature. The impact of flowrate and inlet temperature on the PVT performance has also been investigated.

3.4.1.1 Simulation model

The structure of the PVT in this study is shown in Figure 3-10. The module consists of a glass cover, photovoltaic panel, absorber made of copper, riser water pipes and insulation. The efficiency of crystalline was in the range of 13% to 22%, which is a high-level comared to 7% to 13% for amorphous silicon. Polycrystalline-silicon (pc-Si) delivers higher electrical efficiency than the thin film technology and one of the most used (Aste et al. 2014). For these advantages and because it is available in the literature to validate the model, photovoltaic type that consider in this study was polycrystalline-silicon with reference temperature of 0.0045/K (Yazdanifard et al. 2016).

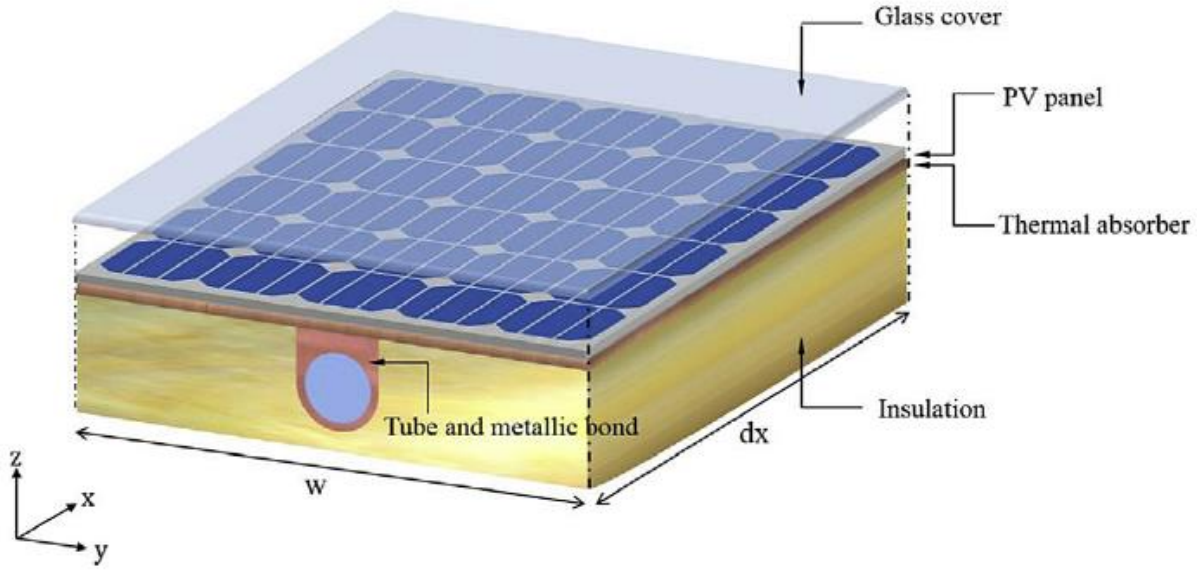

Figure 3-10 Schematic diagram of the PVT (Yazdanifard et al. 2016).

3.4.1.2 Geometry description and meshing

A benchmark model was selected based on Yazdanifard et al. (2016). The PVT was characterised by absorber plate of 2 m length and 1 m width, with riser copper pipes along the absorber plate of 0.008 m outer diameter and 0.0012 m thickness. Ten riser pipes were located under the bottom surface of the absorber plate. Materials properties of the PVT in this study are reported in Table 3-2.

Table 3-2: PVT geometries and materials properties (Pierrick et al. 2015; Yazdanifard et al. 2016).

Material	Density (kg/m3)	Thermal conductivity (W/m K)	Heat capacity (J/kg K)	Thickness (m)	
Glass	2500	1.4	750	0.004	τ =0.92
PV	2330	148	700	0.0005	α =0.9
Absorber	8954	310	385	0.0005	
Insulation	200	0.03	850	0.05	

The CFD model was simplified to a single riser pipe in order to reduce the time cost of simulation. The flowrate in the riser tube is the ratio of the total flowrate of the PVT to the number of riser.

3.4.1.3 Grid independence

In order to guarantee that the number of grids or the size of cells in the computational domain does not affect the results, grid independence study is necessary for CFD simulations. The mesh was generated in ANSYS mesh tool with automatic method for a sequence of coarse, medium and fine meshes. The mesh study (Numerical sensitivity) test was applied on outlet fluid temperature and average temperature of the PV as in Figure 3-11. The number of elements was increased in order to increase the quality of the mesh and across each increment; there was no real variation in the accuracy. There was only 0.2 K variation temperature when the number of elements was increased from 332,492 to 388,040. Therefore, the number of elements for the chosen mesh was 332,492, which is a compromise of good quality and accuracy.

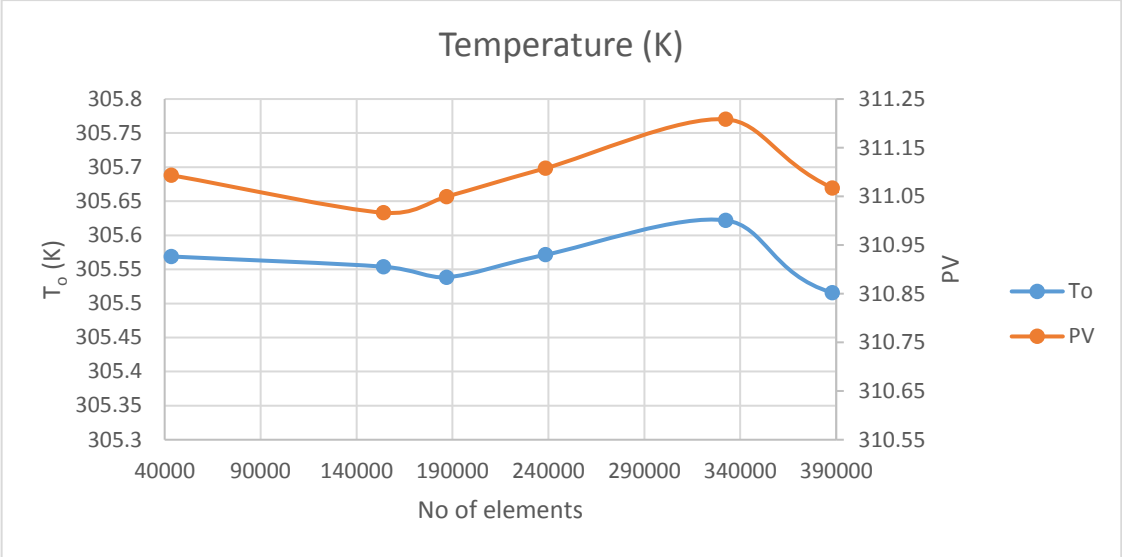

Figure 3-11 Grid independent study for the PVT computational domain.

3.4.1.4 Boundary conditions

The following assumptions have been applied in this study:

- Steady state and uniform flow normal to the inlet (Cerón et al. 2015).
- Physical properties for materials are constant (Zhou et al. 2017).
- The flow in each riser is 1/10 of the total mass flowrate (Khanjari et al. 2016).
- Solar radiation is perpendicular to the photovoltaic sheet (Khanjari et al. 2016).
- Radiation heat loss to the ambient is neglected (Khanjari et al. 2016).
- Fully insulated boundary is applied on sides of the collector.
- Perfect contact region between the PV sheet, absorber plate and riser pipe.
- Heat loss from the bottom by convection (Gunjo et al. 2017).

As discussed in the FPC section, constant heat flux was applied on the top of the photovoltaic sheet. The value of the heat flux was calculated based on equation 3-12. Constant mass flowrate ($\dot{m}$) was applied normal to the boundary as a momentum boundary condition at the inlet while a constant inlet temperature (T_{in}) was applied as a thermal inlet boundary. On the bottom of the PVT, convective boundary condition has been applied. The convective heat transfer coefficient was determined based on equation

3-13. The boundary condition on the rest of surfaces that are in contact with the surroundings were fully insulated (zero heat flux).

3.4.2 PVT Model validation

Outlet fluid temperature of the PVT was determined and compared to Yazdanifard et al. (2016). Figure 3-12 shows that outlet water temperature in this study followed the same trend compared to Yazdanifard et al. (2016) with a maximum relative error of 0.56 %. This validation clarified that the 3-D CFD model provides accurate results in predicting outlet temperature compared to the literature which reached the range of 5.2-30 % (Rangababu et al. 2015; Gunjo et al. 2017).

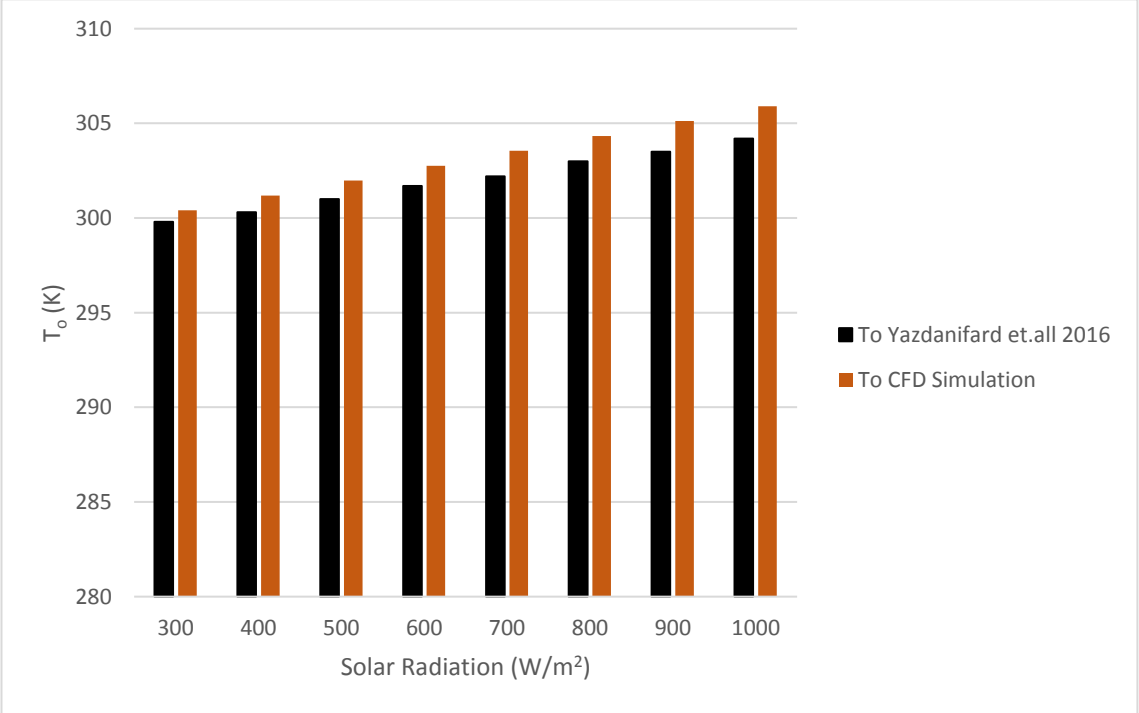

Figure 3-12 The validation of outlet fluid temperature of the PVT-CFD model.

Average temperature of the PV sheet was determined and compared to Yazdanifard et al. (2016). Figure 3-13 shows that the temperature of the PV followed the same trend as Yazdanifard et al. (2016) with a maximum relative error of 0.22 %.

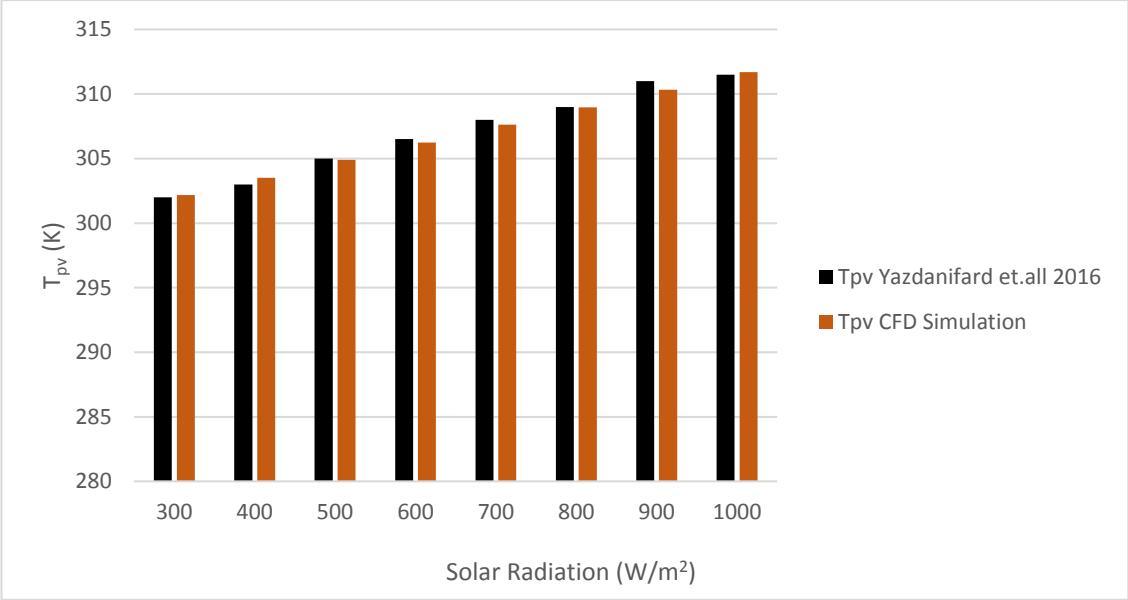

Figure 3-13 The validation of average PV temperature.

3.5 Mathematical model performance of PVT

In order to study the effect of PVT systems on the performance (the effect of the number of panels that are connected in series), a mathematical model of PVT was presented. To find out the performance of the PVT module, the performance of PVT are presented in this section, which includes thermal and electrical efficiency.

3.5.1 Mathematical thermal performance

The assumptions applied to the mathematical PVT model in this section, which were employed by Duffie and Beckman (1980) for FPC, were:

- Steady state performance.
- There is no absorption of heat by the cover.
- One directional heat flow through layers.
- Properties are independent of temperature.

Thermal efficiency is determined as described in the FPC section (equation 3-14):

$$\eta_{th} = C_p \dot{m} \frac{T_o - T_i}{G \; A_c}$$

Useful energy is calculated as describes in the FPC section (equation 3-17):

$$Q_u = F_R A_c [\alpha\tau G - U_L (T_i - T_a)]$$

PVT outlet fluid temperature (T_o) is written as in the FPC section (equation 3-18):

$$T_o = T_i + \frac{Q_u}{m \cdot Cp}$$

3.5.2 Mathematical electrical performance

The method that is widely used in the literature to calculate PVT electrical performance is to calculate the maximum current power and voltage especially for experimental projects (Chow 2010; Bahaidarah et al. 2013; Aste et al. 2014). PV needs to be connected to an electrical load to measure or calculate the value of voltage and current in order to determine electrical efficiency. The method used in this section was to calculate electrical performance based on the average temperature of the PV layer.

By applying energy balance to the PV layer, PV cell temperature (T_{cell}) can be written as in equation 3-22 (Bahaidarah et al. 2013):

$$T_{cell} = \frac{\alpha\tau G + U_T T_a + U_T T_{bs}}{U_t + U_T} \qquad (3\text{-}22)$$

The back surface of Tedlar temperature (T_{bs}) can also be written as in (Bahaidarah et al. 2013):

$$T_{bs} = \frac{h_{p1}\, \alpha\tau G + U_T T_a + h_f T_f}{U_{tT} + h_f} \qquad (3\text{-}23)$$

Where:

- h_f: Convective heat transfer coefficient inside the water duct (W/ m^2).
- T_f: Fluid Temperature (K).
- U_{tT}: The overall heat transfer coefficient from glass to Tedlar through solar cell (W/m^2 K).
- U_T: The overall heat transfer coefficient from solar cell to flowing water (W/m^2 K).

- h_{p1}: Penalty factor due to the presence of solar cell material, glass and EVA.

Electrical efficiency is then determined by knowing the reference cell efficiency (η_o) and reference cell temperature (T_{sc}) as in equation 3-21 which is discussed in the PVT modelling system (Evans 1981, Hosseinzadeh et al. 2018):

$$\eta_{ele} = \eta_o[1 - \beta\ (T_{sc} - 298\ K)]$$

Output electrical power ($\dot{E_{PV}}$) is written as in equation 3-24:

$$\dot{E_{PV}} = \eta_o\ A_m\ G \qquad (3\text{-}24)$$

3.5.3 Experimental setup to validate the mathematical methods for PVT

The parameters of the PVT and the weather data were mainly taken from the experiment conducted by Bahaidarah et al. (2013). Some parameters, which included U_L, U_T and U_{tT}, were assumed based on Dubey and Tay (2014) theoretical model. In this study the inlet temperature was assumed to be less than ambient temperature and the fluid temperature T_f was assumed to be $(T_i + T_o)/2$. PV cell temperature was predicted during the day by the mathematical model and validated with the experimental results from the literature (Bahaidarah et al. 2013).

In order to calculate PV temperature, back surface temperature was worked out based on the PVT configuration and the model shown in Figure 3-14:

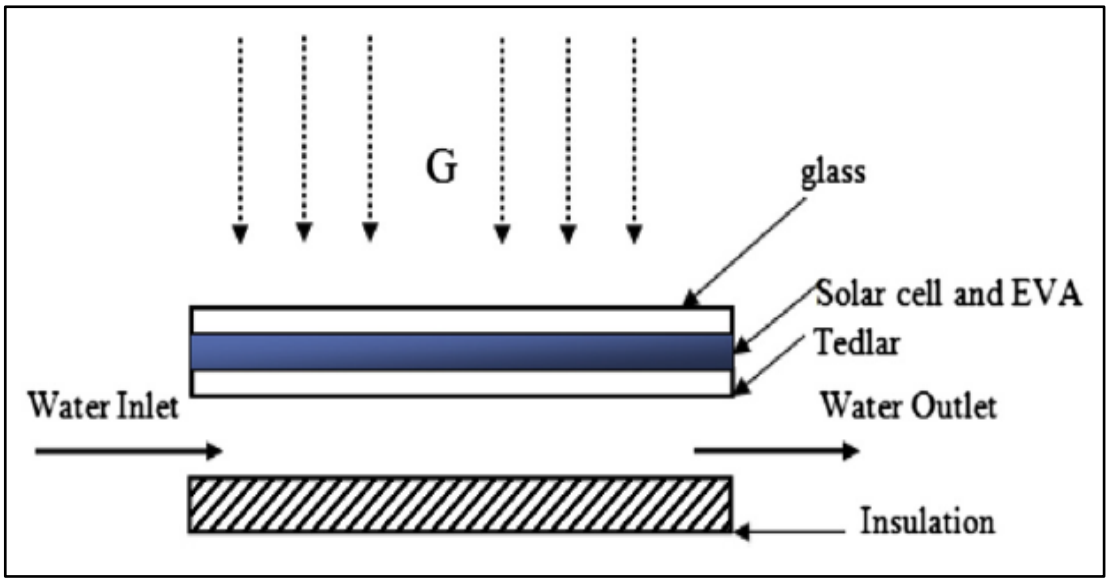

Figure 3-14 Schematic diagram PVT system (Bahaidarah et al. 2013).

Table 3-3 shows the values of design parameters used in the mathematical model of the PVT.

Table 3-3 The values of design parameters used in the mathematical model.

Parameter	**Value**	**Parameter**	**Value**
A_c [m^2]	1.24	h_T [W/m^2 k]	45
C_p [J/kg k]	4190	hp_1	0.954
L_g [m]	0.003	hp_2	0.854
L_{si} [m]	0.0003	α_{sc}	0.9
β_c	0.83	β_o	0.0045
F_R	0.948	η_o	0.15
$\dot{m}$ [kg/s]	0.1	τ_g	0.96
U_b [W/m^2 k]	0.84	U_T [W/m^2 k]	150
U_L [W/m^2 k]	5.81	U_{tT} [W/m^2 k]	6.81
Number of cells (Mono Crystalline)	72		

Weather data in Figure 3-15 were used in the mathematical model to determine the temperatures that affect PVT performance. This included PV cell temperature, back surface temperature and outlet water temperature, which are influenced by instant solar radiation and ambient temperature.

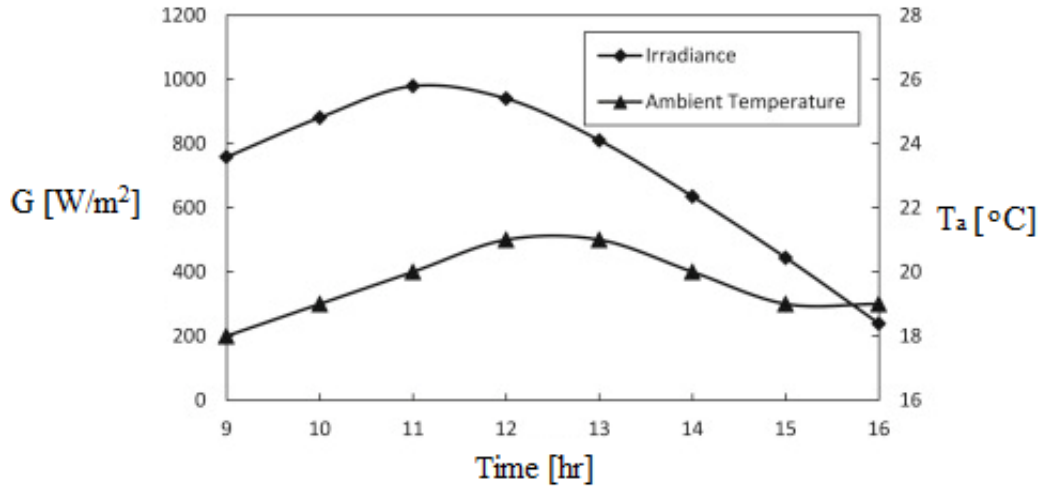

Figure 3-15 Variation of the solar radiation and ambient temperature throughout the test day (Bahaidarah et al. 2013).

3.5.3.1 Mathematical model validation

The mathematical model of the PVT was validated to the experiment from the literature (Bahaidarah et al. 2013). Figure 3-16 shows the agreement between T_{pv} for the PVT model and the experiment. Both the experimental and calculated values followed the same trend which increased during the day due to the increase in solar radiation and ambient temperature, reaching the maximum temperature at 12 pm before decreasing until the end of the day. The temperature difference between the PV cell temperatures in the mathematical model of the PVT and in the experiment was in the range of 0.3 ^{o}C to 6.5 ^{o}C.

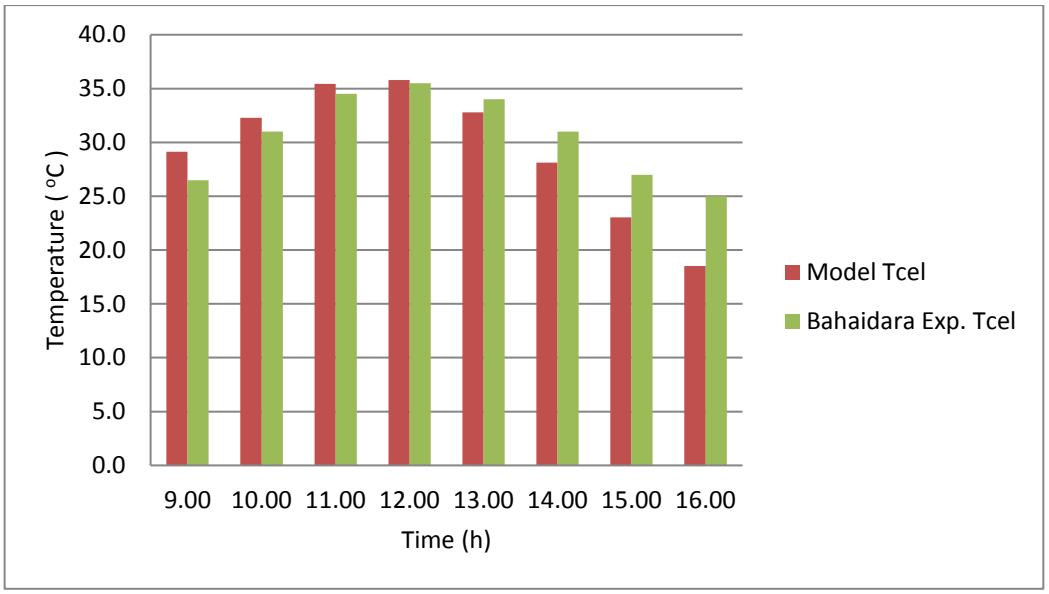

Figure 3-16 Calculated PV cell temperature (T_{cel}) vs Bahaidarah experimental data (Bahaidarah et al. 2013) (Saudi Arabia-Dhahran).

3.6 The optimisation method

Optimisation study focuses on the design parameters that significantly affected the objective of the study (Ansys 2015). In designing processes, it's important to explore the relationships between input parameters and the output. The common approach for optimisation is to vary one variable at a time, keeping all other variables in the process fixed, which might be misleading or time-consuming and may produce a false optimum condition. In order to implement an optimisation study for any system such as solar collectors, it is important to distinguish the controllable factors from the uncontrollable factors that affect performance (Antony 2014). In this study, inlet temperature and flow rate of water are considered controllable factors, while parameters such as ambient temperature and solar radiation are considered uncontrollable factors because they are environmental conditions. In order to conduct the optimisation study efficiently, controllable factors should be included as variable parameters while the uncontrollable parameters are kept as fixed values.

Figure 3-17 shows workflow for the response surface optimisation method which is considered in order to study the effect of inlet water temperature and flowrate on the performance of FPC and PVT. In ANSYS workbench, the CFD model is defined for both FPC and PVT using FLUENT. A set of controllable parameters, which included inlet temperature and flowrate, is defined in FLUENT as well as the output parameters, which included outlet temperature and average temperature of the PV. The parameters set is used as a bridge between the CFD model and the optimisation algorithm. The function of thermal efficiency and electrical efficiency are imported and defined in the parameter set in order to be controlled by the optimisation algorithm. Response surface optimisation in ANSYS workbench then linked to the parameter set. Deign of experiments type is defined (central composite design) and the lower and upper bound are specified for the controllable parameter. Based on that a set of designs point are generated automatically in ANSYS and the output of the design point based on individual simulations for each point. The design point is employed in ANSYS in order produce the response surface and generate sensitivity results. In the last section in the optimisation, multi objectives which included seeking the target outlet temperature and maximise thermal efficiency is defined. Also constrains can be added such as minimum and maximum temperature,. in the final stage, number of candidate points are generated and verified by new simulations runs.

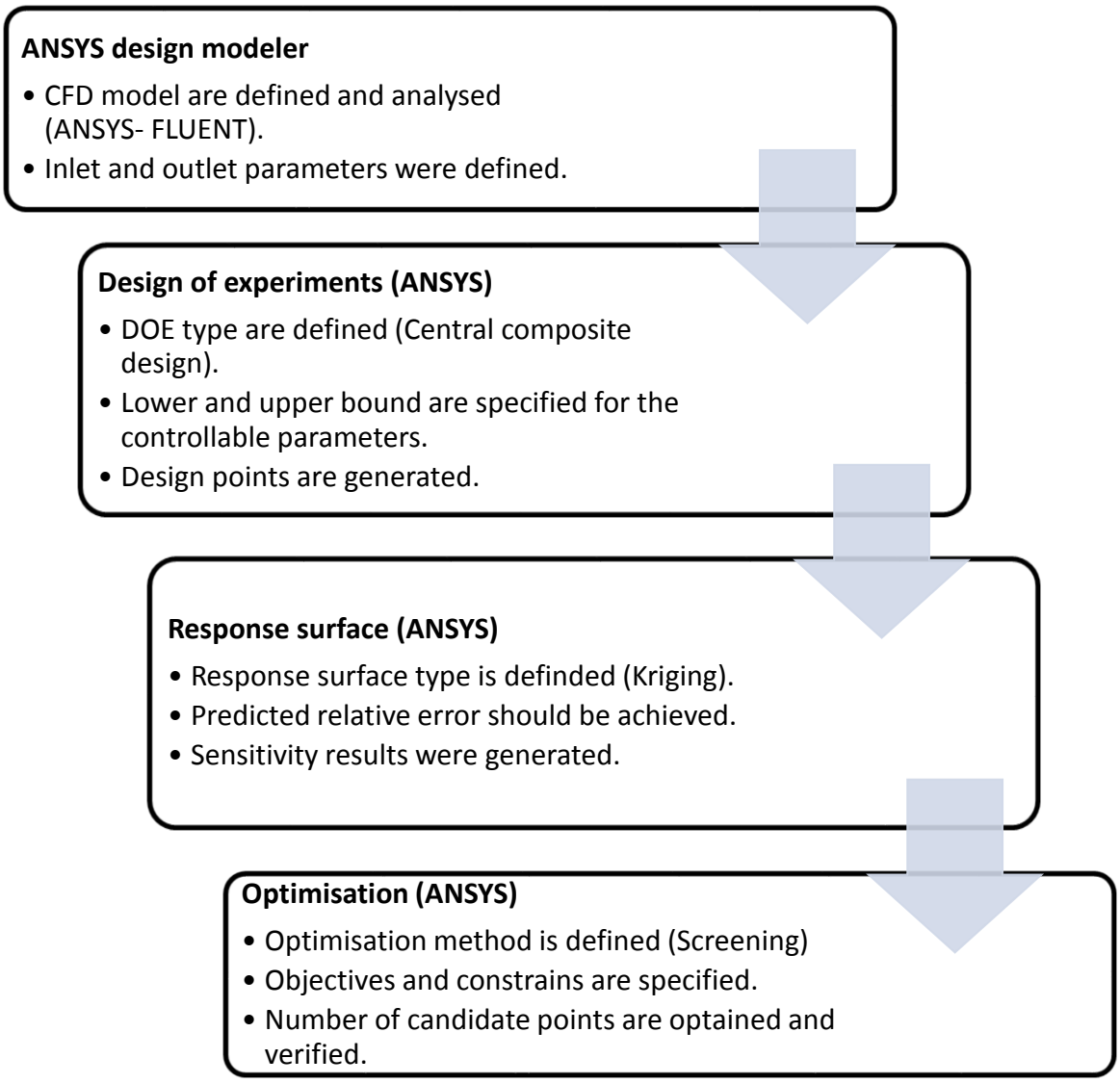

Figure 3-17 Workflow for response surface optimisation method.

3.6.1 Design of experiment (DOE)

When several parameters affected a certain output, then the design of experiment approach (DOE) would produce a trustworthy influence relationship between the input and output parameters. Some input parameters affect the outputs strongly, while the others may have lower impact, or some outputs might not be affected by some parameters. In addition, the impact of one parameter such as inlet temperature might

change when the conditions of the other parameters such as flowrate change. DOE helps to recognise the influence of the input parameters on each output parameters and then define levels for the impact of input on output (Antony 2014).

A set of input parameters of the FPC and PVT, such as inlet temperature and flowrate are generated based on the design of experiment type (DOE) and the upper and lower bounds of the parameters. DOE technique has been employed in this study to provide the design points in the domain of input parameters in order to show the effect of input parameters on the performance of the FPC and PVT. A set of design of experiment points (DOE) was generated in ANSYS in accordance with the design parameters of the PVT. A central composite design method was used by Sofotasiou et al. (2016) to define DOE points for space ventilation. The central composite design method was also employed by Moghimi et al. (2015) for a two dimensional linear Fresnel reflector optimisation study. This method is employed in this study with enhanced Face-Centre type in order to provide a more efficient design point. The method also supports the use of Kriging meta-models in the response surface, which was implemented in this study. Figure 3-18 gives an example with seventeen design points for the inputs parameters of the PVT at specified inlet temperature and flowrate ranges. This explain how can input in the CFD (in the chart P20 and P21) affected the output for the 17 points. For example, the upper level in flow rate with lower level of inlet temperature would produce outlet temperature of 323.65 K and 0.828 thermal efficiency.

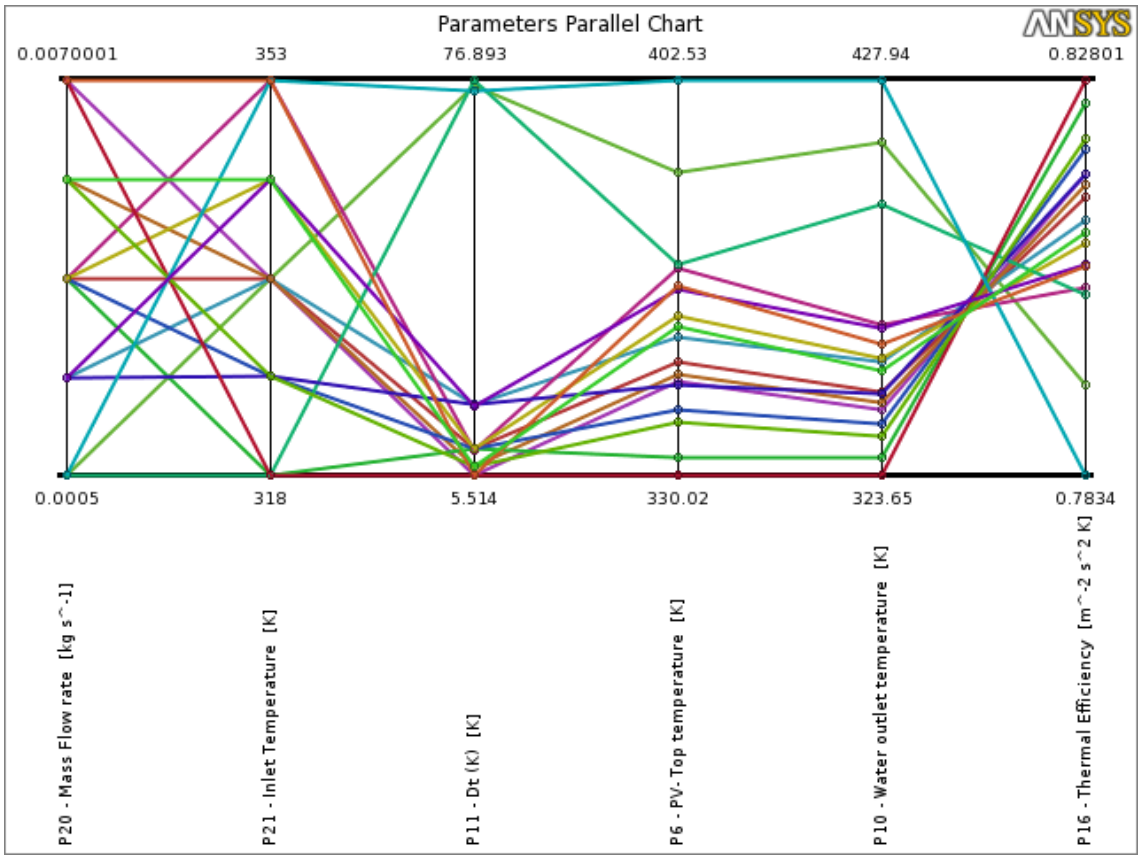

Figure 3-18 Parameters parallel chart for 17 design points and two input parameters.

3.6.2 Response surface optimisation model

In optimisation studies, the important thing is to know the interaction between the input parameters rather than the single effect of each parameter on the output. Response surface helps to recognise the relationship between input parameters and the response (the output).

Predicting response function which represent the relationship between the design parameters and the response is obtained by employing a regression model approach. A regression model take the following form (Antony 2014):

$$y = \beta_0 + \beta_1 x_1 + \beta_2 x_2 + \cdots + \beta_{12} x_1 x_2 + \beta_{13} x_1 x_3 + \varepsilon \qquad (3\text{-}25)$$

Where β_0 is the average response (from the observed results), β_1, β_2 ... are the regression coefficients, and ε is the random error.

Kriging meta-models are considered in this study which interpolates the DOE points to improve the accuracy of response surfaces. This type of response surface was used by Mwesigye et al. (2015) for a multi-objective optimisation study of a parabolic trough receiver with predicted relative error of 5%. Kriging model was also used for a multi-objective optimisation of a solar air heater as in Kulkarni et al. (2015) and in Moghimi et al. (2015) for a 2-D optimisation study of a linear Fresnel reflector. In this study, automated refinement, which improves the accuracy of the response surface by adding extra design points, was applied to create the response surface. Figure 3-19 shows an example of a response surface charts designed for a PVT optimisation study using ANSYS16.1.

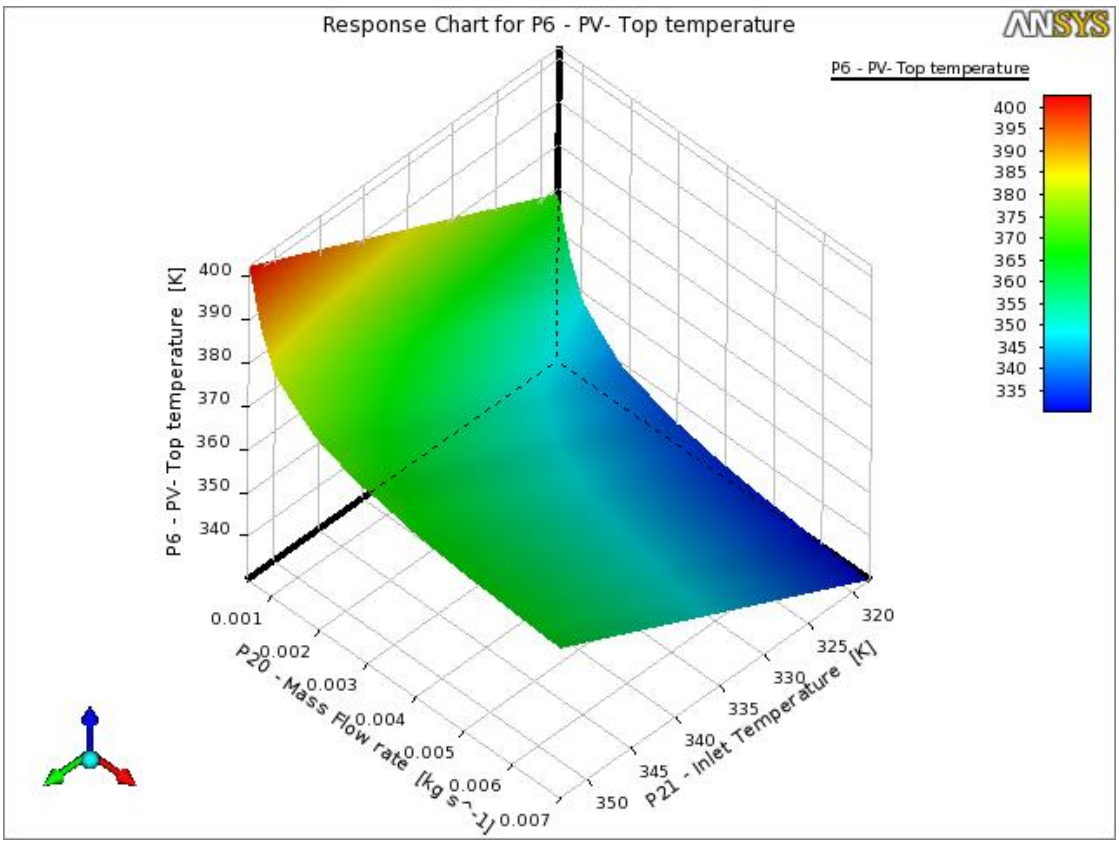

Figure 3-19 Response chart for the average photovoltaic temperature of the PVT.

The screening optimisation method, which uses an approach based on sampling and sorting, is considered in this study. The method was used by Sofotasiou et al. (2016) and supports multiple objectives and constraints as well as all types of input parameters.

3.7 Summary

This chapter presented the CFD theory to solve governing equations for fluid flow, which is intended for use in the investigation in this study. Flat plate collector (FPC) configuration and boundary conditions were described. The computational method (FLUENT) to determine thermal performance of FPC, which included thermal efficiency, useful energy and outlet fluid temperature, was presented and validated with an experiment from literature. Furthermore, photovoltaic thermal collector (PVT) configuration and the boundary conditions were presented. The computational method (FLUENT) to determine thermal and electrical performance was highlighted and validated to an experiment from the literature. In addition, mathematical, thermal and electrical performance were presented and validated for use in investigating the impact of PVT systems (the effect of the number of panels that are connected in series).

Finally, the multi-objective optimisation method employed in this investigation was presented. Response surface optimisation in ANSYS16.1, which is intended to optimise inlet conditions of the FPC and PVT, was discussed.

Chapter 4. Results and Discussion (FPC and PVT)

4.1 Introduction

In this chapter, the effect of inlet temperature on thermal efficiency for the FPC and PVT, which is the second objective in the study, was investigated. Also investigated was the effect of flow rate on thermal efficiency for FPC and PVT, which is the third objective of the study. The computational FPC and PVT models which were discussed in sections 3.3 and 3.4 are presented in order to achieve the objectives. The mathematical model of PVT, which was discussed in section 3.5, was employed in this chapter to study the effect of the PVT system on overall performance, in order to achieve the fourth objective.

A computational investigation using the CFD model of the FPC was presented in section 4.2, which investigated the effect of flow rate on FPC performance at high and low levels of inlet temperature. In addition, the effect of inlet temperature on FPC performance at high and low levels of flow rate was investigated. A computational investigation of PVT was employed to determine thermal and electrical performance in section 4.3. The effect of flow rate on PVT performance at high and low levels of inlet temperature was investigated. Also investigated was the effect of inlet temperature on PVT performance at high and low levels of flow rate. In section 4.4, the mathematical model of the PVT was employed to study the effect of the PVT system on overall performance.

4.2 Computational FPC investigation

The benchmark model of the FPC, which was discussed in section 3.3.3, is employed in this section. The validated CFD model was also employed in this section to study the effect of flow rate on the performance of FPC at high and low levels of inlet temperature. Inlet temperature was also examined at high and low levels of flow rate. The investigation determined thermal efficiency of the FPC and predicted outlet temperature accurately. The output from the CFD model is utilised to establish a new efficiency curve and equations for calculating thermal efficiency for FPC at low and high levels of flow rate in order to generalise the results in this study for other conditions.

4.2.1 Temperature distribution along the riser pipes and the absorber plate

As in Figure 4-1, the absorber temperature of FPC increased from the inlet to the outlet due to the incident solar heat flux by approximately 26 k. 5 K was the deviation of the temperature across the width of the absorber plate between riser and riser. The input parameters of the FPC were based on the real weather data (ambient temperature and solar radiation) and inlet water at 11.00 pm as was illustrated in Figure 3-8 in section 3.3.3.

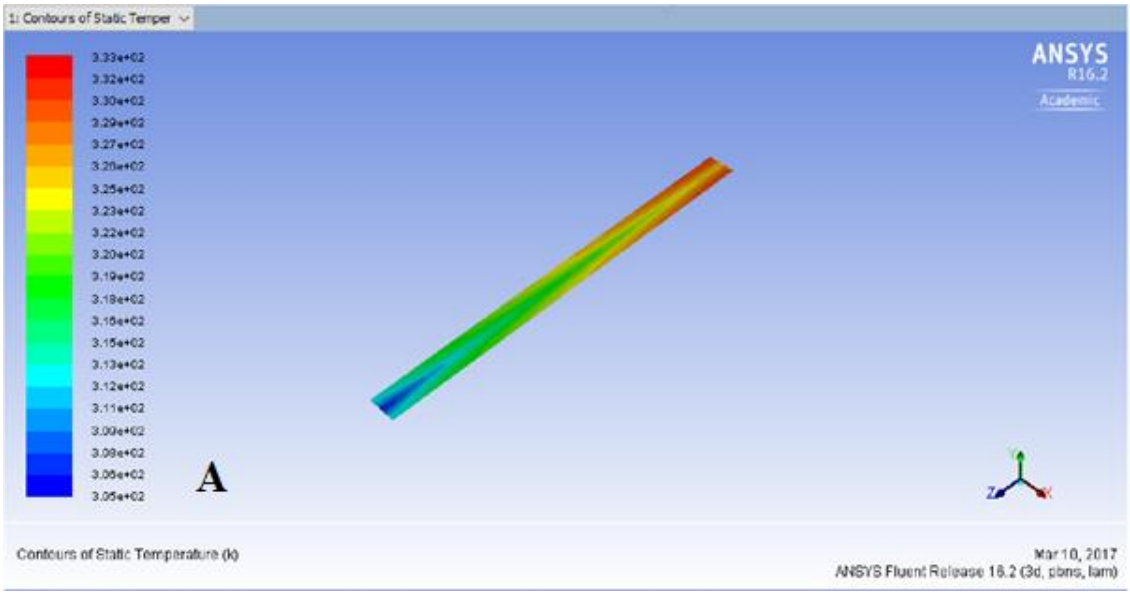

Figure 4-1 Simulated absorber plate at the top surface at 11:00 h.

In addition, Figure 4-2 shows temperature distribution along the riser pipes of the flat plate collector. The water stream entered the FPC towards the z-axis (-z). Water temperature in the riser pipe increased from inlet temperature (T_{in}), due to heat transfer from the absorber plate to the fluid, and reaches the maximum at the outlet.

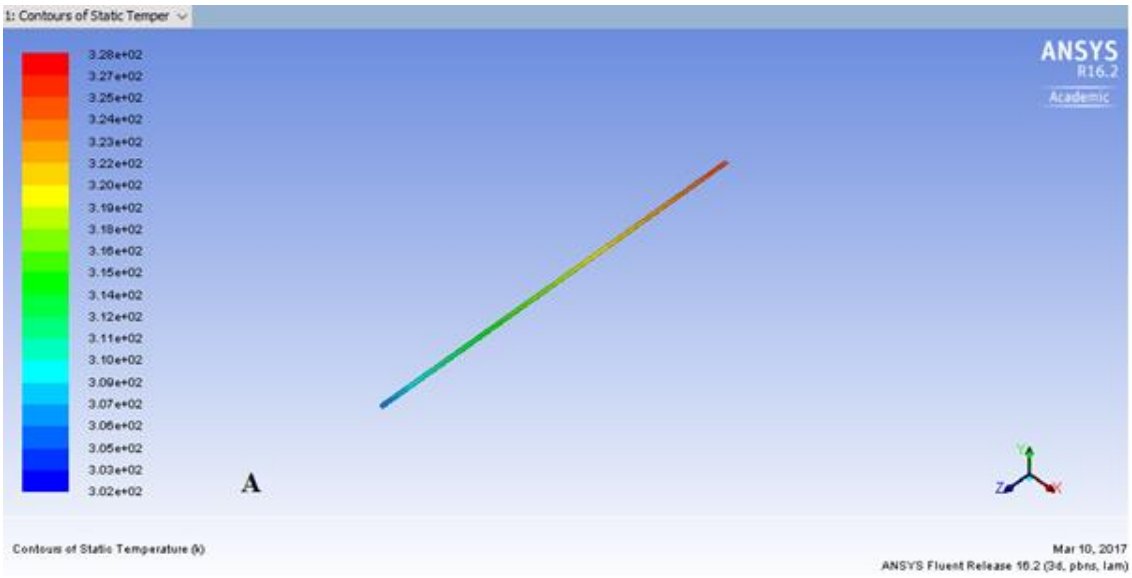

Figure 4-2 Variation of water temperature along the riser pipe at 11:00 h.

4.2.2 Effect of flowrate on FPC performance at high and low level of inlet temperature

The effect of inlet flowrate on useful energy, thermal efficiency, outlet fluid temperature and the temperature rise (T_o-T_{in}) was studied. All parameters such as solar radiation (G=1000 W/m^2), ambient temperature (T_{amb}=298 K) and inlet temperature (T_{in} =298 K if it is not mentioned) were taken as constant input parameters. The maximum flowrate under the geometry of the FPC to keep the flow at laminar regime was 0.0225 kg/s (Re= 2300) which is the maximum flowrate (in each riser) in this investigation.

There was a suggestion of an interaction between the inlet temperature and flowrate. The impact of flowrate at low inlet temperature might be changed at high level inlet temperature and vice versa. Therefore, the impact of flowrate need to be studied at more than one level of inlet temperature. The effect of flowrate on the performance of the FPC in this section was investigated at Low-Level (T_{in} = 298 K) and High-Level (T_{in} =370 K) inlet temperature.

Figure 4-3 shows the impact of inlet flowrate on thermal efficiency at high and low levels of inlet temperatures. It can be observed that the significant impact of the mass flowrate on thermal efficiency occurred at the range of $\dot{m}$ =5 x10^{-4} kg/s to $\dot{m}$ =60 x10^{-4} kg/s inside

each riser pipe. Therefore, in the following discussion, the impact of flowrate will be investigated in this range.

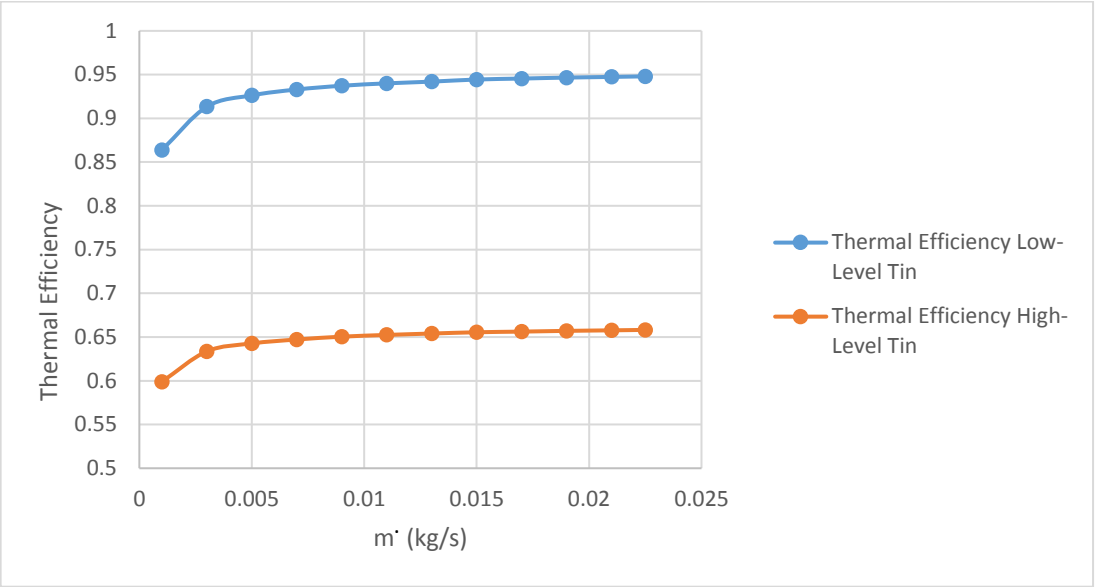

Figure 4-3 The effect of inlet flowrate on thermal efficiency at Low-Level and High-Level inlet temperature.

Figure 4-4 illustrates the effect of inlet flowrate on the useful energy per square meter of the absorber plate (Q_u /m^2). At Low-Level inlet temperature, useful energy increased with increasing mass flowrate due to the increase of surface heat transfer coefficient between the pipe and the water. A maximum useful energy of 930 W/m^2 occurred at the maximum flowrate inside the riser pipe ($\dot{m}$ =60 x10^{-4} kg/s), while the minimum of 800 W/m^2 occurred at the minimum flowrate (5 x10^{-4} kg/s). At High-Level inlet temperature, useful energy increased with the increase in mass flowrate while the gradient decreased with the increase of flowrate. At all cases of flowrate, the useful energy was lower than that at Low-Level inlet temperature, as the bulk temperature (T_f) was higher, which decreased heat transfer from the absorber to the fluid and increased losses to the environment. A maximum useful energy of 646 W/m^2 occurred at the maximum flowrate ($\dot{m}$ =60 x10^{-4} kg/s) while the minimum of 555 W/m^2 occurred at the minimum flowrate (5 x10^{-4} kg/s).

For both Low- and High-Level inlet temperature, useful energy increased significantly for 87.1 W/m^2 and 60.5 W/m^2 respectively, with flow rate changing from 5 x10^{-4} kg/s to 15 x10^{-4} kg/s. The effect of flowrate on useful energy decreased to 20.7 W/m^2 and 14.2

W/m^2 by increasing flowrate from 15 x10^{-4} kg/s to 25 x10^{-4} kg/s while it was 10 W/m^2 and 7 W/m^2 from 25 x10^{-4} kg/s to 35 x10^{-4} kg/s respectively. The effect of flowrate on Q_u then decreased to 6.3 W/m^2 and 4.4 W/m^2 by increasing flowrate from 35 x10^{-4} kg/s to 45 x10^{-4} kg/s while it was less than 4.4 W and 3.0 W/m^2 for the same change in flowrate below 45 x10^{-4} kg/s. The gradient of useful energy decreased with the increase in flowrate, due to the decrease in contact time between the fluid and the pipe, which decreased the heat transfer to the fluid inside the pipe.

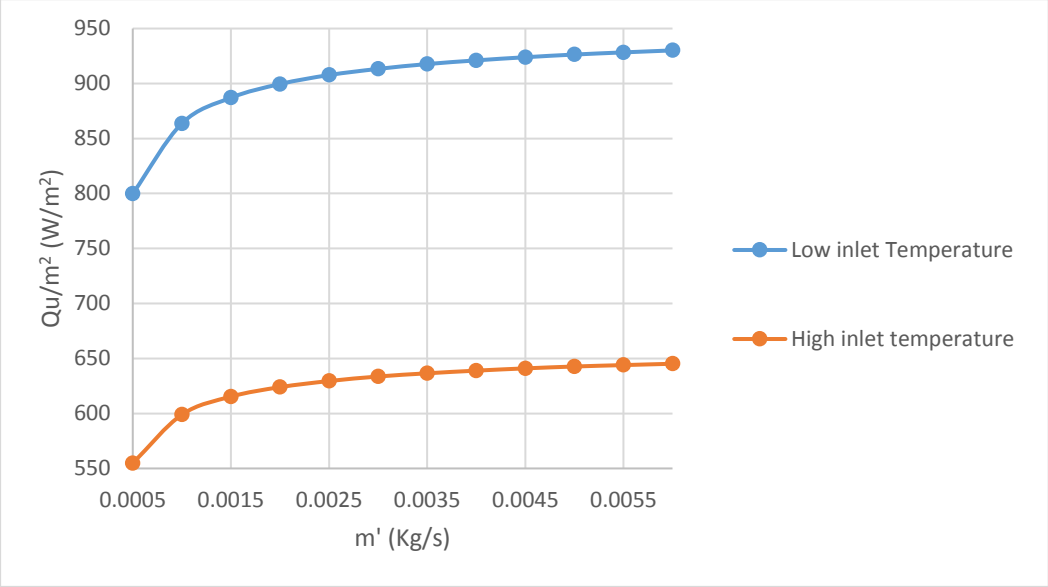

Figure 4-4 The effect of inlet flowrate on the useful energy per unit area of the absorber plate at High- and Low-Level inlet temperature.

Figure 4-5 illustrates the effect of inlet flowrate on the outlet water temperature. At Low-Level inlet temperature, outlet water temperature decreased with the increase in flowrate due to the increase in useful energy, which was explained in equation 3-18. Outlet water temperature decreased significantly for 38 K with increasing flow rate from 5 x10^{-4} kg/s to 15 x10^{-4} kg/s. The effect of flowrate on T_o decreased to 10 K by increasing flowrate from 15 x10^{-4} kg/s to 25 x10^{-4} kg/s and to 4.5 K by increasing it from 25 x10^{-4} kg/s to 35 x10^{-4} kg/s respectively. The effect of flowrate on T_o then decreased to 2.5 K by increasing flowrate from 35 x10^{-4} kg/s to 45 x10^{-4} kg/s and to less than 1.75 K for the same change in flowrate below 45 x10^{-4} kg/s. At High-Level inlet temperature, as in the Low-Level

inlet temperature, outlet water temperature decreased with increasing flowrate inside the riser pipe. Outlet water temperature decreased significantly for 27 K with changing flow rate from 5 x10^{-4} kg/s to 15 x10^{-4} kg/s which is less than the decrease at Low-Level inlet temperature. The effect of flowrate on T_o was decreased to 7 K by increasing flowrate from 15 x10^{-4} kg/s to 25 x10^{-4} kg/s and to 3 K from 25 x10^{-4} kg/s to 35 x10^{-4} kg/s respectively. The effect of flowrate on T_o then decreased to 1.3 K by increasing flowrate from 35 x10^{-4} kg/s to 45 x10^{-4} kg/s and to less than 1.2 K for the same change in flowrate below 45 x10^{-4} kg/s.

The gradient of outlet water temperature decreased with the increase in flowrate, due to the decrease in contact time between the fluid and the pipe, which decreased heat transfer from the absorber to the fluid.

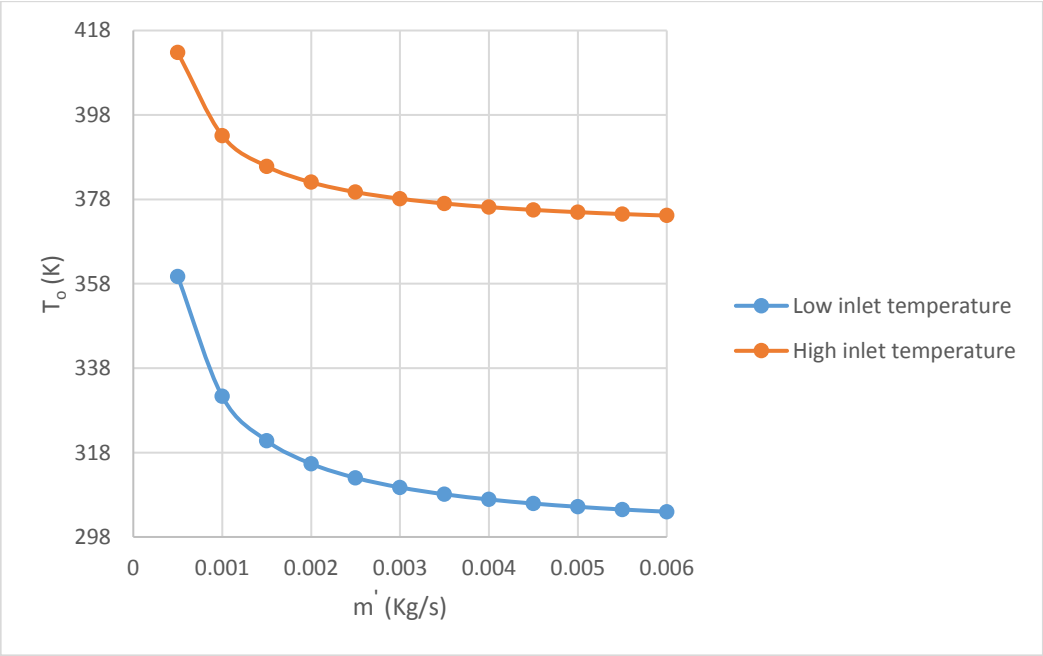

Figure 4-5 The effect of inlet flowrate on the outlet water temperature at High- and Low-Level inlet temperature.

As with the effect on T_o, both the increase in inlet temperature (T_o-T_{in}) and the gradient decreased with the increase in flowrate. A maximum increase in (T_o-T_{in}) of 62 K occurred at the minimum flowrate inside the riser pipe ($\dot{m}$=5 x10^{-4} kg/s) at Low-Level inlet temperature, while the minimum of 6 K occurred at the maximum flowrate ($\dot{m}$=60 x10^{-4} kg/s), as in Figure 4-6. As with Low-Level inlet temperature, both the increase in inlet

temperature and the gradient for High-Level inlet temperature decreased with the increase in flowrate. A maximum increase in (T_o-T_{in}) of 43 K occurred at the minimum flowrate inside the riser pipe ($\dot{m}$=5 x10^{-4} kg/s) while the minimum of 4.1 K occurred at the maximum flowrate ($\dot{m}$= 60 x 10^{-4} kg/s). For all cases of flowrate, (T_o-T_{in}) at Low-Level inlet temperature was higher than at High-Level temperature as the useful energy was higher at all cases.

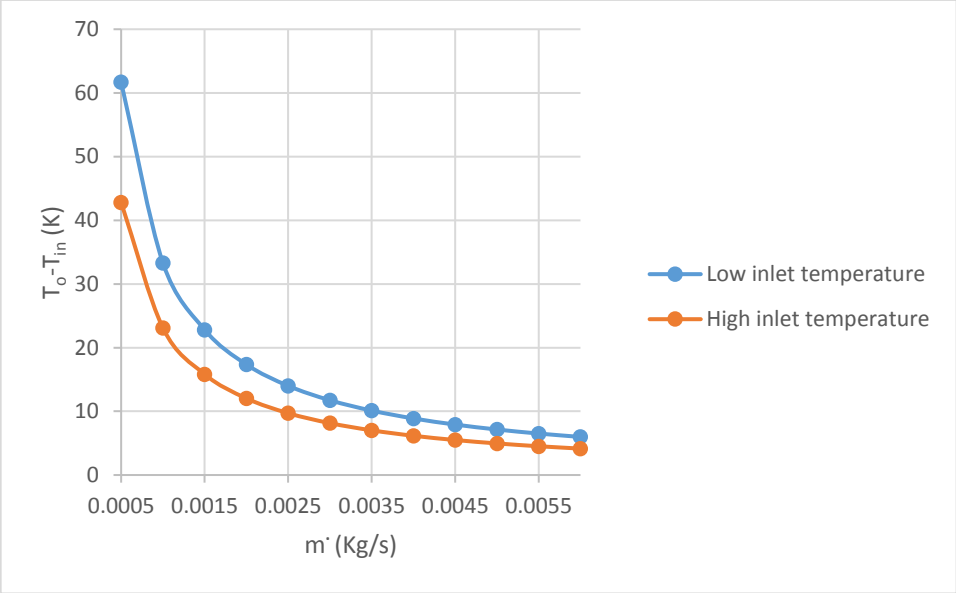

Figure 4-6 The effect of inlet flowrate on (T_o-T_{in}) at High- and Low-Level inlet temperature.

Figure 4-7 illustrates the effect of inlet flowrate on thermal efficiency (η_{th}). At low-level inlet temperature, η_{th} increased with the increase in mass flowrate due to the increase in useful energy. A maximum η_{th} of 93% occurred at the maximum flowrate ($\dot{m}$=60 x10^{-4} kg/s), while the minimum of 80 % occurred at the minimum flowrate ($\dot{m}$ =5 x10^{-4} kg/s). η_{th} increased significantly for 8.7% with increasing flow rate from 5 x10^{-4} kg/s to 15 x10^{-4} kg/s. The effect of flowrate on η_{th} decreased to 2% by increasing flowrate from 15 x10^{-4} kg/s to 25 x10^{-4} kg/s, and to 1% from 25 x10^{-4} kg/s to 35 x10^{-4} kg/s respectively. The effect of flowrate on η_{th} then decreased to 0.6 % by increasing flowrate from 35 x10^{-4} kg/s to 45 x10^{-4} kg/s, and to less than 0.4 % for the same change in flowrate below 45 x10^{-4} kg/s. At High-Level inlet temperature, η_{th} increased with the increase in mass flowrate but less than at Low-Level inlet temperature due to the increase in temperature

difference between the water inside the pipe and the ambient temperature, which leads to increased loss. A maximum η_{th} of 64.5 % occurred at the maximum flowrate ($\dot{m}$=60 x10^{-4} kg/s) while the minimum of 55.5 % occurred at the minimum flowrate (5 x10^{-4} kg/s). η_{th} increased significantly for 6% with increasing flow rate from 5 x10^{-4} kg/s to 15 x10^{-4} kg/s. The effect of flowrate on η_{th} decreased to 1.41 % by increasing flowrate from 15 x10^{-4} kg/s to 25 x10^{-4} kg/s, and to 0.7 % from 25 x10^{-4} kg/s to 35 x10^{-4} kg/s respectively. The effect of flowrate on η_{th} then decreased to 0.4 % by increasing flowrate from 35 x10^{-4} kg/s to 45 x10^{-4} kg/s, and to less than 0.3 % for the same change in flowrate below 45 x10^{-4} kg/s.

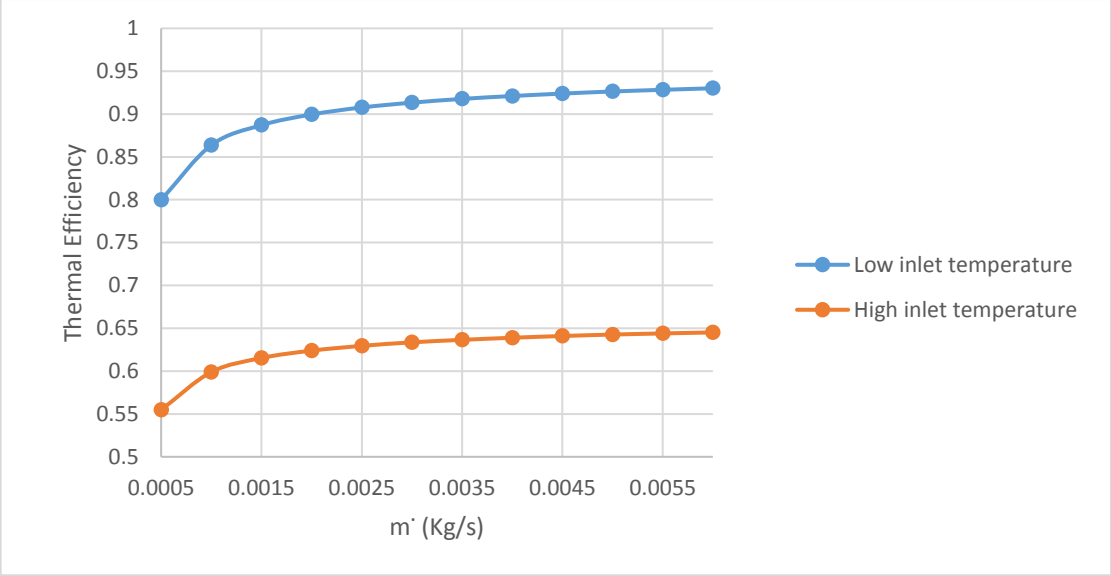

Figure 4-7 The effect of inlet flowrate on η_{th} at High- and Low-Level inlet temperature.

Achieving relatively high thermal efficiency was due to the high solar radiation and the high ambient temperature (318 K) which decreased losses from the collector. This due to the decrease in the temperature difference between the fluid inside the pipe and the ambient. In addition, the low wind velocity decreased losses by convection which improved the efficiency. Thermal efficiency of 71% was achieved at 60 ^{o}C outlet temperature (Gunjo et al. 2017) and was in the range of 70-77% (Nasrin et al. 2018).

4.2.3 Effect of inlet temperature on FPC performance at high and low level of flowrate

The effect of inlet temperature on useful energy, thermal efficiency, outlet fluid temperature and the temperature rise (T_o-T_{in}) was investigated. All parameters such as solar radiation (G=1000 w/m^2), ambient temperature (T_{amb}=298 K) and flowrate ($\dot{m}$ = 0.001 and 0.0225 kg/s) were taken as fixed input parameters. The maximum flowrate under the geometry of the FPC to keep the flow at laminar regime is 0.0225 kg/s (Re= 2300) which is the maximum flowrate in this investigation.

Outlet water temperature T_o has been examined and was found to be highly affected by inlet water temperature. There was an increase in T_o due to the increase in inlet water temperature for both High- and Low-Level flowrate. Maximum outlet temperature of 394 K for the FPC was achieved at Low-Level flowrate and the maximum inlet temperature (370 K) as in Figure 4-8.

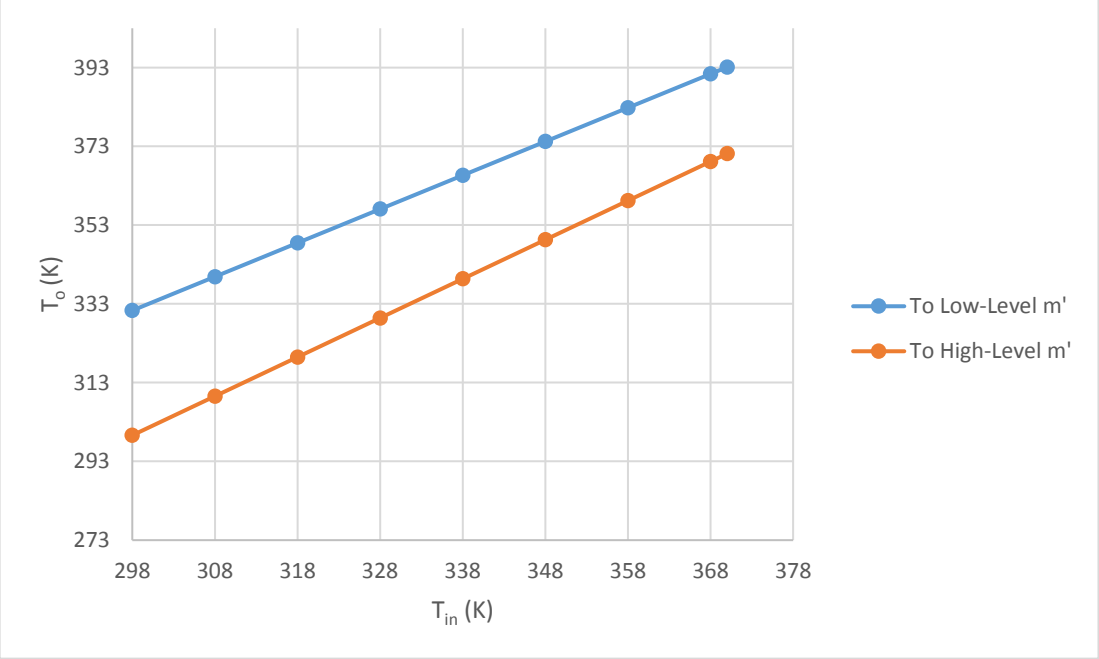

Figure 4-8 Effect of flowrate on outlet temperature of the FPC.

Figure 4-9 illustrates the fact that the inlet temperature rise (T_o-T_{in}) was highly affected by inlet temperature at Low-Level flow rate, while there was, approximately, no effect at High-Level flowrate. A maximum temperature rise of 33 K occurred at Low-Level

flowrate and minimum inlet temperature due to a high temperature difference between the absorber plate and the bulk temperature of water inside the pipe (T_p-T_f), which incresed heat transfer. At High-Level flowrate, the potential to rise the water temperature inside the pipe is also high due to the temperature difference between the absorber and water, but doesn't affect the temperature rise because of the high flowrate.

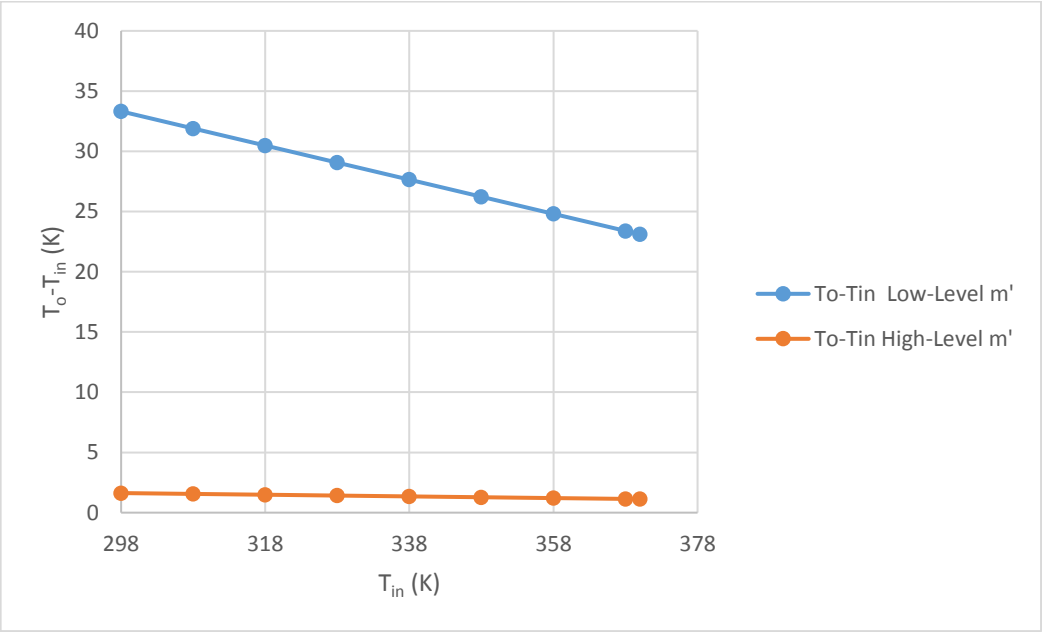

Figure 4-9 Effect of flowrate on (T_o-T_{in}) at two levels flowrate of FPC.

Thermal efficiency (η_{th}) was also examined and found to be highly affected by inlet water temperature. There was a decrease in η_{th} with the increase in inlet water temperature due to the increase in temperature difference between the water inside the pipe and the ambient temperature (T_f-T_{amb}), which increased the losses. Maximum η_{th} of 94 % for the FPC was achieved at High-Level flowrate and the minimum inlet temperature, as in Figure 4-10. Thermal efficiency at High-Level flowrate is higher than at Low-Level flowrate in all cases. In contrast, the temperature rise was higher at Low-Level flowrate for all cases. However, for any application, inlet temperature and flowrate need to be optimised in order to achieve a specified outlet temperature (T_o) with high thermal efficiency.

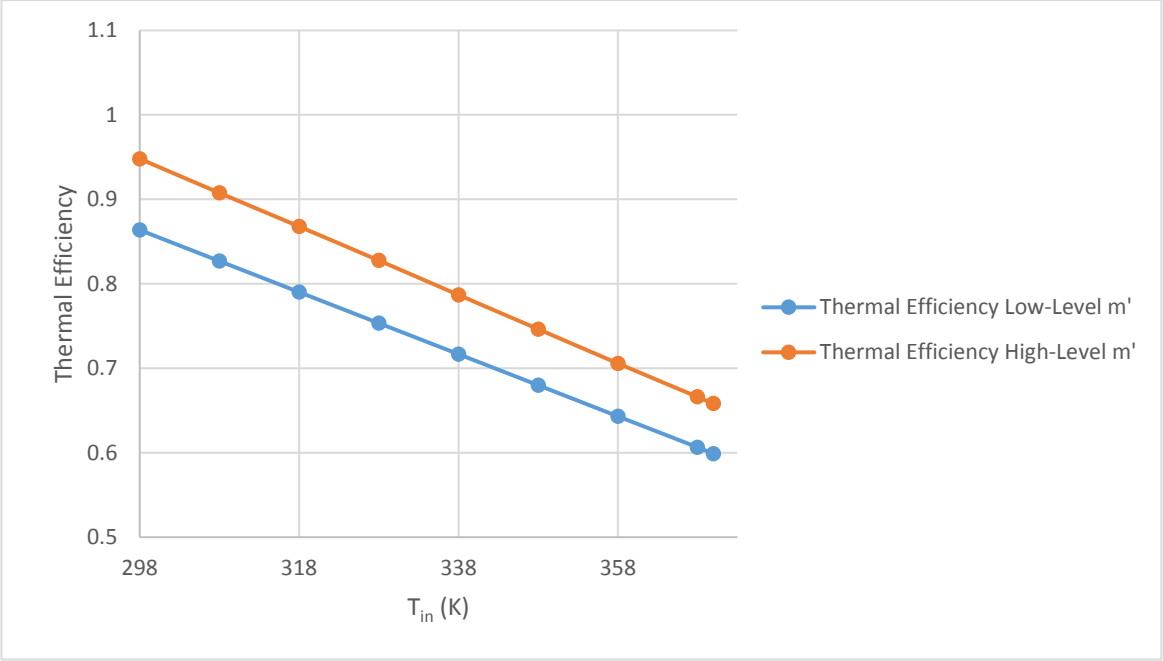

Figure 4-10 Effect of inlet water temperature on thermal efficiency of FPC.

4.2.4 Performance of FPC versus energy loss parameter

The influence of energy loss parameter $((T_i - T_a)/G)$ on FPC performance was investigated for High- and Low-Level flowrate by varying inlet water temperature. Figure 4-11 illustrates the thermal efficiency curve of the FPC for High- and Low-Level flowrate. There was a decrease in η_{th} due to the increase in energy loss parameter for both levels of water flowrate.

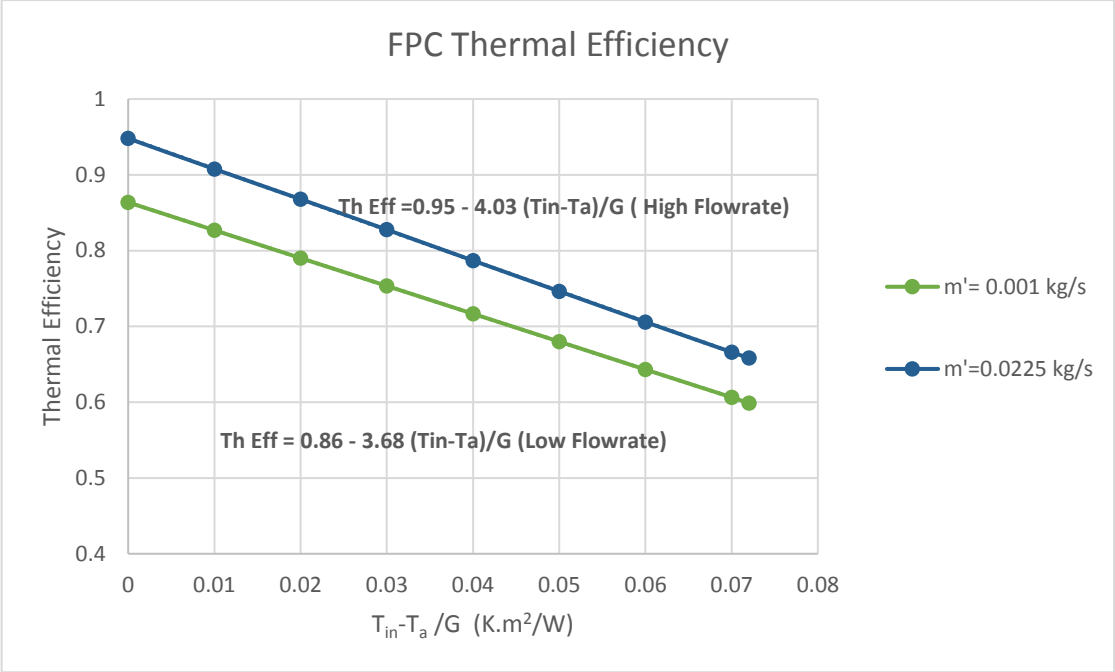

Figure 4-11 Thermal efficiency of FPC versus energy loss parameter.

Thermal efficiency equations were carried out from Figure 4-11 in order to determine the thermal efficiency of the FPC in different weather conditions. As explained in section 3.3.2 based on equation 3-19, $F_R * (\tau\alpha)$ is the intercept of thermal efficiency versus energy loss parameter and the slope is $-F_R U_L$. Based on the simulation results, equations 4-1 and 4-2 represent thermal efficiency for the Low- and High-Level flowrate respectively:

$$\eta_{th} = 0.86 - 3.68 \ \frac{\mathrm{Ti} - \mathrm{Ta}}{\mathrm{G}} \qquad (4-1)$$

$$\eta_{th} = 0.95 - 4.03 \ \frac{\mathrm{Ti} - \mathrm{Ta}}{\mathrm{G}} \qquad (4-2)$$

As explained in section 3.3.2 based on equation 3-20, theoretical maximum equilibrium temperature T_{max} was calculated for different ambient temperatures for the FPC. This temperature represents any part of the collector in the condition of no flow. In this condition, maximum theoretical equilibrium temperature (which represents any part of the collector) can be estimated. This temperature is a function of the absorbed heat by the collector (S), ambient temperature T_{amb} and heat loss coefficient U_L and given as Duffie and Beckman (1980): $T_{max} = T_{amb} + S/U_L$. Figure 4-12 shows the maximum

temperature which can be achieved by the FPC theoretically (and computationally in this study for $\dot{m}$=0), based on heat absorbed by the absorber, ambient temperature, and heat losses coefficient in this study for Low-Level flow rate (U_L=3.66 W/ m^2K). The maximum temperature of the outlet temperature can be raised 233 K above the ambient temperature.

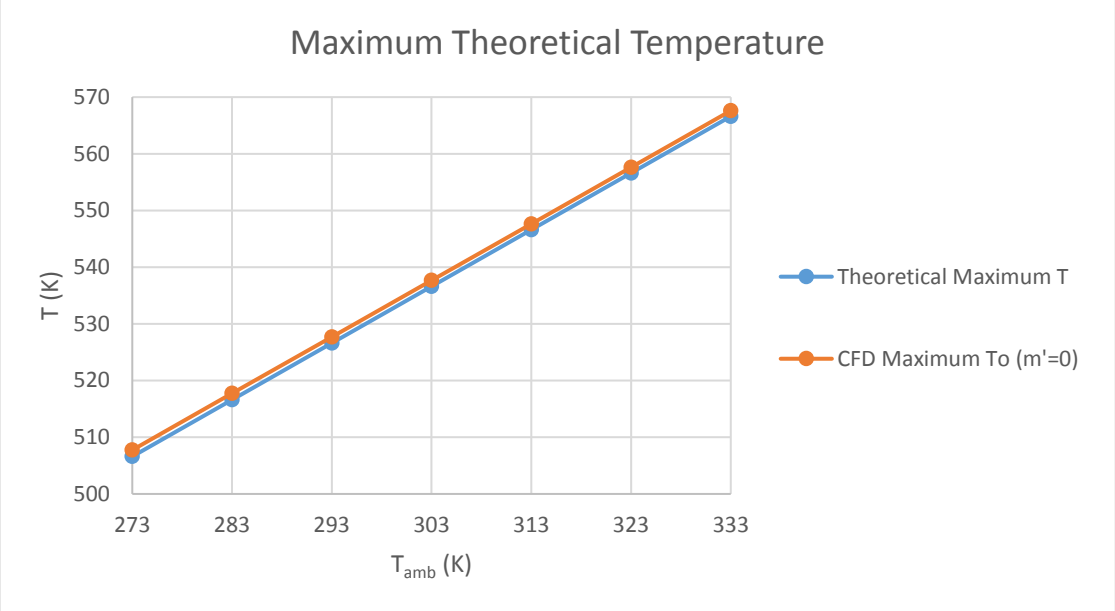

Figure 4-12 Theoretical maximum equilibrium temperature T_{max} for different ambient temperatures.

4.2.5 FPC investigation summary

In this section, the effect of inlet temperature (T_{in}) and flowrate ($\dot{m}$) on FPC performance which included efficiency(η_{th}) was investigated. The FPC was examined using the 3-D CFD model for High- and Low-Level flowrate and for different inlet temperatures, which varied from 298 K to 373 K. Thermal efficiency of 93% and 65% was achieved at 298 K and 370 K inlet temperature respectively. A maximum temperature increase (T_o-T_{in}) of 62 K in the inlet temperature was achieved at flowrate of 5 x10^{-4} kg/s inside the riser pipe. As a conclusion of this section, the heat transfer coefficient between the pipe and water increased with increasing water flowrate of the FPC, which increased useful energy. Useful energy also increased with decreasing inlet temperature due to the

increase in (T_p-T_f). In contrast, thermal efficiency decreased with the increase in inlet temperature due to the increase in (T_f-T_{amb}).

4.3 Computational PVT investigation

The benchmark model for the computational PVT model which was discussed in section 3.4.1 is employed in this section. The effect of inlet flowrate on outlet fluid temperature, thermal efficiency, electrical efficiency and average temperature of the PV were studied. All parameters such as solar radiation (G=1000 W/m^2), ambient temperature (T_{amb}=298 K if it is not mentioned) and inlet temperature (T_{in} =298 K if it is not mentioned) were taken as constant input parameters. The maximum flowrate under the geometry of the PVT to keep the flow at laminar regime is 0.02018 kg/s (Re= 2300), which is the maximum flowrate (in each riser) in this investigation.

4.3.1 Temperature distribution along the riser pipes and the photovoltaic layer

As in Figure 4-13, the temperature distribution on the photovoltaic layer increased from the inlet to the outlet due to the incident solar heat flux by 89 K. The deviation of the temperature across the width of the photovoltaic layer was approximately 5 K between riser and riser.

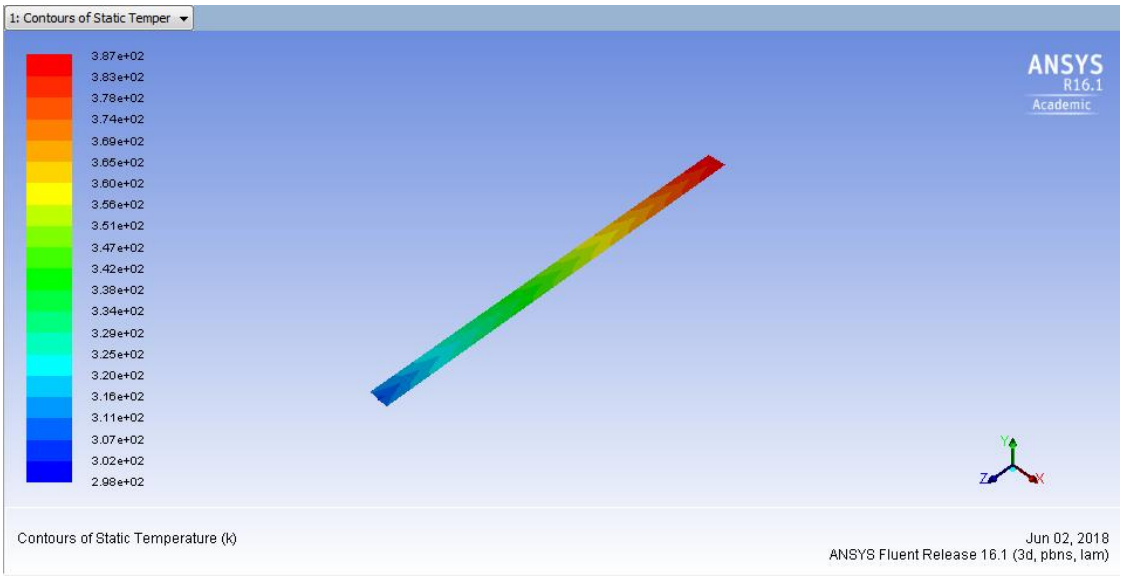

Figure 4-13 Variation of water temperature on the top of photovoltaic layer.

Figure 4-14 shows temperature distribution along the riser pipes of the PVT. The water stream entered the PVT towards z-axis (-z). Water temperature in the riser pipe increased from inlet temperature (T_{in}), due to the heat transfer from the absorber plate to the fluid, and reached the maximum at the outlet.

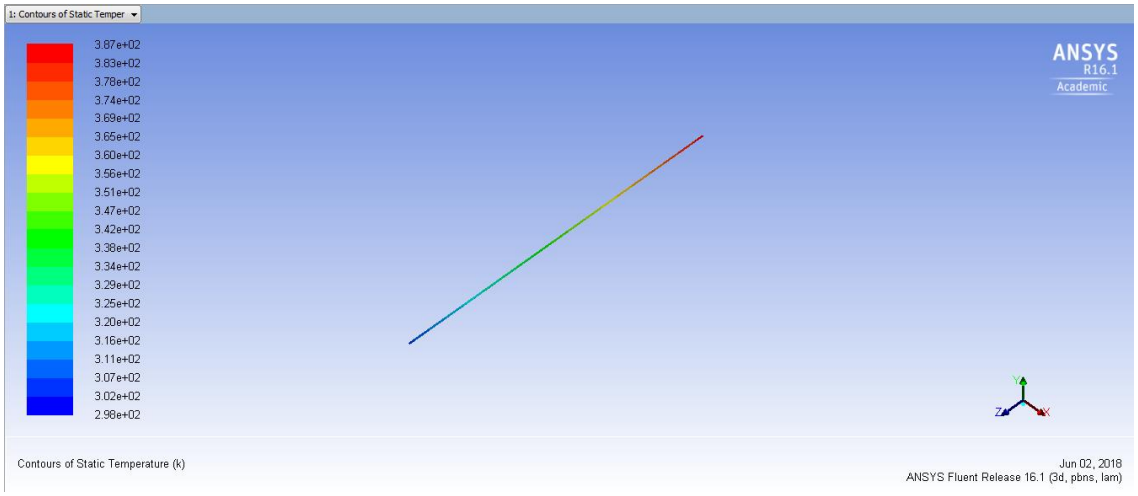

Figure 4-14 Variation of water temperature along the riser pipe of the PVT.

4.3.2 Effect of flowrate on PVT performance at high and low level of inlet temperature

The significant impact on performance of mass flow rate inside each riser pipe occurred in the range of 5 x10^{-4} kg/s to 70 x10^{-4} kg/s. Figure 4-15 shows the effect of inlet flowrate on the useful energy per square meter of the absorber plate (Q_u /m^2) for both Low-Level (T_{in}=298 K) and High-Level (T_{in}=370 K) inlet temperatures. As explained in section 4.2.2 for FPC, the useful energy increased with the increase in mass flowrate due to the increase in heat transfer coefficient between the pipe and the water. At all cases of flowrate, the useful energy for High-Level inlet temperature was lower than that at Low-Level inlet temperature, as the bulk temperature (T_f) was higher, which decreased heat transfer from the absorber to the fluid and increased losses to the environment. A maximum useful energy of 828 W/m^2 occurred at the maximum flowrate ($\dot{m}$ =95 x10^{-4} kg/s) at Low-Level inlet temperature, while the minimum of 761 W/m^2 occurred at the minimum flowrate ($\dot{m}$ = 5 x10^{-4} kg/s) at High-Level inlet temperature.

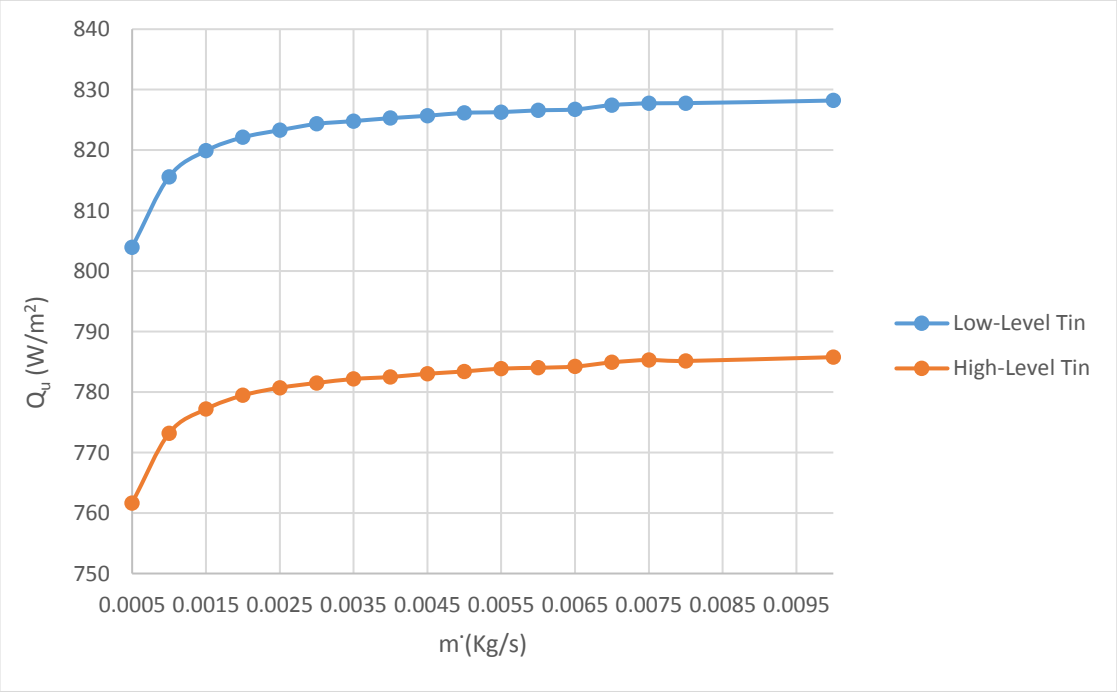

Figure 4-15 The effect of inlet flowrate on the useful energy per unit area of the absorber plate of the PVT.

Figure 4-16 shows the effect of inlet flowrate on the outlet water temperature for both Low-Level (T_{in}=298 K) and High-Level (T_{in}=370 K) inlet temperatures. Outlet water temperature decreased with the increase in flowrate due to the increase in useful energy, which was explained in equation 3-18 and section 4.2.2 for FPC. Outlet temperature for Low- and High-Level inlet temperature decreased significantly for 50 K and 48 K respectively, with increasing flow rate from 5 x10^{-4} kg/s to 15 x10^{-4} kg/s. The effect of flowrate decreased to 1 K when the flowrate exceeded 80 x10^{-4} kg/s. In addition, the increase in flowrate decreased the contact time between the fluid and the pipe, which decreased heat transfer.

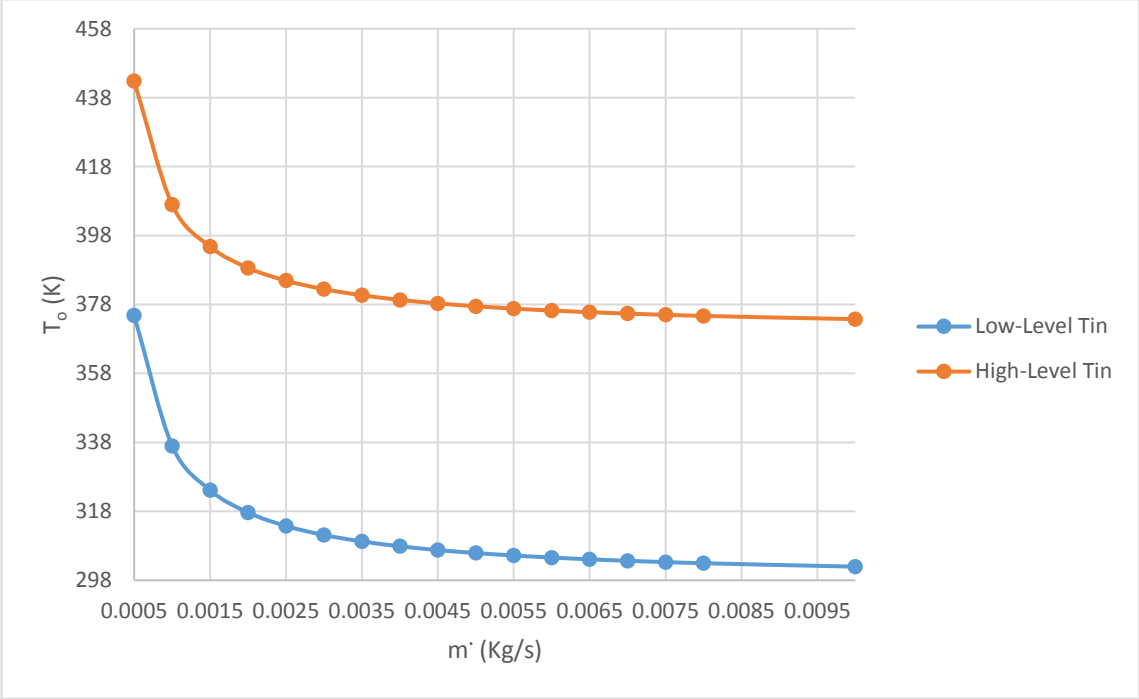

Figure 4-16 The effect of inlet flowrate on the outlet water temperature for the PVT.

For specified absorbed energy, increasing flowrate decreased the temperature rise (T_o-T_{in}). It can be observed that (T_o-T_{in}) for both High- and Low-Level inlet temperature decreased with the increase in flowrate as in Figure 4-17. A maximum increase of 76 K occurred at the minimum flowrate inside the riser pipe ($\dot{m}$=5 x10^{-4} kg/s) at Low-Level inlet temperature while the minimum of 3.7 K occurred at the maximum flowrate ($\dot{m}$=95 x10^{-4} kg/s). Similarly to FPC (As discussed in section 4.22), the gradient of (T_o-T_{in}) decreased with the increase in flowrate due to the decrease in the contact time between the fluid and the pipe, which decreased the impact on the heat transfer.

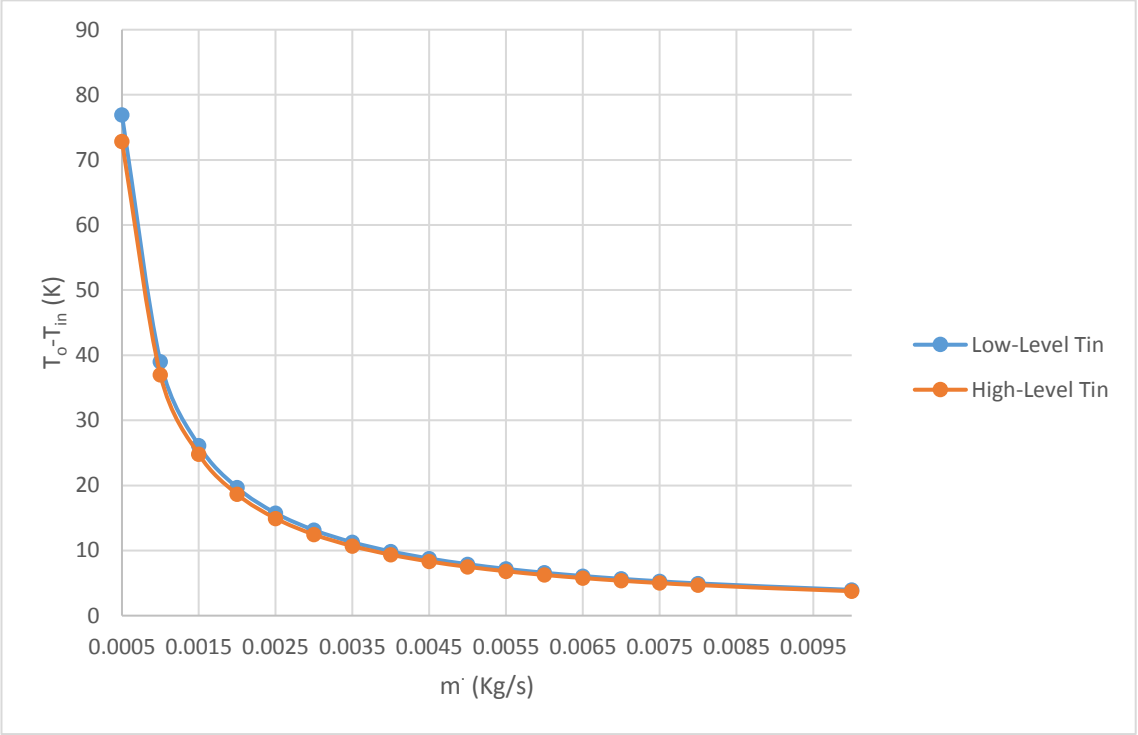

Figure 4-17 The effect of inlet flowrate on the outlet water temperature raise of the PVT.

Figure 4-18 illustrates thermal efficiency (η_{th}) at Low- and High-Level inlet temperature. η_{th} increased with the increase in mass flowrate due to the increase in useful energy (Q_u). One drawback of increasing the flow rate is that total annual cost increased due to the increase in the pressure drop, which required more power for pumping (Hajabdollahi and Hajabdollahi 2017). A maximum η_{th} of 82% and 78 % occurred at the maximum flowrate ($\dot{m}$ =95 x10^{-4} kg/s), while the minimum of 80 % and 76 % occurred at the minimum flowrate ($\dot{m}$ =5 x10^{-4} kg/s) for Low- and High-Level inlet temperature respectively. For both low and high level inlet temperature, η_{th} increased with increasing flowrate from 5 x10^{-4} kg/s to 15 x10^{-4} kg/s for 2 % and 1.5 % respectively. There was just a slight effect when the flowrate exceeded 25 x10^{-4} kg/s.

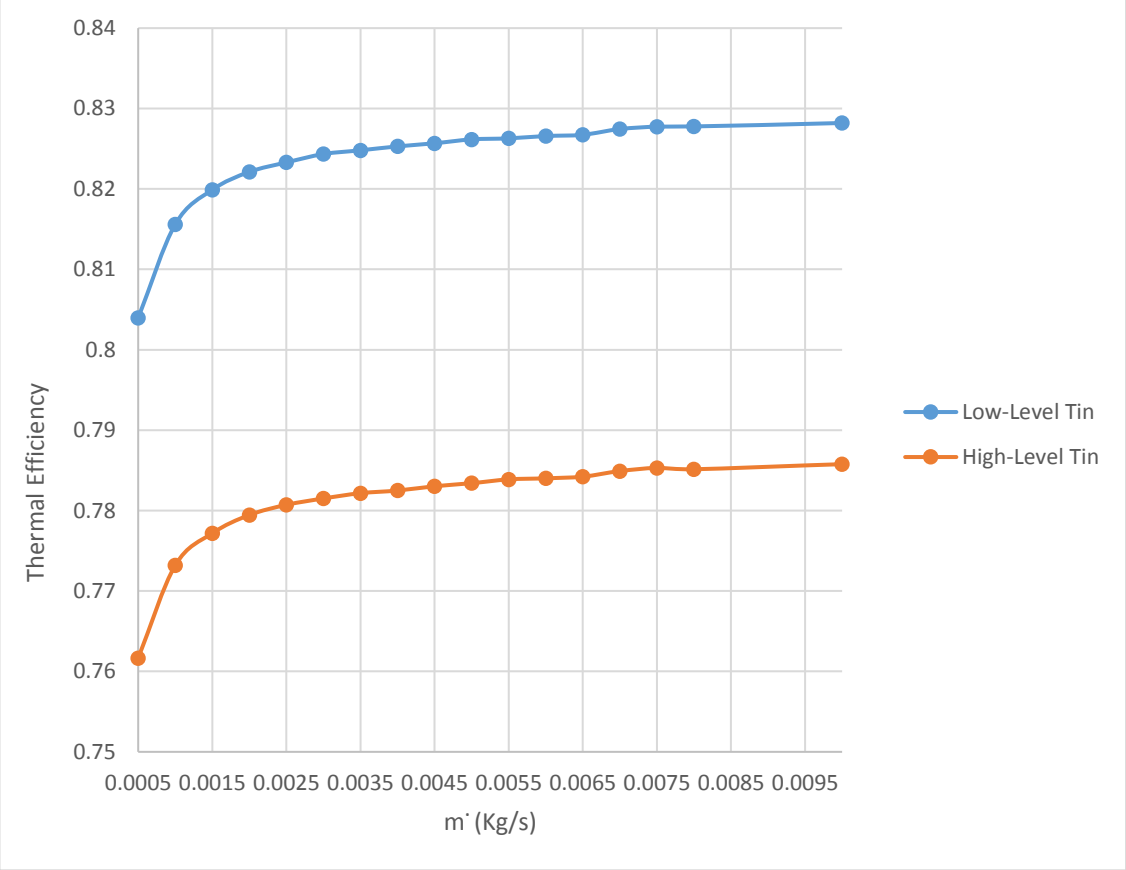

Figure 4-18 The effect of inlet flowrate on η_{th} of the PVT.

Figure 4-19 illustrates electrical efficiency (η_{elc}) at Low- and High-Level inlet temperature. η_{elc} increased with the increase in mass flowrate due to the decrease in average temperature of the PV. A maximum η_{elc} of 14.3 % and 9.5 % occurred at the maximum flowrate ($\dot{m}$=95 x10^{-4} kg/s) while the minimum of 11.6 % and 6.9 % occurred at the minimum flowrate ($\dot{m}$=5 x10^{-4} kg/s) for Low- and High-Level inlet temperature respectively. For all cases of the flowrate, High-Level inlet temperature affected η_{elc} adversely. However, for any application, inlet temperature and flowrate need to be optimised in order to achieve a specified outlet temperature with high thermal and electrical efficiency.

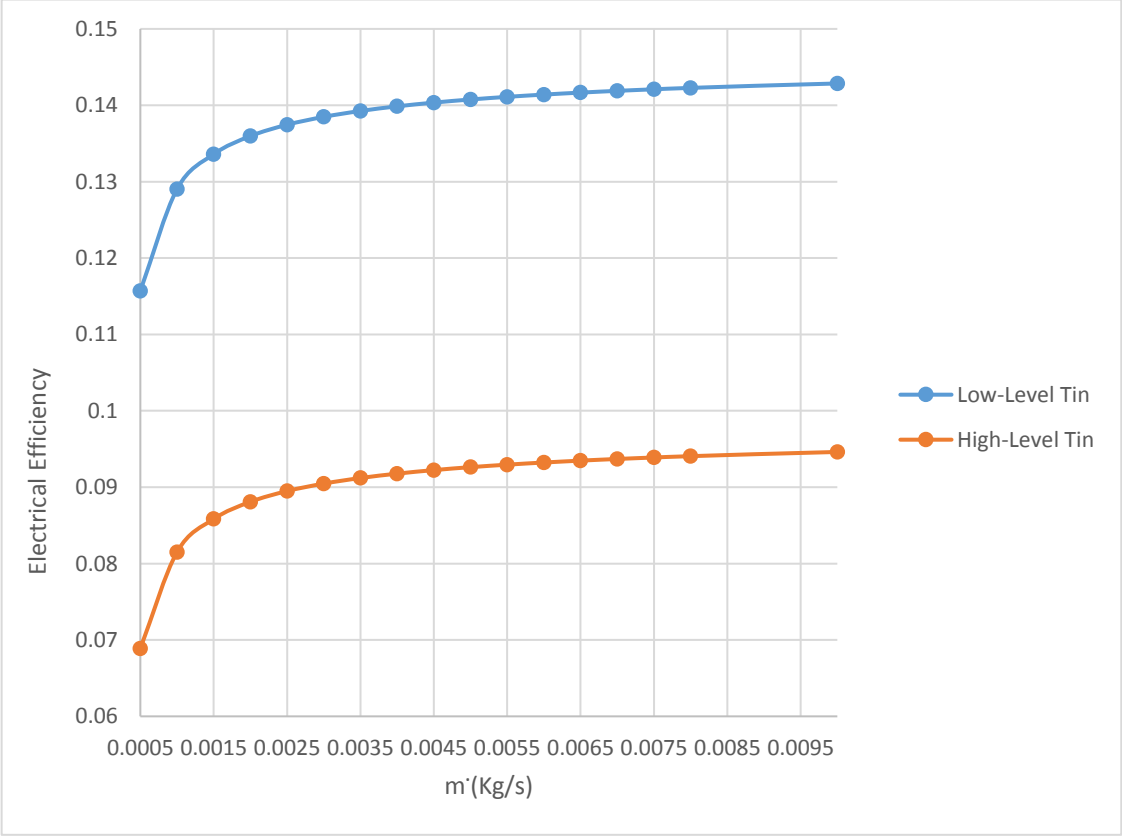

Figure 4-19 The effect of inlet flowrate on electrical efficiency of the PVT.

It is found that thermal and electrical efficiency increased with the increase in flowrate while the outlet fluid temperature decreased. On the other hand, thermal and electrical efficiency at Low-Level inlet temperature was higher than that at High-Level, while the outlet water temperature was lower; hence multi-objective optimisation study is required.

Figure 4-20 shows the effect of inlet flowrate on the electrical output power per square meter of PV (E_p/m^2) at High-Level and Low-Level inlet temperature. The output power increased with the increase in mass flowrate while the gradient decreased with the increase of flowrate due to the decrease in electric efficiency, as discussed in this section. A maximum E_p/m^2 of 128 W/m^2 and 85 W/m^2 occurred at the maximum flowrate ($\dot{m}$=95 x10^{-4} kg/s) while the minimum of 104 W/m^2 and 61 W/m^2 occurred at the minimum flowrate ($\dot{m}$=5 x10^{-4} kg/s) for Low- and High-Level inlet temperature respectively.

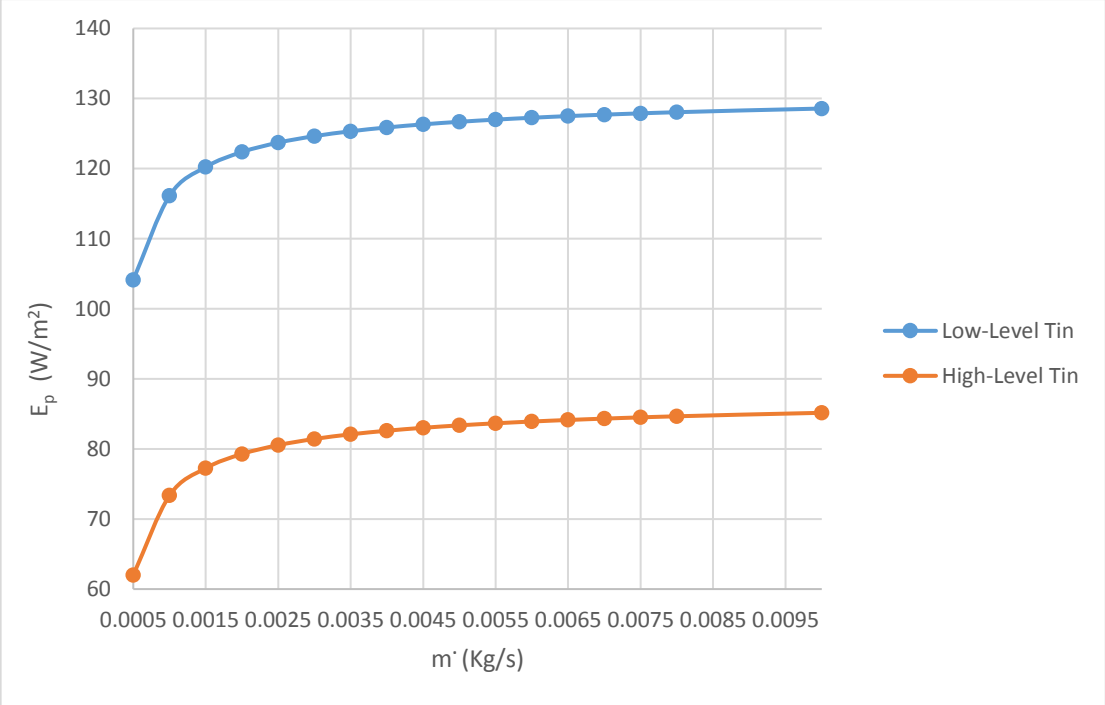

Figure 4-20 The effect of inlet flowrate on the output electrical power per unit area of the photovoltaic sheet of the PVT.

4.3.3 Effect of inlet temperature on PVT performance at high and low level of flowrate

The effects of inlet temperature on useful energy, outlet fluid temperature, the temperature rise (T_o-T_{in}) and thermal efficiency were investigated. Electrical efficiency and the output electrical power were also examined. All parameters such as solar radiation (G=1000 w/m^2), ambient temperature (T_{amb}=298 K) and flowrate ($\dot{m}$ = 0.001 and $\dot{m}$ = 0.02 kg/s) were taken as fixed input parameters. The maximum flowrate under the geometry of the PVT to keep the flow at laminar regime is 0.02018 kg/s (Re= 2300) which is the maximum flowrate (in each riser) in this investigation.

Outlet water temperature (T_o) of PVT was highly affected by inlet water temperature. There was an increase in T_o due to the increase in inlet water temperature for both High- and Low-Level flowrate. Maximum outlet temperature of 409 K for the PVT was achieved at Low-Level flowrate and the maximum inlet temperature as in Figure 4-21.

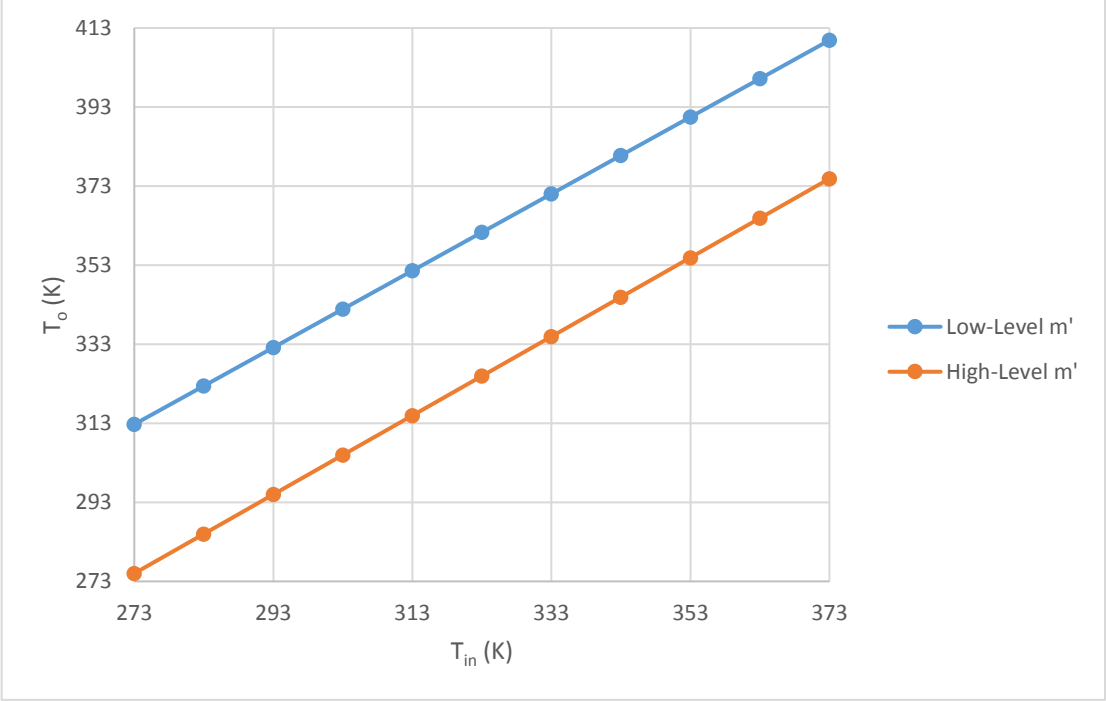

Figure 4-21 Effect of flowrate on outlet temperature of the PVT.

Figure 4-22 illustrates the fact that the inlet temperature rise (T_o-T_{in}) was highly affected by inlet temperature at Low-Level flow rate while there was approximately no effect at High-Level flowrate. A maximum temperature rise of 39.7 K occurred at Low-Level flowrate and minimum inlet temperature due to a high temperature difference between the absorber plate and the bulk temperature of water inside the pipe (T_p-T_f), which increased heat transfer. At High-Level flowrate, the potential to raise the water temperature inside the pipe is also high due to the temperature difference between the absorber and water, but didn't affect the temperature raise because of the high flowrate.

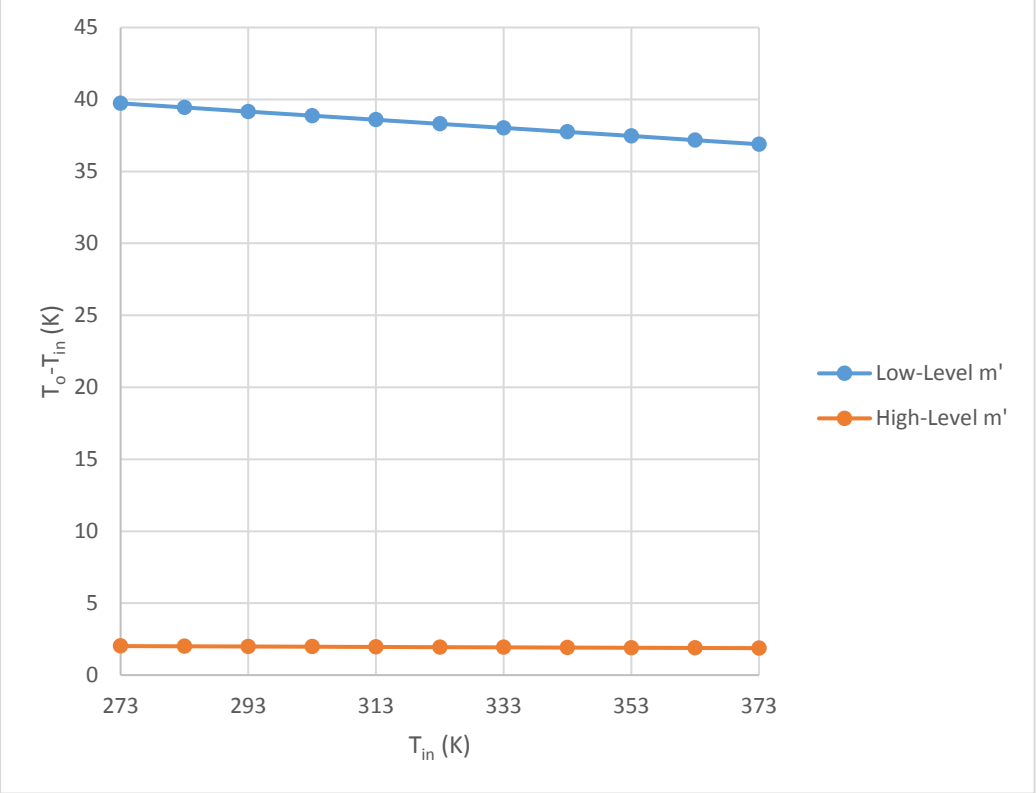

Figure 4-22 Effect of flowrate on (T_o-T_{in}) at two levels of flowrate of PVT.

Thermal efficiency (η_{th}) was also examined and found to be highly affected by inlet water temperature. There was a decrease in η_{th} with the increase in inlet water temperature due to the increase in temperature difference between the water inside the pipe and the ambient temperature (T_f-T_{amb}), which increased the losses. Maximum η_{th} of 84.3 % for the PVT was achieved at High-Level flowrate and the minimum inlet temperature as in Figure 4-23. Thermal efficiency at High-Level flowrate is higher than that at Low-Level flow at all cases. In contrast, the temperature raise was higher at Low-Level flowrate for all cases. However (as discussed in FPC section), inlet temperature and flowrate of the PVT need to be optimised in order to achieve a specified outlet temperature with high thermal efficiency.

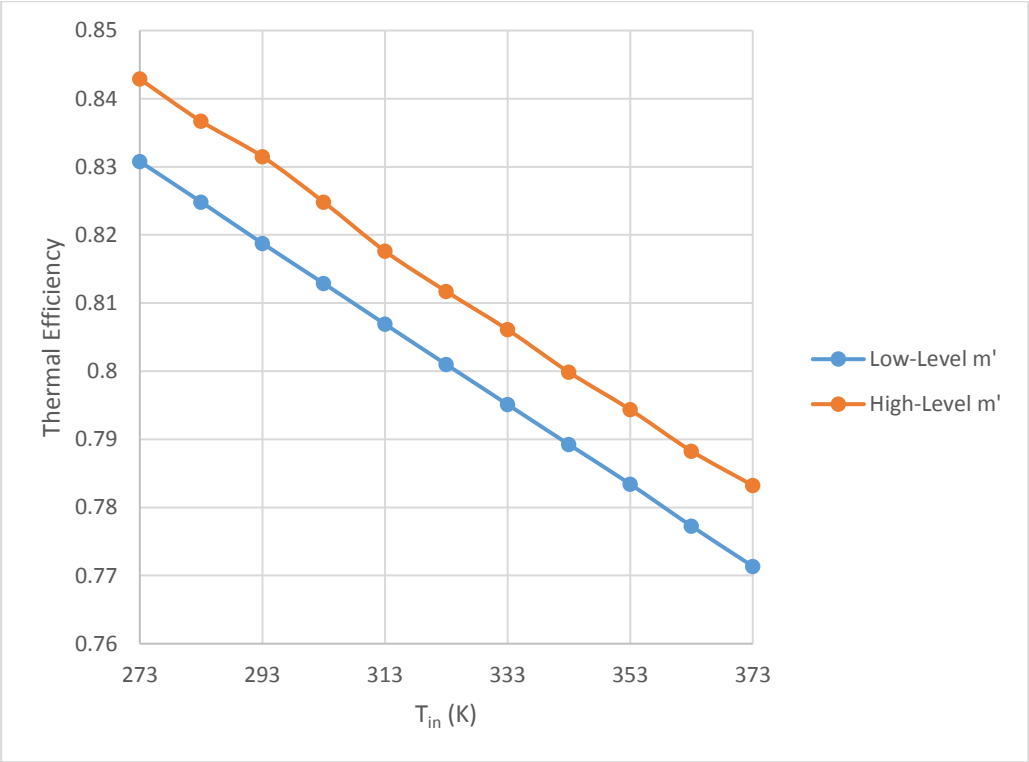

Figure 4-23 Effect of flowrate thermal efficiency of PVT.

Figure 4-24 illustrates the effect of inlet temperature on electrical efficiency (η_{elc}) at Low and High-Level inlet temperature. η_{elc} decreased with the increase in inlet temperature due to the increase in the average temperature of the photovoltaic layer. A maximum η_{elc} of 16.1 % and 14.6 % occurred at the minimum inlet temperature, while the minimum of 9.4 % and 7.6 % occurred at the maximum inlet temperature for High- and Low-Level flowrate respectively. For all cases of inlet temperature, η_{elc} at High-Level flowrate was higher than that at Low-Level flowrate due to the average temperature of the photovoltaic layer. The lower the PV temperature, the higher the electrical efficiency.

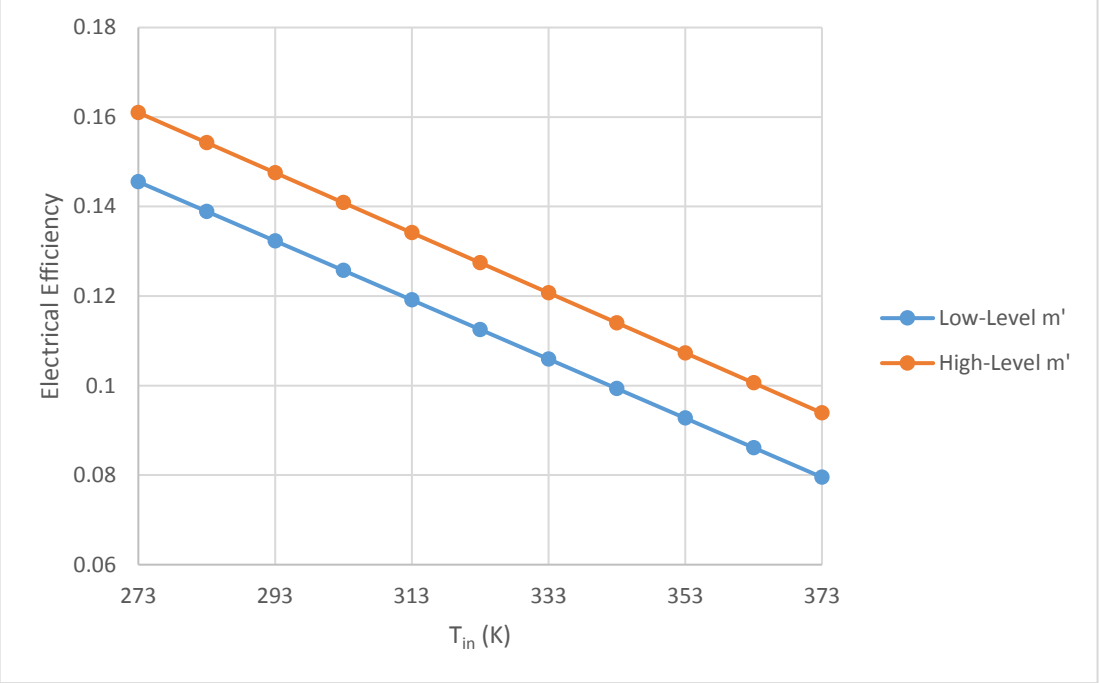

Figure 4-24 Effect of inlet water temperature on electrical efficiency of PVT.

4.3.4 Performance of PVT versus energy loss parameter

The influence of energy loss parameter (($T_i - T_a$)/G) on thermal efficiency of the PVT was investigated for High- and Low-Level flowrate by varying inlet water temperature. Figure 4-25 illustrates the fact that there was a decrease in η_{th} due to the increase in energy loss parameter for both levels of water flowrate.

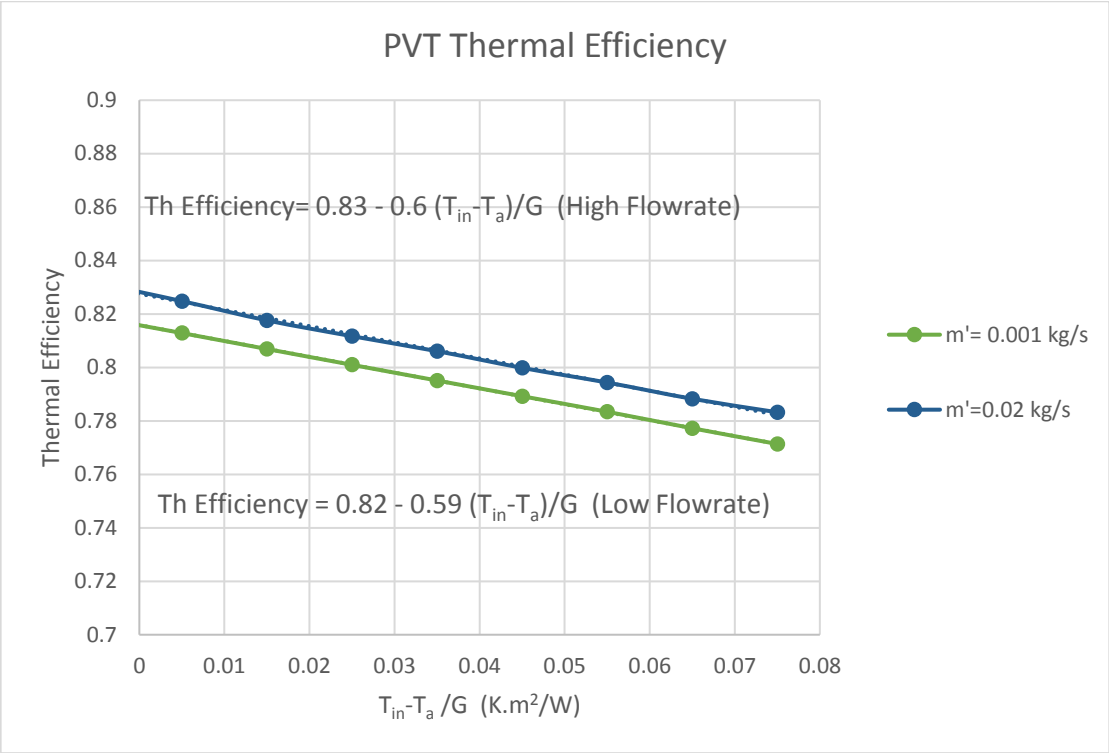

Figure 4-25 Thermal efficiency of PVT versus energy loss parameter.

Thermal efficiency equations were carried out from Figure 4-25 in order to determine the thermal efficiency of the PVT in different weather conditions. As explained in section 3.3.2 based on equation 3-19, $F_R * (\tau\alpha)$ is the intercept of thermal efficiency versus energy loss parameter and the slope is $-F_R U_L$. Based on the simulation results, equations 4-3 and 4-4 represent thermal efficiency for the Low- and High-Level flowrate respectively:

$$\eta_{th} = 0.82 - 0.59 \frac{Ti - Ta}{G} \qquad \text{Low} - \text{Level Flowrate} \quad (4-3)$$

$$\eta_{th} = 0.83 - 0.6 \frac{Ti - Ta}{G} \qquad \text{High} - \text{Level Flowrate} \quad (4-4)$$

The influence of energy loss parameter ((T_i− T_a)/G) on the electrical efficiency of the PVT was also investigated for High- and Low-Level flowrate by varying inlet water temperature. Figure 4-26 illustrates the fact that there was a decrease in η_{elc} with the increase in energy loss parameter for both levels of water flowrate.

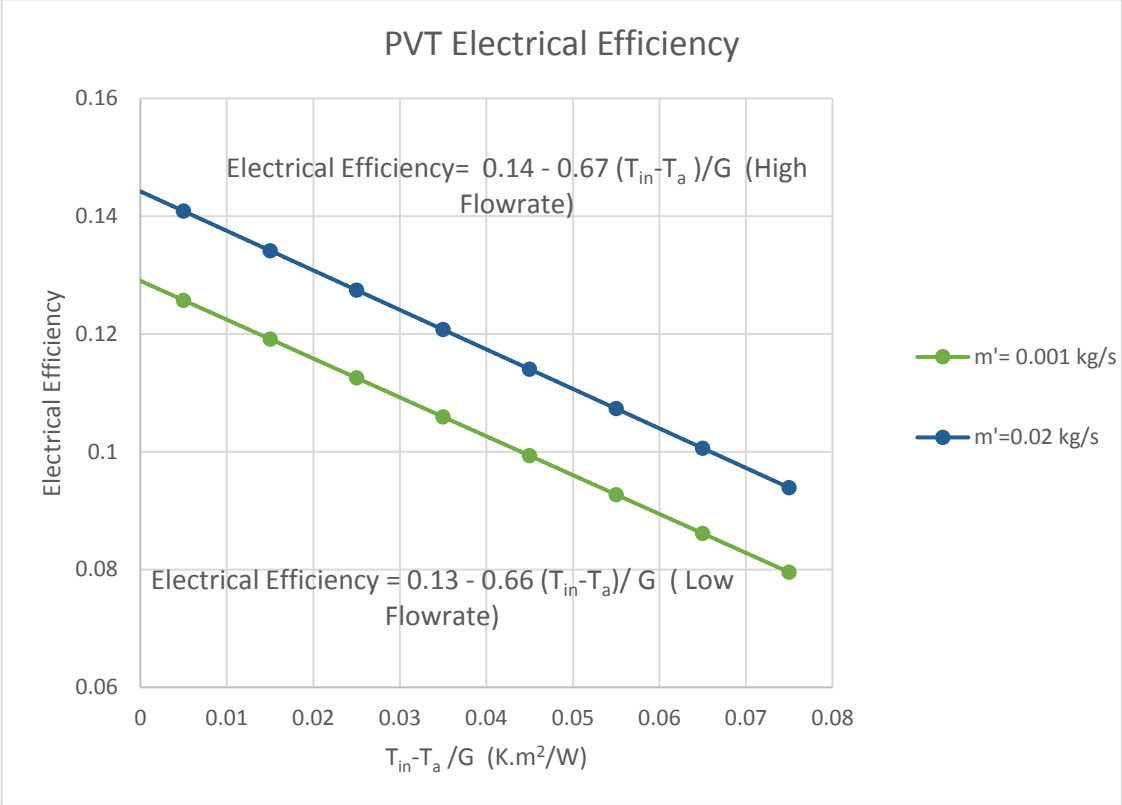

Figure 4-26 Electrical efficiency of PVT versus energy loss parameter.

Electrical efficiency equations were carried out from Figure 4-26 in order to determine electrical efficiency of the PVT in different weather conditions. Based on the simulation results, equations 4-5 and 4-6 represent electrical efficiency for the Low- and High-Level flowrate respectively:

$$\eta_{elc} = 0.13 - 0.66 \ \frac{\mathrm{Ti} - \mathrm{Ta}}{\mathrm{G}} \qquad \text{Low} - \text{Level Flowrate} \qquad (4-5)$$

$$\eta_{elc} = 0.14 - 0.67 \ \frac{\mathrm{Ti} - \mathrm{Ta}}{\mathrm{G}} \qquad \text{High} - \text{Level Flowrate} \qquad (4-6)$$

4.3.5 PVT Summary

In this section, the effects of flowrate ($\dot{m}$) and inlet temperature (T_{in}) on thermal efficiency (η_{th}) and electrical efficiency (η_{elc}) of PVT were investigated. The PVT was examined using the 3-D CFD model for High- and Low-Level flowrate and for different inlet temperatures, which varied from 298 K to 373 K. Thermal and electrical efficiency of 82 % and 14.3 % respectively was achieved at the minimum inlet temperature (298 K) and the maximum flowrate inside the riser pipe (95 x10^{-4} kg/s). Similar to the findings for FPC, the heat transfer coefficient between the pipe and water increased with increasing water flowrate of the PVT, which increased useful energy. Useful energy also increased with decreasing inlet temperature due to the increase in (T_p-T_f). In contrast, thermal efficiency decreased with the increase in inlet temperature due to the increase in (T_f-T_{amb}).

4.4 Effect of PVT system on overall performance (Mathematical)

The benchmark model for the mathematical PVT model which was discussed in section 3.5 is employed in this section. In the previous chapter, Figure 3-14 showed the schematic diagram of the PVT panel and the design parameters were reported in Table 3-3. The mathematical model of PVT was employed in this section in order to study the effects of the PVT system on overall performance, in order to achieve the fourth objective of this study.

The behaviour of a dynamic system would be described better with transient system but steady state model is giving a clear understanding about the effect of different parameters on the performance with lower simulation time. However, the steady state model is more efficient when the average weather conditions (hourly, daily, weekly or monthly) is used as an input parameters in the model (Tagliafico et al. 2014). In this section, the mathematical model of PVT was validated with an experiment from Bahaidarah et al. (2013). To validate the model (steady state model), one-hour interval has been considered as input parameters for each hours based on the operation conditions in Bahaidarah et al. (2013).

4.4.1 Effect of modules temperatures on thermal efficiency

As discussed in section 3.5, water flowrate of the mathematical model of PVT was constant while inlet temperature varied in accordance with the environment's conditions during the day. Figure 4-27 shows ambient temperature, inlet fluid temperature, outlet fluid temperature, PV cell temperature and back surface temperature during the day based on weather data from Bahaidarah et al. (2013).

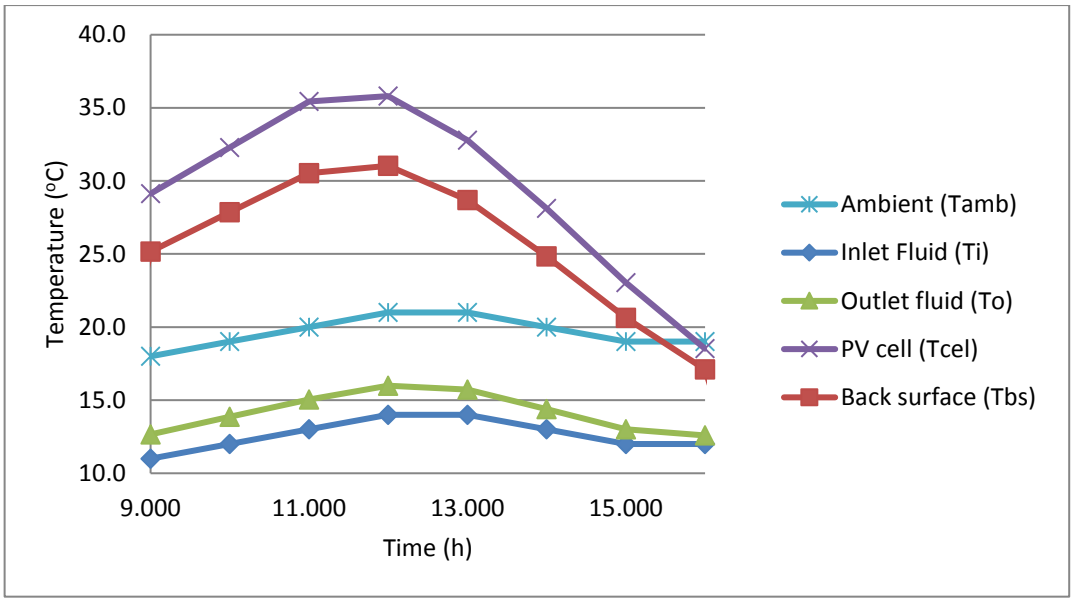

Figure 4-27 Variation of different temperatures that affected the PVT module during the day.

The results show that the PVT performance was influenced by several factors that included instant solar radiation, ambient temperature, inlet fluid temperature, PV cell temperature and back surface temperature. As shown in Figure 4-28, thermal efficiency was in the range of 72% at 9 am to 83% at 4 pm and the minimum efficiency was 70.6 % between 11 and 12 pm. Thermal efficiency was influenced by several factors such as instant solar radiation, ambient temperature, inlet temperature and outlet fluid temperature. Electrical efficiency was in the range of 14.7% at 9 am to 15.5% at 4 pm. The minimum efficiency was 14.3 % between 11 am and 12 pm due to the increase in the PV cell temperature. Electrical efficiency decreased by 2.72% due to the increase in PV cell temperature by 19.4% from the morning until 11 pm, and by 7.6% due to the decrease in PV cell temperature by 48.32 % from 12 pm until 4 pm. Figure 4-28 shows thermal and electrical efficiency during the day.

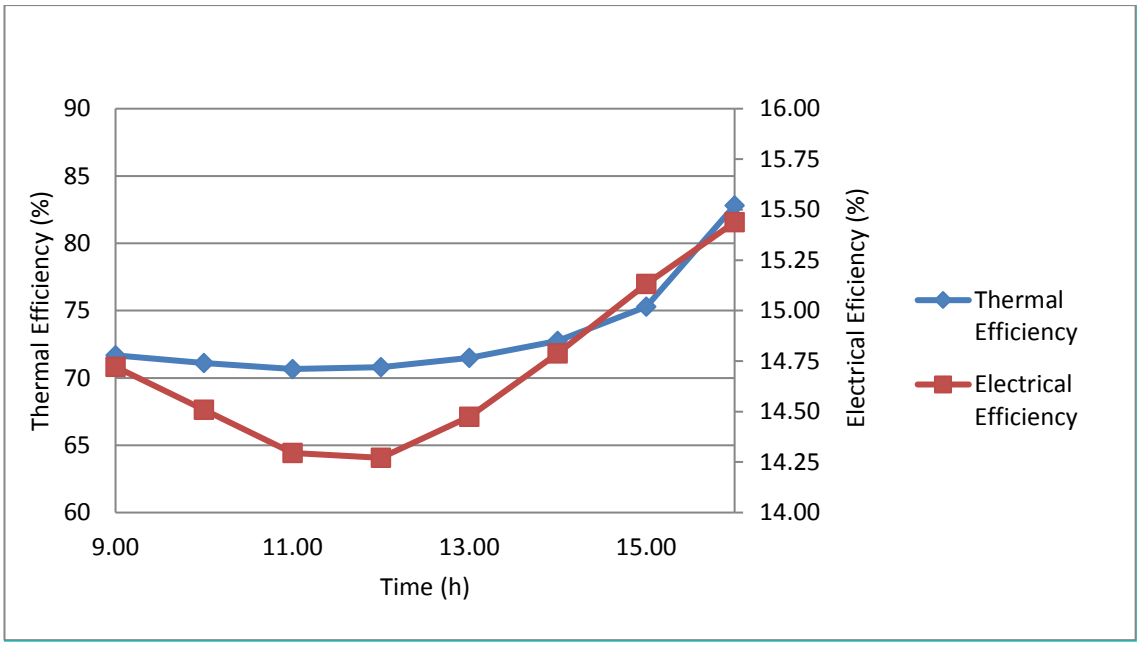

Figure 4-28 Thermal and electrical efficiency of the PVT module during the day.

The maximum electrical power during the day was 174 W at 11 pm due to the solar radiation and ambient temperature values, while it was measured at 210 W at the same time by Bahaidarah et al. (2013). Figure 4-29 shows the comparison between calculated electrical power by the PVT model and the data from Bahaidarah et al. (2013). The electrical power difference between the mathematical model of the PVT and the experiment was in the range of 4 W to 36 W.

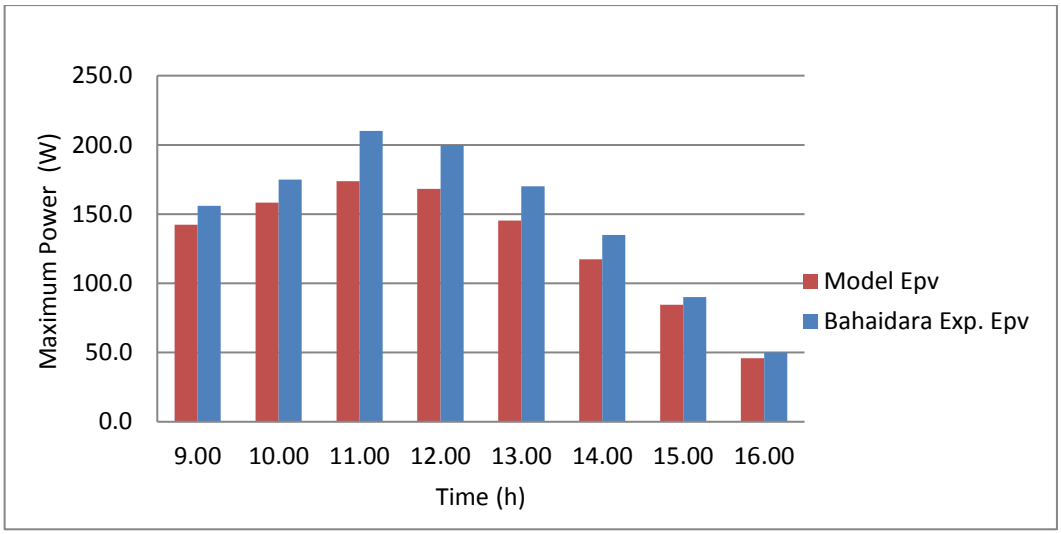

Figure 4-29 Calculated maximum electrical power vs Experimental data (Saudi Arabia-Dhahran).

4.4.2 PVT performance for different inlet temperature and different numbers of panels in series

The performance of PVT was calculated based on the heat transfer equations that were discussed in section 3.5.1 and 3.5.2. To meet the requirements for solar cooling systems, the best options based on PVT outlet temperature need to be selected. The average PV cell temperature should not exceed the maximum operating temperature in the manufacturing specifications of the photovoltaic cells. The proposed PVT system in this section was based on the mathematical model that validated to Bahaidarah et al. (2013). Solar absorption cooling systems require a high outlet temperature from solar collector. To maximise the outlet temperature from multi solar panels, multi panels need to be connected in series as shown in Figure 4-30.

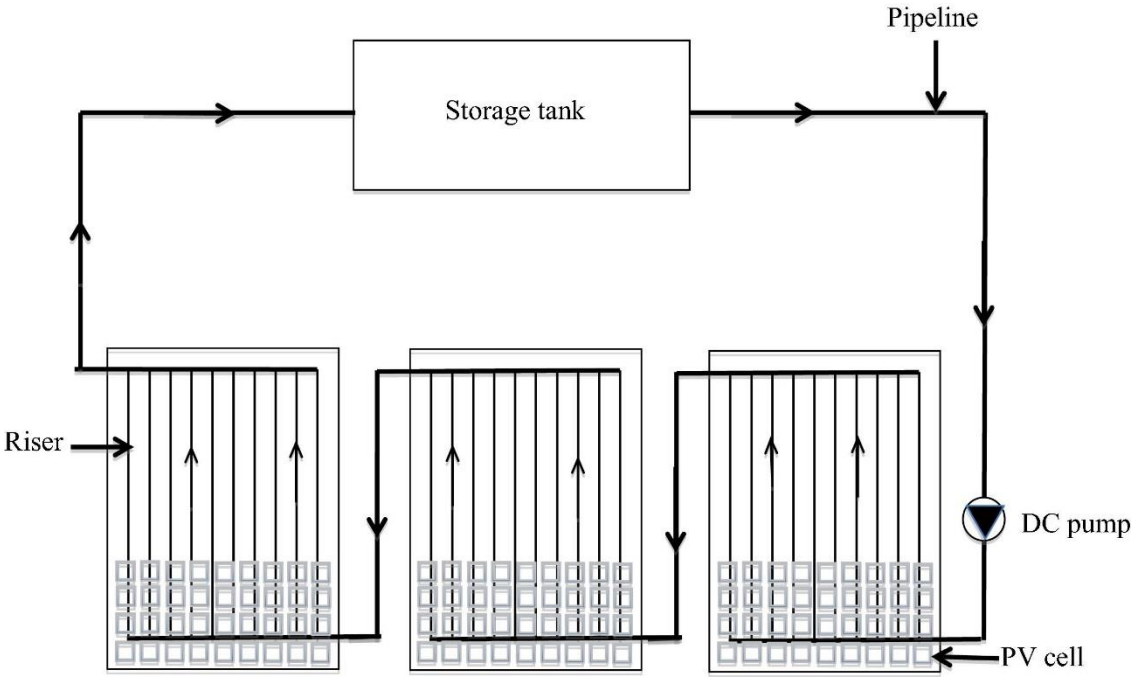

Figure 4-30 layout of connected PVT panels in series (Shyam et al. 2016).

It was found that for PVT system, outlet temperature could reach 120 ^{o}C by connecting 10 panels in series (Shyam et al. 2015). In order to evaluate the output performance for an overall PVT system, a given number of panels in this study (72 in this investigation) are suggested. The possible options to connect the panels in one arrangement in an array are presented in Figure 4-31**.** The following performance figures in this section are based on 72 panels connected in an array. There are many options for the number of panels that should be linked in series in order to achieve specified outlet temperature. Figure 4-31 shows the possible arrangements for a PVT system that could be made of 72 panels. The arrangements could include: one line of 72 panels connected in series (L=1 and N=72), 2 lines of 36 panels in series, 3 lines of 24 panels in series, 4 lines of 18 panels in series, 6 lines of 12 panels in series, 8 lines of 9 panels in series, 9 lines of 8 panels in series, 12 lines of 6 panels in series, 18 lines of 4 panels in series, 36 lines of 2 panels in series or 72 panels connected in parallel to the inlet and outlet header (L=72 and N=1).

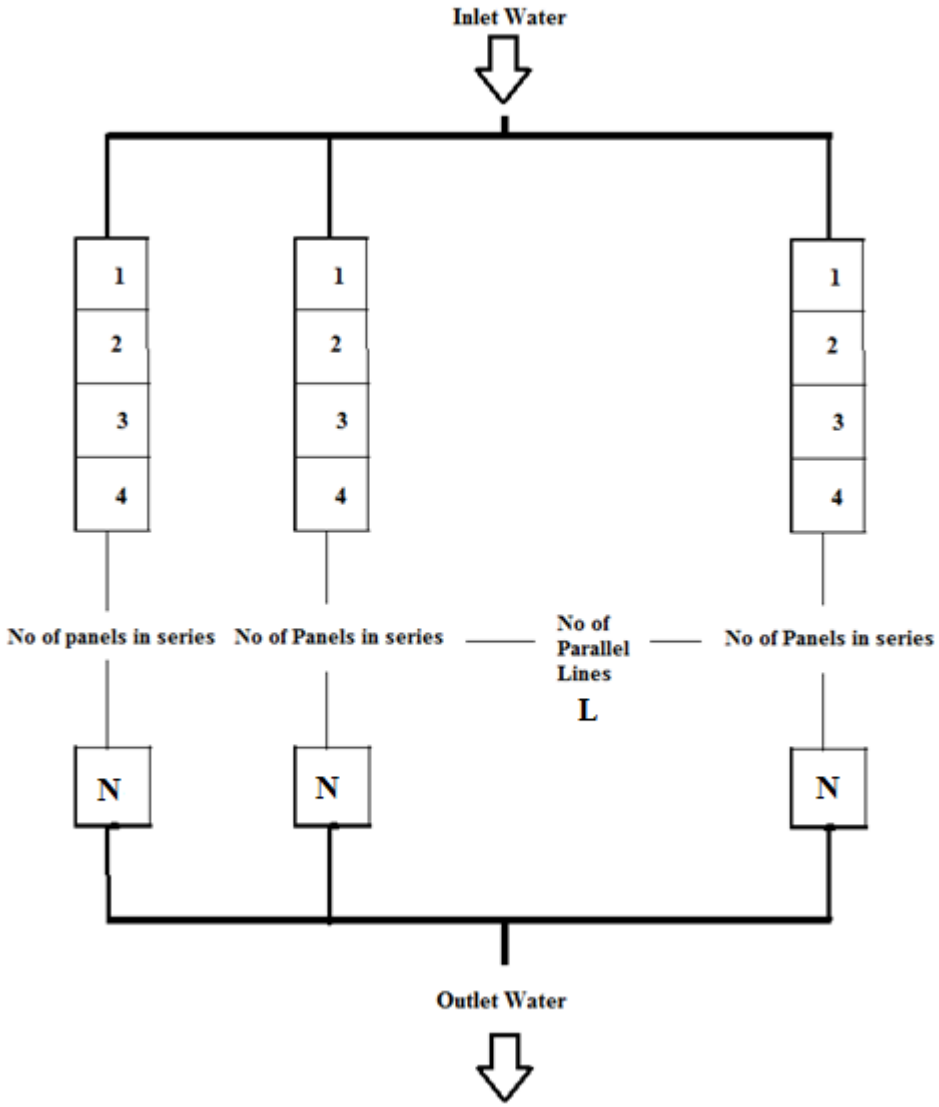

Figure 4-31 The proposed arrangement for a PVT system based on 72 panels connected in an array.

The following figures in this section illustrate the performance of the mathematical PVT system, which starts by cooling each panel individually (N=1), then two panels in series (N=2), up to 72 panel in series (N=72). As an example, the number 4 (N=4) in the x-axis means that the configuration consists of 18 lines (L=18) in parallel, each line consisting of 4 panels connected in series and the outlet for each line supplying the main header.
For the same number of panels, the configuration connecting them affected the outlet water temperature which was in the range of 25 ^{o}C to 110 ^{o}C. The more panels that are connected in series, the higher the outlet temperature that is.

Figure 4-32 shows outlet water temperature for different inlet temperatures, which have the same trend, in that the higher the inlet temperature, the higher the observed outlet temperature. The performance of the PVT system was examined for different range of inlet temperatures. In solar cooling applications, the return temperature to the collector could reach 85 ^{o}C (Ghafoor and Munir 2015). For a target outlet temperature of 70 ^{o}C as in Figure 4-32, there would be five options. This can be achieved by linking 6 panels in series for an inlet temperature of 65 ^{o}C. This system in this option would produce thermal power of 44.88 kW as in Figure 4-33 for an average thermal efficiency of 39% as in Figure 4-34. The remain options to achieve the target outlet temperature are; 18 panels with an inlet temperature of 55^{o}C, 28 panels with an inlet temperature of 45^{o}C, 40 panels with an inlet temperature of 35^{o}C and 52 panels with an inlet temperature of 25 ^{o}C.

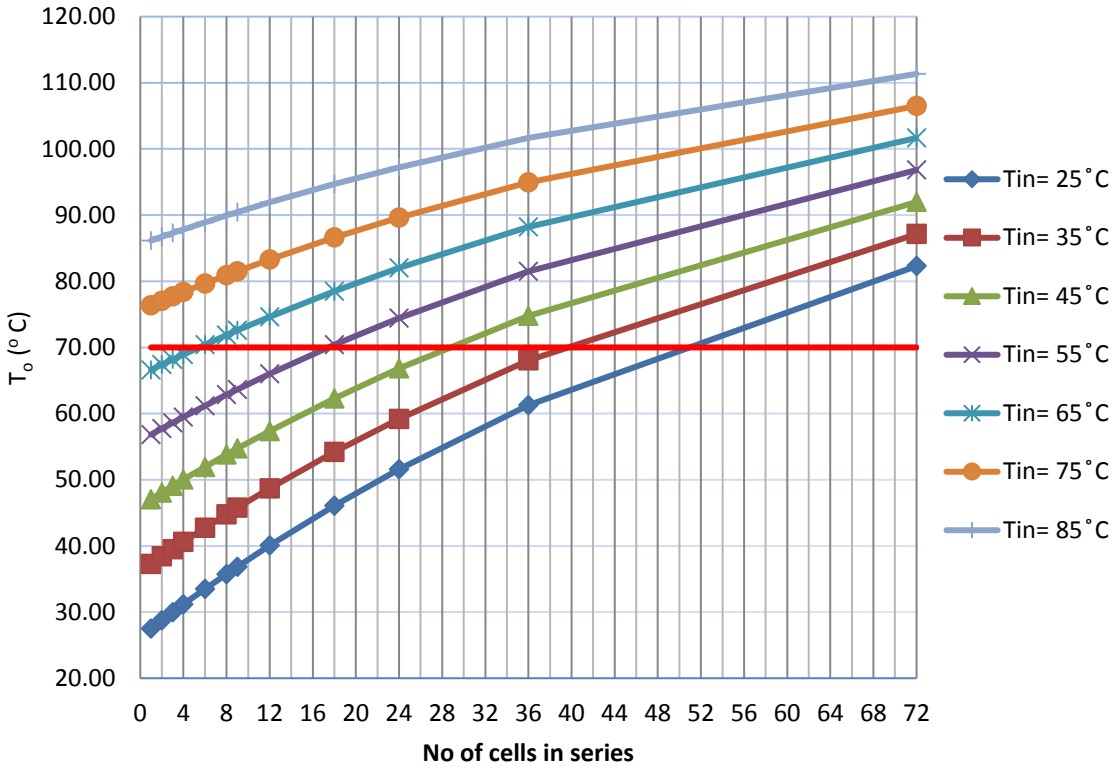

Figure 4-32 PVT outlet fluid temperature for different inlet temperatures**.**

The total numbers of PVT panels in the overall system was constant (72 panels) but the arrangement of connecting them were different. Connecting more panels in series increased the average temperature for the overall system, which increased losses to the ambient. Results of that, Q_u (kW) decreased with the increase in the number of panels connecting in series. Figure 4-33 shows total thermal power for different inlet temperatures based on 72 panels. The higher the inlet temperature, the lower the observed useful energy. Useful energy decreased with the increase in the number of panels in series for all cases of inlet temperature, due to the increase in temperature inside the water stream, which decreased the heat transfer from the absorber to the fluid.

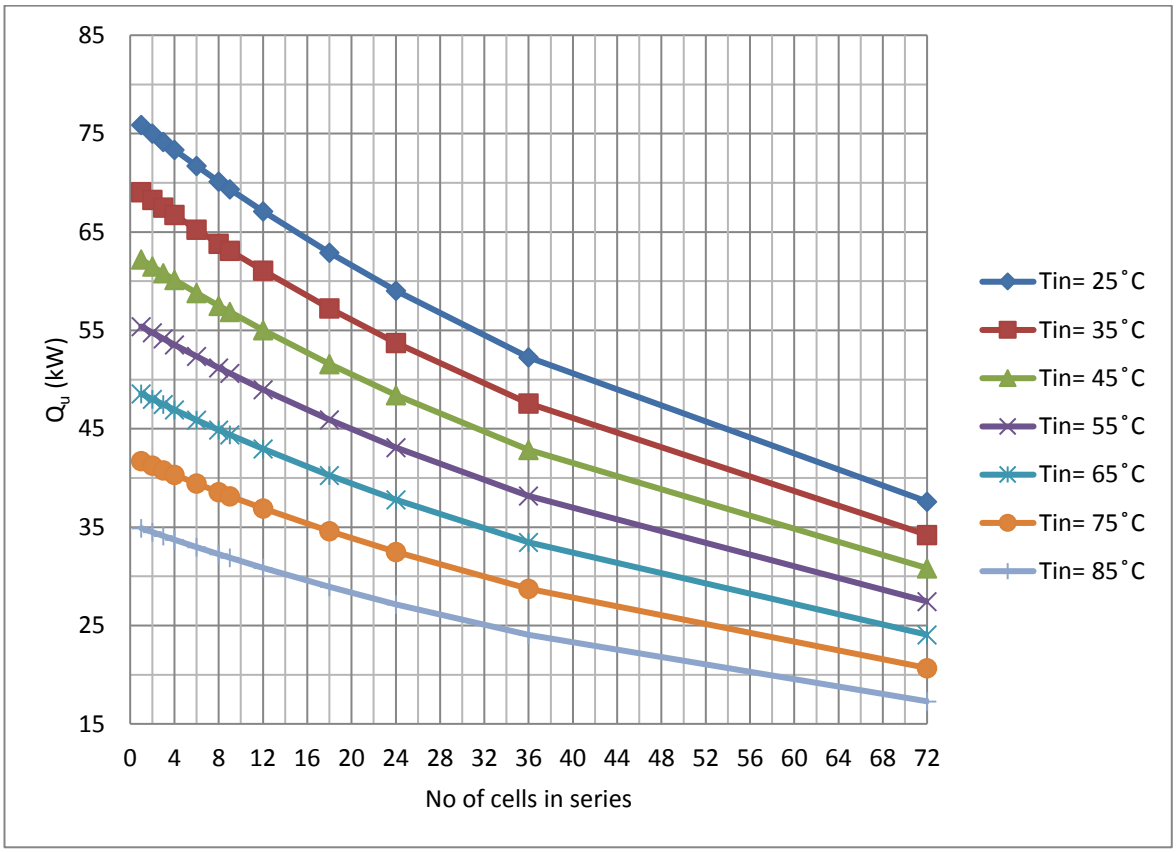

Figure 4-33 PVT total thermal power for different inlet temperatures based on 72 panels**.**

Figure 4-34 shows average thermal efficiency for different inlet temperatures, which was in the range of 15 % to 65 %. For all cases, the lower the inlet temperature, the higher the observed thermal efficiency. Thermal efficiency decreased with the increase in the number of panels in series due to the increase in fluid temperature, which decreased the heat transfer to the fluid and increased loses to the environment.

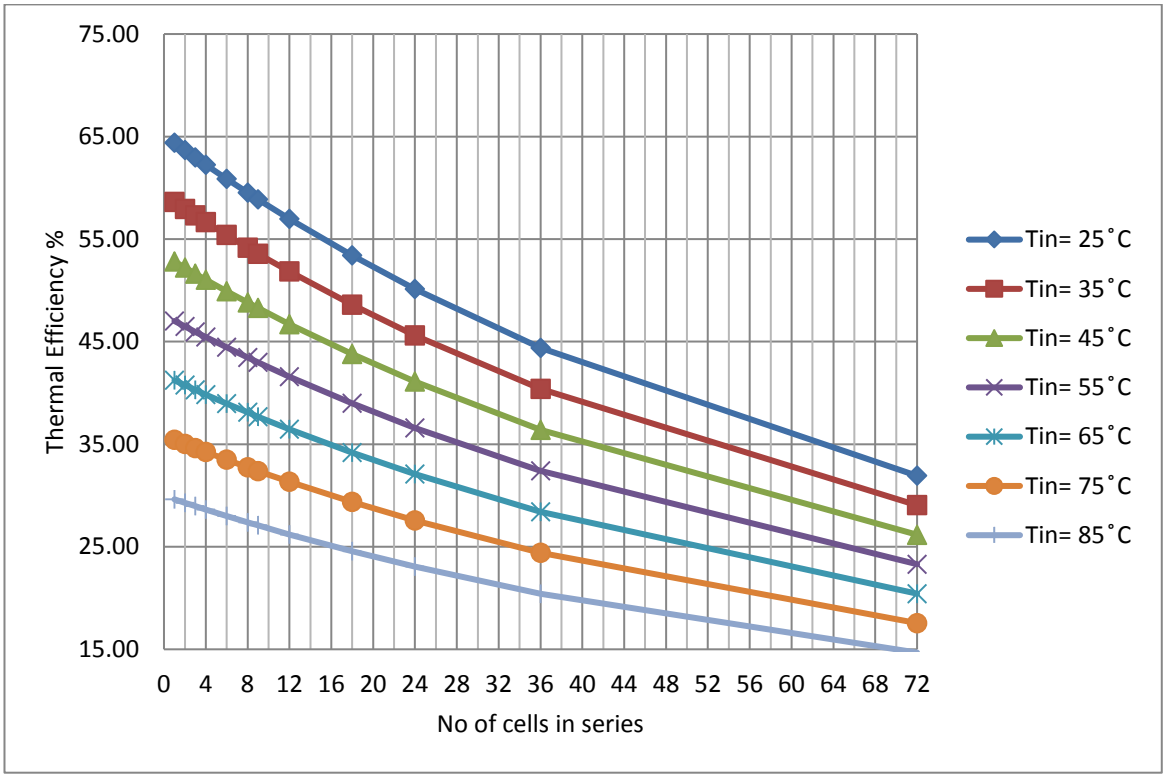

Figure 4-34 PVT thermal efficiency for different inlet temperatures**.**

As for outlet temperature, the configuration of connecting panels affected the average temperature of the photovoltaic layer which was in the range of 45 ºC to 115 ºC. The more panels connected in series, the higher the photovoltaic temperature achieved. Figure 4-35 shows photovoltaic temperatures for different inlet water temperatures, which have the same trend, in that the higher the inlet temperature, the higher the observed photovoltaic temperature. The panels' temperature is an important factor in selecting the configuration, which should not exceed the manufacturing specification for the maximum temperature.

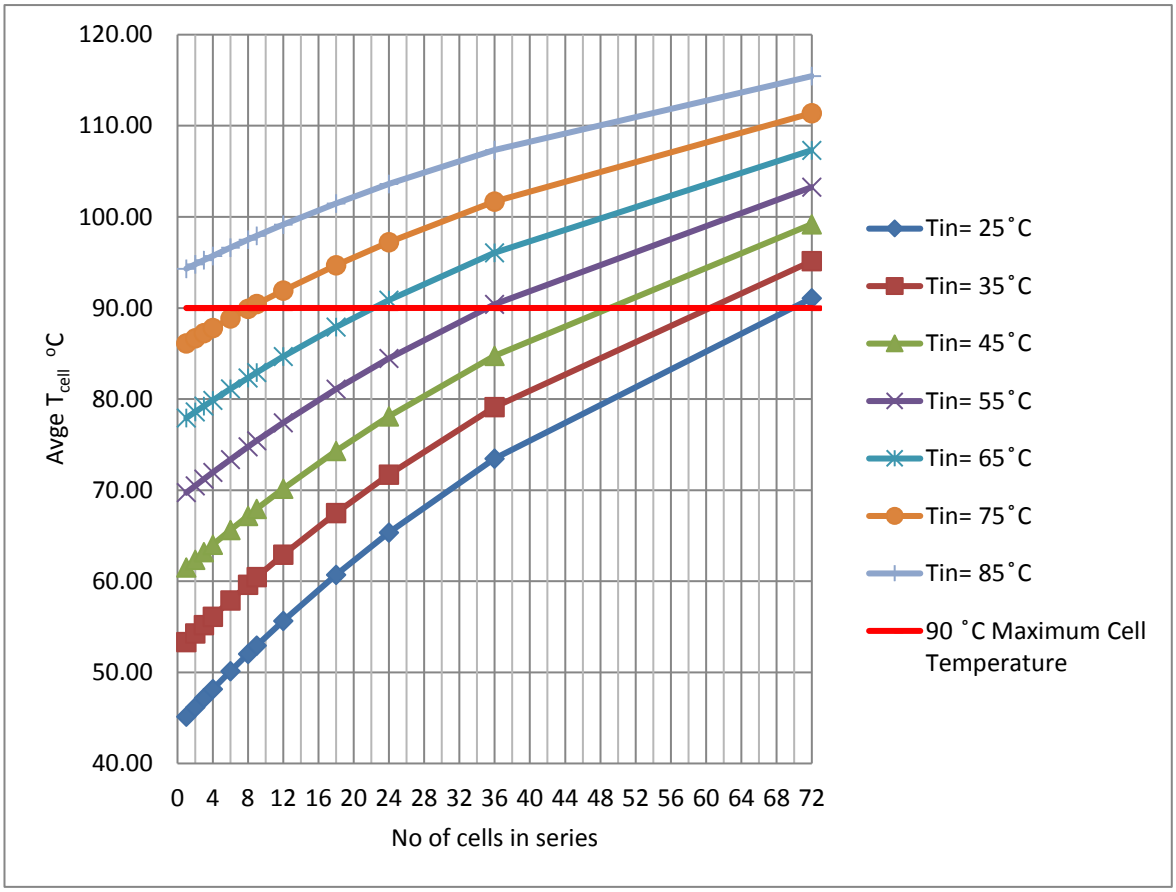

Figure 4-35 PVT average cells temperature for different inlet temperatures**.**

Average electrical efficiency, which was in the range of 8.9 % to 13.7 %, was also influenced by the configuration of the PVT. The lower the inlet temperature, the higher the observed electrical efficiency, as in Figure 4-36. Electrical efficiency decreased with an increase in the number of panels in series for all cases of inlet temperature due to the increase of the photovoltaic temperature.

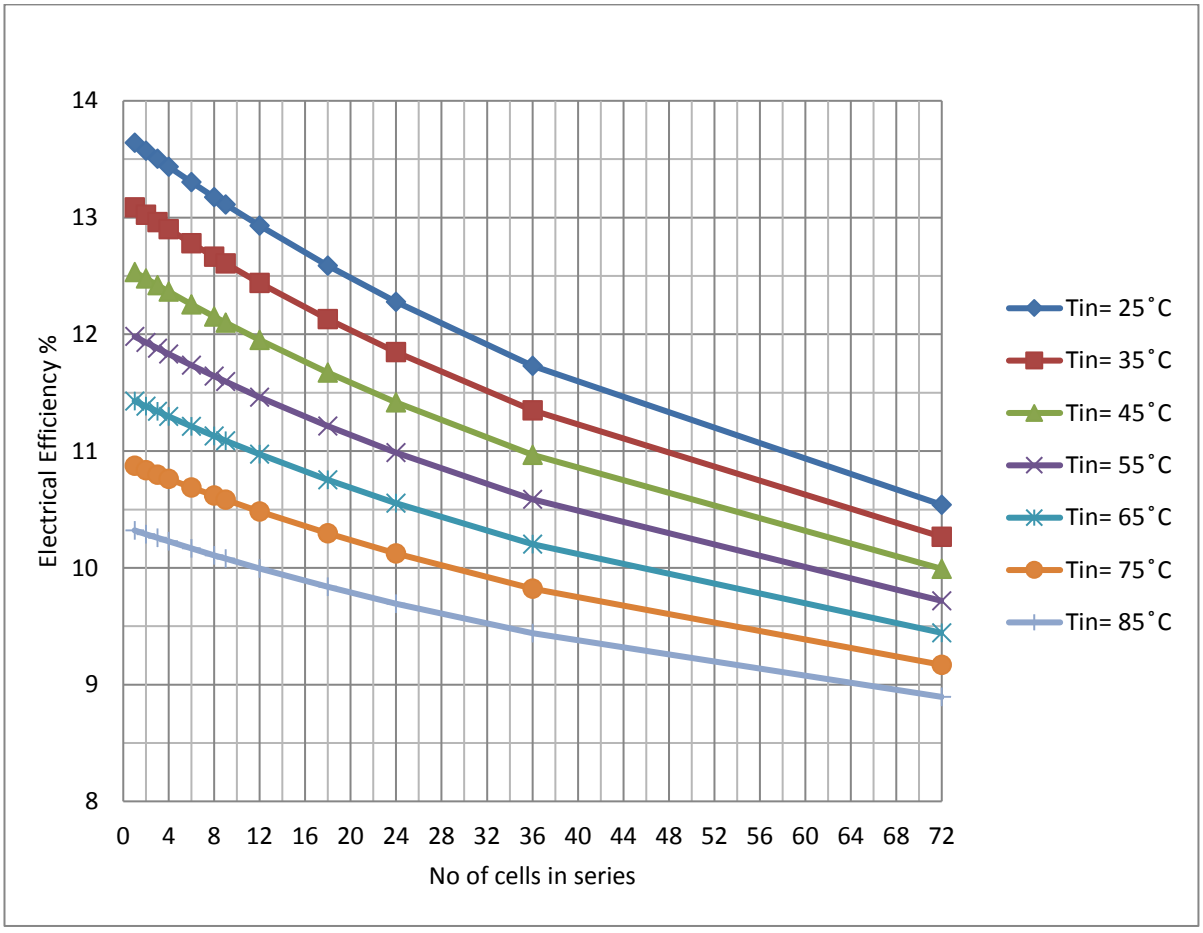

Figure 4-36 PVT electrical efficiency for different inlet temperatures.

Figure 4-37 shows total electrical power (E_p) for different inlet temperatures based on 72 panels. The higher the inlet temperature, the lower the observed electrical power. The power decreased with the increase in the number of panels in series for all cases of inlet temperature due to the increase in temperature of the photovoltaic layer, which decreased electrical efficiency.

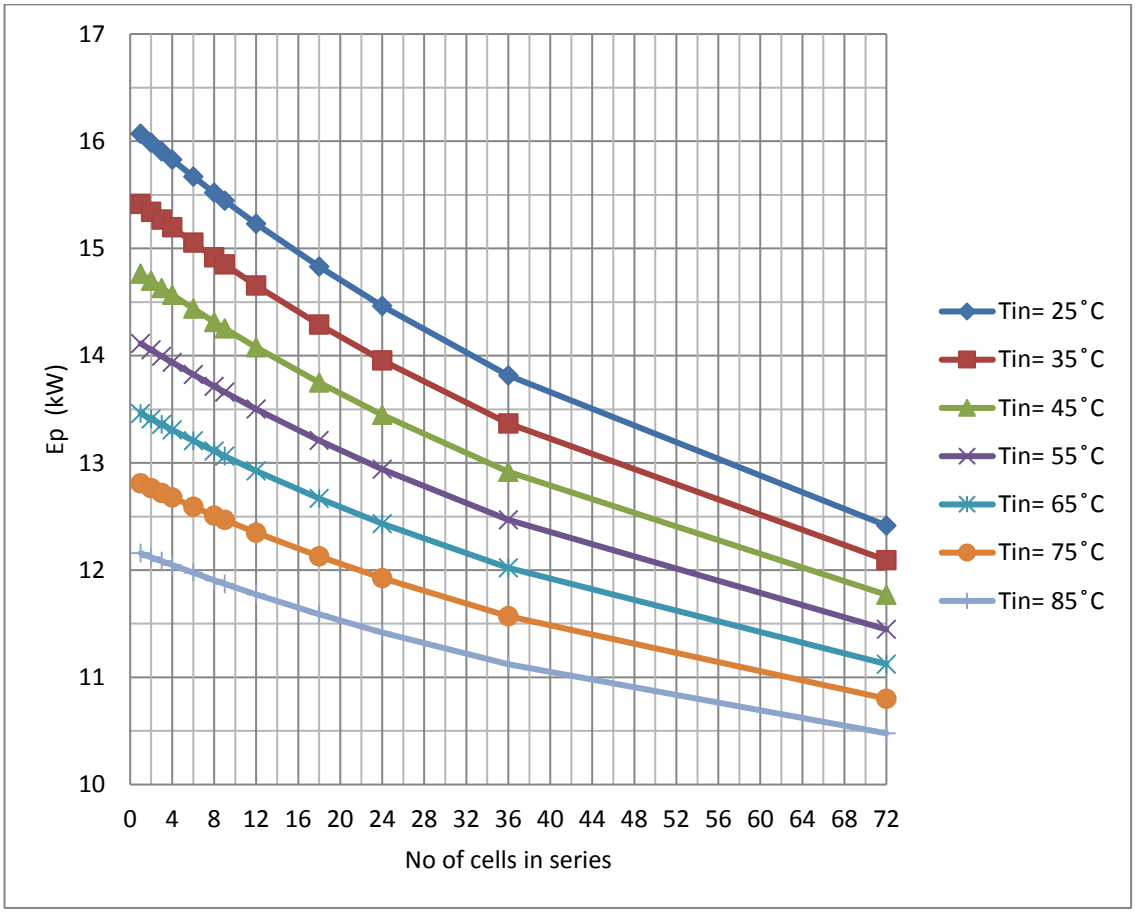

Figure 4-37 PVT total electrical power based on 72 panels**.**

The percentage of thermal power to the total power (thermal and electrical power) of the PVT, based on 72 panels, is illustrated in Figure 4-38. The higher the inlet temperature, the lower the observed thermal power percentage. The percentages of thermal power decreased with the increase in the number of panels in series for all cases of inlet temperature, which were in the range of 62 % to 83% of the total produced power.

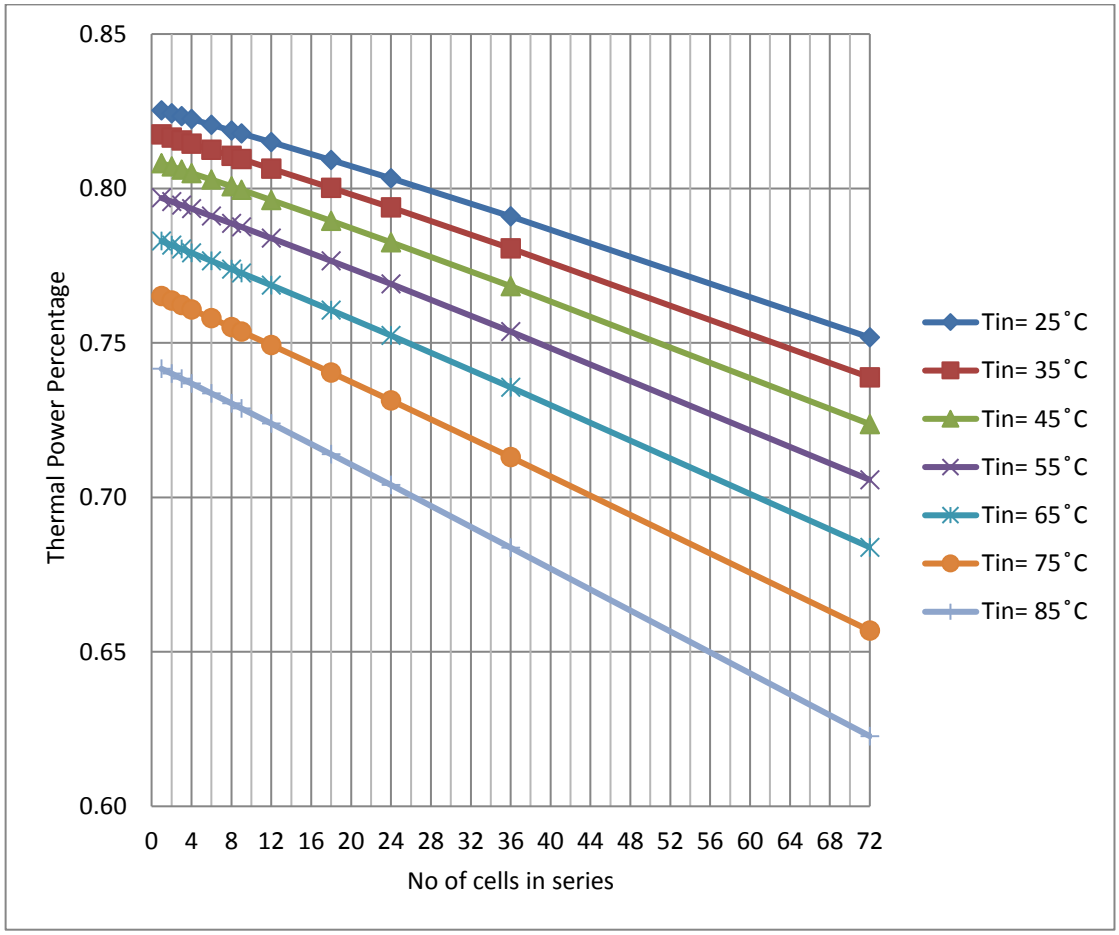

Figure 4-38 The percentage of the thermal power to the total power of PVT based on 72 panels**.**

The percentage of the electrical power to the total power (thermal and electrical power) of the PVT based on 72 panels is illustrated in Figure 4-39. The higher the inlet temperature, the higher the observed electrical power percentage. The percentages of electrical power increased with the increase in the number of panels in series for all cases of inlet temperature, which were in the range of 17 % to 38% of the total produced power.

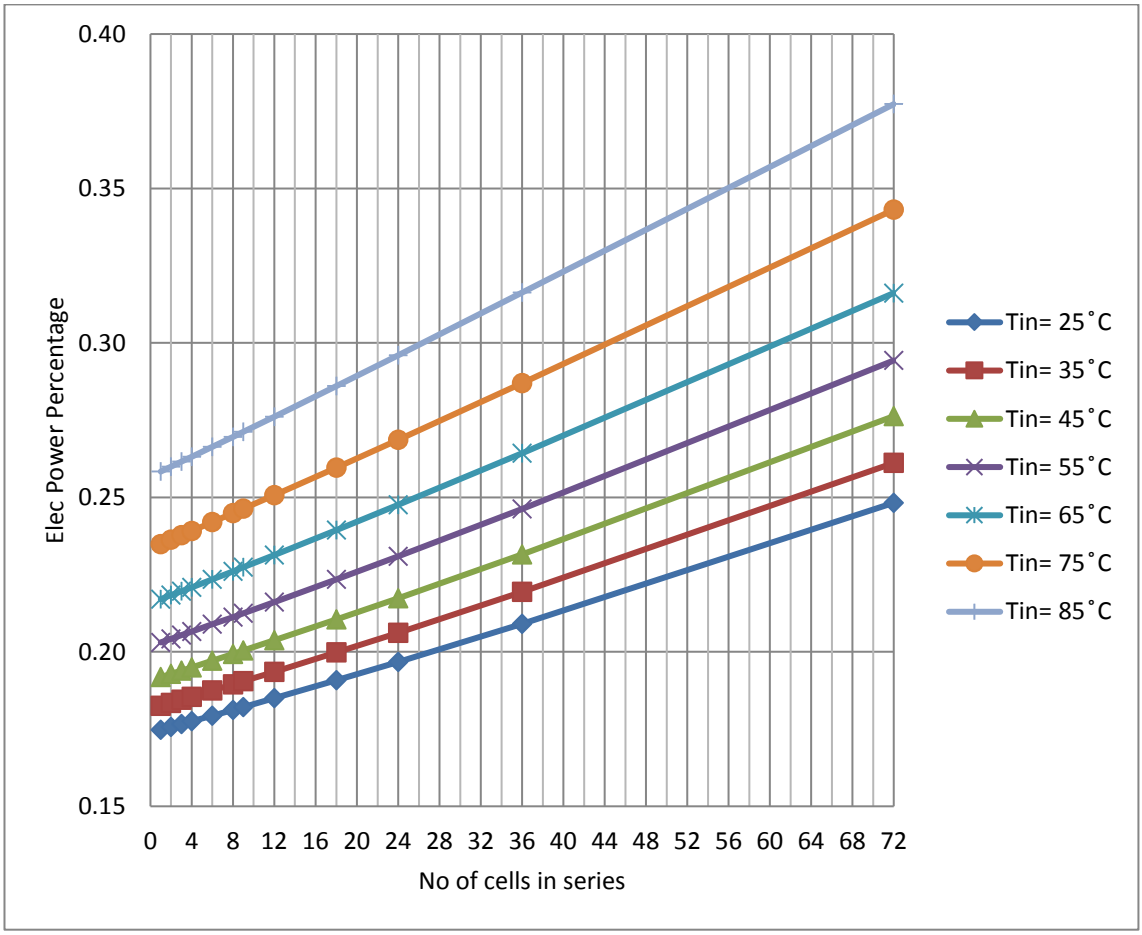

Figure 4-39 The percentage of the electrical power to the total power of PVT based on 72 panels.

4.4.3 Mathematical PVT summary

The mathematical model of a PVT system was employed to calculate the PVT system's performance. The effect of the PVT system (the configuration of connecting panels in series) was investigated for different range of inlet water temperature. The results show that the PVT performance was influenced by several factors that included instant solar radiation, ambient temperature, inlet fluid temperature, PV cell temperature and back surface temperature.

For the same numbers of panels, the configuration of connecting panels affected the performance of the PVT. The more panels that were connected in series, the higher the outlet temperature and photovoltaic temperature that were achieved. Useful energy and thermal efficiency decreased with the increase in the number of panels in series for all cases of inlet temperature due to the increase in temperature inside the water stream, which decreased the heat transfer from the absorber to the fluid. Electrical efficiency also decreased with the increase in the number of panels in series for all cases of inlet temperature due to the increase in the photovoltaic temperature.

The higher the inlet temperature, the higher the observed outlet temperature and the lower the observed useful energy. In addition, the higher the inlet temperature, the lower the observed thermal efficiency. Furthermore, the higher the inlet temperature, the higher the observed photovoltaic temperature and the higher the observed electrical efficiency.

Chapter 5. Results and Discussion (Multi-objective optimisation)

5.1 Introduction

As discussed in chapter 1, the fifth objective in the study was to optimise inlet conditions of the flat plate collector (FPC) and photovoltaic thermal collector (PVT). Multi objective optimisation with response surface method was applied to the computational model of the FPC and PVT, which were explained and validated in chapter 3, in order to achieve the highest efficiency for specified outlet temperature. The outlet temperatures of FPC and PVT were selected in accordance with the minimum absorption cooling driving temperature currently available in the market. Design of experiment technique (DOE) was employed to provide the design points for response surface optimisation.

5.2 Optimum inlet conditions of FPC

The thermal power which can be utilised from FPCs is the dominant driving power in solar absorption cooling systems. Thermal energy is delivered from solar collectors such as FPC and PVT to a storage tank via a hydraulic pump. A backup heating system is normally connected to the storage tank in order to maintain the required feed temperature for the absorption chiller. According to Alobaid et al. (2017), the minimum driving temperature (T_g) for small capacity absorption chillers in the market (Sonnenklima, Germany, 10 kW) is 75 ^oC (348 K) with return temperature (T_r) from the chiller of 65 ^oC (338 K).

5.2.1 Single effect optimisation of FPC

In order to achieve the highest energy saving in solar absorption systems, inlet water temperature and flowrate need to be optimised (Alobaid et al. 2018). Different ranges of inlet water temperature were examined at high ambient temperature (318 K) in order to achieve the driven temperature for the chiller with high FPC thermal efficiency. As shown in Figure 5-1, the minimum required feed temperature (348 K) can be achieved at five options of inlet temperature and flowrate, namely: T_{in}=313 K and $\dot{m}$= 0.001 kg/s; T_{in}=323 K and $\dot{m}$ = 0.0013 kg/s; T_{in}=333 K and $\dot{m}$ = 0.0022 kg/s; T_{in}=338 K and $\dot{m}$ = 0.0034 kg/s; and T_{in}=343 K and $\dot{m}$ = 0.005 kg/s.

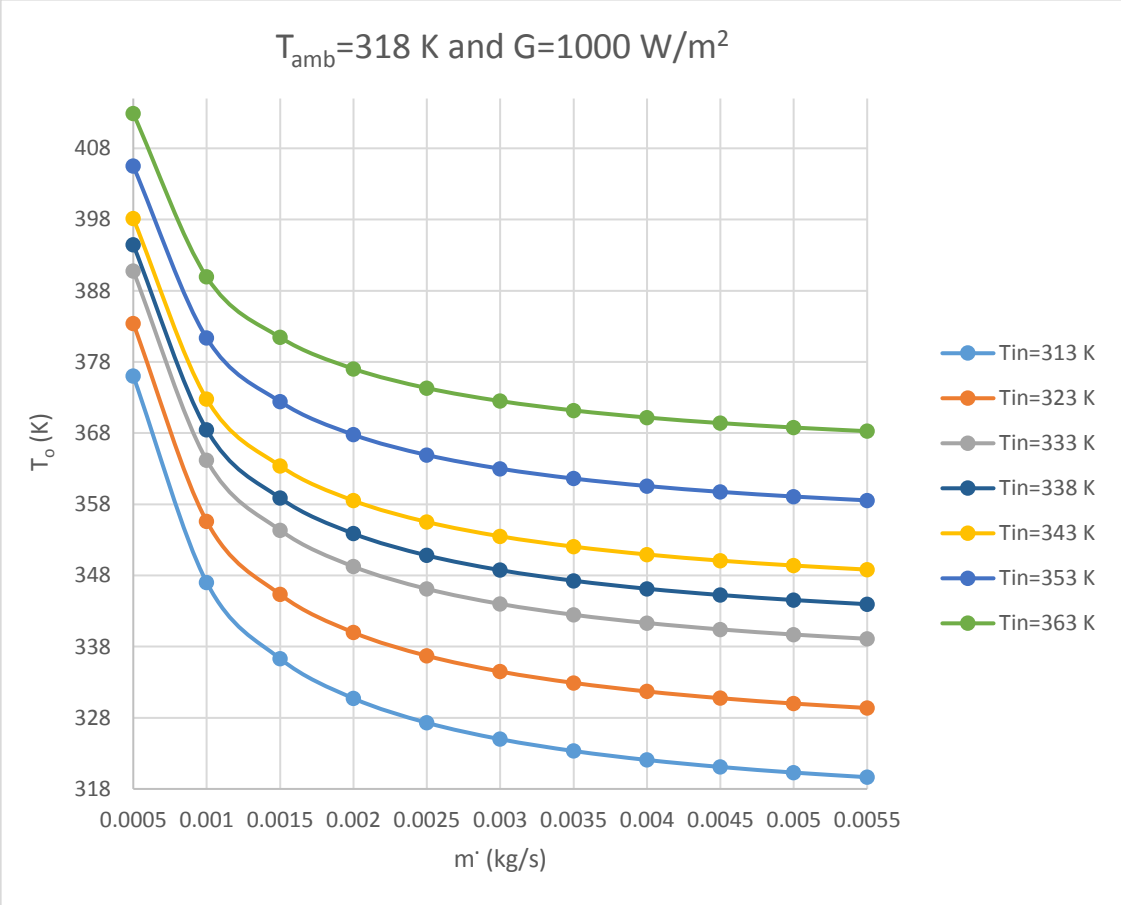

Figure 5-1 Outlet water temperature for different inlet temperatures versus flowrate.

The optimum inlet temperature and flowrate - to meet the minimum feed temperature for the absorption chiller- based on the highest thermal efficiency for the FPC, was (T_{in}=313 K and $\dot{m}$=0.001 kg/s, for η_{th}=88%) as in Figure 5-2. Based on the design criteria of the selected absorption chiller and the losses to the environment from the piping system and from the storage tank, $T_{amb} < T_{in} < T_r$. This constraint minimised the options to: (T_{in}=323 K and $\dot{m}$ = 0.0013 kg/s and η_{th}= 86%) or (T_{in}= 333 K and $\dot{m}$ =0.0022 kg/ and η_{th}=84 %)**.** (Note that, as mentioned, the flowrate here is for one riser pipe which is 1/10 of the total flowrate of the FPC).

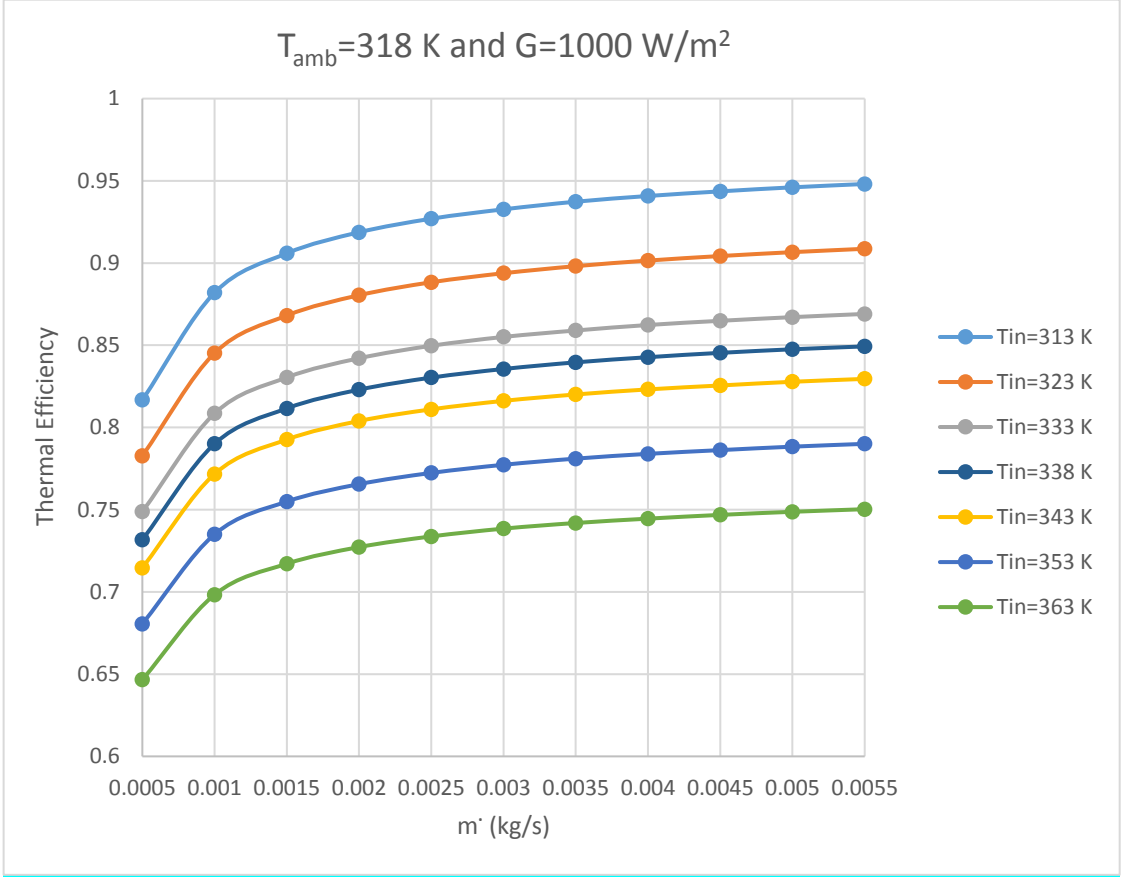

Figure 5-2 Thermal efficiency (η_{th}) for different inlet temperature versus flowrate.

T_{in} and $\dot{m}$ were optimised for highest η_{th} in order to achieve the minimum required feed temperature for a 10 kW absorption chiller. The optimum results of the FPC based on Figure 5-1 and Figure 5-2 were T_{in} = 323 K and $\dot{m}$ = 0.0013 kg/s for η_{th}= 86%. In optimisation studies, the important thing is to illustrate the interaction between input

parameters and study the effect on the output (response), as discussed in section 3.6.2, instead of studying each parameter individually (single effect of each parameter). The response surface optimisation method were presented in the following section, which details the relationship between input parameters and the response (the output).

5.2.2 Response surface optimisation for FPC

The fifth objective in this study was to apply the multi-objective optimisation method to a FPC and PVT. The aim of using this method was to achieve a specified outlet temperature with high thermal efficiency within the domain of the optimisation parameters. The outlet temperature of the FPC was selected in accordance with the minimum absorption cooling driving temperature available in the market in order to increase the coefficient of performance of a solar cooling absorption system (SCOP). The minimum driving temperature (T_g) in the market, according to (Alobaid et al. 2017), for small capacity absorption chillers (Sonnenklima, Germany, 10 kW) is 348 K (75 ^oC) with return temperature (T_r) from the chiller of 338 K (65 ^oC).

As discussed in section 3.6.1, a set of design of experiments points (DOE) was generated in ANSYS in accordance with the design parameters of the FPC using the central composite design method. A parameters parallel chart for the FPC is shown in Figure 5-3. Inlet temperature was in the range of 298 K to 370 K and the flowrate was in the range of 5 $x10^{-4}$ kg/s to 60 $x10^{-4}$ kg/s inside the riser pipe. In the range of inputs parameters, outlet temperature varied from 304.4 K to 416.8 K, temperature rise (T_o-T_{in}) varied from 4.5 K to 65.6 K, the average temperature of fluid inside the pipe varied from 301.21 K to 395.07 K, and thermal efficiency (η_{th}) varied from 0.61 to 0.99.

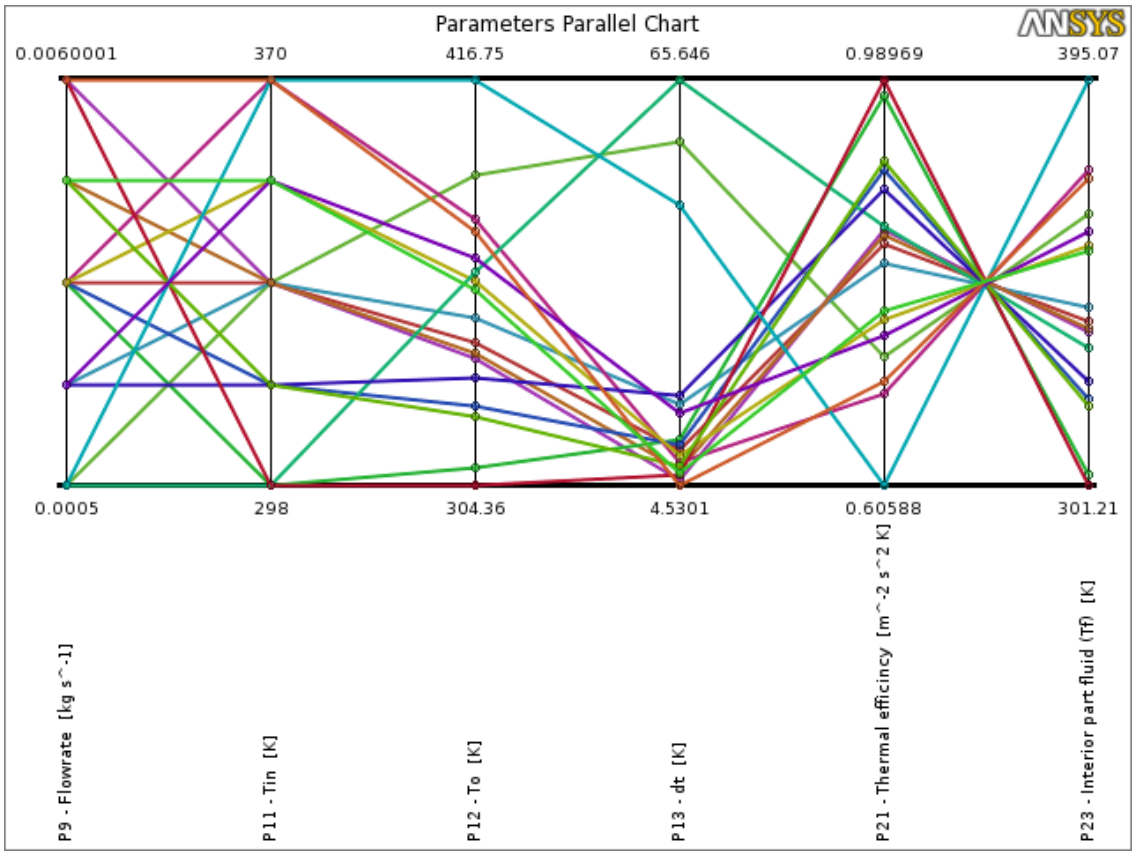

Figure 5-3 Parameters parallel chart for 17 design points and two inputs parameters of FPC.

As discussed in section 3.6.2, Kriging response surface type was employed to predict the behaviour of the output parameters based on the DOE results. The predicted relative error of 0.7 % was achieved for all outputs and the solution converged at 10 refinement points.

The response chart for water outlet temperature of the FPC showed the maximum outlet temperature of 415 K at the minimum flowrate and maximum input temperature. Minimum outlet temperature of 304 K occurred at the maximum flowrate and the minimum inlet temperature as in Figure 5-4. It can be observed that both flowrate and inlet temperature influenced the outlet temperature at each point in the domain by different levels of impact, which requires optimisation.

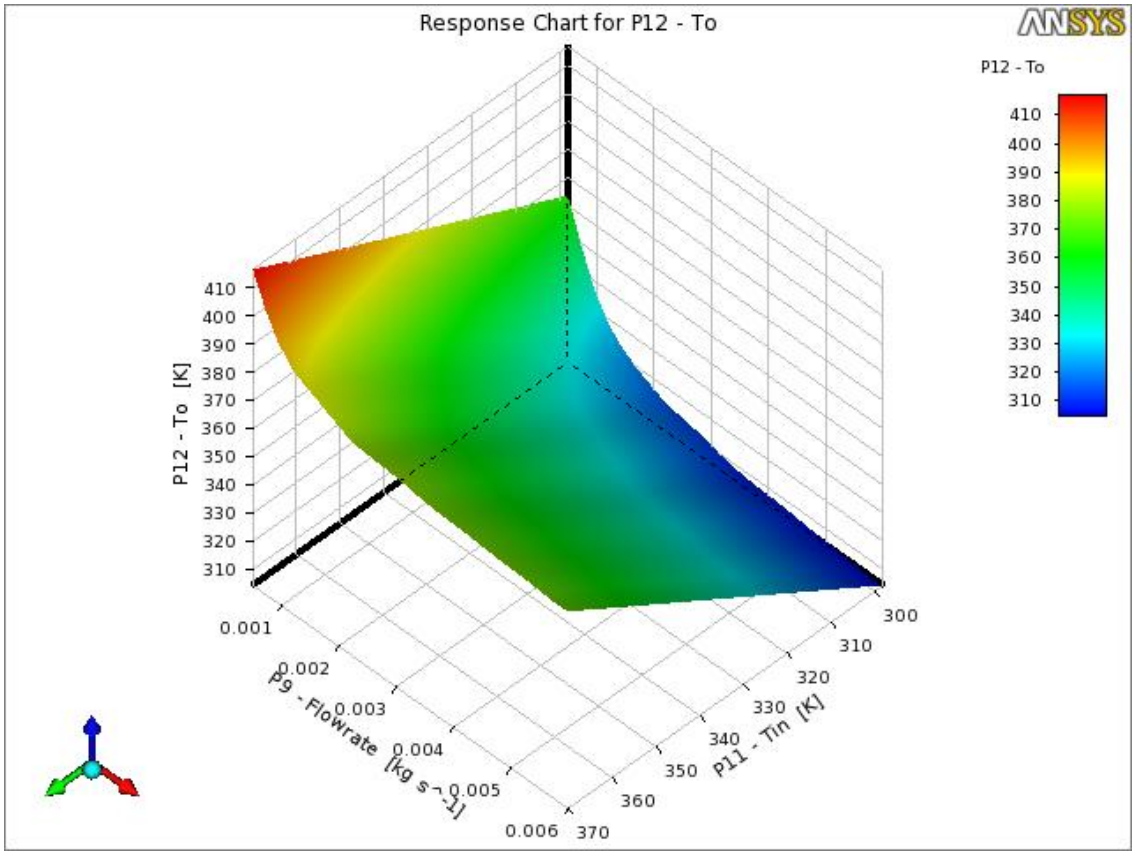

Figure 5-4 Response chart for the outlet water temperature of the FPC.

The response chart for the temperature raise (T_o-T_{in}) is illustrated in Figure 5-5, which shows the maximum expected temperature rise (T_o-T_{in}) of 65.6 K at the minimum inlet temperature and flowrate. This is similar to the results in section 4.2.2. It can be observed that the inlet flowrate has the significant impact on (T_o-T_{in}), whereas the inlet temperature has relatively lower impact on (T_o-T_{in}).

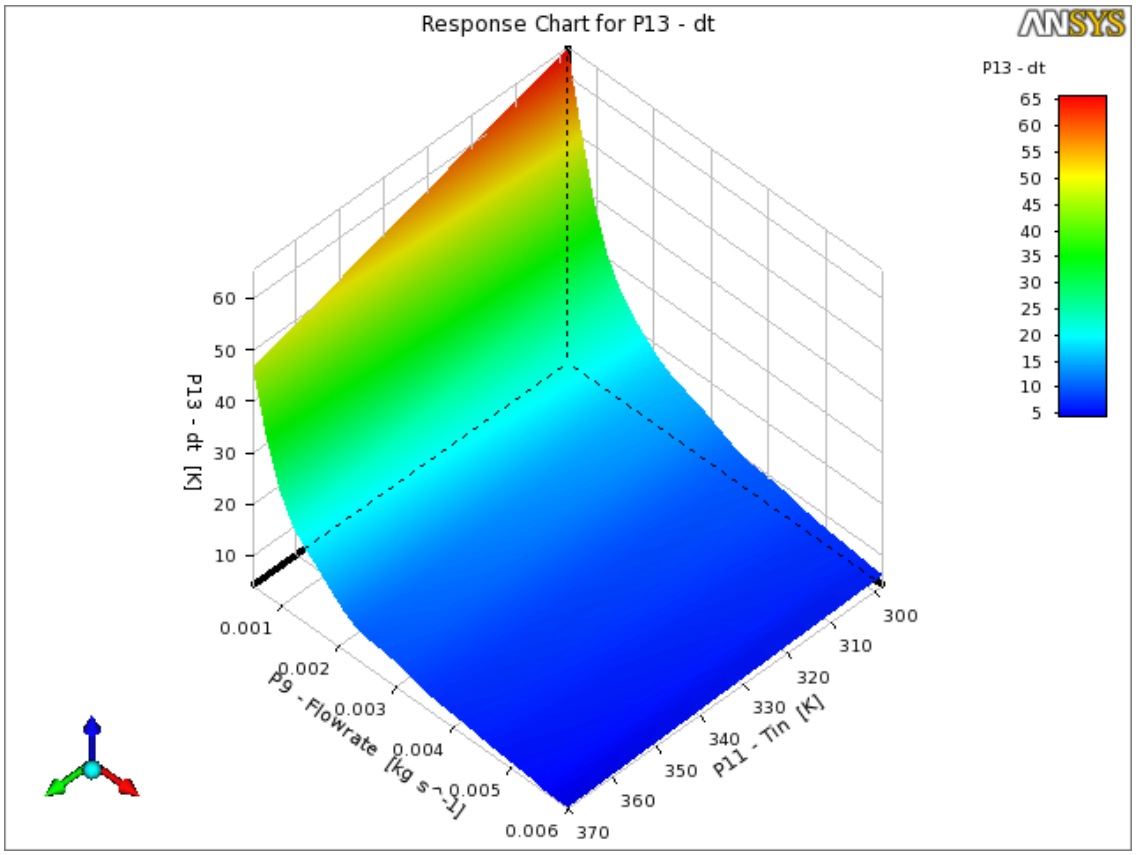

Figure 5-5 Response chart for the temperature rise in the inlet temperature of the FPC.

In order to maximise overall efficiency in a solar absorption system coupled with FPC, flowrate and inlet water temperature were optimised for the FPC. Multiple objectives optimisation was applied in order to achieve the driven temperature for the chiller with high thermal efficiency of the FPC. As explained in chapter 3, by employing the response surface optimisation method in ANSYS16.1, multiple objectives and constraints were chosen in this section with screening optimisation type. 1000 samples were provided in the domain of the study in order to propose five candidates results. The initial goal in this study was to seek a 348 K outlet temperature and the second goal was to maximise

thermal efficiency. The optimum candidate's points, which achieved the target temperature with maximum thermal efficiency, were also verified as in Table 5-1. The second and fourth candidates' points in Table 5-1 satisfied the conditions of the optimisation study. The optimum results were: $\dot{m}$ =11 x10^{-4} kg/s with inlet temperature of 320.98 K (or 321.60 K) for thermal efficiency of 84 %.

Table 5-1 Optimum flowrate and inlet water temperature of the FPC.

Optimisation Method Name: Screening Response surface type: Kriging, Max. No. of refinement point =10 0.7 % relative error DOE Type: Face cantered enhanced design type Central composite design Configuration: Generate 10000 samples and find 5 candidates. T_o: Seek Target 353 K , lower band 348 K Maximise thermal efficiency Constrains ($T_{amb}<T_{in}<T_r$): $318<T_{in}<338$ K										
	Point 1	Point 1 (verified)	Point 2	Point 2 (verified)	Point 3	Point 3 (verified)	Point 4	Point 4 (verified)	Point 5	Point 5 (verified)
Flowrate (kg/ s)	0.0009		0.0011		0.0010		0.0011		0.0010	
T_{in} (K)	318.7913		320.9788		323.4788		321.6038		323.7913	
T_o (K)	354.86	353.10	352.46	351.67	354.94	354.13	350.29	350.02	358.50	356.99
Useful Energy (W)	163.63	155.63	159.48	155.49	157.71	153.66	157.45	155.98	159.31	152.38
T_{in}-T_o (K)	36.07	34.31	31.48	30.69	31.46	30.65	28.68	28.41	34.71	33.20
Thermal Efficiency	0.88	0.84	0.86	0.84	0.85	0.83	0.85	0.84	0.86	0.82

Global sensitivities are based on all possible values of the input parameters in the generated sample points under the domain of the input parameters. The sensitivities chart which is presented in Figure 5-6 provides a graphic view of the impact of inlet parameters on each output parameter. The temperature rise (T_o-T_{in}) was the most sensitive output for the flowrate whereas it wasn't affected by the inlet temperature. The temperature of the top absorber increased with the increase in inlet temperature and decreased with the increase in flowrate. However, it was affected by the inlet temperature (0.7) more than the flowrate (-0.6). Water outlet temperature was less sensitive to the inlet temperature (0.58) compared to flowrate (-0.72). The outlet temperature increased with the increase in inlet temperature but decreased with the increase in flowrate. Thermal efficiency was more sensitive to the inlet temperature (-0.7) compared to the flowrate (0.35).

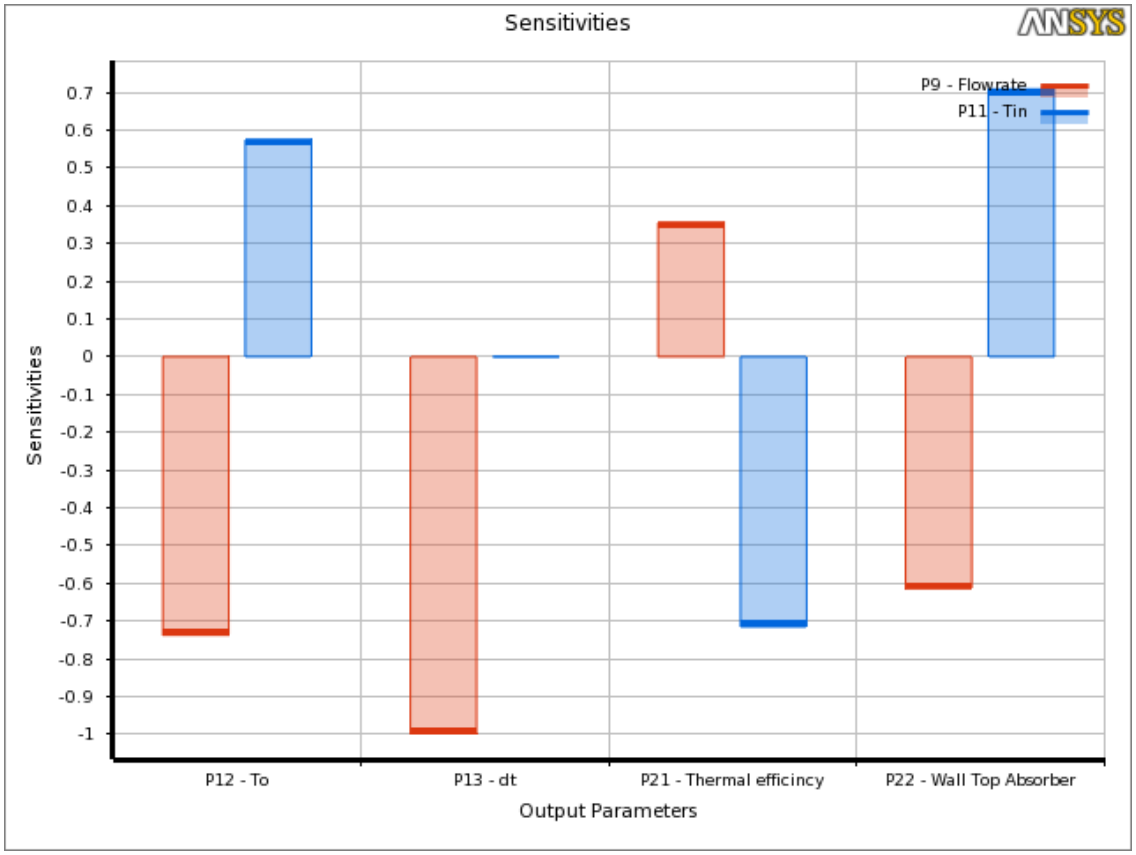

Figure 5-6 Global sensitivities chart of FPC for the temperature raise (T_o-T_{in}), average absorber temperature, outlet water temperature and thermal efficiency.

5.3 PVT Multi-objective optimisation

The effect of flowrate and inlet temperature on electrical and thermal efficiency were optimised in accordance with the minimum absorption cooling driving temperature available in the market in order to increase the coefficient of performance of the solar cooling absorption system (SCOP). As discussed in the previous section for FPC optimisation, thermal energy can be utilised from PVT then delivered to a storage tank via a hydraulic pump in order to supply solar absorption cooling systems. Minimum driving temperature (T_g) in the market, according to (Alobaid et al. 2017), for small capacity absorption chillers (Sonnenklima, Germany, 10 kW) is 348 K (75 ^oC) with return temperature (T_r) from the chiller of 338 K (65 ^oC).

Based on the design criteria of the selected absorption chiller, inlet temperature needs to be maintained above the ambient and below the return temperature from the chiller ($T_{amb} < T_{in} < T_r$). A parameters parallel chart for 17 design points and two inputs parameters is shown in Figure 5-7. Inlet temperature was in the range of 318 K to 353 K and the flowrate was in the range of 5 $x10^{-4}$ kg/s to 70 $x10^{-4}$ kg/s inside the riser pipe. In the range of inputs parameters, temperature rise varied from 5.5 K to 77 K, average temperature of PV varied from 330 K to 402.5 K, outlet temperature varied from 323.7 K to 428 K and thermal efficiency varied from 0.78 to 0.83.

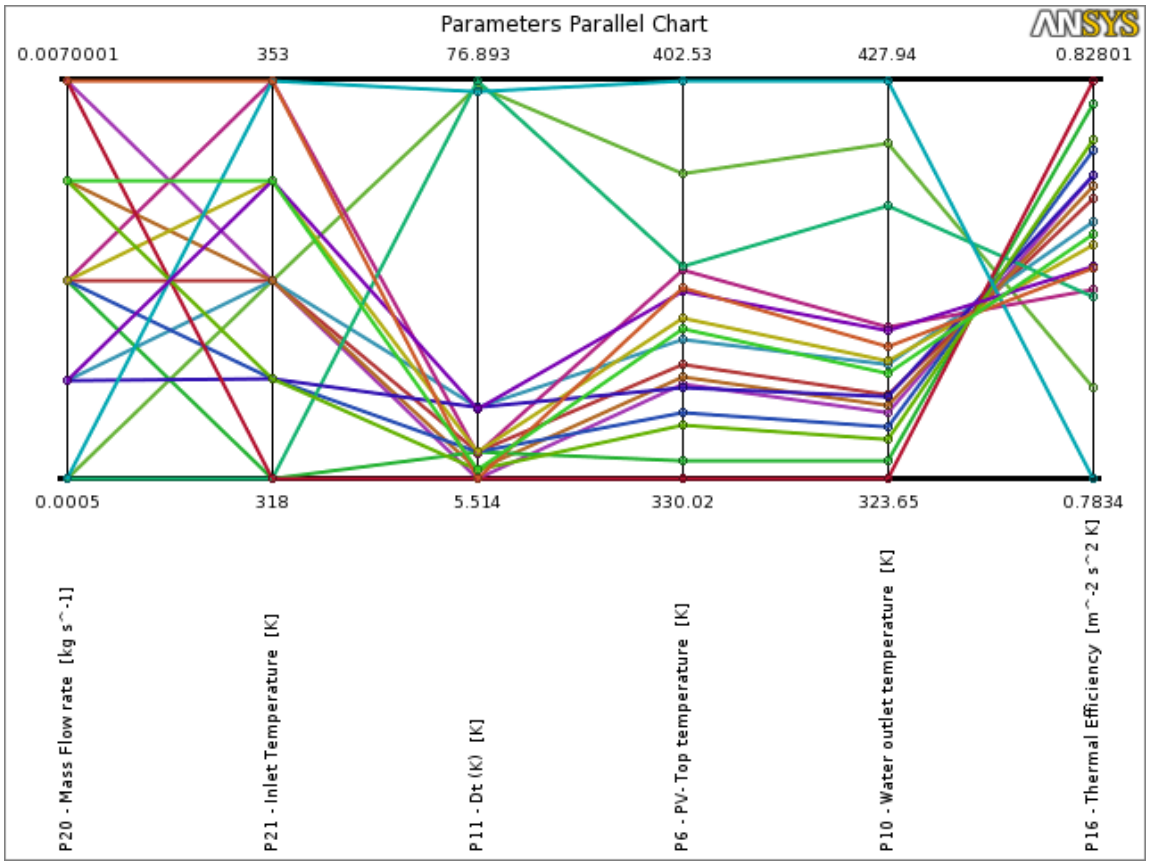

Figure 5-7 Parameters parallel chart for 17 design points and two inputs parameters of PVT.

Kriging response surface type was employed to predict the behaviour of the output parameters based on the results from DOE. Predicted relative error of 1.7 % was achieved for all outputs and converged at 22 refinement points. The response chart for the temperature rise (T_o-T_{in}) is illustrated in Figure 5-8, which shows the maximum expected rise (T_o-T_{in}) of 77 K at the minimum inlet temperature and flowrate; this is similar to the results in section 4.3.2. It can be observed that the inlet flowrate has the significant impact on (T_o-T_{in}), whereas the inlet temperature has a relatively slight impact on (T_o-T_{in}).

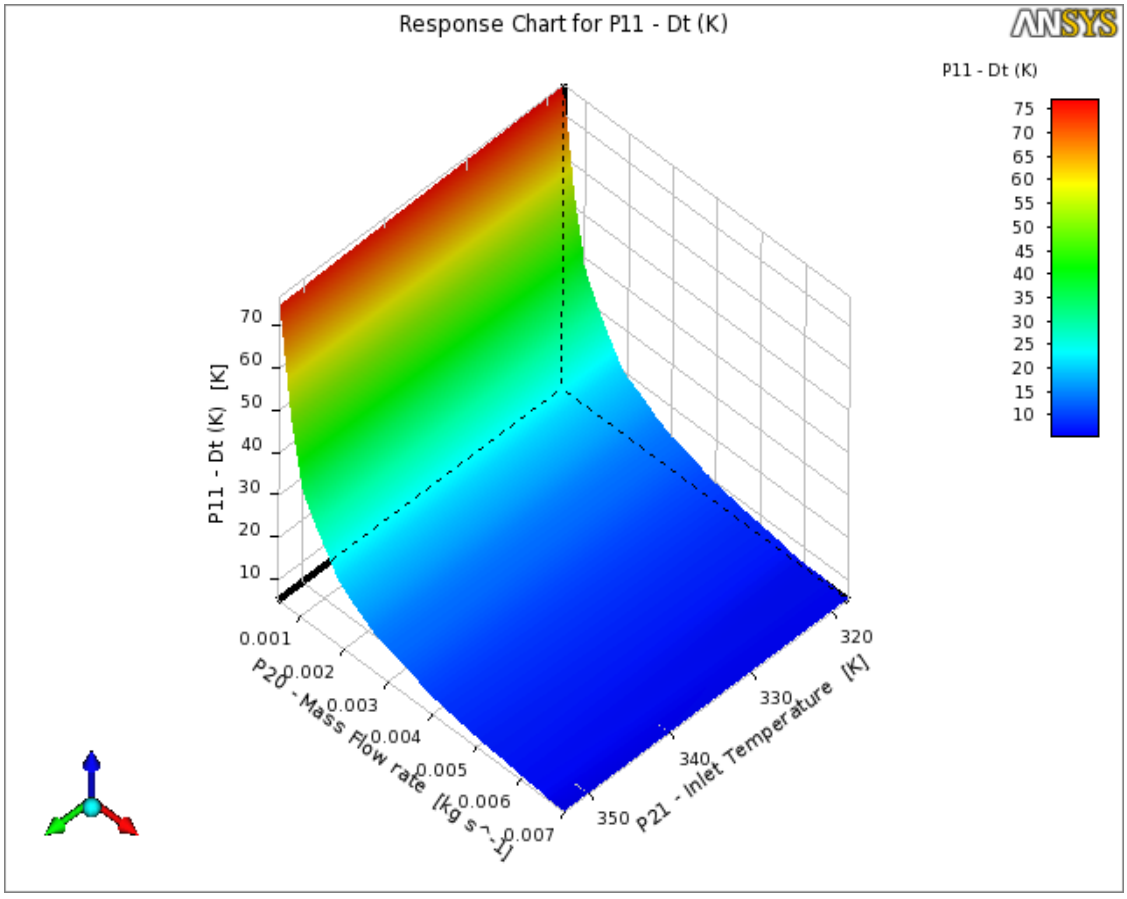

Figure 5-8 Response chart for the temperature rise in the inlet temperature (T_o-T_{in}) of the PVT.

The response chart for water outlet temperature of the PVT showed the maximum outlet temperature of 428 K at the minimum flowrate and maximum input temperature. Minimum outlet temperature of 323 K occurred at the maximum flowrate and the minimum inlet temperature as in Figure 5-9. It can be observed that both flowrate and inlet temperature influenced the outlet temperature at each point in the domain by different levels of impact, which requires optimisation.

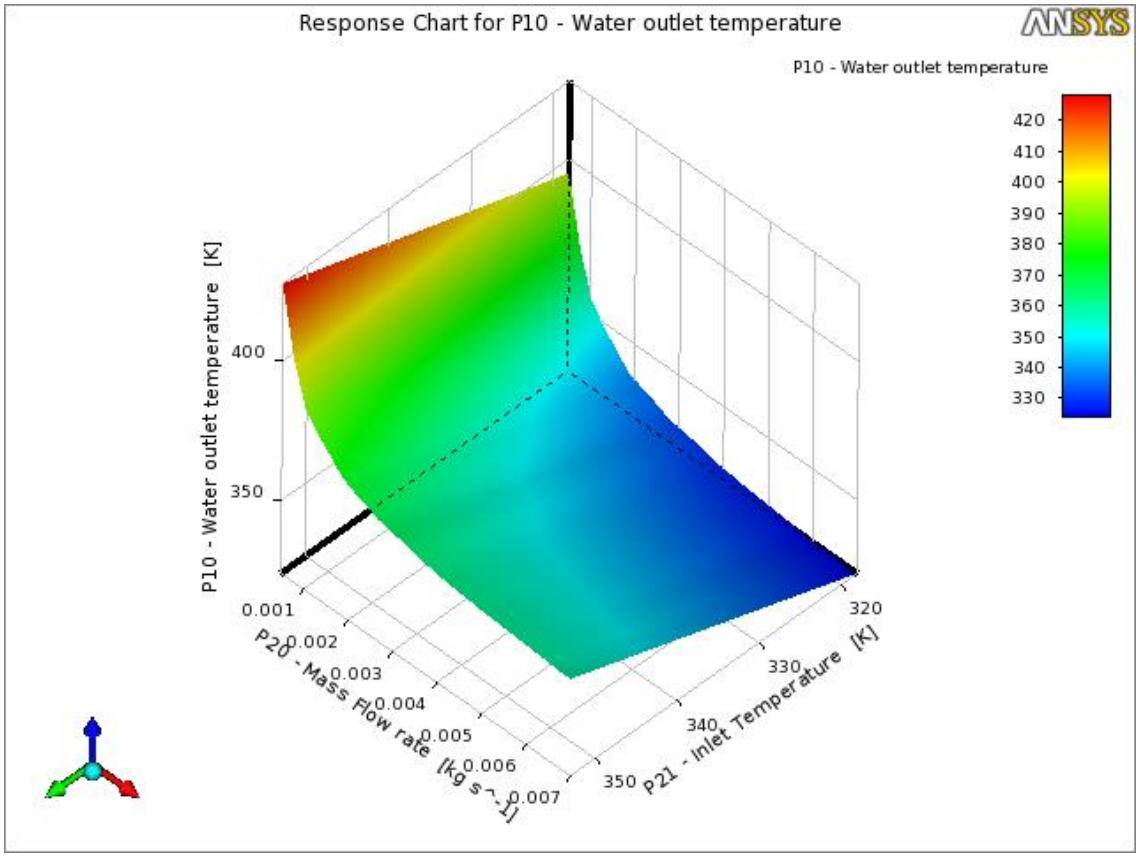

Figure 5-9 Response chart for the outlet temperature of the PVT.

The response chart of the average temperature of the photovoltaic layer is shown in Figure 5-10. Maximum average photovoltaic temperature of 402 K occurred at the minimum flowrate and maximum inlet temperature, while the minimum of 330 K occurred at the maximum flowrate and minimum inlet temperature. Similarly to the impact on outlet temperature, both flowrate and inlet temperature influenced the average temperature of the photovoltaic layer at each point in the domain by a different level.

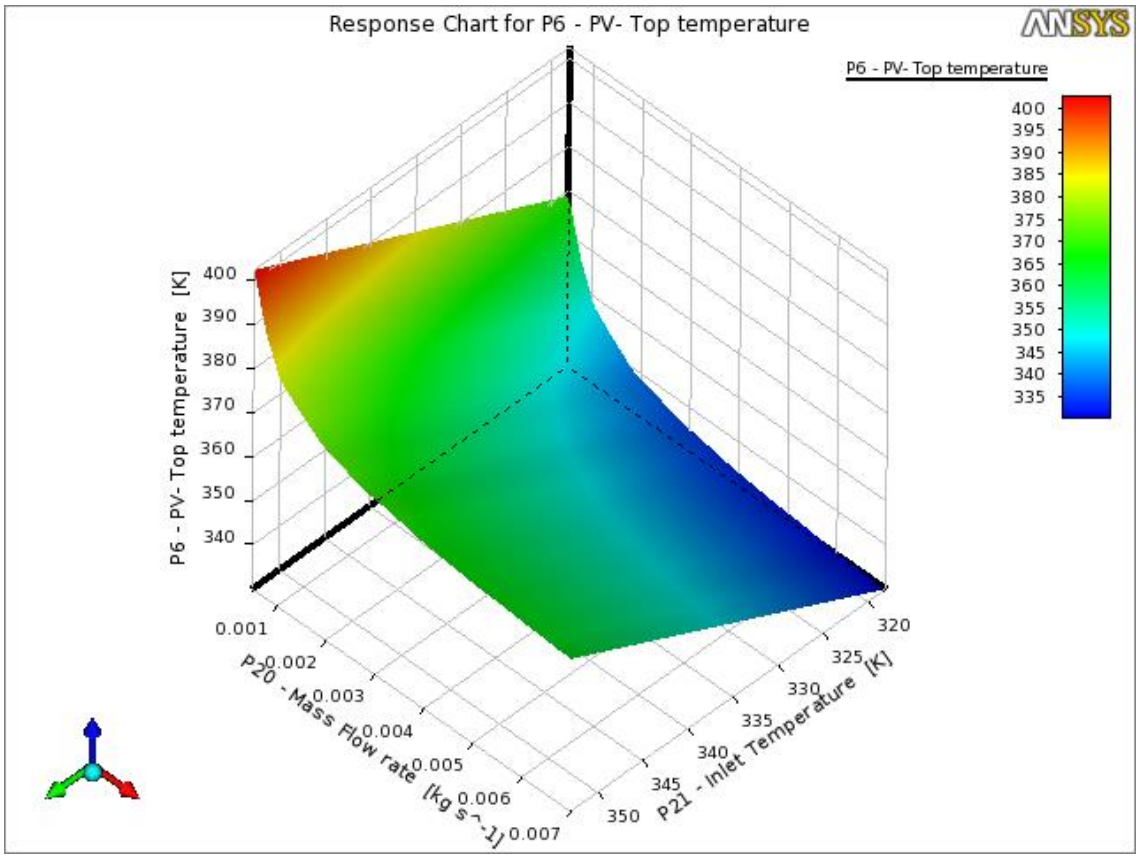

Figure 5-10 Response chart for the average photovoltaic temperature of the PVT.

In order to maximise overall efficiency in a solar absorption system coupled with PVT, flowrate and inlet water temperature were optimised for the PVT. Multiple objectives optimisation was applied in order to achieve the driven temperature for the chiller with high PVT thermal efficiency. As explained in chapter 3, by employing the response surface optimisation method in ANSYS16.1, multiple objectives and constraints were chosen in this section with screening optimisation type. 1000 samples were provided in the domain of the study in order to propose five candidate results. The initial goal in this study was to seek a 348 K outlet temperature (P10), and the additional goal was to maximise thermal efficiency (P16). The optimum candidates' points, which achieved the target temperature with maximum thermal efficiency, were also verified as in Table 5-2. From the details in Table 5-2, the optimum flowrate was 33 $x10^{-4}$ kg/s with inlet temperature of 337.36 K, which satisfied the inlet temperature condition:$T_{amb} < T_{in} < T_r$. The optimum thermal and electrical efficiencies were 81.32 % and 11.26 % respectively while the average temperature of the photovoltaic was 353.44 K.

Table 5-2 Optimum flowrate and inlet water temperature of the PVT.

Optimisation Method Name: Screening Response surface type : Kriging, refinements points = 22 1.7 % relative error DOE Type: Face cantered enhanced design type Central composite design Configuration: Generate 10000 samples and find 5 candidates. T_o: Seek Target 353 K , lower band 348 K Maximise thermal efficiency Constrains ($T_{amb}<T_{in}<T_r$): $318<T_{in}<338$ K										
	Point 1	Point 1 (verified)	Point 2	Point 2 (verified)	Point 3	Point 3 (verified)	Point 4	Point 4 (verified)	Point 5	Point 5 (verified)
Flowrate (kg/ s)	0.0033		0.0015		0.0034		0.0015		0.0033	
T_{in} (K)	337.36		321.44		339.55		323.62		341.74	
T_o (K)	349.60	349.08	348.60	347.66	351.57	351.07	351.22	350.27	353.85	353.33
Thermal Efficiency %	84.88	81.32	84.71	81.78	84.68	81.19	84.54	81.64	84.68	81.06
Avg. T_{pv} (K)	353.69	353.44	346.24	345.76	355.74	355.49	348.65	348.15	357.97	357.71
Electrical Efficiency %	11.24	11.26	11.74	11.78	11.10	11.12	11.58	11.61	10.95	10.97

Global sensitivities, based on all possible values of the input parameters in the generated sample points under the domain of the input parameters, were employed. A sensitivities chart, as in Figure 5-11, provides a graphic view of the impact of inlet parameters on each output parameter. The temperature rise (T_o-T_{in}) was the most sensitive output for the flow rate, whereas it wasn't affected by the inlet temperature. The average photovoltaic temperature increased with the increase in inlet temperature and decreased with the increase in flowrate. However, it was affected by the inlet temperature (0.81) more than the flowrate (-0.45). Water outlet temperature was more sensitive to the inlet temperature (0.7) compared to flowrate (-0.61). The outlet temperature increased with the increase in inlet temperature but decreased with the increase in flowrate.

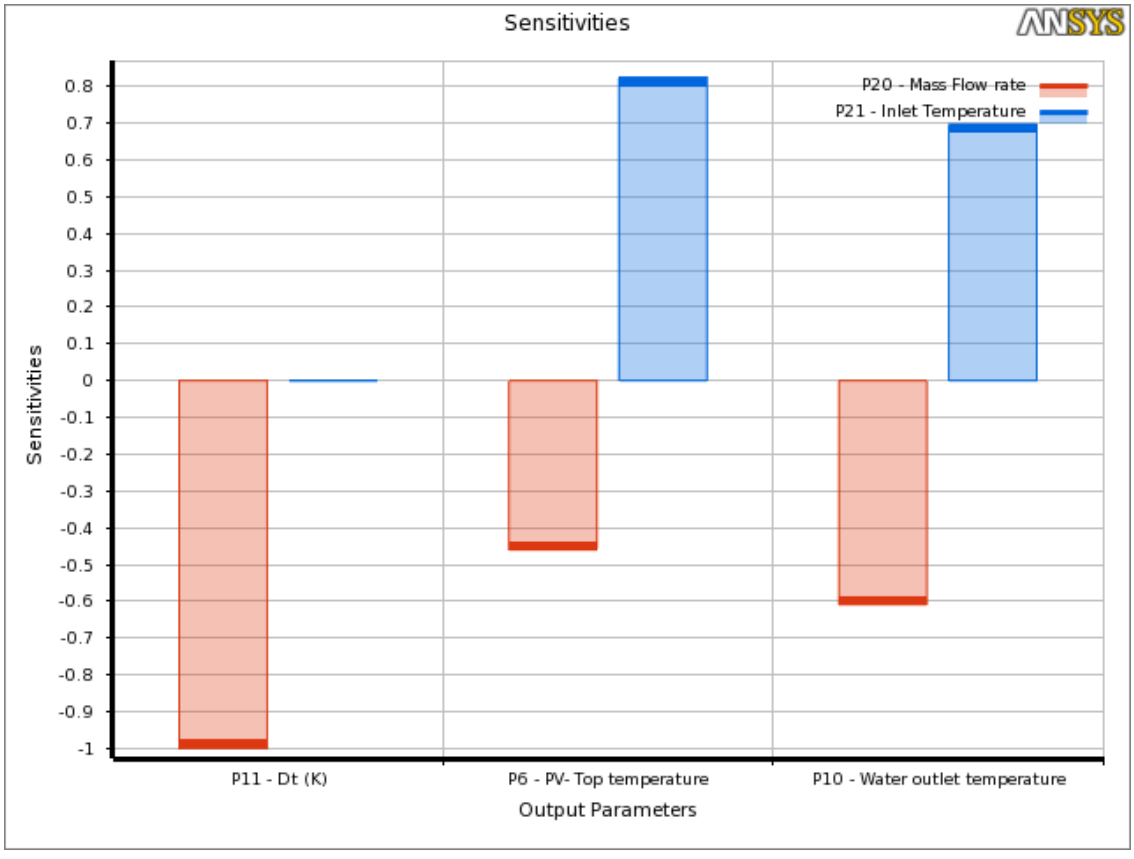

Figure 5-11 Global sensitivities chart of PVT for the temperature rise (T_o-T_{in}), average photovoltaic temperature and outlet water temperature.

5.4 Summary

The inlet conditions of FPC and PVT were optimised in this section for the highest efficiency with specified outlet temperature. The outlet temperatures of FPC and PVT were selected in accordance with the minimum absorption cooling driving temperature currently available in the market. Firstly, the single effect optimisation method was applied to the FPC in order to achieve the driven temperature for the chiller with high FPC thermal efficiency. T_{in} and $\dot{m}$ were optimised for the highest thermal efficiency (η_{th}). The optimum results of the FPC, based on the single effect optimisation method, were T_{in} = 323 K and $\dot{m}$ = 0.0013 kg/s for η_{th} = 86%.

In addition, a multi-objective optimisation study was applied to the computational model of the FPC by employing the response surface optimisation method in ANSYS16.1. The aim of using this method was to achieve a specified outlet temperature with high thermal efficiency within the domain of the optimisation parameters. The optimum results were $\dot{m}$ =11 x10^{-4} kg/s with inlet temperature of 321 K for thermal efficiency of 84 %. Based on the response surface optimisation of FPC, the temperature raise of the FPC (T_o-T_{in}) was the most sensitive output for the flowrate, whereas it wasn't affected by the inlet temperature. Furthermore, water outlet temperature was less sensitive to inlet temperature (0.58) compared to flowrate (-0.72), whereas thermal efficiency was more sensitive to the inlet temperature (-0.7) compared to the flowrate (0.35).

A multi-objective optimisation study was also applied to the computational model of the PVT by employing the response surface optimisation method in ANSYS16.1 with the same target. The optimum results were $\dot{m}$ =33 x10^{-4} kg/s with inlet temperature of 337.36 K for thermal and electrical efficiency, that is, 81.32 % and 11.26 % respectively. Based on the response surface optimisation of PVT, as for FPC, the temperature raise of the PVT (T_o-T_{in}) was the most sensitive output for the flowrate, whereas it wasn't affected by the inlet temperature. The average photovoltaic temperature was affected by the inlet temperature (0.81) more than the flowrate (-0.45). Furthermore, water outlet temperature was more sensitive to the inlet temperature (0.7) compared to flowrate (-0.61).

Chapter 6. Conclusion and Future Work

6.1 Conclusion

The aim of this study was to investigate and optimise the thermal efficiency of solar collectors for a sustainable cooling system. The opportunity to improve the overall performance of solar cooling systems is achievable by increasing the thermal efficiency of solar collectors in the system. This study has managed to achieve 84% thermal efficiency of flat plate collector (FPC) associated with absorption chiller by optimising the operation conditions of the FPC. The improvement in the thermal efficiency of FPC was 35% compare to the literature (maximum thermal efficiency of FPC collectors in cooling system was 55%). In addition, 81.3 % thermal efficiency of photovoltaic thermal collector (PVT) associated with single absorption chiller was achieved. The improvement in the thermal efficiency of PVT was 52 % compare to the literature (maximum thermal efficiency of PVT collectors in cooling system was 39%). The multi objective optimisation method was employed to seek the target outlet temperature with maximise the thermal efficiency based on a given weather data. At this specified conditions, the efficiency could exceed 80%. Including radiation losses to the model would reduce thermal efficiency. In addition considering higher wind speed would also reduce thermal efficiency. 71% thermal efficiency of a FPC was achieved, experimentally and numerically, at outlet temperature of 60 ^{o}C (Gunjo et al. 2017). Also the efficiency was in the range of 37% to 81% in another work from Gunjo et al. (2017). 79 % thermal efficiency was achieved by Hajabdollahi and Hajabdollahi (2017) for FPC. For PVT, thermal efficiency was in the range of 70-80 % (Khanjari et al. 2016). Presented here are the specific conclusions against each objective:

Objective 1- Critical literature review

In order to achieve the first objective in this study, the current developments in the use of FPC and PVT for cooling purposes were reviewed. The study also covered current developments in the field of solar absorption cooling systems from the standpoint of solar collecting options. Based on the performance and the initial cost of solar cooling systems, single effect absorption systems were estimated to be more efficient with lower costs. Solar absorption cooling systems showed the opportunity to act as an alternative to conventional cooling technologies, with a relatively high COP (0.5-0.8) for generating temperatures in the range of 70°C and 90°C. It was also shown that a sufficient efficiency for the PVT was achieved in the range of outlet temperatures of 60 ^{o}C to 80 ^{o}C. Despite the fact that there was an improvement in the electrical efficiency due to reducing the PV temperature by the coolant in the PVT system, a worthwhile opportunity existed to utilise the outlet water from the PVT to supply absorption chillers.

Objective 2- Effect of inlet temperature on thermal efficiency (FPC and PVT)

There was a decrease in η_{th} of FPC due to the increase in inlet water temperature. Increasing inlet water temperature of the FPC from 298 K to 370 K reduced thermal efficiency by 30%. The explanation is that the useful energy of the FPC decreased with increasing inlet temperature due to the decrease in the temperature difference between the absorber plate and the fluid inside the pipe (T_p-T_f) which reduced heat transfer. In addition, the temperature difference between the fluid inside the pipe and the ambient temperature (T_f-T_{amb}) increased due to the increase in inlet temperature, which increased the losses from the collector to the surroundings; this also minimised thermal efficiency. Similarly, there was a decrease in thermal efficiency (η_{th}) and electrical efficiency (η_{elc}) of PVT due to the increase in inlet water temperature. Increasing inlet water temperature of PVT from 273 K to 373 K reduced thermal efficiency by 7%, while there was a significant reduction in electrical efficiency by 45% due to the increase in photovoltaic layer temperature.

Objective 3- Effect of flowrate on thermal efficiency (FPC and PVT)

There was an increase in η_{th} of the FPC due to the increase in the water flowrate for all cases of inlet temperature. The reason was that the heat transfer coefficient between the pipe and water increased with the increase in water flowrate of the FPC which increased useful energy. The significant impact of total flowrate on the performance of the FPC occurred at the range of $\dot{m}$ =5 x10^{-3} kg/s to $\dot{m}$ =60 x10^{-3} kg/s, or in other words, there was no significant impact when the total flowrate of FPCs exceeded 36.4 x10^{-3} kg/s/m^2. Thermal efficiency was increased by 14 % (or by 15.4 % for high temperature inlet temperature) while the increase in inlet water temperature (T_o-T_{in}) was reduced by 90% due to the increase in total water flowrate from 3x10^{-3} kg/s/m^2 to 36.4 x10^{-3} kg/s/m^2. Similarly, η_{th} of the PVT increased due to the increase in the water flowrate for the all cases. The significant impact of the total flowrate on the performance of the PVT occurred in the range of $\dot{m}$ =5 x10^{-3} kg/s to $\dot{m}$ =70 x10^{-3} kg/s, or in other words, there was no significant impact when the total flowrate of PVTs exceeded 35 x10^{-3} kg/s/m^2. Thermal efficiency was increased by 2.8 % (or by 2.9 % for high temperature inlet temperature) while the increase in inlet water temperature (T_o-T_{in}) reduced by 93% due to the increase in total water flowrate from 2.5x10^{-3} kg/s/m^2 to 35 x10^{-3} kg/s/m^2.

Objective 4- Effect of PVT system on overall performance

In order to achieve the fourth objective in this study, a mathematical model of a PVT system was employed to determine the anticipated system performance. The more panels connected in series, the higher the outlet temperature and the higher the photovoltaic temperature that were achieved. Thermal efficiency decreased with the increase in the number of panels in series due to the increase in the temperature inside the water stream, which decreased heat transfer from the absorber to the fluid. Electrical efficiency also decreased with an increase in the number of panels in series for all cases of inlet temperature due to the increase in the photovoltaic temperature. The effect of the PVT system was investigated for different range of inlet water temperature. The method of connecting a specified number of panels has a significant impact on the performance characteristics of the PVT system. For an array consisting of 72 panels with inlet water temperature of 298 K, the outlet temperature increased for 54.8 K by increasing the

number of panels that connected in series from one to 72. This also increased the average temperature of the photovoltaic layer for 45 K, which reduced electrical efficiency by 23.4% while thermal efficiency was reduced by 50.44%. The impact of the configuration of the PVT system was reduced significantly by increasing the inlet water temperature.

Objective 5- Multi objective optimisation of FPC and PVT

The computational models of FPC and PVT were considered to achieve the fifth objective in this study. The inlet conditions of FPC and PVT were optimised for the highest efficiency in accordance with the minimum absorption cooling driving temperature currently available in the market. Firstly, the single effect optimisation method was applied to the FPC in order to meet the driven temperature for the chiller with high FPC thermal efficiency. T_{in} and $\dot{m}$ were optimised for the highest thermal efficiency (η_{th}). The optimum flowrate per square meter of the FPC based on the single effect optimisation method was $\dot{m} = 0.0079$ kg/s/m^2 and T_{in} = 323 K for η_{th} = 86%.

In addition, a multi- objective optimisation study was applied to the computational model of the FPC by employing the response surface optimisation method in ANSYS16.1. The aim of using this method was to achieve the specified outlet temperature with high thermal efficiency within the domain of the optimisation parameters. The optimum flowrate was $\dot{m}$ =0.0067 kg/s/m^2 with inlet temperature of 321 K for thermal efficiency of 84 %. Based on the response surface optimisation of FPC, the temperature rise of the FPC (T_o-T_{in}) was the most sensitive output for the flowrate. Furthermore, water outlet temperature was less sensitive to the inlet temperature (0.58) compared to flowrate (-0.72), whereas thermal efficiency was more sensitive to the inlet temperature (-0.7) compared to the flowrate (0.35).

A multi-objective optimisation study was also applied to the computational model of the PVT by employing the response surface optimisation method in ANSYS16.1 with the same aim. The optimum flowrate per square meter of the PVT was $\dot{m}$ =0.0165 kg/s/m^2 with inlet temperature of 337.36 K for thermal and electrical efficiency of 81.32 % and 11.26 % respectively. Based on the response surface optimisation of the PVT, as with the FPC, the temperature rise of the PVT (T_o-T_{in}) was the most sensitive output for the flowrate. The average photovoltaic temperature was affected by the inlet temperature

(0.81) more than the flowrate (-0.45). Furthermore, water outlet temperature was more sensitive to the inlet temperature (0.7) compared to flowrate (-0.61).

6.2 Challenges and Future Work

Steady state model is more efficient when the average operations parameters are considered (daily, weekly or monthly). The output from the steady state model, which is based on the average operations parameters such as efficiency curve, could be employed as input parameters in realistic transient system. Steady state in CFD describes the behaviour of the system in low computational cost with respect of governing equations, which included the conservation of mass, momentum and energy. The steady state model is commonly applied with solar collectors to investigate thermal performance. The major challenge in the use of the flat plate collector and photovoltaic thermal collectors for solar cooling systems is to achieve high thermal and electrical efficiency along with producing the required outlet fluid temperature. An economic feasibility study for the overall system is also an important factor and further research is suggested as follows:

- Dynamics of the flow and thermal behaviour for solar collectors within solar cooling absorption systems need to be studied throughout the year for specified countries.
- Control strategies for PVT absorption cooling system and operating scenarios with cooling load profile need to be investigated.
- The economic feasibility of solar absorption systems, including capital and running costs based on electricity prices and the need for cooling, need to be investigated.
- A case study of a building system needs to be specified and cooling load for the building needs to be simulated and validated to the literature or to alternative software.
- A comparative economic study between solar cooling absorption system and conventional air conditional units needs to be highlighted for a specified country.
- Further research is required to determine the optimum outlet water temperature and flowrate of the collector for the highest coefficient of performance (SCOP) for a solar cooling system throughout the year.

- The performance characteristics of solar collectors which is achieved in steady state approach in this study, would be considered as an input parameters for an overall transient system (solar cooling system which includes solar collectors, storage tank and absorption chiller) in future work. This can be utiliseed by linking the CFD software with transient software such as TRANSYS.
- Including transient approach instead of steady state in the CFD model of the FPC and PVT would describe the behaviour of the collectors better. However, this would significantly increase the simulation time especially in multi optimisation study.
- A radiation model in the CFD could be employed to include the radiation losses. This can be applied with the collector with discrete ordinate model (DO). However, including a radiation model would significantly increase the simulation time especially in multi optimisation study.

List of References

Abd-ur-Rehman, H. M. and F. A. Al-Sulaiman (2016). "Optimum selection of solar water heating (SWH) systems based on their comparative techno-economic feasibility study for the domestic sector of Saudi Arabia." Renewable and Sustainable Energy Reviews **62**: 336-349.

Agrouaz, Y., T. Bouhal, A. Allouhi, T. Kousksou, A. Jamil and Y. Zeraouli (2017). "Energy and parametric analysis of solar absorption cooling systems in various Moroccan climates." Case Studies in Thermal Engineering **9**: 28-39.

Agyenim, F., I. Knight and M. Rhodes (2010). "Design and experimental testing of the performance of an outdoor LiBr/H 2 O solar thermal absorption cooling system with a cold store." Solar energy **84**(5): 735-744.

Al-Ajlan, S., H. Al Faris and H. Khonkar (2003). "A simulation modeling for optimization of flat plate collector design in Riyadh, Saudi Arabia." Renewable Energy **28**(9): 1325-1339.

Al-Alili, A., Y. Hwang and R. Radermacher (2014). "Review of solar thermal air conditioning technologies." International Journal of Refrigeration **39**: 4-22.

Al-Alili, A., Y. Hwang, R. Radermacher and I. Kubo (2012). "A high efficiency solar air conditioner using concentrating photovoltaic/thermal collectors." Applied Energy **93**: 138-147.

Al-Alili, A., M. Islam, I. Kubo, Y. Hwang and R. Radermacher (2012). "Modeling of a solar powered absorption cycle for Abu Dhabi." Applied Energy **93**: 160-167.

Al-Ugla, A. A., M. A. I. El-Shaarawi and S. A. M. Said (2015). "Alternative designs for a 24-hours operating solar-powered LiBr–water absorption air-conditioning technology." International Journal of Refrigeration **53**: 90-100.

Al-Ugla, A. A., M. A. I. El-Shaarawi, S. A. M. Said and A. M. Al-Qutub (2016). "Techno-economic analysis of solar-assisted air-conditioning systems for commercial buildings in Saudi Arabia." Renewable and Sustainable Energy Reviews **54**: 1301-1310.

Aliane, A., S. Abboudi, C. Seladji and B. Guendouz (2016). "An illustrated review on solar absorption cooling experimental studies." Renewable and Sustainable Energy Reviews **65**: 443-458.

Allouhi, A., T. Kousksou, A. Jamil, P. Bruel, Y. Mourad and Y. Zeraouli (2015). "Solar driven cooling systems: An updated review." Renewable and Sustainable Energy Reviews **44**: 159-181.

Alobaid, M., B. Hughes, J. K. Calautit, D. O'Connor and A. Heyes (2017). "A review of solar driven absorption cooling with photovoltaic thermal systems." Renewable and Sustainable Energy Reviews **76**: 728-742.

Alobaid, M., B. Hughes, D. O'Connor, J. Calautit and A. Heyes (2018). "Improving Thermal and Electrical Efficiency in Photovoltaic Thermal Systems for Sustainable Cooling System Integration." Journal of Sustainable Development of Energy, Water and Environment Systems https://doi.org/10.13044/j.sdewes.d5.0187.

Aman, J., D.-K. Ting and P. Henshaw (2014). "Residential solar air conditioning: Energy and exergy analyses of an ammonia–water absorption cooling system." Applied Thermal Engineering **62**(2): 424-432.

Ansys, I. (2015). "CFD." ICEM CFD theory guide, Ansys inc.

Antony, J. (2014). Design of Experiments for Engineers and Scientists, Elsevier.

Asadi, J., P. Amani, M. Amani, A. Kasaeian and M. Bahiraei (2018). "Thermo-economic analysis and multi-objective optimization of absorption cooling system driven by various solar collectors." Energy Conversion and Management **173**: 715-727.

Aste, N., C. del Pero and F. Leonforte (2014). "Water flat plate PV–thermal collectors: A review." Solar Energy **102**: 98-115.

Aste, N., C. Del Pero, F. Leonforte and M. Manfren (2016). "Performance monitoring and modeling of an uncovered photovoltaic-thermal (PVT) water collector." Solar Energy **135**: 551-568.

Ayompe, L., A. Duffy, S. McCormack and M. Conlon (2011). "Validated TRNSYS model for forced circulation solar water heating systems with flat plate and heat pipe evacuated tube collectors." Applied Thermal Engineering **31**(8): 1536-1542.

Bahaidarah, H., A. Subhan, P. Gandhidasan and S. Rehman (2013). "Performance evaluation of a PV (photovoltaic) module by back surface water cooling for hot climatic conditions." Energy **59**: 445-453.

Bahaidarah, H. M., S. Rehman, P. Gandhidasan and B. Tanweer (2013). Experimental evaluation of the performance of a photovoltaic panel with water cooling. Photovoltaic Specialists Conference (PVSC), 2013 IEEE 39th, IEEE.

Baldwin, C. and C. A. Cruickshank (2012). "A review of solar cooling technologies for residential applications in Canada." Energy Procedia **30**: 495-504.

Balghouthi, M., M. Chahbani and A. Guizani (2012). "Investigation of a solar cooling installation in Tunisia." Applied Energy **98**: 138-148.

Bataineh, K. and Y. Taamneh (2016). "Review and recent improvements of solar sorption cooling systems." Energy and Buildings **128**: 22-37.

Beccali, M., P. Finocchiaro and B. Nocke (2009). "Energy and economic assessment of desiccant cooling systems coupled with single glazed air and hybrid PV/thermal solar collectors for applications in hot and humid climate." Solar energy **83**(10): 1828-1846.

Bellos, E., C. Tzivanidis and K. A. Antonopoulos (2016). "Exergetic, energetic and financial evaluation of a solar driven absorption cooling system with various collector types." Applied Thermal Engineering **102**: 749-759.

Bermejo, P., F. J. Pino and F. Rosa (2010). "Solar absorption cooling plant in Seville." Solar Energy **84**(8): 1503-1512.

Buonomano, A., F. Calise and A. Palombo (2013). "Solar heating and cooling systems by CPVT and ET solar collectors: a novel transient simulation model." Applied Energy **103**: 588-606.

Buonomano, A., F. Calise and A. Palombo (2018). "Solar heating and cooling systems by absorption and adsorption chillers driven by stationary and concentrating photovoltaic/thermal solar collectors: Modelling and simulation." Renewable and Sustainable Energy Reviews **82**: 1874-1908.

Calautit, J. K., H. N. Chaudhry, B. R. Hughes and S. A. Ghani (2013). "Comparison between evaporative cooling and a heat pipe assisted thermal loop for a commercial wind tower in hot and dry climatic conditions." Applied Energy **101**: 740-755.

Calise, F., A. Cipollina, M. D. d'Accadia and A. Piacentino (2014). "A novel renewable polygeneration system for a small Mediterranean volcanic island for the combined production of energy and water: Dynamic simulation and economic assessment." Applied Energy **135**: 675-693.

Calise, F., M. D. d'Accadia, A. Palombo and L. Vanoli (2013). "Dynamic simulation of a novel high-temperature solar trigeneration system based on concentrating photovoltaic/thermal collectors." Energy **61**: 72-86.

Calise, F., M. D. d'Accadia and L. Vanoli (2012). "Design and dynamic simulation of a novel solar trigeneration system based on hybrid photovoltaic/thermal collectors (PVT)." Energy Conversion and Management **60**: 214-225.

Calise, F., M. Dentice d'Accadia, R. D. Figaj and L. Vanoli (2016). "A novel solar-assisted heat pump driven by photovoltaic/thermal collectors: Dynamic simulation and thermoeconomic optimization." Energy **95**: 346-366.

Calise, F. and L. Vanoli (2012). "Parabolic trough photovoltaic/thermal collectors: design and simulation model." Energies **5**(10): 4186-4208.

Cengel, Y. A., M. A. Boles and M. Kanoğlu (2011). Thermodynamics: an engineering approach, McGraw-Hill New York.

Cerón, J. F., J. Pérez-García, J. P. Solano, A. García and R. Herrero-Martín (2015). "A coupled numerical model for tube-on-sheet flat-plate solar liquid collectors. Analysis and validation of the heat transfer mechanisms." Applied Energy **140**: 275-287.

Chidambaram, L., A. Ramana, G. Kamaraj and R. Velraj (2011). "Review of solar cooling methods and thermal storage options." Renewable and sustainable energy reviews **15**(6): 3220-3228.

Chow, T. T. (2010). "A review on photovoltaic/thermal hybrid solar technology." Applied Energy **87**(2): 365-379.

Cristofari, C., G. Notton and J. L. Canaletti (2009). "Thermal behavior of a copolymer PV/Th solar system in low flow rate conditions." Solar Energy **83**(8): 1123-1138.

Darkwa, J., S. Fraser and D. Chow (2012). "Theoretical and practical analysis of an integrated solar hot water-powered absorption cooling system." Energy **39**(1): 395-402.

Deng, J., R. Wang and G. Han (2011). "A review of thermally activated cooling technologies for combined cooling, heating and power systems." Progress in Energy and Combustion Science **37**(2): 172-203.

Dubey, S. and A. A. Tay (2014). "The theoretical modelling and optimization of a 10 KWP photovoltaic thermal system for a student hostel in Singapore." International Journal of Green Energy **11**(3): 225-239.

Duffie, J. A. and W. A. Beckman (1980). Solar engineering of thermal processes, Wiley New York etc.

Ebrahim Ghasemi, S. and A. Akbar Ranjbar (2017). "Numerical thermal study on effect of porous rings on performance of solar parabolic trough collector." Applied Thermal Engineering **118**: 807-816.

Eicker, U., A. Colmenar-Santos, L. Teran, M. Cotrado and D. Borge-Diez (2014). "Economic evaluation of solar thermal and photovoltaic cooling systems through simulation in different climatic conditions: An analysis in three different cities in Europe." Energy and Buildings **70**: 207-223.

Eicker, U. and D. Pietruschka (2009). "Design and performance of solar powered absorption cooling systems in office buildings." Energy and Buildings **41**(1): 81-91.

Evans, D. L. (1981). "Simplified method for predicting photovoltaic array output." Solar Energy **27**(6): 555-560.

Falahatkar, A. and M. Khalaji Assad (2011). Analysis of solar lithium bromide-water absorption cooling system with heat pipe solar collector. World renewable energy congress.

Fang, G., H. Hu and X. Liu (2010). "Experimental investigation on the photovoltaic–thermal solar heat pump air-conditioning system on water-heating mode." Experimental Thermal and Fluid Science **34**(6): 736-743.

Ferreira, C. I. and D.-S. Kim (2014). "Techno-economic review of solar cooling technologies based on location-specific data." International journal of refrigeration **39**: 23-37.

Fong, K., T. T. Chow, C. K. Lee, Z. Lin and L. Chan (2010). "Comparative study of different solar cooling systems for buildings in subtropical city." Solar Energy **84**(2): 227-244.

Fong, K., T. T. Chow, C. K. Lee, Z. Lin and L. Chan (2011). "Solar hybrid cooling system for high-tech offices in subtropical climate–Radiant cooling by absorption refrigeration and desiccant dehumidification." Energy Conversion and Management **52**(8): 2883-2894.

Fong, K. and C. Lee (2014). "Performance advancement of solar air-conditioning through integrated system design for building." Energy **73**: 987-996.

Fortuin, S., M. Hermann, G. Stryi-Hipp, P. Nitz and W. Platzer (2014). "Hybrid PV-thermal Collector Development: Concepts, Experiences, Results and Research Needs." Energy Procedia **48**: 37-47.

Fudholi, A., K. Sopian, M. H. Yazdi, M. H. Ruslan, A. Ibrahim and H. A. Kazem (2014). "Performance analysis of photovoltaic thermal (PVT) water collectors." Energy Conversion and Management **78**(0): 641-651.

Fumo, N., V. Bortone and J. Zambrano (2013). "Comparative Analysis of Solar Thermal Cooling and Solar Photovoltaic Cooling Systems." Journal of Solar Energy Engineering **135**(2): 021002.

Garcia-Heller, V., S. Paredes, C. L. Ong, P. Ruch and B. Michel (2014). "Exergoeconomic analysis of high concentration photovoltaic thermal co-generation system for space cooling." Renewable and Sustainable Energy Reviews **34**: 8-19.

Ghafoor, A. and A. Munir (2015). "Worldwide overview of solar thermal cooling technologies." Renewable and Sustainable Energy Reviews **43**: 763-774.

Gunjo, D. G., P. Mahanta and P. S. Robi (2017). "CFD and experimental investigation of flat plate solar water heating system under steady state condition." Renewable Energy **106**: 24-36.

Gunjo, D. G., P. Mahanta and P. S. Robi (2017). "Exergy and energy analysis of a novel type solar collector under steady state condition: Experimental and CFD analysis." Renewable Energy **114**: 655-669.

Guo, J., S. Lin, J. I. Bilbao, S. D. White and A. B. Sproul (2017). "A review of photovoltaic thermal (PV/T) heat utilisation with low temperature desiccant cooling and dehumidification." Renewable and Sustainable Energy Reviews **67**: 1-14.

Hajabdollahi, Z. and H. Hajabdollahi (2017). "Thermo-economic modeling and multi-objective optimization of solar water heater using flat plate collectors." Solar Energy **155**(Supplement C): 191-202.

Hartmann, N., C. Glueck and F. Schmidt (2011). "Solar cooling for small office buildings: Comparison of solar thermal and photovoltaic options for two different European climates." Renewable Energy **36**(5): 1329-1338.

Hassan, H. and A. Mohamad (2012). "A review on solar cold production through absorption technology." Renewable and sustainable energy reviews **16**(7): 5331-5348.

Hawwash, A. A., A. K. Abdel Rahman, S. A. Nada and S. Ookawara (2018). "Numerical Investigation and Experimental Verification of Performance Enhancement of Flat Plate Solar Collector Using Nanofluids." Applied Thermal Engineering **130**: 363-374.

Hepbasli, A. and Z. Alsuhaibani (2011). "A key review on present status and future directions of solar energy studies and applications in Saudi Arabia." Renewable and Sustainable Energy Reviews **15**(9): 5021-5050.

Hoffmann, W. (2006). "PV solar electricity industry: Market growth and perspective." Solar energy materials and solar cells **90**(18): 3285-3311.

Hossain, M. S., R. Saidur, H. Fayaz, N. A. Rahim, M. R. Islam, J. U. Ahamed and M. M. Rahman (2011). "Review on solar water heater collector and thermal energy performance of circulating pipe." Renewable and Sustainable Energy Reviews **15**(8): 3801-3812.

Hosseinzadeh, M., A. Salari, M. Sardarabadi and M. Passandideh-Fard (2018). "Optimization and parametric analysis of a nanofluid based photovoltaic thermal

system: 3D numerical model with experimental validation." Energy Conversion and Management **160**: 93-108.

Hung, T.-C., T.-J. Huang, D.-S. Lee, C.-H. Lin, B.-S. Pei and Z.-Y. Li (2017). "Numerical analysis and experimental validation of heat transfer characteristic for flat-plate solar air collector." Applied Thermal Engineering **111**: 1025-1038.
Jesch, L. F. (1981). Solar energy today, UK-ISES.

Ketfi, O., M. Merzouk, N. K. Merzouk and S. E. Metenani (2015). "Performance of a Single Effect Solar Absorption Cooling System (Libr-H2O)." Energy Procedia **74**: 130-138.

Ketjoy, N. and K. Mansiri (2013). "Performance Evaluation of 35kW LiBr–H 2 O Solar Absorption Cooling System in Thailand." Energy Procedia **34**: 198-210.

Khan, M. M. A., N. I. Ibrahim, R. Saidur, I. M. Mahbubul and F. A. Al-Sulaiman (2016). "Performance assessment of a solar powered ammonia–water absorption refrigeration system with storage units." Energy Conversion and Management **126**: 316-328.

Khanjari, Y., F. Pourfayaz and A. B. Kasaeian (2016). "Numerical investigation on using of nanofluid in a water-cooled photovoltaic thermal system." Energy Conversion and Management **122**: 263-278.

Kim, D. and C. Infante Ferreira (2008). "Solar refrigeration options–a state-of-the-art review." International journal of refrigeration **31**(1): 3-15.

Knier, G. (2002). "How do photovoltaics work?" Science@ NASA.

Koronaki, I. P., E. G. Papoutsis and V. D. Papaefthimiou (2016). "Thermodynamic modeling and exergy analysis of a solar adsorption cooling system with cooling tower in Mediterranean conditions." Applied Thermal Engineering **99**: 1027-1038.

Kulkarni, K., A. Afzal and K.-Y. Kim (2015). "Multi-objective optimization of solar air heater with obstacles on absorber plate." Solar Energy **114**(Supplement C): 364-377.

Lari, M. O. and A. Z. Sahin (2018). "Effect of retrofitting a silver/water nanofluid-based photovoltaic/thermal (PV/T) system with a PCM-thermal battery for residential applications." Renewable Energy **122**: 98-107.

Lee, S.-M. and K.-Y. Kim (2015). "Multi-objective optimization of arc-shaped ribs in the channels of a printed circuit heat exchanger." International Journal of Thermal Sciences **94**(Supplement C): 1-8.

Li, M., C. Xu, R. H. E. Hassanien, Y. Xu and B. Zhuang (2016). "Experimental investigation on the performance of a solar powered lithium bromide–water absorption cooling system." International Journal of Refrigeration **71**: 46-59.

Li, Z., X. Ye and J. Liu (2014). "Optimal temperature of collector for solar double effect LiBr/H2O absorption cooling system in subtropical city based on a year round meteorological data." Applied Thermal Engineering **69**(1): 19-28.

Li, Z. Y., X. Y. Ye and J. P. Liu (2014). Performance analysis of solar double effect LiBr/H2O absorption chiller in subtropical city based on the year round meteorological data. Applied Mechanics and Materials, Trans Tech Publ.

Liang, R., J. Zhang and C. Zhou (2015). "Dynamic Simulation of a Novel Solar Heating System Based on Hybrid Photovoltaic/Thermal Collectors (PVT)." Procedia Engineering **121**: 675-683.

Lin, W., Z. Ma, M. I. Sohel and P. Cooper (2014). "Development and evaluation of a ceiling ventilation system enhanced by solar photovoltaic thermal collectors and phase change materials." Energy conversion and Management **88**: 218-230.

Lizarte, R., M. Izquierdo, J. Marcos and E. Palacios (2012). "An innovative solar-driven directly air-cooled LiBr–H 2 O absorption chiller prototype for residential use." Energy and Buildings **47**: 1-11.

Lu, Z., R. Wang, Z. Xia, X. Lu, C. Yang, Y. Ma and G. Ma (2013). "Study of a novel solar adsorption cooling system and a solar absorption cooling system with new CPC collectors." Renewable Energy **50**: 299-306.

Lu, Z. H. and Q. Yao (2007). "Energy analysis of silicon solar cell modules based on an optical model for arbitrary layers." Solar Energy **81**(5): 636-647.

Marc, O., F. Lucas, F. Sinama and E. Monceyron (2010). "Experimental investigation of a solar cooling absorption system operating without any backup system under tropical climate." Energy and Buildings **42**(6): 774-782.

Martínez, P. J., J. C. Martínez and M. Lucas (2012). "Design and test results of a low-capacity solar cooling system in Alicante (Spain)." Solar Energy **86**(10): 2950-2960.

Martínez, P. J., J. C. Martínez and P. Martínez (2016). "Performance comparison of solar autonomous and assisted absorption systems in Spain." International Journal of Refrigeration **71**: 85-93.

Mateus, T. and A. C. Oliveira (2009). "Energy and economic analysis of an integrated solar absorption cooling and heating system in different building types and climates." Applied Energy **86**(6): 949-957.

Michael, J. J., S. Iniyan and R. Goic (2015). "Flat plate solar photovoltaic–thermal (PV/T) systems: a reference guide." Renewable and Sustainable Energy Reviews **51**: 62-88.

Mittelman, G., A. Kribus and A. Dayan (2007). "Solar cooling with concentrating photovoltaic/thermal (CPVT) systems." Energy Conversion and Management **48**(9): 2481-2490.

Moghimi, M. A., K. J. Craig and J. P. Meyer (2015). "Optimization of a trapezoidal cavity absorber for the Linear Fresnel Reflector." Solar Energy **119**(Supplement C): 343-361.

Moss, R., S. Shire, P. Henshall, F. Arya, P. Eames and T. Hyde (2018). "Performance of evacuated flat plate solar thermal collectors." Thermal Science and Engineering Progress **8**: 296-306.

Mwesigye, A., T. Bello-Ochende and J. P. Meyer (2015). "Multi-objective and thermodynamic optimisation of a parabolic trough receiver with perforated plate inserts." Applied Thermal Engineering **77**(Supplement C): 42-56.

Nasrin, R., M. Hasanuzzaman and N. A. Rahim (2018). "Effect of high irradiation and cooling on power, energy and performance of a PVT system." Renewable Energy **116**: 552-569.

Pampuri, L., N. Cereghetti, D. Strepparava and P. Caputo (2016). "Analysis of the electricity consumptions: A first step to develop a district cooling system." Sustainable Cities and Society **23**: 23-36.

Papoutsis, E. G., I. P. Koronaki and V. D. Papaefthimiou (2017). "Numerical simulation and parametric study of different types of solar cooling systems under Mediterranean climatic conditions." Energy and Buildings **138**: 601-611.

Parida, B., S. Iniyan and R. Goic (2011). "A review of solar photovoltaic technologies." Renewable and Sustainable Energy Reviews **15**(3): 1625-1636.

Pazheri, F. R., N. H. Malik, A. A. Al-Arainy, S. Ottukulotk, M. F. Othman, E. A. Al-Ammar and I. Ahamed (2012). "Use of renewable energy sources in Saudi Arabia through smart grid." Journal of Energy and Power Engineering **6**(7): 1065-1070.

Peng, Z. J., M. R. Herfatmanesh and Y. M. Liu (2017). "Cooled solar PV panels for output energy efficiency optimisation." Energy Conversion and Management **150**: 949-955.

Pierrick, H., M. Christophe, G. Leon and D. Patrick (2015). "Dynamic numerical model of a high efficiency PV–T collector integrated into a domestic hot water system." Solar Energy **111**: 68-81.

Pongtornkulpanich, A., S. Thepa, M. Amornkitbamrung and C. Butcher (2008). "Experience with fully operational solar-driven 10-ton LiBr/H 2 O single-effect absorption cooling system in Thailand." Renewable Energy **33**(5): 943-949.

Praene, J. P., O. Marc, F. Lucas and F. Miranville (2011). "Simulation and experimental investigation of solar absorption cooling system in Reunion Island." Applied Energy **88**(3): 831-839.

Prasartkaew, B. (2013). "Mathematical Modeling of an Absorption Chiller System Energized by a Hybrid Thermal System: Model Validation." Energy Procedia **34**: 159-172.

Qu, M., H. Yin and D. H. Archer (2010). "A solar thermal cooling and heating system for a building: experimental and model based performance analysis and design." Solar energy **84**(2): 166-182.

Raja, V. B. and V. Shanmugam (2012). "A review and new approach to minimize the cost of solar assisted absorption cooling system." Renewable and sustainable energy reviews **16**(9): 6725-6731.

Rangababu, J. A., K. Kiran Kumar and S. Srinivasa Rao (2015). "Numerical Analysis and Validation of Heat Transfer Mechanism of Flat Plate Collectors." Procedia Engineering **127**: 63-70.

Rejeb, O., M. Sardarabadi, C. Ménézo, M. Passandideh-Fard, M. H. Dhaou and A. Jemni (2016). "Numerical and model validation of uncovered nanofluid sheet and tube type photovoltaic thermal solar system." Energy Conversion and Management **110**: 367-377.

Rosell, J. I., X. Vallverdú, M. A. Lechón and M. Ibáñez (2005). "Design and simulation of a low concentrating photovoltaic/thermal system." Energy Conversion and Management **46**(18–19): 3034-3046.

Sadiq Munfath Khan, M. and J. Orfi (2014). "Cooling performance and energy saving analysis of cascade refrigeration system powered by solar energy for Riyadh region (Saudi Arabia)." International Journal of Sustainable Building Technology and Urban Development **5**(1): 44-52.

Said, S. A. M., K. Spindler, M. A. El-Shaarawi, M. U. Siddiqui, F. Schmid, B. Bierling and M. M. A. Khan (2016). "Design, construction and operation of a solar powered ammonia–water absorption refrigeration system in Saudi Arabia." International Journal of Refrigeration **62**: 222-231.

Sanaye, S. and A. Sarrafi (2015). "Optimization of combined cooling, heating and power generation by a solar system." Renewable Energy **80**: 699-712.

Sarbu, I. and C. Sebarchievici (2013). "Review of solar refrigeration and cooling systems." Energy and Buildings **67**: 286-297.

Shirazi, A., R. A. Taylor, S. D. White and G. L. Morrison (2016). "A systematic parametric study and feasibility assessment of solar-assisted single-effect, double-effect, and triple-effect absorption chillers for heating and cooling applications." Energy Conversion and Management **114**: 258-277.

Shojaeizadeh, E., F. Veysi and A. Kamandi (2015). "Exergy efficiency investigation and optimization of an Al2O3–water nanofluid based Flat-plate solar collector." Energy and Buildings **101**: 12-23.

Shyam, G. N. Tiwari and I. M. Al-Helal (2015). "Analytical expression of temperature dependent electrical efficiency of N-PVT water collectors connected in series." Solar Energy **114**: 61-76.

Shyam, G. N. Tiwari, O. Fischer, R. K. Mishra and I. M. Al-Helal (2016). "Performance evaluation of N-photovoltaic thermal (PVT) water collectors partially covered by photovoltaic module connected in series: An experimental study." Solar Energy **134**: 302-313.

Siddiqui, M. U. and S. A. M. Said (2015). "A review of solar powered absorption systems." Renewable and Sustainable Energy Reviews **42**: 93-115.

Sofotasiou, P., J. K. Calautit, B. R. Hughes and D. O'Connor (2016). "Towards an integrated computational method to determine internal spaces for optimum environmental conditions." Computers & Fluids **127**: 146-160.

Sumathy, K., Z. Huang and Z. Li (2002). "Solar absorption cooling with low grade heat source—a strategy of development in South China." Solar energy **72**(2): 155-165.

Šúri, M., T. A. Huld, E. D. Dunlop and H. A. Ossenbrink (2007). "Potential of solar electricity generation in the European Union member states and candidate countries." Solar Energy **81**(10): 1295-1305.

Tagliafico, L. A., F. Scarpa and M. De Rosa (2014). "Dynamic thermal models and CFD analysis for flat-plate thermal solar collectors – A review." Renewable and Sustainable Energy Reviews **30**: 526-537.

Tsai, H.-L. (2015). "Modeling and validation of refrigerant-based PVT-assisted heat pump water heating (PVTA–HPWH) system." Solar Energy **122**: 36-47.

Vokas, G., N. Christandonis and F. Skittides (2006). "Hybrid photovoltaic–thermal systems for domestic heating and cooling—a theoretical approach." Solar Energy **80**(5): 607-615.

Wang, N., S. Zeng, M. Zhou and S. Wang (2015). "Numerical study of flat plate solar collector with novel heat collecting components." International Communications in Heat and Mass Transfer **69**: 18-22.

White, F. M. (2011). Fluid mechanics, in SI units, McGraw-Hill.

Xu, Z. and C. Kleinstreuer (2014). "Concentration photovoltaic–thermal energy co-generation system using nanofluids for cooling and heating." Energy Conversion and Management **87**: 504-512.

Yazdanifard, F., E. Ebrahimnia-Bajestan and M. Ameri (2016). "Investigating the performance of a water-based photovoltaic/thermal (PV/T) collector in laminar and turbulent flow regime." Renewable Energy **99**: 295-306.

Yin, Y., X. Zhai and R. Wang (2013). "Experimental investigation and performance analysis of a mini-type solar absorption cooling system." Applied Thermal Engineering **59**(1): 267-277.

Zhai, X., M. Qu, Y. Li and R. Wang (2011). "A review for research and new design options of solar absorption cooling systems." Renewable and sustainable energy reviews **15**(9): 4416-4423.

Zhang, D., J. Li, Z. Gao, L. Wang and J. Nan (2016). "Thermal performance investigation of modified flat plate solar collector with dual-function." Applied Thermal Engineering **108**: 1126-1135.

Zhou, F., J. Ji, J. Cai and B. Yu (2017). "Experimental and numerical study of the freezing process of flat-plate solar collector." Applied Thermal Engineering **118**: 773-784.

A